Ryszard Buchalik

Experimental and simulation studies of steady- and transient-state operation of thermoelectric systems for cooling and electricity generation

---

PhD Thesis

Supervisor: dr hab. inż. Grzegorz Nowak, prof. PŚ

Scientific discipline:

Environmental Engineering, Mining and Energy

Gliwice, 2022

Author:

mgr inż. Ryszard Buchalik
Department of Power Engineering and Turbomachinery,
Faculty of Energy and Environmental Engineering,
Silesian University of Technology, Gliwice, Poland
ryszard.buchalik@polsl.pl

Supervisor:

dr hab. inż. Grzegorz Nowak, prof. PŚ
Department of Power Engineering and Turbomachinery,
Faculty of Energy and Environmental Engineering,
Silesian University of Technology, Gliwice, Poland
grzegorz.nowak@polsl.pl

Reviewers:

prof. dr hab. inż. Dariusz Mikielewicz
Institue of Energy,
Faculty of Mechanical Engineering,
Gdańsk University of Technology, Gdańsk, Poland
dariusz.mikielewicz@pg.edu.pl

prof. dr hab. inż. Jarosław Milewski
Institute of Heat Engineering,
Faculty of Power and Aeronautical Engineering,
Warsaw University of Technology, Warsaw, Poland
milewski@itc.pw.edu.pl

Polish title:

Eksperymentalne i symulacyjne badania pracy układów termoelektrycznych w układach pompy ciepła oraz generatora elektryczności w stanach ustalonych i nieustalonych

Department of Power Engineering and Turbomachinery,
Faculty of Energy and Environmental Engineering,
Silesian University of Technology, Gliwice, July 2022

ACKNOWLEDGEMENTS

I wish to thank Professor Grzegorz Nowak for his scientific supervision of this dissertation. I am particularly grateful for his guidance in my scientific development, the fruitful cooperation in research and the discussions leading to new ideas and the feedback on my own. I appreciate the friendly atmosphere conducive to creativity and the support shown to me. I would also like to extend my thanks to the co-authors of the papers that make up this dissertation and to the staff and people associated with the Faculty of Energy and Environmental Engineering who have helped me even in the slightest and on various levels to complete this task.

CONTENTS

MONOTHEMATIC PUBLICATIONS

[A] **Ryszard Buchalik**, Grzegorz Nowak, Iwona Nowak, Mathematical model of a thermoelectric system based on steady- and rapid-state measurements, Applied Energy, Vol. 293:1-11, 2021, doi:10.1016/j.apenergy.2021.116943. **IF: 11.446; MNISW: 200**

[B] **Ryszard Buchalik**, Iwona Nowak, Krzysztof Rogoziński, Grzegorz Nowak, Detailed model of a thermoelectric generator performance, Journal of Energy Resources Technology – Transactions of the ASME, 2020, Vol. 142(2):1-8, doi:10.1115/1.4044367. **IF: 2.903; MNISW: 100**

[C] **Ryszard Buchalik**, Grzegorz Nowak, Iwona Nowak, Comparative analysis and optimization of one- and two-stage cooling systems with thermoelectric cells with respect to supercooling, Energy Conversion and Management, Vol. 259:115587, 2022, https://doi.org/10.1016/j.enconman.2022.115587. **IF: 11.533; MNISW: 200**

[D] **Ryszard Buchalik**, Grzegorz Nowak, Technical and economic analysis of a thermoelectric air conditioning system, Energy and Buildings, Vol. 268:112168, 2022, https://doi.org/10.1016/j.enbuild.2022.112168. **IF: 7.201; MNISW: 140**

[E] **Ryszard Buchalik**, Krzysztof Rogoziński, Grzegorz Nowak, The potential of thermoelectric energy harvesting in vehicles equipped with ICE, Combustion Engines, Vol. 4:70-74, 2019, doi:10.19206/CE-2019-411. **MNISW: 70**

[F] **Ryszard Buchalik**, Grzegorz Nowak, Krzysztof Rogoziński, Modelling the internal combustion engine waste heat recovery using thermoelectric modules, 34th International Conference on Efficiency, Cost, Optimization, Simulation and Environmental Impact of Energy Systems (ECOS 2021), Taormina, Sicily 28 June – 2 July 2021:1565-1576. **MNISW: 5**

The author's contributions to each of the papers mentioned above were as follows:

[A] Conceptualization, Methodology, Validation, Investigation, Resources, Data Curation, Writing – Original Draft; Author's contribution was equal to **75%**

[B] Conceptualization, Methodology, Validation, Investigation, Resources, Writing – Original Draft; Author's contribution was equal to **75%**

[C] Conceptualization, Methodology, Software, Validation, Investigation, Resources, Data Curation, Writing – Original Draft, Visualization; Author's contribution was equal to **80%**

[D] Conceptualization, Methodology, Software, Validation, Investigation, Resources, Data Curation, Writing – Original Draft, Visualization; Author's contribution was equal to **80%**

[E] Conceptualization, Methodology, Software, Validation, Investigation, Resources, Data Curation, Writing – Original Draft, Visualization; Author's contribution was equal to **80%**

[F] Conceptualization, Methodology, Software, Validation, Investigation, Resources, Data Curation, Writing – Original Draft, Visualization; Author's contribution was equal to **80%**

SUPPLEMENTARY PUBLICATIONS

[G] Iwona Nowak, **Ryszard Buchalik**, Grzegorz Nowak, Reconstruction of selected operating parameters of a thermoelectric device, Computer Assisted Methods in Engineering and Science, Vol. 26(1):35-46, 2019, doi:10.24423/cames.251. **MNISW: 70**

The author's contributions were as follows:

[G] Conceptualization (partially), Resources (partially); Author's contribution was equal to **20%**

SYMBOLS

LATIN

COP – coefficient of performance, -

EMF – electromotive force, V

$ETCC$ – economic total cooling capacity, W/USD

HTF – heat transfer coefficient, W/K

I – electric current, A

n – number of the module legs, $-$

P – power, W

$\dot{Q}$ – heat, W

T – temperature, K

Z – thermoelectric figure of merit, $1/K$

ZT – dimensionless thermoelectric figure of merit, -

GREEK

α – Seebeck coefficient, V/K

η – efficiency, $-$

λ – thermal conductivity, $W/(mK)$

π – Peltier coefficient, $\frac{W}{A}$

ρ – electrical resistivity, Ωm

SUBSCRIPTS

c – cold side of the TEG

el – electric

h – hot side of the TEG

Abbreviations

TEM – thermoelectric module

TEG – thermoelectric generator

TEC – thermoelectric cooler

I. INTRODUCTION

Increasing environmental pollution and the ongoing energy crisis are prompting mankind to seek new and develop already known energy conversion methods. One of them is use of thermoelectric phenomena for recovery of waste heat from various energy and technological processes, or for heat pumping. In the latter case no dangerous refrigeration agents are required. Therefore, intensive research has been observed in recent years on the possibility of using the phenomena occurring in thermoelectric modules [1, 2] and in systems and devices based on them.

1. Basics of thermoelectric phenomena

1.1 Concepts and historical outline

The essence of the phenomena used in thermoelectric devices is the mutual interaction and the relationship between the temperature field and the electric field [3]. They can be used for a bidirectional transformation between electricity and heat [4, 5]. On the one hand, it is possible to generate electricity due to the temperature gradient applied to the thermoelectric module and the heat flow resulting therefrom. On the other hand, the process of forced heat transport can be triggered by the supply of electric energy to the thermoelectric module (heat pump). Although these processes are manifestations of the same physical phenomenon, they can be regarded as opposite. The basis for the existence of thermoelectric phenomena is the Seebeck effect [3]. It was scientifically observed for the first time in the 18th century and it was described more extensively and explained in the 19th. The Seebeck effect consists in generating an electromotive force (EMF) in a circuit composed of two different types of conductors if their junctions are in different temperatures. The generated electric voltage is proportional to the difference between the temperatures of the junctions and the difference in the Seebeck coefficients of the two materials. The Seebeck coefficient is a material property resulting at the microscopic level from different binding energies of the elements carrying the electric charge in the atomic structure and involved in the flow of the current. Also important is the diffusion of charges resulting from a non-zero temperature and the change in its intensity with temperature. Together, these phenomena can lead to a change in the concentration of electric charges in the vicinity of the junction and thus to the formation of electric voltage. Thermoelectric devices most often use semiconductors due to their lower concentration of carriers of electric energy compared to conductors. As a result, the voltage related to the diffusion of charges through the contact is higher in them. Usually one semiconductor is p-type, whereas the other is n-type.

1.2 Using thermoelectric phenomena

One of the most common applications of the Seebeck effect is the temperature measurement using a thermocouple. In this case, the voltage generated in a circuit of two conductors (or semiconductors) with significantly different Seebeck coefficients is measured. One of the junctions is placed in the environment with the temperature being measured and the other – in the reference temperature. The voltage generated in the circuit is proportional to the difference between these temperatures. Ideally, the voltage measurement should be performed at zero

current to measure the electromotive force directly. In practice, however, it is realized when an electrical meter with a relatively high electrical resistance is incorporated into the circuit.

Another important application of thermoelectric phenomena, which is identical in terms of physical fundamentals, is the recovery of thermal energy, which involves converting some of the heat flowing through a thermoelectric module into electricity. In this case, an external electrical receiver with an electrical resistance similar to that of the thermoelectric module is connected to the junction. Since the voltage generated by a single thermoelectric couple is very small, thermoelectric modules consisting of multiple thermoelectric junctions connected in series or parallel (usually both types – mixed connection) are used in this type of application [6-9]. The electromotive force generated in this case is proportional to the temperature difference, the difference in Seebeck coefficients and the number of thermoelectric junctions electrically connected in series. Although the in-series electrical connection of thermoelectric couples inside the module increases the electromotive force, it also increases the (disadvantageous due to the decrease in the output voltage with increasing current) internal electrical resistance. The parallel connection, on the other hand, leads to a reduction in this resistance, thereby increasing the current output while keeping the generated electromotive force constant. In a thermoelectric module intended for energy generation one side of the module is kept at a high temperature by supplying heat (e.g. process waste heat), whereas the other side is kept at a low temperature by absorbing heat (e.g. cooling to ambient temperature). Example thermoelectric modules are shown in Fig. 1.

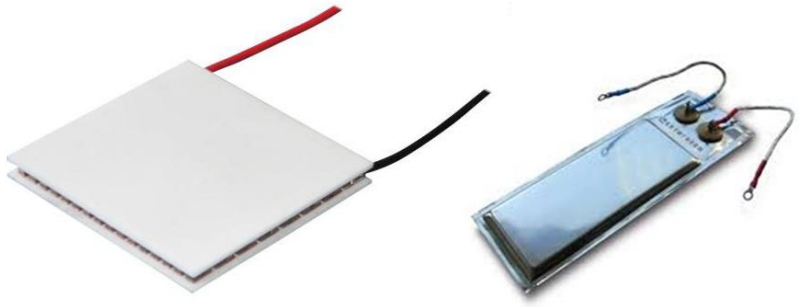

Fig. 1. Example thermoelectric modules

A thermoelectric module usually consists of legs placed between two parallel ceramic plates that form the housing. The legs are a number of small elements, usually with the shape of a rectangular prism, which are made of materials with useful thermoelectric properties. The heat usually flows through all the legs in parallel, while the current usually flows in series. A schematic diagram of an example thermoelectric module is shown in Fig. 2.

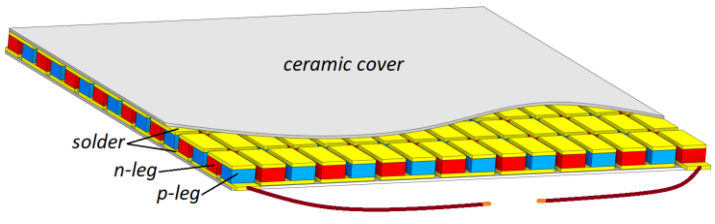

Fig. 2. Schematic diagram of a thermoelectric module; legs made of two materials are visible with their connections (solders), housing and connecting wires

The cross-sectional area of the current flow path should be large enough to ensure low electrical resistance and a significant flow of current. Low resistance makes it possible to obtain a higher current and a bigger electric power output at a given voltage level at the terminals, i.e. in specific temperature conditions of the module operation. Due to that it is possible to power an external electrical receiver. On the other hand, a larger total cross-sectional area of the legs results in a greater amount of heat conducted by the module and has a negative effect on the temperature gradient for a heat source with a limited output (whose temperature decreases with the amount of collected heat). The amount of heat conducted through the module can also affects its efficiency. Another element shaping the module external characteristics is the height of the legs. A rise in the leg height reduces heat conduction through the module (longer heat conduction path), but causes an unfavourable increase in the module electrical resistance by lengthening the electrical path. Thus, considering the entirety of the phenomena signalled above, the selection of the module geometry has to be optimized. Non-standard configurations where the leg is not a rectangular prism are possible [10-17].

The Seebeck effect can be expressed by the relationship between the generated electromotive force for a single junction pair and the difference between the temperatures of the junctions. The proportionality factor between the two quantities is the Seebeck coefficient, which is the difference between the Seebeck coefficients of the two materials:

$$EMF = (\alpha_1 - \alpha_2)(T_H - T_L) = \alpha \Delta T \quad (1)$$

In thermoelectric modules, in addition to the Seebeck effect and the voltage generation related to it (consequently – the possible flow of electric current), an opposite effect also occurs. The current flow through the thermoelectric junction (or module) causes heat to be emitted or absorbed at the junction – the Peltier effect. Its existence follows directly from the existence of the Seebeck effect and the energy conservation principle [3]. The amount of the absorbed/emitted heat depends on the value of the Peltier coefficient, which is related to the Seebeck coefficient (the difference between the Seebeck coefficients of the two materials), the temperature of the junction and the value of the current in the circuit:

$$\dot{Q}_{pelt} = \Pi I = \alpha T I \quad (2)$$

When the thermoelectric module operates in the power generation mode, the Peltier effect increases the heat flow through the module with a rise in current, leading, in the case of a real non-ideal heat source or in the presence of thermal resistances in the path, to a reduction in the effective temperature difference between the thermoelectric junctions and a weakening of the generated EMF [18]. This, in turn, translates into a lower power output. On the other hand, the described Peltier effect can be used to force a heat flow by forcing a current flow through the module (e.g. using an external power supply), thus creating a heat pump. Here, however, the opposite phenomenon, i.e. the Seebeck effect, also occurs, which will generate an electric voltage with the direction opposite to the applied external supply voltage. As a result, the Seebeck voltage will counteract the current forcing and can limit the heat transport through the module. Keeping a specific level of the heat transport will therefore involve the need to increase the power

supply with a rise in the temperature gradient forced by this process. The heat absorbed/emitted at a thermoelectric junction is proportional to the current flowing through the junction and the junction temperature (2). In any thermoelectric module the Seebeck effect and the Peltier effect always occur simultaneously (except for an open-circuit condition); one of them is usually a useful phenomenon whereas the other is undesirable. The simultaneous occurrence of the two effects follows from (1) and (2) and is an immanent feature of thermoelectric systems.

Thermoelectric legs usually have the structure of a rectangular prism with identical dimensions of the two materials forming a couple. However, it may happen that for significantly different physical properties of the thermoelectric couple materials, the p and n legs will have different dimensions [19, 20]. Also, the cross-sectional area of a single leg may vary along its length [10, 21-24]. In some applications, especially involving the flow of a medium being a heat source or a heat sink in a pipe, annular modules are used [25-27], also in a multi-stage configuration [28].

1.3 Energy conversion efficiency

Each thermoelectric device can, in principle, operate as both an electricity generator and a heat pump. Alternate operation is also possible [29]. In practice, the working parameters of the modules (including the allowable temperature range) vary depending on the intended use [30]. This is the effect of the selected thermoelectric materials, the geometry of the module and of the legs, the used binder, etc. The module output parameters are mainly determined by the thermoelectric materials used to make thermoelectric legs. A single quantity describing the properties of a thermoelectric material in terms of its use in thermoelectric modules is the thermoelectric figure of merit (Z) [31]. The dimensionless product of Z and absolute temperature, referred to as the dimensionless figure of merit (ZT), is frequently used to determine the quality of the energy conversion process in a thermoelectric module made of a given material at a given temperature (3). The Z and ZT indices can also be determined in a similar way for the whole module [31]. The higher the ZT value, the more efficient the material/module, and the better the material is for thermoelectric applications at a set temperature range.

$$ZT = \frac{\alpha^2}{\rho\lambda}T \tag{3}$$

The figure of merit has an effect on the indicators used to quantify the operating efficiency of thermoelectric modules, i.e. the efficiency of electricity generation in the generator-mode operation or the COP for heat pump-mode operation. It also has an impact on the ratio between the achieved thermal/electric power and the size/volume of the material/module, i.e. the number of legs.

It follows from the figure of merit that a good thermoelectric material should be characterized by a high Seebeck coefficient and low values of electrical resistance and thermal conductivity. Hypothetically, an infinitely small electrical resistance or an infinitely small thermal conductivity (and thus an infinitely high figure of merit) would result in a thermoelectric system efficiency at the level of the Carnot cycle, as would an infinitely high Seebeck coefficient. Detailed relationships between efficiency, the COP, and the figure of merit and other indicators are shown in [32].

The science of thermoelectric materials continues to develop rapidly, with the visible result being the continuous development of new thermoelectric materials with improved performance, as measured by the aforementioned figure of merit (ZT) and temperature resistance [5]. Along with this, there is ongoing development in the field of finding applications for thermoelectric modules [1]. However, it is important to bear in mind the distinction between materials intended for high-end scientific applications and those that can be relatively cheaply produced on a large scale for use in consumer equipment.

The efficiency of the energy conversion process during the operation in the mode of electricity generation is expressed as:

$$\eta = \frac{P_{el}}{\dot{Q}_h} \tag{4}$$

and in the heat pump mode as:

$$COP_{c,h} = \frac{\dot{Q}_{c,h}}{P_{el}} \tag{5}$$

In order to improve the COP or the energy generation efficiency, selected parameters of the whole module, as well as of the material (intensive and extensive parameters), should meet the following conditions:

- the module electrical resistance should be as low as possible, as it is a source of losses in the supplied/generated electricity due to the release of Joule heat (heating of the material due to the presence of electrical resistance and the current flow),
- thermal conductivity should be as low as possible, as it affects the heat flux transferred through the module and not used in any way through thermoelectric phenomena (generator), or causes a heat flow in the undesirable direction opposite to the pumping of heat (cooler) [33-35],
- the Seebeck coefficient for the module should be as high as possible to enhance the phenomena of heat absorption and release for a single junction for small currents (heat pump) or the useful voltage at a set temperature (generator).

At the microscopic level, the phenomena of electrical resistance and thermal resistance are interrelated and have to do with the freedom of electrons and the form of the material crystal lattice [34]. Usually, a change in one of the parameters causes the same direction of change in the value of the other (e.g. an increase in electrical conductivity causes an increase in thermal conductivity), hence the difficulty in developing better thermoelectric materials because, generalizing, one of these changes has, when it comes to thermoelectric applications, a positive effect and the other a negative one. By creating suitable semiconductor materials, it is possible to increase the value of the ZT parameter.

Behind the Seebeck coefficient of a module is the difference between the Seebeck coefficients of the thermoelectric pair (cf. (1)) of which the module is made multiplied by the number of their electrical in-series connections (assuming the same temperature of all junctions on each side of

the module). It is thus the ratio between the electromotive force generated by the module and the difference in the temperatures of thermoelectric junctions on both sides of the module. If the Seebeck coefficient is relatively high, the current can then be relatively small. As a result, little Joule heat is released (the amount of this heat is proportional to the square of the electric current). Joule heat is a disadvantageous phenomenon because it reduces the power of the produced electrical energy for a module operating as a generator or heats up the whole system including the cooled space (also increases the amount of heat that has to be carried away by an external heat sink) when operating as a heat pump. The Peltier heat for the junction (for a set current value) and the EMF generated due to the Seebeck effect are linearly dependent on temperature (assuming a constant value of α and the temperature of the other side of the module).

An additional thermoelectric phenomenon is the Thomson effect consisting in Seebeck and Peltier phenomena "distributed" along the length of the thermoelectric material if the Seebeck coefficient changes significantly with temperature. In such a situation its value can be different in different cross-sections of the legs, changing gradually, which results in a release or absorption of heat at the current flow and generation of voltage in a manner distributed over the volume [36, 37].

2. Heat transfer problems in thermoelectric systems

In practical applications, a thermoelectric system consists of the previously discussed module, or modules connected to each other, and cooperating heat exchangers [38-40]. Usually, the selection of the module dimensions is based not only on an analysis of thermodynamic processes. The capacity for power generation, the practical aspects of operation and the characteristics of cooperating heat sources and heat exchangers are also taken into account [7]. Exchangers are elements that mediate the heat exchange between the thermoelectric module and the environment (source/sink). The heat exchange process can take place by means of heat conduction and free or forced convection [41]. Therefore, the operating parameters of the thermoelectric system depend not only on the characteristics of the module itself (including the characteristics of the thermoelectric material and the geometry of the legs [11]), but also on the parameters of the heat exchangers and the quality of the thermal contact at the interface between these elements [42, 43]. Heat exchangers must be used because, for typical configurations of thermoelectric modules, their external surface area is usually too small to ensure proper heat transfer due to convection in the case of gases (whether free or forced, e.g. directly through the air or exhaust gases of a combustion engine). The heat transfer coefficient value is in this case too low, and the heat transfer surface needs to be developed. From a thermodynamic point of view, the answer regarding the dimensions and efficiency of the exchangers is obvious – they should be as large as possible. However, when economic criteria are taken into account in the selection of exchangers, the task is not so easy to solve. Practical aspects related to the size, weight or conditions of the system installation are also a limitation.

In the case of a thermoelectric module, heat transfer due to both convection and radiation can occur in the spaces between the legs, which will modify the module performance characteristics [44, 45]. Usually, however, this influence is negligibly small and therefore omitted in analyses.

Total resistance in the heat transfer between the thermoelectric junction and the final cooled/heating medium consists of:

- thermal resistance on the boundary of the medium (environment) and the exchanger,
- conduction resistance in the exchanger material,
- contact thermal resistance between the exchanger and the module housing,
- thermal conduction resistance of the module housing material (ceramics usually),
- thermal resistance of electrical contacts.

Between thermoelectric junctions heat is conducted by thermoelectric legs.

An example of the effect of thermal resistance on the path from the heat source to the thermoelectric junction (in this case a thermal grease between TEM housing and the heat exchangers) for the minimum achievable temperature as a function of the leg height for a thermoelectric cooler is shown in Fig. 3. The figure includes the situation with no thermal resistance (actually the resistance is non-zero, but negligibly small $r = 1\mu Km^2/W$) and with a reasonable resistance value of $r = 100\mu Km^2/W$.

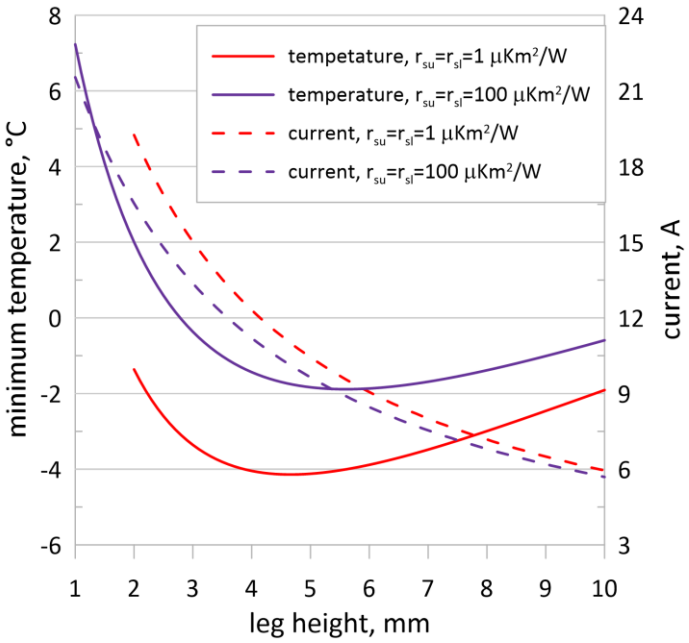

Fig. 3. Impact of the leg height on the minimum cooling temperature and the electric current corresponding to it for the case with thermal resistance taken into account ($100\mu Km^2$) and without thermal resistance ($1\mu Km^2$)

In order to improve the efficiency of the module operation by minimizing the thermal resistance between the thermoelectric module and the heat reservoir, in addition to the conventional solution of increasing the active surface of the heat exchanger, a phase change material (PCM) can also be used to utilize the phase change heat [36, 46]. This makes it possible to substantially reduce the size of the exchanger and increase the heat transfer efficiency.

Because the efficiency of the heat-to-electricity conversion in the generator-mode operation depends on the temperature difference between the hot and the cold heat source, it makes sense

to increase the hot source temperature while maintaining the temperature of the heat discharge (ambient temperature). Unfortunately, the temperature resistance of the modules becomes a significant problem here. For the most popular commercial models, reaching temperatures of 150-200°C will result in the module destruction. Models with the temperature resistance of 300-400°C are frequently referred to as suitable for high-temperature operation and are characterized by a much higher price and operating problems. Modules with a declared operating temperature of up to 600°C can also be found on the market, but their price is disproportionate to the results.

An important issue affecting the energy conversion efficiency is the level of heat losses. Care must therefore be taken to ensure that heat exchangers are adequately insulated, especially if their temperature differs significantly from the ambient temperature. In the case of a refrigerator, for example, good insulation of the cooled space ensures a lower unit cost of operation, less heat to be dissipated to the environment and the possibility of achieving a lower temperature. In the case of a generator, where the cold heat source/sink is usually the environment or a reservoir with a temperature close to ambient, heat losses from the hot heat exchanger have a negative impact on the system efficiency and power output [47]. This can be the result of either a drop in the temperature of this source and a consequent decrease in the efficiency of the thermoelectric energy conversion process, or the fact that heat is lost outside the thermoelectric module to the surroundings.

During the thermoelectric module operation in the mode of electricity generation, an important issue is the selection of the value of electrical resistance of the power receiver. In the steady state, there are resistance values corresponding to operation with maximum electric power or with maximum efficiency [3, 48]. However, the two maxima usually do not occur simultaneously and operation at maximum efficiency means a power output lower than maximum. During the operation as a generator, the change in the temperature of the junctions caused by external heat will cause (with the power receiver connected) a change in the current flowing in the circuit, and this will reciprocally affect the temperature of the thermoelectric junctions through Joule and Peltier effects when using a heat source with a non-constant temperature or at the occurrence of thermal resistance between the source and the thermoelectric junction [47].

A similar situation occurs during the selection of the supply current (and the related supply power) of a thermoelectric heat pump. In such a case it is usually possible to distinguish the working point with the maximum efficiency and maximum cooling/heating power depending on temperatures and heat flow characteristics. Like above, the former usually corresponds to a lower supply power.

2.1 Module-exchanger contact layer

The heat transfer between the heat exchanger and the module is most often realized by means of conduction through physical contact between the two elements (radiation is also possible). In such a situation, the problem of ensuring proper thermal contact, i.e. minimizing thermal resistance on the interface, requires attention [49]. The quality of the contact surface, the surface clamping force and the thermal grease improving the contact quality are of key importance here [43]. The described problem remains even if the intermediary in the heat transfer is a heat pipe or another system using a PCM. In this case, there are several thermal resistance components

with an aggregate effect occurring in an in-series configuration to be dealt with [50]. The existence of thermal resistance in contact layers between the thermoelectric module and the rest of the system deteriorates the system performance [51]. The problem is similar to the case of cooling electronic components requiring a heat sink, of which the PC CPU is an example. Minimizing thermal resistance on the system-heat sink interface is then necessary to ensure proper cooling. In thermoelectric modules, the occurrence of thermal resistance reduces the effective temperature difference between the module junctions in the case of the TEG and increases it in the case of the TEC, adversely affecting the module operation in both cases. For this reason, the module surfaces should have the best possible thermal contact with the mediums they exchange heat with. Above all, unnecessary layers of thermal insulation should be avoided. The effective temperature difference is understood as the temperature difference between the thermoelectric junctions and not the usually given temperature difference between the heat sources or the exchangers in contact with the module. In the case of thermoelectric modules, thermal resistance is usually reduced using thermal grease. Some modules are factory-coated with a layer of material (e.g. copper or graphite grease) that acts as thermal grease. The thermal resistance at the surface of contact between the materials where the grease has been applied is a function of two essential groups of parameters. One includes the quantities that characterize the thermal paste itself, mainly its thermal conductivity and mechanical parameters, such as relation between stress, strain, velocity occurring in it. This nature is the effect of the properties of the paste, which for small stresses behaves like a solid body, but at a slight increase in their value acts more like a fluid. The other group includes mechanical parameters of the interface between the two materials. Among the most important of these are the irregularities in the form of both fine burrs and roughness, as well as the non-parallelism of the contacting surfaces, their stiffness and the clamping force. The precision of the paste application, i.e. the thickness of the paste layer and the uniformity of its spreading, is important. It should be noted that a change in the operating conditions of a given interface relative to the assembly conditions can result in a change in its properties. This mainly concerns a change in temperature and in the clamping force. Typically, a reduction in temperature can result in reduced adhesion and hardening of the paste, while an increase in temperature can result in accelerated drying, degassing of some components and increased fluidity (paste oozing from the interface).

The thermal resistance of the thermal grease layer changes also with time [52-54]. This phenomenon can be enhanced due to high temperature and cyclic operation. In most cases, the paste properties are degraded, which involves an increase in thermal resistance. The rate of this process depends on the history of changes in the clamping force, temperature and the paste moisture content. The main problem is the thermal paste drying out, which means that the paste loses the desired physical properties. In certain conditions, gentle movements resulting from thermal deformations arising during heating/cooling cycles can assist in the thermal grease spreading, which may have a positive effect, especially in the initial period after the assembly. Another phenomenon that deteriorates the heat transfer is the oxidation of the boundary layers of the heat exchanger material (metal), resulting in the formation of a layer of oxides with poor thermal conductivity. The same phenomena can also cause the deterioration of the module internal components, ranging from the oxidation of their surfaces to the formation of cracks, also due to thermal stresses. This can take place both in the thermoelectric material itself and in the

joints connecting the legs. In order to protect the inside of the module from mechanical damage, chemical damage (corrosion) or invasion by foreign bodies, silicone filling is often used between the surfaces of the housing. Modules enclosed in a sealed metal housing can also be found (cf. Fig. 1). In addition, cyclic thermal expansion phenomena can enhance the processes of the module internal structure disintegration related to different values of the linear expansion coefficient of the thermoelectric material, the joints and the housing. This leads to an increase in the contact resistance between the thermoelectric junctions and the heat exchanger, or damage to the internal structure of the module, thus worsening its overall performance.

Fig. 3 and Fig. 4 show the effect of taking account of the contact layer thermal resistance on the start-up of a thermoelectric cooler and its minimum steady-state temperature. It can be seen that the lack of contact resistance lowers the achievable cooling temperature, which occurs at a smaller current value.

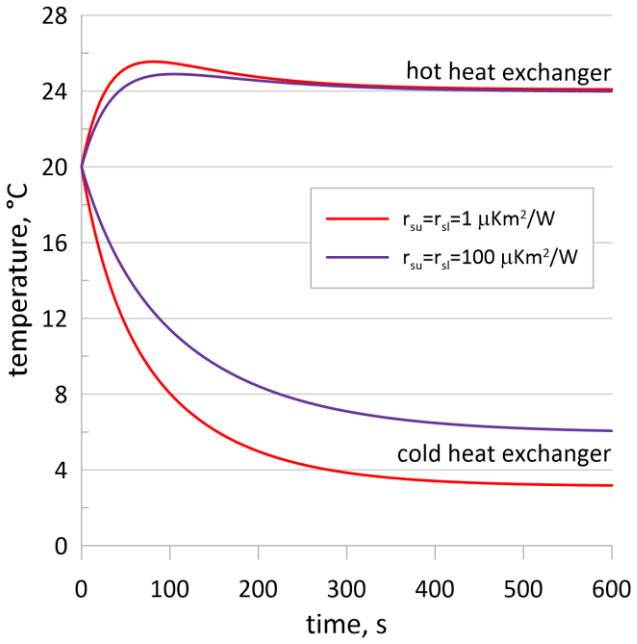

Fig. 3. Example of the effect of the presence of thermal contact resistance between the module and the heat exchangers on their temperatures during the start-up process of a cooler

The change in the temperature of the system components, combined with their thermal expansion, also affects the clamping force of the exchangers to the module. Depending on the applied method of the system assembly, this change can manifest itself in an increase or decrease in the clamping force with a rise in the operating temperature. The clamping force increases due to the expansion of the elements which together with the module form a compact structure with an in-series arrangement. On the other hand, it decreases due to thermal deformation of the clamping elements, e.g. an increase in the temperature of the fixing screws. Typically, one of these effects predominates significantly, leading to considerable variations in the clamping force during operation with variable temperature.

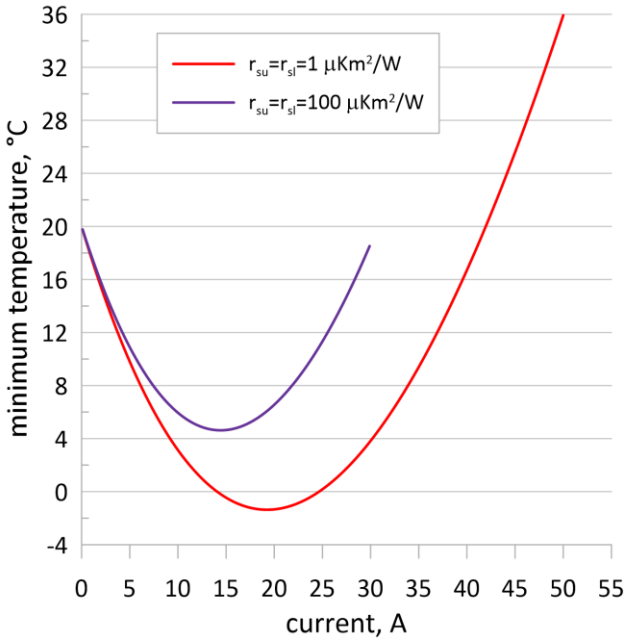

Fig. 4. Effect of the current flowing in the circuit on the steady-state cooling temperature

The temperature of the fixing elements usually changes much more slowly than the temperature of the heat exchangers and the module, which further complicates the course of changes in the clamping force over time. At relatively high operating temperatures and during long-term operation, the material of the fixing elements may creep leading in consequence to stress relaxation. Considering the above-mentioned phenomena, it is desirable to use relatively elastic elements in the fixing system to minimize the clamping force variations depending on momentary temperature values and possible external forces. Another possibility is to use an active or passive actuator (pneumatic/hydraulic with constant pressure or a mechanical servomechanism that is actively regulated based on signals from a strain gauge). Such solutions, however, are only observed in research applications. A very important element of correct operation is to ensure the module load uniformity during assembly and during the system operation. Exceeding the load at any point, especially in the corner area, can result in the module destruction (also in a break in the electrical path completely invisible from the outside). This is where a very significant problem appears which is related to the accuracy of the thermoelectric module manufacturing (deviations in the leg height). Insufficient accuracy of the height of the legs causes a non-uniform distribution of stresses in the legs and housing. The applied clamping force can of course be very precisely controlled, but its distribution between the legs is a quantity that depends on the accuracy of the system components geometry. It is assumed to be uniform, and a deviation from this assumption can lead to the destructive stress value being locally exceeded.

3. Example applications and practical aspects of the use of thermoelectric modules

Currently, thermoelectric modules are used in niche or experimental systems for electricity generation or cooling [1, 55]. One of their few common applications is in a portable refrigerator, often powered by the car electrical system.

Possible applications of the thermoelectric phenomenon include electricity generation using the heat of radioactive disintegration (e.g. powering space probes) [56] or the heat of stellar radiation [57]. Portable fuel-fired micro-generators of electricity can also be found on the market, as well as exhaust waste heat recovery device built into the exhaust system of an internal combustion engine [43, 58-64]. In addition, waste heat can also be recovered from hot gases, not necessarily exhaust gases, resulting from technological processes [65, 66] or in CHP systems [67]. It is also possible to use deliberately stored thermal energy [68]. The thermal energy released by the human body can be used to power wearable handheld gadgets [69, 70].

A promising idea is to combine thermoelectric modules with photovoltaic modules (PV-TEG), which can be done in several ways [71-76]. Modules of both types can form a series-combined system, where incident radiation causes the PV module to produce electricity and heats it. Since the increase in the PV module temperature negatively affects the efficiency of the energy transformation taking place in it, attempts are made to use the accumulated heat as a heat source to power the TEG module. The other side of the module is cooled to a temperature close to ambient. Different solutions are also possible, where part of the radiation, with an appropriately selected wavelength, is directed to the PV module, ensuring that its efficiency is as high as possible, and the rest of the radiation heats the hot end of the TEG module.

It is also possible to combine thermoelectric modules with fuel cell systems, where waste heat is released during operation [37]. Moreover, the heat generated during the production of useful cool by the thermoelectric module can be used effectively [77], for example to heat tap water [78].

Thermoelectric modules operating in the heat pump mode can find application in air-conditioning systems. They can also be part of a nearly zero-emission building system [79-81], or they can be used for space radiation cooling [82, 83]. If used in thermoelectric air-conditioning systems in vehicles [84, 85], their main advantages are rapid response, small size, light weight, reversible operation (heating) [86] and the possibility of using heat/cool not only to provide comfort to passengers, but also to ensure thermal management of vehicle systems, such as electric batteries [87]. The idea of using a thermoelectric generator in combination with an internal combustion engine to power a car air-conditioning system is shown in [88].

An interesting concept of using thermoelectric modules is their application in medical equipment, where the efficiency of energy conversion does not play a primary role. The application of thermoelectric modules for sterilization and disinfection of air using elevated temperature which is then cooled to a temperature appropriate for the medical process is presented in [89]. Papers [90, 91] present the use of thermoelectric systems in neonatal incubators and in medical procedures that require accurate and flexible temperature control through interchangeable heating and cooling. Cases can also be found of using TECs for direct cooling of electronic systems [92-95].

The main disadvantage of modules operating based on thermoelectric phenomena is the low efficiency of the process of electrical-to-thermal energy conversion [96, 97]. This applies to both heat pumps and electricity generators. On the one hand, for most refrigeration or energy generation applications there are much more efficient processes based on thermodynamic cycle

of the working medium circulating in the system (compressor-based); on the other hand, thermoelectric devices are characterized by noiseless operation, small size and weight, lack of moving parts, ease of scaling (down to a microscopic size [98]) and maintenance-free operation. In addition, refrigeration systems based on thermoelectric modules can operate with no intermediate mediums (usually harmful or hazardous refrigerants).

Wherever the efficiency of energy conversion is not paramount, thermoelectric modules may find many applications in the future, especially in small systems. There, the above-mentioned advantages of thermoelectric systems make them potentially unbeatable.

4. Multi-stage thermoelectric modules

Thermoelectric module systems can have a multi-stage design for both a generator [99, 100] and a heat pump [101-105]. Such a system consists of multiple thermoelectric modules connected thermally in series arranged in a sandwich configuration. However, in each of the cases this type of configuration is used for a different reason. It is less common in energy generation systems. The rationale for its use is that some thermoelectric materials may have desirable (or non-destructive) operating parameters (e.g. figure of merit) only over a relatively narrow temperature range compared to the entire operating range of the system, from the heat source to the heat sink [12, 30]. The successive modules are then thermally connected in series, and in the optimal operating state there is a temperature difference on each of them covering a narrow range of the total range of the temperature difference of the sources. However, a practical implementation of such a system requires stable and predictable heat sources that will not cause too frequent accidental exceedances of the optimal temperature or exceed the allowable temperature of individual modules of the cascade. The process of optimizing the operation of multi-stage systems both in terms of their design and operation is in general more complicated than for one-stage systems [106, 107].

A cascade system of multiple modules connected in series (multi-stage system) in the case of a heat pump/cooler makes it possible, in some configurations, to achieve cooling temperatures unachievable in a one-stage system [108, 109]. Compared to a one-stage configuration, in a multi-stage system the maximum thermal power that can be “pumped” through the system decreases significantly with each added stage. The efficiency of the whole process also tends to decrease substantially. This is mainly due to Joule heat, which is released in each module. Part of this heat emitted at the cold end of the module, located closer to the cooled space, must be “transferred” through subsequent modules of the cascade. Too many modules (more than required to achieve the set temperature) can also result in a deterioration of performance (achieved minimum temperature) as a result of greater total thermal resistance and consequently a reduction in the efficiency of the entire process. Such systems are used when it is necessary to achieve a very low temperature with a limited heat flux required to keep it. Also, successive modules are usually characterized by different parameters (and dimensions) due to the changing the heat flowing through each stage, as well as (in the case of parameters varying with temperature) their operating temperature. It should be noted that the design of such a system requires multi-objective optimization, due to the interaction of modules with each other. The hot side of one module contacts the cold side of the next, and so on. Thus, for each of the modules of the cascade, for set operating temperatures, there is an optimal value of the supply current, ensuring

maximization of cooling power. Each module also operates in a different temperature, which can result in a different value of the figure of merit and consequently affect the selection of the module material and/or characteristics.

5. Transient TEG/TEC operation

In transient operating conditions it is possible to observe phenomena and processes that do not occur in the steady state. They involve, among other things, the possibility of momentarily achieving operating parameters beyond the range of values achievable in the steady state. Transient-state conditions can also result from the variability of the heat source parameters and the possible continuous tuning of the thermoelectric system to the operation of the source [110-116]. An example of transient conditions is also the start-up of a "cold" system and its reaching the steady state [117-120]. Another manifestation of a transient state is the quasi-steady-state pulsed operation at constant ambient conditions, and the variations in the operation are mainly due to the current changes [121-126].

In the case of cooling operation, it is possible to induce the so-called supercooling phenomenon [105]. Its essence is to achieve a momentary lower temperature of the cooled space than the minimum achievable in the steady state. This happens as a result of the thermal inertia (thermal capacity) of the heat reservoirs cooperating with the thermoelectric module. In the steady state the temperature of each component in the system is independent of its thermal capacity; it depends only on the resulting heats and thermal resistances. Taking advantage of the relatively large thermal capacity of some elements of the system compared to the others, at appropriate initial thermal conditions, it is possible for example to achieve a significant temperature drop on the system cooled side compared to the steady-state minimum. Moreover, this phenomenon is stronger in multi-stage systems, especially if additional heat reservoirs are introduced between modules connected thermally in series.

Supercooling can only occur (or be enhanced) at certain power supply conditions of the modules. In most cases, reaching the minimum temperature usually requires power supply using current pulses with complex shapes [127-130]. A period of intensive cooling and reaching the minimum (supercooling) temperature is followed by a recovery period, where the temperature of the system rises strongly an then returns the heat accumulated throughout the system to the environment [126, 131]. If the spatial distribution of the temperature field in the cooled reservoir in contact with the thermoelectric module is taken into account, the level of supercooling that can be achieved depends on the distance from the module [132]. The idea of supercooling is schematically illustrated in Fig. 5 for a one-stage system, for which the thermal capacity of the hot-side reservoir (the heat sink giving up heat to the environment) is much larger than the thermal capacity of the cooled space. In the first phase, when the current is constant, the temperature of the cooled reservoir has a value higher than the steady-state minimum. Then follows a phase during which the current increases. Intensive cooling of the cooled space is observed at that time, and its temperature decreases rapidly as a result of the relatively small thermal capacity. Simultaneously, the heat sink giving up heat to the environment is heated up. After a while, the heat sink temperature is so high that the conduction of heat through the module prevents a further drop in the temperature of the cooled reservoir. At this stage, the total thermal energy accumulated in the system is much higher than in the initial phase.

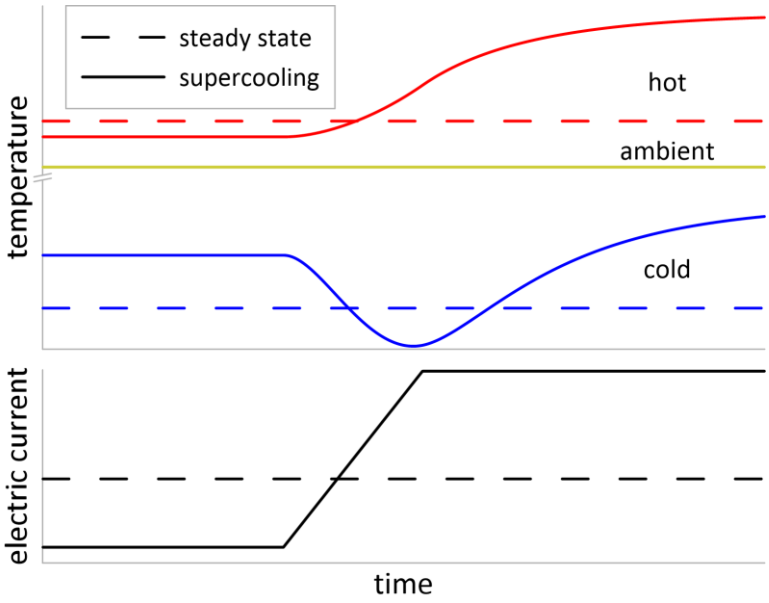

Fig. 5. The idea of supercooling: temperatures of the heat reservoirs on both sides of the module and the current in the module circuit; the case of the minimum temperature achievable in the steady state (dashed line), the case of reaching the minimum supercooling temperature (solid line)

A phenomenon analogous to supercooling can also be distinguished in generator systems [133], but it is of less practical importance. It consists in regulating the heat absorbed by the module to raise the temperature of the hot heat reservoir (and/or lower the temperature of the cold one) contacting the module. This can be achieved by regulating the current in the module circuit, i.e. changing the electrical resistance of the connected receiver of power. The module transfers the least heat for zero current (omitting negative values, for which it is necessary to supply energy from the outside – heat pump mode). For this reason, a temporary opening of the electrical circuit can increase the temperature difference between the module junctions due to a smaller heat flow through the module. Closing the circuit will then cause the voltage on the external power receiver to rise to a level that exceeds the steady-state value. Appropriate control of the current makes it possible to momentarily obtain the maximum power higher than the steady-state level. This is due to the accumulation of thermal energy and consequently to the increase in temperature of hot heat exchanger. This is only valid for the heat source with a limited output or with additional thermal resistance. Such a situation may be desirable in the case of momentary demand for power higher than possible to provide in the steady state.

The described transient phenomena, both for heat pumping and electricity generation, are based on the possibility of inducing changes in the heat flow through the module cooperating with the system capacitive components (heat reservoirs). In the case of multi-stage systems, a change in the current in one module has an effect on the distribution of heat fluxes in the system and on the temperature distribution, changing the operating conditions of the other modules. This, in turn, will cause a change in the optimal current in the circuits of individual modules.

6. Thermoelectric module durability and reliability

Most publications commonly cite the argument that thermoelectric modules have a low failure rate and a high mean time between failures (MTBF), mainly due to the lack of moving parts, as well as the absence of liquid working mediums. However, as indicated by own and yet partially unpublished studies, relatively frequent occurrences of the module failure have been observed. A few dozen percent of the tested modules intended for operation as a generator for relatively high hot heat source temperatures (>300°C) were damaged during the tests, with a total operating time of much less than a hundred hours. It should be noted that in no case were the allowable operating conditions, in this case the temperature of the hot heat source and the value and uniformity of the clamping force distribution, exceeded during assembly process and testing. The damage usually occurred as a direct result of the heating/cooling cycle. In some cases, the electrical path was completely broken, resulting in zero voltage at the terminals and their mutual galvanic isolation. In others, the internal electrical resistance increased significantly, while the electromotive force remained almost unchanged for a given temperature difference (the Seebeck coefficient of the module was preserved). The increase in electrical resistance ranged from a few dozen percent to levels a few dozen times higher. This may indicate a failure (complete or partial loss of electrical conductivity) of parts of the electrical paths at a series-parallel configuration of internal electrical connections.

7. Experimental studies

The parameters of thermoelectric modules can be determined experimentally using various methods of measurement and data analysis. The measurements can be supported by numerical models or used for mutual tuning of the models [18, 116]. Using an appropriately selected experimental method makes it possible to determine the module sought parameters while minimizing the number of required measurements. Basic measurements and analyses are usually performed at a constant temperature in a selected operation point of the system or at a constant heat flux [134]. There are also methods based on a dynamic change in the module operating conditions [135] and measurements conducted under such a condition [136]. Paper [137] shows the differences in the values of material parameters determined by means of different measurement methods. The subject of the analysis can be pure material properties [34], as well as effective values of the module parameters from the point of view of the module external characteristics [4, 138].

Analysing the datasheets made available by module manufacturers/suppliers, it was noted that they usually failed to provide all factual information. First of all, the testing parameters, such as the clamping force and the type of the thermal grease, for which the selected parameters were obtained, are unclear. The heat flux is often given, but the conditions to which this value applies are not specified – Peltier heat is not considered. Measurements indicated a significant discrepancy in actual and datasheet parameters. Also, the differences between the indicators describing different items of brand-new modules of the same model and of the same series (excluding obviously defective pieces) reached a few dozen percent, with 10-15% being common.

Therefore it is necessary to carry out own research until generally accepted procedures for testing thermoelectric modules and relevant standards are developed and introduced. The constructed test stand and a schematic diagram of its cross-section are shown in Fig. 6.

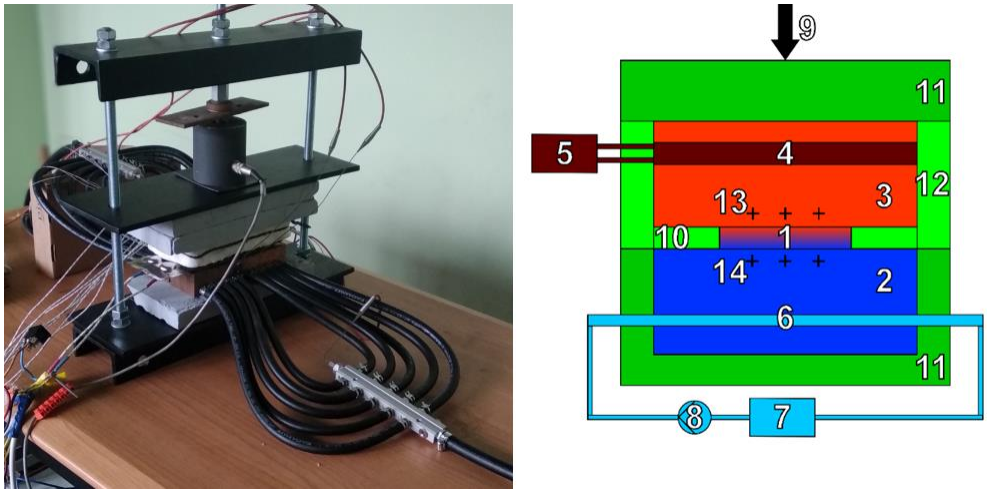

Fig. 6. Photo and schematic diagram of the test stand 1. TEG/TEC, 2. Lower block, 3. Upper block, 4. Electric heater, 5. Power supply/receiver and power measurement, 6. Cooling channels, 7. Radiator, 8. Water pump, 9. Measured force, 10. Internal soft thermal insulation, 11. Bottom hard insulation, 12. Middle soft insulation, 13, Hot side thermocouples and thermoresistive thermometer, 14. Cold side thermocouples and thermoresistive thermometer

8. Aim and scope of work

Many works, both past and present, address the issue of thermoelectricity, as evidenced by the number of available publications in this field. Some of them focus on materials and solid-state physics, while others address the development and optimization of the thermoelectric module geometry and dimensions, the leg geometry. The last category comprises analyses of complex thermoelectric systems that take account of the three-dimensional character of the heat flow in the entire system [2], as well as studies that evaluate the sensibility of using such systems and their economic evaluation [64]. Based on the cited information and the conducted literature review, it is possible to see significant potential for the development of thermoelectricity as a field of knowledge, both from a scientific and engineering perspective, and room for further advancement in research in this area.

The main subject of the research presented in this dissertation is the analysis of the operation of systems equipped with thermoelectric modules. This concerns systems operating to generate electricity, as well as in the heat pump mode. Because it was observed that some information was missing from the available scientific literature, and considering the areas still requiring in-depth analysis and the concepts not yet analysed, research was undertaken to supplement and expand knowledge in this area. Many works on thermoelectricity ignore the occurrence of the thermal resistance to the heat flow between heat exchangers and the thermoelectric junction, assuming the temperatures of the exchangers to be the temperatures of the junctions. This leads to a simplification of the computational model and, consequently, to inaccuracies in estimating the actual operating indicators of such a system. The works that take this phenomenon into account deal with selected special cases and aspects of the system operation.

The aim of the research was to develop simulation tools and experimental methods enabling comprehensive evaluation of thermoelectric modules and operation, in steady-state and transient conditions, of systems equipped with thermoelectric modules. This was achieved by:

- development and construction of a fully computerized test stand intended for testing thermoelectric systems,
- development of a method of rapid-state measurements to evaluate thermal contact resistance and basic parameters of modules,
- development of a model of a thermoelectric system taking account of thermal resistance and thermal capacity of the system components,
- development of a method of evaluating contact thermal resistance at a temperature close to ambient,
- development of software modelling steady- and transient-state operation of systems with thermoelectric modules,
- development of numerical procedures and experimental testing of one- and two-stage thermoelectric systems,
- numerical simulations of waste heat recovery and cooling systems in the exhaust system of an internal combustion engine (including simulation of its operation),
- numerical simulations of the operation and economy of using a thermoelectric air-conditioning system,
- analysis and optimization of the supercooling phenomenon in one- and two-stage thermoelectric systems.

The first stage of the research focused on analysing the effect of thermal resistance on the performance characteristics of the thermoelectric system. Analytical models were developed to describe the operation of thermoelectric systems taking into consideration, among other things, thermal resistance on each contact layer. Based on that, an own simulation tool was created in the form of the ThermoelectricCalc computer program, enabling comprehensive analysis of the operation of one- and two-stage systems, including supercooling and optimisation of electric current. The simulations can be carried out in steady or transient states, taking account of thermal capacity of the system components. The software includes the possibility of optimizing the operation of analysed systems for a number of defined decision variables. The software was used to perform simulations according to original, novel and purpose-designed methodologies.

As part of the experimental testing, and thanks to the developed rapid-state method using the difference in the temperature field and the electric field inertia, a procedure was formulated for determining thermal resistance of the heat flow between heat source/sink and thermoelectric junctions. Additionally, based on the developed analytical model and the measurements carried out in steady and rapid states, a way was found to determine the thermoelectric module material parameters. An own method was also created of evaluating contact resistance using measurements in the vicinity of the ambient temperature.

Using the developed software and available commercial codes, a wide range of numerical simulations were performed of thermoelectric systems operating in the mode of both a generator and a heat pump. In the case of the generator-mode operation, a system for waste heat recovery from the exhaust of a car reciprocating engine was proposed and simulated. An example

air-conditioning system using thermoelectric modules for heat pumping was also proposed and analysed thoroughly from the technical and economic point of view.

A detailed review of performed works is presented in the chapters that follow.

II. PAPER [A] – Mathematical model of a thermoelectric system based on steady- and rapid-state measurements

This paper presents the concept of determining, using the rapid-state method, the parameters of a thermoelectric module and thermal resistance between the module and the heat exchangers cooperating with it. Although measurements using the dynamics of phenomena and the inertia of processes are known in the literature, this is, to the best of the author's knowledge, the first study presenting such a use of dynamic phenomena. It is mainly about the use of the order difference in the inertia of electrical and thermal phenomena (the change in the electric voltage field and the change in the temperature field, respectively) to study thermoelectric modules.

1. Determination of the thermoelectric module operating parameters

The proposed method in its basic version consists in bringing the system to a steady state at the module short-circuit current. Then the circuit is abruptly broken – transition to an open-circuit state. During this process, the voltage history on the module terminals is recorded at a sampling frequency of tens of kHz. Just after the change in the electrical state, the temperature field still corresponds to the steady short-circuit state. The electric field, or more precisely the output voltage, changes much more rapidly, and the trace delay may be due to the electrical capacity and inductance of the electrical path. The delay resulting from the system reaching a new thermal steady state is by orders of magnitude bigger. Such circumstances make it possible to read the voltage just after the change in the state and after the new steady state has stabilized. Based on the difference between these readings, the short-circuit current and the heat measurement, selected parameters characterizing the module can be determined. The number of the quantities that need measuring depend on the number of output parameters being determined. The developed method makes it possible not only to determine the quantities characterizing the thermoelectric module, such as Seebeck and Peltier coefficients, electrical resistance and thermal conductivity between the junctions, but also to quantify thermal resistance between the thermoelectric junctions and the heat source/sink. The knowledge of contact thermal resistance, in turn, makes it possible to determine the actual (practically unmeasurable in a direct way) temperature difference on the thermoelectric junctions, and thus the crucial operating parameters of the system. For this purpose, a dimensionless power factor was introduced, which determines the ratio of the actual power to the maximum power that would occur in the absence of contact thermal resistance.

Thermal resistance can vary over time, especially when thermal grease is used on contacting surfaces. The grease performance strongly depends on the clamping force, the quality of the contacting surfaces and the environmental conditions, due to which it may be subject to degradation over time (mainly dehumidification). In real operating conditions of systems with thermoelectric modules, a drop in the clamping force is also possible due to, for example, the stress relaxation process in the mounting elements. Increased resistance can also be caused by degradation of the module internal structure, particularly the solders and their contact with the legs and the housing.

2. Mathematical model

The mathematical model presented in the paper, based on the energy balance equations and definitions of thermoelectric phenomena, makes it possible to find solutions describing the relationship between the electric current in the circuit, the module electric power, the temperatures of the junctions, the electromotive force, as well as determine the optimal electrical resistance corresponding to maximum power or efficiency. The analytical form of these solutions is characterized by a considerable degree of complexity. The concept of effective parameters considering external thermal resistance as an immanent feature of the thermoelectric module was also introduced into the model. In this way, the thermoelectric system operation along with thermal resistance of contact layers can be described assuming that the temperature of the junctions is equal to the temperature of the exchangers and using the effective values of the Seebeck coefficient, electrical resistance and thermal conductivity. This approach is not an exact representation of the performance characteristics, but is a good enough approximation of them. The accuracy of such an approximation was proven by an error analysis conducted for the presented case. The developed model can be also used to determine contact resistance based on measurements of the performance characteristics of thermoelectric modules.

3. Experimental testing

The paper demonstrates the structure and measurement capabilities of the prepared test stand and presents practical aspects of the realization of measurements in the steady state and at rapid changes in the electrical state of the system. The test stand is fully computerized and automated thanks to the prepared control and measurement software, which enables precise control of each element of the system and collection of data from a large number of measurements at a frequency of up to several kHz. It consists of a mounting frame that ensures a proper electronically controlled clamping force pressing the thermoelectric system elements to each other, two copper blocks acting as heat exchangers and a thermoelectric module placed between them. The hot exchanger is heated by electric heaters, while the cold exchanger is cooled by water. On the electrical side of the module there is an electronically regulated receiver of electric power. The main quantities measured on the stand are the temperatures of the exchangers (and their distribution inside each exchanger), the power supply to the exchanger heaters, the mass flow and temperature of the cooling water, the voltage and the current on the module terminals and the clamping force.

4. Results and conclusions

Using the assumption of the module current-voltage characteristics linearity, from the practical point of view contact resistance should be determined between two extreme states of the module operation, i.e. the short circuit and the open circuit.

Studies have shown that the existence of thermal resistance introduces nonlinearity into the module characteristics in a way that cannot be achieved by modifying the thermoelectric material parameters (in other words, by introducing effective parameters).

The results of the assessment of the effect of contact thermal resistance in various operating conditions make it possible to determine the actual temperature range of the thermoelectric material, including the most significant maximum temperature, which decides the module failure. The higher the value of the resistance, the higher the temperature of the hot source can be, even tens of K above the module allowable temperature. In addition, the performed sensitivity analysis of the determination of the module parameters based on measurements shows that the results are affected the most by the measurement of electrical voltage, which interestingly enough is one of the most accurately measured quantities.

The developed, relatively simple method of determining the contact layer thermal resistance provides an answer to the question of the potential for improvement in the module performance characteristics by improving the contact with heat exchangers (in practice, for example, by replacing the thermal grease and adjusting the clamping force). It also makes it possible to indicate possible damage to the internal thermal path in the module (e.g. if the ceramic surface of the housing comes unstuck from the thermoelectric junctions).

III. PAPER [B] – Detailed model of the thermoelectric generator performance

This paper analyses the effect of contact resistance with a symmetric distribution on the operation of a thermoelectric generator. A mathematical model and its numerical solution for a specific commercially available module are developed and shown.

1. Mathematical model

The mathematical model describes the power and the energy conversion efficiency of a thermoelectric module cooperating with heat exchangers with set temperatures. The input data are the parameters describing the module and the outdoor temperatures. The temperatures of the thermoelectric junctions in this case are a function of the temperatures of the exchangers, the current in the circuit and the value of thermal resistance along the exchanger-thermoelectric junction path. The thermal resistance can be set individually for each side. If the exchangers absorb/give up heat by convection, e.g. from hot exhaust gases, the amount of the exchanged heat will additionally be a function of the flow velocity, the geometry and size of the heat transfer surface, and the medium-exchanger temperature difference. The presented model takes account of the radiative heat transfer as well. The temperature of the thermoelectric junction also depends on the parameters of the legs and the quantities directly resulting from them, i.e. thermal conductivity, the amount of released Peltier heat and Joule heat. The current in the circuit can be determined by electrical resistance of the power receiver. The model equations can be used to find relations describing optimal electrical resistance of the connected power receiver while maximizing the module output power or efficiency. The degree of the model complexity is thus considerable. EMF varies due to the current in the circuit as a result of the Peltier heat. This, in turn, changes the current corresponding to desired optimized condition creating a coupled problem.

2. TEG operation for constant temperatures

Solving the model equations numerically, it was established how the output electrical power and efficiency changed as a function of the circuit current for different values of contact thermal resistance. The effect of this resistance on the shaping of selected operating parameters, the value of the current in particular, was discussed with a view to achieving operation with the maximum, possible to obtain in given conditions, generated electrical power or maximum total efficiency. Efficiency is understood as the ratio of the generated electrical power to the thermal power received by the module from the hot heat source.

Literature analyses usually make use of an approximation stating that the point of the maximum power corresponds to the current value equal to half the short-circuit current. Therefore the paper examines the deviation from this rule for the situation when contact thermal resistance is taken into account in the system. A function was determined that describes the optimal value of electrical resistance of the connected power receiver depending on thermal resistance. As a result, analysing relevant values of relative deviations of the system operating parameters, it was found that the deviation of the actual power from the maximum power was insignificant

(much less than 1%) when using the simplified rule assuming the maximum power for the current value equal to 50% of the short-circuit current. A similar situation occurs assuming a constant value of external electrical resistance of the power receiver which is equal to the value of the module internal resistance. Analogous considerations were also made for the criterion of maximum efficiency. The optimal values of electrical resistance in both cases can be adopted independently of the thermal resistance of the layer at a usually negligibly small deviation of the output parameters. The range of the analysed thermal resistances was from zero to a value corresponding to a few-centimetre layer of the insulating material.

3. Heat source maximum temperature

Considering that the temperature of the hot junctions of the thermoelectric module decreases with a rise in thermal resistance, an analysis was made of possible increase in the temperature of the heat source depending on the value of the thermal resistance. For each of the analysed operating states, this temperature was selected so that for zero current in the circuit (the maximum temperature of the thermoelectric junction) the allowable temperature of the module should not be exceeded. For the operating states under analysis, the effect of the current in the circuit, and – consequently – Peltier heat, on the temperature of the thermoelectric junctions was presented. It is shown that for at least one constant-temperature heat source, there is an external thermal resistance value for which the effect (between zero and short circuit current) is the greatest. For very small values of thermal resistance, the temperature of the thermoelectric junction differs only a little from the temperature of the constant-temperature heat reservoir, so also its variations with changes in current are slight. On the other hand, for very large values of thermal resistance, the short-circuit current has a relatively low value due to the small useful temperature gradient on the module. Therefore the potential for changing the junction temperature (by changing the current value from open circuit condition to short circuit) is also small (a small current means a small Peltier effect).

4. Conclusions

It is shown that the presence of the contact thermal resistance between the module and the heat exchanger modifies, to a significant extent, the thermoelectric system operating parameters. This mainly concerns the temperature of the thermoelectric junctions, which has a direct impact on output power. It is also shown that the presence of thermal resistance affects the optimal, in terms of output power or efficiency, electrical resistance values of the connected power receiver. Moreover, it is substantiated that the use of approximation-based methods makes it possible to obtain results with satisfactory accuracy. It is demonstrated how, in the presence of thermal resistance of the layer, the temperature of the hot heat source can be increased above the allowable temperature of the module without damaging it. The so-determined maximum temperature varies depending on whether the module operates under conditions of maximum power, efficiency, or under any conditions (in practice corresponding to no current flow).

IV. PAPER [C] – Comparative analysis and optimization of one- and two-stage cooling systems with thermoelectric cells with respect to supercooling

This paper deals with the analysis of a cooler operating based on thermoelectric phenomena, with special attention given to the phenomenon of supercooling, understood as a momentary achievement by the system of a temperature lower than the minimum achievable in the steady state. Such a situation may occur due to the presence in the system of heat reservoirs with a certain thermal capacity. In transient states, their momentary temperatures, combined with an appropriate value of the module supply electric power and the resulting heat fluxes in the system, can result in the achievement of a supercooling temperature. An analysis is conducted of the methods of shaping current over time to achieve the temperature minimum.

1. Model of the system

Because better supercooling results can be achieved in a two-stage system, most of the simulations were carried out for this configuration. It consists of two thermoelectric modules connected thermally in series, so the “pumped heat” flows sequentially through each module. The main advantage of the two-stage system is the possibility of obtaining a lower temperature than for a single module (both – steady state and supercooling). The disadvantage is the relatively low cooling power compared to supply power (low COP), the module size and the amount of the thermoelectric material used for construction. In the work described here, the two-stage thermoelectric system model was extended by an additional heat reservoir placed in between the modules. The system thus has 3 heat reservoirs with specific thermal capacities and two thermoelectric modules (layers with a varied size). The analyses were carried out both with and without taking account of contact thermal resistances of the layers. The issue was investigated using the own program.

2. Software validation

The developed simulation program was validated on an in-house test stand. This time, a two-stage system equipped with two identical thermoelectric modules was tested. The validation was carried out for the steady state and the transient variations in the supply current of the modules. The numerical simulations carried out for the tested system were then reproduced on the test stand with satisfactory agreement of the obtained temperatures courses.

3. Numerical simulations

In the first step of the calculations, the focus was on the value of the minimum temperature achievable in the steady state as a result of the optimal selection of the supply current of the modules. In this case the thermal capacities in the system are irrelevant. The results here are curves illustrating changes in the steady-state temperature as a function of currents in the circuits of the modules.

Next, the analysis concentrated on the process of the system start-up from the initial state (with the temperature of all components equal to the ambient temperature) at a constant value of the

current supplying the modules. In this case, for certain current values and an appropriate combination of thermal capacities of the reservoirs, the phenomenon is observed of a momentary achievement of a temperature below the steady-state level on the cold side of the system, which may also be lower than the minimum temperature achievable by the system in the steady state (supercooling). This is illustrated in the charts, showing both the steady-state temperature and the minimum temperature over the entire time under analysis (from activation to reaching the steady state). Moreover, current values are marked for which the steady-state temperature is at the same time the minimum in the entire cycle (overlap of the analysed areas). The analyses also made it possible to determine the limit value of the internal heat reservoir thermal capacity below which the minimum achievable temperature occurs in the steady state, and above which it is achievable only temporarily. The changes in the minimum temperature of the cooled reservoir are shown as a function of this capacity.

The supercooling phenomenon can potentially be achieved by supplying modules with currents with a constant value, depending on the initial state. However, better results are achieved if the module is supplied with a variable current pulse. For this purpose, a few methods of modelling current changes over time were analysed to achieve the maximum supercooling effect. A linear increase in current (from the initial value maintained for a certain period of time) for each module individually was considered as the most efficient. To describe such a history, 4 values were required (degrees of freedom – initial value, time of the beginning of the increase, the increase rate, the final value), which were determined based on the optimization procedure; the objective of the process was momentary temperature minimization. The adopted method of the current modelling ensured much lower resultant temperatures than a step change from the initial to the final value of the current, while a more complex description of the current shape did not bring a noticeable improvement on the results.

The results are shown both in the form of the minimum temperature and characteristic values describing the current modelling, as a function of the thermal capacity of the internal reservoir. In this case, two characteristic phases can be distinguished during the process of obtaining the minimum temperature. In the first, the system is brought to the steady state (at constant initial currents), and then the phase of the increase in current begins. During that phase, or just after the current final value is reached, the moment occurs when the minimum temperature of the cooled space is observed. For a relatively high thermal capacity of the internal reservoir in the initial phase, the current in one of the modules may even be negative – both modules work to “cool” the middle reservoir. Owing to its large capacity, the “cool” accumulated in it can be used for intensive cooling of the cooled space in the next phase, which results in a low minimum temperature. Moreover, the size of the modules was for each of them optimized individually to achieve the lowest possible temperature, both with and without taking account of contact resistances.

4. Summary and conclusions

The results of the studies prove that both in one-stage and in multi-stage systems, with proper adjustment of the histories of currents, it is possible to achieve a temperature momentarily lower than the minimum steady-state temperature. In a multi-stage system the phenomenon is much more pronounced. The paper presents the features and the performance characteristics (mainly

the supercooling capacity) of the two-stage system, and an analysis is conducted of their variation as a function of the internal reservoir thermal capacity. In addition, it is proved that the characteristics of the system performance under variable conditions can be shaped considerably by placing such a reservoir in a multi-stage system. The optimal method of current shaping to achieve the strongest possible supercooling effect is determined. It is also shown that for some of the tested configurations/conditions the minimum temperature is also achievable in the steady state – the supercooling phenomenon does not occur. For each of the configurations it was proved that optimizing the size of the thermoelectric layer (the number of modules/legs in a single layer) in terms of the minimum steady-state temperature resulted in a substantial temperature drop, but at the same time the potential for supercooling decreased considerably. The optimization results differed significantly for cases where thermal resistances of the contact layer between the module and heat exchangers were taken into account and where they were omitted.

V. PAPER [D] – Technical and economic analysis of the thermoelectric air-conditioning system

This paper presents an analysis of the system of a portable thermoelectric air conditioner. Its main part is based on simulations performed using the author's own, previously mentioned, software. The considerations include, among other things, the economic aspect, which resulted in a comprehensive techno-economic analysis of the proposed system. The system was also optimized with a view to minimizing the cost of cool production.

1. Experimental testing

The testing was performed using a module that is easily available on the market and relatively inexpensive. The main criterion for the module selection was the ratio of the cooling power to the purchase price. The experimental tests were carried out to determine the analysed module actual parameters. The research novelty, among others, is the presented method of determining contact thermal resistance between heat exchangers and the module. It is based on static and rapid measurements performed in temperatures close to ambient. The method includes measurements that enable compensation for losses to the environment. The developed procedure is realized in such a way that the cold side of the module is in contact with the heated exchanger causing its cooling. For this reason, maintaining the exchanger constant temperature involves supplying it with adequate thermal power from heaters. Performing such measurements (including rapid measurements) makes it possible to determine the hypothetical state of the zero temperature gradient in the thermoelectric material, i.e. the absence of heat conduction through the module. The known temperature difference between the exchangers is then due only to the thermal resistances occurring on contact layers. Additionally, the paper presents the results of a quantitative analysis for two different classes of thermoelectric grease.

2. Simulations of the system operation

The first stage was to simulate the behaviour of a system consisting of a thermoelectric module and heat exchangers with set constant temperatures. Based on that, characteristics of cooling power and the COP were determined as a function of the module supply current and the temperature difference of the exchangers. The simulations were then enriched by considering the characteristics of the heat exchangers in contact with the surrounding air (indoor and outdoor). The quality and the size of the exchangers were independently described for each of them using the heat transfer factor (HTF) defining the ratio between the exchanged heat and the temperature difference. For comparison, characteristics of systems consisting of one and of ten reference modules using the same heat exchangers are shown. It is demonstrated that in this case the system with one module has higher maximum COP and cooling power values per module. In the next stage of the simulation, an analysis was conducted of the effect of the number of modules on the characteristics of a system at fixed dimensions of the heat exchangers and at a fixed temperature difference between the cooled space and the environment to which heat is discharged. Contour maps were created of cooling power and the COP as a function of the size of the thermoelectric layer (number of legs) and the supply current. They indicate clearly that cooling power reaches a global maximum for a certain number of thermoelectric couples and

an appropriate supply current value. Moreover, for any size of the thermoelectric layer or any value of current, there is a value of the latter parameter that corresponds to the maximum cooling power. The maximum COP for the set size of the thermoelectric layer is obtained at very small currents, which corresponds to a very low cooling power. Due to these observations, a graph was plotted illustrating the dependence of the maximum COP and the corresponding supply current of the module as a function of the demand for cooling power (minimum cooling power), optimizing for each point both the current value and the thermoelectric module size. The resulting graph has practical significance in the design of this type of the air conditioner and its economic analyses.

3. Economic simulations

In the next step, the economic aspect related to the design and operation of a thermoelectric air conditioner with the cooling capacity of 2kW was introduced into the analyses. The calculations took account of the market price of thermoelectric modules and heat exchangers, as well as the cost of electricity for a retail consumer. The simulations were carried out for a 5-year service time at the operating time of 480h/year.

This section discusses the optimization procedure and defines the parameter called Economic Total Cooling Capacity ($ETCC$), which determines the ratio of the cooling energy delivered over the assumed lifetime of the device to the total cost of the device purchase and operation. It mainly consisted in the maximization of the $ETCC$ indicator performed for the entire temperature range of the air conditioner operation, i.e. from 0°C to 25°C of the indoor/outdoor difference, and a wide range of unit costs of electricity. The decision variables of the optimization problem were the coefficients and characteristics describing the unit cost and efficiency of the heat exchangers, the modules and the electric power supplying the system. The reference point to which the obtained values were compared was adopted as a 5°C indoor/outdoor temperature difference and the cost of electricity at the mean level in the EU. The obtained results show how, the size of heat exchangers, the number of modules and the module supply current change. Contour maps were also determined, which illustrate the deviation of the $ETCC$ indicator and cooling power for the system operation in the whole field of temperature differences and electricity costs under analysis, assuming that the system is designed and optimized in terms of the adopted reference point. The assumption does not concern the current because this can easily be matched to actual operating conditions (which may require no changes in the design).

In the next phase of the simulations, the height of the legs making up the thermoelectric layer was added to the task decision variables. This captures the potential possibility of ordering dedicated modules (with a specific leg geometry). The system optimization performed in this way showed the possibility of improving the $ETCC$ indicator. The problem in this procedure was to determine the share of material costs in the cost of the thermoelectric module, in other words, how the module price varied with a change in the height of the legs (while keeping their number and their cross-sectional area constant). The calculations were carried out assuming a 20%-share of the material cost in the cost of the module. For the reference point, the optimization results were also presented for extreme assumptions – 0% (the module cost does not depend on the leg height) and 100% (the cost changes linearly with the leg height).

In the last part of the considerations, an analysis was carried out of the possibility of increasing the cooling power of a device optimized to maximize the $ETCC$ indicator, which in this situation does not operate with maximum cooling power. It was shown that this power could be significantly increased (e.g. temporarily) at the expense of a decrease in the COP and the $ETCC$. In the latter case, the change in overall lifetime indicators is dependent on the operating time beyond design conditions.

4. Summary and conclusions

Based on a detailed analysis of the air conditioner system built using thermoelectric modules, the features and the characteristics of its operation were presented. Such a system has a significantly lower cooling efficiency and higher investment and operating costs compared to conventional compressor solutions. However, the proposed system has hardly quantifiable advantages, which can be crucial in certain applications, such as the lack of a circulating medium, the noiseless operation, the small size and weight, and the system scalability in a wide range of cooling power (especially small ones). The introduced $ETCC$ indicator is a quantity independent of the system size. For the reference point, the obtained $ETCC$ value totalled 0.58 W/USD for the case with the original geometry of the leg, and 0.64 W/USD after optimization taking account of the possibility of its modification.

VI. PAPER [E] – The potential of thermoelectric energy harvesting in vehicles equipped with the ICE

This paper deals with the possibility of integrating thermoelectric systems into the exhaust system of an internal combustion engine. The considered solution is characterized by the following features: ease of installation, as there is no need to modify the internal combustion engine (except the exhaust system), possibility of retrofitting and a number of advantages of the thermoelectric module.

1. Model of the system

The computational model was created using the AVL software package, in particular the BOOST module. It enables one-dimensional calculations of the internal combustion engine layout, taking into account the phenomena of gas dynamics, thermodynamics, energy conversion, etc. The modelled engine had a single-cylinder structure with the displacement of 500 ccm and spark ignition, representing a simple motorcycle engine. The thermoelectric system was designed as a “user-defined element” by developing a C-language script. Catalogue data of a commercially available module were used as a source of TEG characteristics. The heat exchanger was modelled in the software by a fragment of the exhaust gas duct with a set diameter, clad with thermoelectric modules on the outside. The heat transfer coefficients are determined by the software based on momentary parameters of the exhaust gas in the duct (temperature, velocity, pressure, composition). It is assumed that the cold end of the thermoelectric modules is placed in a temperature close to ambient. In practice, this can be implemented through a structure of heat sinks or a liquid cooling system. It is also possible to use the liquid cooling system of the engine, for example, by drawing the liquid to cool the thermoelectric system just after the radiator. The assumption is that the current in the module circuit is at all times set to a value which ensures the maximum electric output power, which is almost exactly equal to the maximum total efficiency. This is because the efficiency of the system is understood as the ratio of generated electricity not only to the heat flowing through the module, but to the heat contained in the exhaust gas. Based on the current temperatures of both sides of the module, the heat flow through the module is calculated. This heat affects the temperature of the duct wall, which, due to the adopted assumptions, is also the temperature of the hot side of the thermoelectric module, which translates into the heat conducted by the module and then again it affects the duct temperature. This means that the thermoelectric system operating conditions are determined iteratively. It is further assumed that a single “thermoelectric segment” is made of 20 modules, while the entire recovery system consisted of multiple segments connected in series, i.e. the exhaust gas flowed sequentially through each segment and was finally carried away to the environment. Inside a single segment all thermoelectric modules operate at the same temperature on both sides, also the temperature of the inner wall of the heat exchanger (in contact with the exhaust gas) has a uniform temperature along the entire segment in this case. The pressure increment resulting from the pumping of the exhaust gas through the heat recovery segments was negligibly small. In addition, a reservoir was placed in the exhaust system, after the last segment and before the outlet to the environment, to prevent the intake of cold air from the environment due to the pulsatory nature of the flow.

2. Calculations

A single working point of the engine – 6000 rpm, full throttle – was assumed for the calculations. In this condition, the engine reaches a brake output power of 27.7 kW (very close to its maximum power), the exhaust gas mass flow rate in the duct totals 24 g/s at the average temperature of 1278 K and the average velocity of 69 m/s (mass- averaged). In the first stage, in order to compensate for the flow pulsations, an insulated reservoir with the capacity of several hundred litres was placed between the simulated thermoelectric system and the engine. In addition, the heat transfer multiplier (representing the physical internal ribbing of the exhaust duct of the segment) was set at 1.02, where 1.0 corresponds to a smooth pipe. This ensured that the temperature was at the limit of the level allowable for the thermoelectric modules for the first segment. At this stage, the segments were assumed to be identical. It is shown how the heat conducted by the modules, the temperature of the hot side, the amount of generated electricity and the gas temperature at the segment inlet and outlet vary for each segment.

3. Optimization of the system

The next step was to adjust the value of the heat transfer multiplier to optimize the operating conditions of the thermoelectric modules in each segment independently. This multiplier was selected for each segment in a manner ensuring that the temperature of the hot end of the TEG should reach (but not exceed) their allowable value. For each successive segment the determined value of the multiplier, and thus the required ribbing of the exchanger, increase substantially. The value of 10 was reached for the fifth segment, which was the upper limit in the optimization process. Using this approach, it was possible to achieve an approximate 30% increase in power in the first four segments compared to the case with identical multiplier (identical ribbing).

In the next stage of the calculations, the capacity of the insulated reservoir between the thermoelectric system and the engine was reduced to a reasonable size of 5 litres. It was determined how the optimal multipliers of the heat transfer changed in such a system.

Next, an analysis was carried out of the electric power recovered in the case of the engine operation under a full range of load for two rotational speeds: 4000 rpm and 6000 rpm. The dependence of the recovered electric power on the mechanical power of the engine was approximately linear. Higher power can of course be observed for the higher rotational speed value, when the efficiency of the recovery system is bigger as a result of its tuning (heat transfer multipliers) to this working point.

4. Conclusions

A quantitative assessment was made of the possible heat recovery for the operation of a single-cylinder engine. The proposed system can partially or fully replace a conventional mechanical alternator (electric generator). The reasonableness of using such a solution and the number of segments strictly depend on the cost of the thermoelectric modules and the heat exchangers, where each successive one was bigger. Each successive segment is characterized by a lower value of the ratio between generated useful energy and the segment cost.

VII. PAPER [F] – Modelling the internal combustion engine waste heat recovery using thermoelectric modules

The paper is based on a similar computational model and assumptions as the work presented in Chapter VI. The AVL BOOST software and an independently prepared script describing a thermoelectric module with a heat exchanger on the exhaust gas side and a constant cold end temperature were used to model the system.

The motivation for the research was the desire to find a way to improve the economic indicators and the environmental impact of the combustion engine car operation by reducing its unit fuel consumption. The road transport market, including passenger cars, is growing rapidly in the world. The efficiency of internal combustion engines reaches 30-40% at best. A significant amount of heat is dissipated in the form of the exhaust gas temperature.

A model of a four-cylinder spark-ignition passenger car engine with the displacement of 1.5 L was used for the study. A car was also modelled, taking account of its weight and gearbox with the gear ratios. A simple model of the driver was also introduced, thus determining the operation of the vehicle drivetrain.

1. Calculations

In the first stage, the dependence of the engine power, torque, average velocity of the exhaust gas stream and its average temperature (mass-averaged) were investigated as a function of rotational speed at a full opening of the throttle. In this case, the thermoelectric system of the exhaust heat recovery consisted of a single segment as described in Chapter VI, but using a different type of thermoelectric module. The initial length and diameter of the segment were 500 mm and 44 mm, respectively. It contained 10 thermoelectric modules, and the heat transfer coefficient multiplier (equal to 7.51) was selected so that at a rotational speed of 3300 rpm (the maximum in the tests, at which the gear changes) the hot side of the module, and thus at the same time – the inner wall of the heat exchanger, should reach the allowable (limit) temperature of the applied thermoelectric modules. The minimum rotational speed of the engine was assumed as 750 rpm (idling).

Then, for the system selected in this way, charts were made showing the relationships between the engine rotational speed and the heat flowing through the modules, the temperature of their hot end and the electrical energy produced by them. Results are shown for three values of the engine rotational speed: 1000, 2500 and 3300 rpm. For these speeds, charts were plotted showing the dependence of the average temperature of the exhaust gas and its average velocity in the duct as a function of the mechanical power generated by the engine. The course of the gas pulsation in the exhaust system is also presented.

Due to the pulsatory nature of the flow, it was checked how the length and position of the heat exchanger (the segment with thermoelectric modules) affected the recovery of energy. The number of modules cooperating with the exchanger was kept constant. As the exchanger is shortened, the heat transferred through it decreases, but the relationship is not linear. Less collected heat (shorter exchanger) causes a smaller temperature drop along the segment.

Moreover, less heat flowing through the segment modules results in a lower temperature at their hot end. Both these phenomena are therefore responsible for a larger average temperature difference (between the exhaust gas and the exchanger), and therefore a larger heat flux.

The analysis then focused on the impact of the exchanger location on the amount of recovered heat. The simulations in this case were carried out for an exchanger with the length of 300 mm. In general, the longer the exchanger, the smaller the impact of wave effects on the heat transfer because what happens then is averaging of both velocity and temperature along the exchanger. On the other hand, for a very short exchanger the histories of momentary values of velocity and temperature (and especially the relationships between them) strictly depend on the distance from the engine. The results indicate that as the recovery segment is moved away from the engine, the amount of the exchanged heat decreases, but the relationship is not homogeneous, with local minima and maxima. The local phenomena are probably due to the pulsatory nature of the flow, and the general decreasing trend is an effect of the "averaging" (mixing and dispersion effects) of the exhaust gas temperature and velocity with the distance covered from the engine.

In the next step, simulations were performed of a driving cycle of the car involving acceleration from a standstill to the speed of about 100 km/h followed by deceleration to a complete stop. In this case, account was taken of the thermal capacity of the heat exchanger transferring heat from the exhaust gas to the thermoelectric modules. An increase in capacity results in slower heating of the system (delayed energy recovery and slow build-up), but also, after a decrease in the engine operating parameters, the accumulated heat is utilized in the thermoelectric modules. This can have a positive effect on the amount of recovered energy at the engine relatively short operation. However, prolonged heating results in a lower hot side average temperature, which has a negative impact on the efficiency of the thermoelectric recovery process. Based on the charts illustrating momentary values of the recovered power and the total recovered energy, it is concluded that there is an optimal value of the exchanger thermal capacity that depends on the assumed drive cycle.

The final step was to simulate a driving cycle following the WLTP standardized cycle and consisting of urban driving of varying intensity and motorway driving. The analysed cycle covered nearly 15 min and 13 km of driving. Based on this, the relations concerning the power and the energy recovered during the cycle were obtained.

2. Conclusions

Based on the obtained results, it can be concluded that the proposed system is not justified for use in a passenger car. During the simulated driving cycle, the vehicle average fuel consumption totalled 9.3 L/100km, and the recovered energy was equivalent to the energy contained in 0.01 litre of fuel (assuming the conversion efficiency of 30%). The resulting saving in fuel consumption only slightly exceeds 0.1%. Much more energy was consumed to decrease the vehicle speed, which points to the potential for using regenerative braking systems. There are some ways of improving the efficiency of the thermoelectric system, such as increasing the heat transfer surface area for example. However, this makes such a recovery system much more complex and expensive.

VIII. SUMMARY AND CONCLUSIONS

The research presented in this work focuses on measuring parameters of thermoelectric modules in various steady- and transient-state operating conditions, and on modelling the operation of systems equipped with such modules. It covers the operation of such devices both in the generator and in the heat pump mode.

A purpose-built test stand was developed and constructed to enable comprehensive experimental evaluation of thermoelectric modules. The stand is fully automated, with self-control systems monitoring its own components, the measured values and indications, including implemented emergency procedures. Algorithms were developed and implemented for steady-state detection, recording of results and automatic performance of measurements in various conditions, including fast-changing ones. The module operating parameters can be adjusted over a wide range fully covering the entire field of operation of most commercially available modules. The stand can operate at the hot source temperatures of up to 600°C and enables testing of multi-stage systems, including those with thermal capacities in between modules. It was used to develop the performance characteristics of the tested thermoelectric modules. The calculations were based on own measurements, the modelling results were validated for systems with TEGs and TECs, and new measurement methods were developed. The results were characterized by a high degree of repeatability and by confirmed accuracy.

A transient-state measurement method was developed to determine thermal contact resistance on the thermoelectric module-heat exchanger interface. The method consists in rapid electrical measurements when the operating conditions of the module change abruptly, and takes advantage of the large difference in the inertia of the thermal and the electric field. In parallel, an analytical model was developed to utilize the measurement results obtained by means of this method to evaluate the operation of a system with a thermoelectric module. An indicator of the system operation quality was also introduced, which indicates the deviation of the current power of the system from the theoretical maximum at ideal thermal contact between the thermoelectric junction and the exchangers. The method makes it possible to determine actual parameters and operating conditions of the thermoelectric module material, the theoretical operating maxima, the potential for improving operation by improving thermal contact, or the degree of wear of the thermal grease. The source maximum temperature was also analysed for a defined allowable temperature of the module. The thermal resistance values measured using the developed methods were found to vary strongly for different type of the thermal grease used on the contact surfaces and for the applied clamping forces.

In the next phase of the investigations, the degradation of operating indicators of thermoelectric modules due to the presence of a thermal resistance layer between the module and constant-temperature heat sources in the case of the TEG was established. The influence of Peltier heat on thermoelectric junction temperatures was examined depending on the circuit current. Based on that, the optimal values of current as a function of contact thermal resistance were determined. They vary depending on whether it is the module power or the module efficiency that is maximized. The optimal electric resistance of the power receiver also differs from the values determined based on an approximate model assuming constant-temperature sources. In

addition, the errors resulting from the use of approximate relations to determine the optimal level of current and other parameters were estimated.

Based on the developed mathematical model of a system with a thermoelectric module, a computer program was prepared that enables complex analyses of thermoelectric systems operating in the mode of electricity generation or heat pump. Using the program, it is possible to simulate both steady- and transient-state operation of one- and two-stage systems, prepare their characteristics and optimize operating conditions and geometric configurations for pre-defined criteria. In addition, it is possible to conduct economic analyses and optimize the shapes of variable current pulses using different current shaping methods. This tool was validated experimentally and then used to simulate the operation of thermoelectric systems.

Using the prepared software and other means, a concept was analysed of a thermoelectric air conditioner based on relatively cheap and commercially available modules. Own experimentally determined characteristics of the thermoelectric module were adopted for the calculations, and own methods were used to determine the system operating parameters. Apart from the analysis of the air-conditioning system technical parameters, a comprehensive economic evaluation of the system was performed, taking account of investment and operating costs. It is shown how individual cost factors affect the introduced $ETCC$ indicator. The results of the performed optimization of the geometry of thermoelectric modules indicate a possibility of improving the economic indicators by proper selection of the leg geometry. It is demonstrated that a system optimized in terms of set technical and economic conditions can operate with an overload of up to 30%, but at the expense of a significant reduction in the value of the $ETCC$ indicator.

The next stage of the works was an analysis of a two-stage system with an additional thermal capacity placed between the modules. Special attention was paid to the possibility of achieving a momentary temperature of the cooled space that is below the steady-state minimum, i.e. achieving the supercooling effect. A comparative analysis of the one-stage and the two-stage system was conducted, and ways of shaping the module supply currents to achieve the minimum temperature were presented. Characteristics defining the minimum achievable temperature and describing the corresponding current pulse history as a function of the values of the thermal capacities of the reservoirs were determined. It was observed that a momentary very large increase in current in the module circuit made it possible to achieve the significant supercooling effect, while the steady-state minimum temperature was reached for relatively low values of current to minimize the impact of the Joule effect. In each case, however, achieving the minimum temperature involves running the process of optimizing the system operating conditions, taking account of the system geometric configuration and the thermoelectric module parameters. The geometric configuration was also subjected to optimization for different operating conditions.

Simulations were performed of internal combustion engine systems (for a motorcycle and a passenger car) equipped with exhaust heat recovery thermoelectric systems built into the exhaust system. A dedicated software package extended with own calculation scripts was used for this purpose. The recovery parameters were determined in selected configurations and operating conditions. It was found that this type of solution was cost-ineffective for a typical passenger car.

Further research

Despite the wide scope of performed works, there are still quite a few closely related issues that require further analysis. Future research will go in the direction of introducing temperature-dependent variations of the module material parameters into numerical simulations, which may be important for high-temperature power generation and cascade systems. This in turn will involve taking account of the Thomson effect in calculations. The experience gained during the research also points to the need to address the problems of thermal strains and stresses, and consequently of the wear of thermoelectric modules.

The results of the research performed so far show that the durability of such devices is surprisingly low in many cases. The damage is suspected to be due to thermal stresses arising on and around thermoelectric junctions and leading to a loss of material cohesion (cracking), as well as to fast oxidation of the thermoelectric material. It is necessary to carry out numerical simulations and experimental testing of the stress field in the module structure (including fatigue testing). In order to draw comprehensive conclusions about the durability of thermoelectric modules, it is necessary to perform tests for a sufficiently large number of modules of a single series to be able to make a reliable statistical inference.

IX. BIBLIOGRAPHY

[1] S. M. Pourkiaei, M.H. Ahmadi, M. Sadeghzadeh, S. Moosavi, F. Pourfayaz, L. Chen, M.A.P. Yazdi, R. Kumar, Thermoelectric cooler and thermoelectric generator devices: A review of present and potential applications, modeling and materials, Energy, Volume 186, 2019, 115849, ISSN 0360-5442, https://doi.org/10.1016/j.energy.2019.07.179.

[2] G. Wu, X. Yu, A holistic 3D finite element simulation model for thermoelectric power generator element, Energy Conversion and Management, Vol. 86, 2014, Pages 99-110, ISSN 0196-8904, https://doi.org/10.1016/j.enconman.2014.04.040.

[3] G.S. Nolas, J. Sharp, H.J. Goldsmid, Thermoelectrics, Basic Principles and New Materials Developments. Heidelberg, New York, Berlin: Springer-Verlag; 2001.

[4] S. Weera, H.S. Lee, A. Attar, Utilizing effective material properties to validate the performance of thermoelectric cooler and generator modules, Energy Conversion and Management, Vol. 205, 2020, 112427, ISSN 0196-8904, https://doi.org/10.1016/j.enconman.2019.112427.

[5] W. He, G. Zhang, X. Zhang, J. Ji, G. Li, X. Zhao, Recent development and application of thermoelectric generator and cooler, Applied Energy, Vol. 143, 2015, Pages 1-25, ISSN 0306-2619, https://doi.org/10.1016/j.apenergy.2014.12.075.

[6] D. Champier, Thermoelectric generators: A review of applications, Energy Conversion and Management, Vol. 140, 2017, Pages 167-181, ISSN 0196-8904, https://doi.org/10.1016/j.enconman.2017.02.070.

[7] D. Ji, Z. Wei, S. Mazzoni, M. Mengarelli, S. Rajoo, J. Zhao, J. Pou, A. Romagnoli, Thermoelectric generation for waste heat recovery: Application of a system level design optimization approach via Taguchi method, Energy Conversion and Management, Vol. 172, 2018, Pages 507-516, ISSN 0196-8904, https://doi.org/10.1016/j.enconman.2018.06.016.

[8] W.H. Chen, C.Y. Liao, C.I. Hung, W.L. Huang, Experimental study on thermoelectric modules for power generation at various operating conditions, Energy, Vol. 45, Issue 1, 2012, Pages 874-881, ISSN 0360-5442, https://doi.org/10.1016/j.energy.2012.06.076.

[9] C.L. Izidoro, O.H. Ando Junior, J.P. Carmo, L. Schaeffer, Characterization of thermoelectric generator for energy harvesting, Measurement, Vol. 106, 2017, Pages 283-290, ISSN 0263-2241, https://doi.org/10.1016/j.measurement.2016.01.010.

[10] S. Shittu, G. Li, X. Zhao, X. Ma, Review of thermoelectric geometry and structure optimization for performance enhancement, Applied Energy, Vol. 268, 2020, 115075, ISSN 0306-2619, https://doi.org/10.1016/j.apenergy.2020.115075.

[11] J. Dongxu, W. Zhongbao, J. Pou, S. Mazzoni, S. Rajoo, A. Romagnoli, Geometry optimization of thermoelectric modules: Simulation and experimental study, Energy Conversion and Management, Vol. 195, 2019, Pages 236-243, ISSN 0196-8904, https://doi.org/10.1016/j.enconman.2019.05.003.

[12] P.E. Ruiz-Ortega, M.A. Olivares-Robles, C.A. Badillo-Ruiz, Transient thermal behavior of a segmented thermoelectric cooler with variable cross-sectional areas, Int. J. Energy Res. 2021, 45(13): 19215- 19225, https://doi.org/10.1002/er.7123.

[13] D. Pandel, A.K. Singh, M.K. Banerjee, R. Gupta, Optimizing thermoelectric generators based on Mg2(Si, Sn) alloys through numerical simulations, Energy Conversion and Management: X, Vol. 11, 2021, 100097, ISSN 2590-1745, https://doi.org/10.1016/j.ecmx.2021.100097.

[14] S. Ferreira-Teixeira, A.M. Pereira, Geometrical optimization of a thermoelectric device: Numerical simulations, Energy Conversion and Management, Vol. 169, 2018, Pages 217-227, ISSN 0196-8904, https://doi.org/10.1016/j.enconman.2018.05.030.
[15] O. Högblom, Multiscale Simulation Methods for Thermoelectric Generators, PhD Thesis, Gothenburg, 2016.
[16] D. Luo, R. Wang, W. Yu, W. Zhou, Performance optimization of a converging thermoelectric generator system via multiphysics simulations, Energy, Vol. 204, 2020, 117974, ISSN 0360-5442, https://doi.org/10.1016/j.energy.2020.117974.
[17] A. Piggott, Detailed Transient Multiphysics Model for Fast and Accurate Design, Simulation and Optimization of a Thermoelectric Generator (TEG) or Thermal Energy Harvesting Device, J. Electron. Mater. 48, 5442–5452, 2019, https://doi.org/10.1007/s11664-019-06952-x.
[18] M. Liao, Z. He, C. Jiang, X. Fan, Y. Li, F. Qi, A three-dimensional model for thermoelectric generator and the influence of Peltier effect on the performance and heat transfer, Applied Thermal Engineering, Vol. 133, 2018, Pages 493-500, ISSN 1359-4311, https://doi.org/10.1016/j.applthermaleng.2018.01.080.
[19] A. Fabián-Mijangos, G. Min, J. Alvarez-Quintana, Enhanced performance thermoelectric module having asymmetrical legs, Energy Conversion and Management, Vol. 148, 2017, Pages 1372-1381, ISSN 0196-8904, https://doi.org/10.1016/j.enconman.2017.06.087.
[20] S. Shittu, G. Li, X. Zhao, X. Ma, Y.G. Akhlaghi, Emmanuel Ayodele, Optimized high performance thermoelectric generator with combined segmented and asymmetrical legs under pulsed heat input power, Journal of Power Sources, Vol. 428, 2019, Pages 53-66, ISSN 0378-7753, https://doi.org/10.1016/j.jpowsour.2019.04.099.
[21] X. Wang, J. Qi, W. Deng, G. Li, X.Gao, L. He, S. Zhang, An optimized design approach concerning thermoelectric generators with frustum-shaped legs based on three-dimensional multiphysics model, Energy, Vol. 233, 2021, 120810, ISSN 0360-5442, https://doi.org/10.1016/j.energy.2021.120810.
[22] A.R.M. Siddique, F. Kratz, S. Mahmud, B. Van Heyst, Energy Conversion by Nanomaterial-Based Trapezoidal-Shaped Leg of Thermoelectric Generator Considering Convection Heat Transfer Effect, ASME. J. Energy Resour. Technol. August 2019; 141(8): 082001, https://doi.org/10.1115/1.4042644.
[23] S. Lin, J. Yu, Optimization of a trapezoid-type two-stage Peltier couples for thermoelectric cooling applications, International Journal of Refrigeration, Vol. 65, 2016, Pages 103-110, ISSN 0140-7007, https://doi.org/10.1016/j.ijrefrig.2015.12.007.
[24] O.I. Ibeagwu, Modelling and comprehensive analysis of TEGs with diverse variable leg geometry, Energy, Vol. 180, 2019, Pages 90-106, ISSN 0360-5442, https://doi.org/10.1016/j.energy.2019.05.088.
[25] X.X. Tian, S. Asaadi, H. Moria, A. Kaood, S. Pourhedayat, K. Jermsittiparsert, Proposing tube-bundle arrangement of tubular thermoelectric module as a novel air cooler, Energy, Vol. 208, 2020, 118428, ISSN 0360-5442, https://doi.org/10.1016/j.energy.2020.118428.
[26] Q. Tan, G. Chen, Y. Sun, B. Duan, G. Li, P. Zhai, Performance of annular thermoelectric couples by simultaneously considering interface layers and boundary conditions, Applied Thermal Engineering, Vol. 174, 2020, 115301, ISSN 1359-4311, https://doi.org/10.1016/j.applthermaleng.2020.115301.

[27] N. Mansouri, E.J. Timm, H.J. Schock, D. Sahoo, A. Kotrba, Development of a Circular Thermoelectric Skutterudite Couple Using Compression Technology, ASME. J. Energy Resour. Technol. September 2016; 138(5): 052003, https://doi.org/10.1115/1.4032619.
[28] S. Asaadi, S. Khalilarya, S. Jafarmadar, A thermodynamic and exergoeconomic numerical study of two-stage annular thermoelectric generator, Applied Thermal Engineering, Vol. 156, 2019, Pages 371-381, ISSN 1359-4311, https://doi.org/10.1016/j.applthermaleng.2019.04.058.
[29] T.H. Kwan, X. Wu, Q. Yao, Complete implementation of the combined TEG-TEC temperature control and energy harvesting system, Control Engineering Practice, Vol. 95, 2020, 104224, ISSN 0967-0661, https://doi.org/10.1016/j.conengprac.2019.104224.
[30] T. Yin, Z.M. Li, P. Peng, W. Liu, Y.Y. Shao, Z.Z. He, Performance analysis of a novel Two-stage automobile thermoelectric generator with the Temperature-dependent materials, Applied Thermal Engineering, Vol. 195, 2021, 117249, ISSN 1359-4311, https://doi.org/10.1016/j.applthermaleng.2021.117249.
[31] M. Chen, S. Lu, B. Liao, On the Figure of Merit of Thermoelectric Generators, ASME. J. Energy Resour. Technol. March 2005; 127(1): 37–41, https://doi.org/10.1115/1.1811120.
[32] S. Lv, Z. Qian, D. Hu, X. Li, W. He, A Comprehensive Review of Strategies and Approaches for Enhancing the Performance of Thermoelectric Module, Energies 13, no. 12: 3142, 2020, https://doi.org/10.3390/en13123142.
[33] Z. Tian, S. Lee, G. Chen, Heat Transfer in Thermoelectric Materials and Devices, ASME. J. Heat Transfer. June 2013; 135(6): 061605, https://doi.org/10.1115/1.4023585.
[34] H.A. Eivari, Z. Sohbatzadeh, P. Mele, M.H.N. Assadi, Low thermal conductivity: fundamentals and theoretical aspects in thermoelectric applications, Materials Today Energy, Vol. 21, 2021, 100744, ISSN 2468-6069, https://doi.org/10.1016/j.mtener.2021.100744.
[35] L. Chen, J. Gong, F. Sun, C. Wu, Effect of heat transfer on the performance of thermoelectric generators, International Journal of Thermal Sciences, Vol. 41, Issue 1, 2002, Pages 95-99, ISSN 1290-0729, https://doi.org/10.1016/S1290-0729(01)01307-2.
[36] P.E. Ruiz-Ortega, M.A. Olivares-Robles, O.Y. Enciso-Montes de Oca, Supercooling in a new two-stage thermoelectric cooler design with phase change material and Thomson effect, Energy Conversion and Management, Vol. 243, 2021, 114355, ISSN 0196-8904, https://doi.org/10.1016/j.enconman.2021.114355.
[37] X. Guo, H. Zhang, J. Wang, J. Zhao, F. Wang, H. Miao, J. Yuan, S. Hou, A new hybrid system composed of high-temperature proton exchange fuel cell and two-stage thermoelectric generator with Thomson effect: Energy and exergy analyses, Energy, Vol. 195, 2020, 117000, ISSN 0360-5442, https://doi.org/10.1016/j.energy.2020.117000.
[38] W. He, S. Wang, Y. Li, Y. Zhao, Structural size optimization on an exhaust exchanger based on the fluid heat transfer and flow resistance characteristics applied to an automotive thermoelectric generator, Energy Conversion and Management, Vol. 129, 2016, Pages 240-249, ISSN 0196-8904, https://doi.org/10.1016/j.enconman.2016.10.032.
[39] Y. Wang, S. Li, Y. Zhang, X. Yang, Y. Deng, C. Su, The influence of inner topology of exhaust heat exchanger and thermoelectric module distribution on the performance of automotive thermoelectric generator, Energy Conversion and Management, Vol. 126, 2016, Pages 266-277, ISSN 0196-8904, https://doi.org/10.1016/j.enconman.2016.08.009.
[40] W. Li, J. Peng, W. Xiao, H. Wang, J. Zeng, J. Xie, Q. Huang, K. Mao, L. Zhang, The temperature distribution and electrical performance of fluid heat exchanger-based

thermoelectric generator, Applied Thermal Engineering, Vol. 118, 2017, Pages 742-747, ISSN 1359-4311, https://doi.org/10.1016/j.applthermaleng.2017.03.022.
[41] X. Ying, F. Ye, R. Liu, H. Bao, Design and Optimization of Thermoelectric Cooling System Under Natural Convection Condition, ASME. J. Thermal Sci. Eng. Appl. October 2018; 10(5): 051008, https://doi.org/10.1115/1.4039926.
[42] Y. Wang, S. Li, X. Xie, Y. Deng, X. Liu, C. Su, Performance evaluation of an automotive thermoelectric generator with inserted fins or dimpled-surface hot heat exchanger, Applied Energy, Vol. 218, 2018, Pages 391-401, ISSN 0306-2619, https://doi.org/10.1016/j.apenergy.2018.02.176.
[43] Z.B. Tang, Y.D. Deng, C.Q. Su, W.W. Shuai, C.J. Xie, A research on thermoelectric generator's electrical performance under temperature mismatch conditions for automotive waste heat recovery system, Case Studies in Thermal Engineering, Vol. 5, 2015, Pages 143-150, ISSN 2214-157X, https://doi.org/10.1016/j.csite.2015.03.006.
[44] J. Gao, Q. Du, M. Chen, B. Li, D. Zhang, Assessing the accuracy of mathematical models used in thermoelectric simulation: Thermal influence of insulated air zone and radiation heat, Applied Thermal Engineering, Vol. 82, 2015, Pages 162-169, ISSN 1359-4311, https://doi.org/10.1016/j.applthermaleng.2015.02.072.
[45] S. Lv, M. Liu, W. He, X. Li, W. Gong, S. Shen, Study of thermal insulation materials influence on the performance of thermoelectric generators by creating a significant effective temperature difference, Energy Conversion and Management, Vol. 207, 2020, 112516, ISSN 0196-8904, https://doi.org/10.1016/j.enconman.2020.112516.
[46] C. Selvam, S. Manikandan, N.V. Krishna, R. Lamba, S.C. Kaushik, O. Mahian, Enhanced thermal performance of a thermoelectric generator with phase change materials, International Communications in Heat and Mass Transfer, Vol. 114, 2020, 104561, ISSN 0735-1933, https://doi.org/10.1016/j.icheatmasstransfer.2020.104561.
[47] H. Lee, J. Sharp, D. Stokes, M. Pearson, S. Priya, Modeling and analysis of the effect of thermal losses on thermoelectric generator performance using effective properties, Applied Energy, Vol. 211, 2018, Pages 987-996, ISSN 0306-2619, https://doi.org/10.1016/j.apenergy.2017.11.096.
[48] M.C. Torrecilla, A. Montecucco, J. Siviter, A.R. Knox, A. Strain, Novel model and maximum power tracking algorithm for thermoelectric generators operated under constant heat flux, Applied Energy, Vol. 256, 2019, 113930, ISSN 0306-2619, https://doi.org/10.1016/j.apenergy.2019.113930.
[49] S. Wang, T. Xie, H. Xie, Experimental study of the effects of the thermal contact resistance on the performance of thermoelectric generator, Applied Thermal Engineering, Vol. 130, 2018, Pages 847-853, ISSN 1359-4311, https://doi.org/10.1016/j.applthermaleng.2017.11.036.
[50] B. Beltrán-Pitarch, J. Maassen, J. García-Cañadas, Comprehensive impedance spectroscopy equivalent circuit of a thermoelectric device which includes the internal thermal contact resistances, Applied Energy, Vol. 299, 2021, 117287, ISSN 0306-2619, https://doi.org/10.1016/j.apenergy.2021.117287.
[51] S. Kim, Analysis and modeling of effective temperature differences and electrical parameters of thermoelectric generators, Applied Energy, Vol. 102, 2013, Pages 1458-1463, ISSN 0306-2619, https://doi.org/10.1016/j.apenergy.2012.09.006.

[52] S. Zheng, X. Du, J. Zhang, Y. Yu, Q. Luo, W. Lu, Monitoring the Thermal Grease Degradation Based on the IGBT Junction Temperature Cooling Curves, IEEE International Power Electronics and Application Conference and Exposition (PEAC), 2018, pp. 1-4, doi: 10.1109/PEAC.2018.8590329.
[53] R. Skuriat, J.F. Li, P.A. Agyakwa, N. Mattey, P. Evans, C.M. Johnson, Degradation of thermal interface materials for high-temperature power electronics applications, Microelectronics Reliability, Volume 53, Issue 12, 2013, Pages 1933-1942, ISSN 0026-2714, https://doi.org/10.1016/j.microrel.2013.05.011.
[54] D. DeVoto, J. Major, P. Paret, G.S. Blackman, A. Wong, J.S. Meth, Degradation characterization of thermal interface greases, 16th IEEE Intersociety Conference on Thermal and Thermomechanical Phenomena in Electronic Systems (ITherm), 2017, pp. 394-399, doi: 10.1109/ITHERM.2017.7992501.
[55] F. Tohidi, S.G. Holagh, A. Chitsaz, Thermoelectric Generators: A comprehensive review of characteristics and applications, Applied Thermal Engineering, Vol. 201, Part A, 2022, 117793, ISSN 1359-4311, https://doi.org/10.1016/j.applthermaleng.2021.117793.
[56] M. Nosek, R. Domański, Simulation of a Thermoelectric Generator with Radioisotope Heat Source as a Long-Lived Energy Source, Journal of KONES Powertrain and Transport, Vol. 23, No. 3, 2016, ISSN: 1231-4005, DOI: 10.5604/12314005.1216596
[57] P. Fleith, A. Cowley, A.C. Pou, A.V. Lozano, R. Frank, P.L. Córdoba, R. González-Cinca, In-situ approach for thermal energy storage and thermoelectricity generation on the Moon: Modelling and simulation, Planetary and Space Science, Vol. 181, 2020, 104789, ISSN 0032-0633, https://doi.org/10.1016/j.pss.2019.104789.
[58] M. Karvonen, R. Kapoor, A. Uusitalo, V. Ojanen, Technology competition in the internal combustion engine waste heat recovery: a patent landscape analysis, Journal of Cleaner Production, Vol. 112, Part 5, 2016, Pages 3735-3743, ISSN 0959-6526, https://doi.org/10.1016/j.jclepro.2015.06.031.
[59] E.S. Mohamed, Development and performance analysis of a TEG system using exhaust recovery for a light diesel vehicle with assessment of fuel economy and emissions, Applied Thermal Engineering, Vol. 147, 2019, Pages 661-674, ISSN 1359-4311, https://doi.org/10.1016/j.applthermaleng.2018.10.100.
[60] C.Q. Su, W.S. Wang, X. Liu, Y.D. Deng, Simulation and experimental study on thermal optimization of the heat exchanger for automotive exhaust-based thermoelectric generators, Case Studies in Thermal Engineering, Vol. 4, 2014, Pages 85-91, ISSN 2214-157X, https://doi.org/10.1016/j.csite.2014.06.002.
[61] R. Wang, W. Yu, X. Meng, Performance investigation and energy optimization of a thermoelectric generator for a mild hybrid vehicle, Energy, Vol. 162, 2018, Pages 1016-1028, ISSN 0360-5442, https://doi.org/10.1016/j.energy.2018.08.103.
[62] A. Royale, M. Simic, P. Lappas, P. Schiffer, R. Palaniswamy, Novel, shape optimised, TEG subsystem design, Procedia Computer Science, Vol. 159, 2019, Pages 2607-2615, ISSN 1877-0509, https://doi.org/10.1016/j.procs.2019.09.255.
[63] Q. Hussain, D. Brigham, C. Maranville, Thermoelectric Exhaust Heat Recovery for Hybrid Vehicles, SAE Int. J. Engines 2(1):1132-1142, 2009, ISSN: 1946-3936, https://doi.org/10.4271/2009-01-1327.

[64] A. Massaguer, E. Massaguer, M. Comamala, T. Pujol, J.R. González, M.D. Cardenas, D. Carbonell, A.J. Bueno, A method to assess the fuel economy of automotive thermoelectric generators, Applied Energy, Vol. 222, 2018, Pages 42-58, ISSN 0306-2619, https://doi.org/10.1016/j.apenergy.2018.03.169.
[65] K. Charilaou, T. Kyratsi, L.S. Louca, Design of an air-cooled thermoelectric generator system through modelling and simulations, for use in cement industries, Materials Today: Proceedings, Vol. 44, Part 4, 2021, Pages 3516-3524, ISSN 2214-7853, https://doi.org/10.1016/j.matpr.2020.11.392.
[66] G. Omer, A.H. Yavuz, R. Ahiska, K.E. Calisal, Smart thermoelectric waste heat generator: Design, simulation and cost analysis, Sustainable Energy Technologies and Assessments, Vol. 37, 2020, 100623, ISSN 2213-1388, https://doi.org/10.1016/j.seta.2019.100623.
[67] J.L. Wang, J.Y. Wu, C.Y. Zheng, Simulation and evaluation of a CCHP system with exhaust gas deep-recovery and thermoelectric generator, Energy Conversion and Management, Vol. 86, 2014, Pages 992-1000, ISSN 0196-8904, https://doi.org/10.1016/j.enconman.2014.06.036.
[68] J.F. Carneiro, F. Gomes de Almeida, Model and simulation of the energy retrieved by thermoelectric generators in an underwater glider, Energy Conversion and Management, Vol. 163, 2018, Pages 38-49, ISSN 0196-8904, https://doi.org/10.1016/j.enconman.2018.02.031.
[69] S. Addanki, D. Nedumaran, Simulation and fabrication of thermoelectric generators for hand held electronic gadgets, Materials Science and Engineering: B, Vol. 251, 2019, 114453, ISSN 0921-5107, https://doi.org/10.1016/j.mseb.2019.114453.
[70] J. Yuan, R. Zhu, A fully self-powered wearable monitoring system with systematically optimized flexible thermoelectric generator, Applied Energy, Vol. 271, 2020, 115250, ISSN 0306-2619, https://doi.org/10.1016/j.apenergy.2020.115250.
[71] G. Li, S. Shittu, T.M.O. Diallo, M. Yu, X. Zhao, J. Ji, A review of solar photovoltaic-thermoelectric hybrid system for electricity generation, Energy, Vol. 158, 2018, Pages 41-58, ISSN 0360-5442, https://doi.org/10.1016/j.energy.2018.06.021.
[72] Q. Zhao, H. Zhang, Z. Hu, S. Hou, Achieving a broad-spectrum photovoltaic system by hybridizing a two-stage thermoelectric generator, Energy Conversion and Management, Vol. 211, 2020, 112778, ISSN 0196-8904, https://doi.org/10.1016/j.enconman.2020.112778.
[73] S. Mahmoudinezhad, A. Rezania, L.A. Rosendahl, Behavior of hybrid concentrated photovoltaic-thermoelectric generator under variable solar radiation, Energy Conversion and Management, Vol. 164, 2018, Pages 443-452, ISSN 0196-8904, https://doi.org/10.1016/j.enconman.2018.03.025.
[74] J. Darkwa, J. Calautit, D. Du, G. Kokogianakis, A numerical and experimental analysis of an integrated TEG-PCM power enhancement system for photovoltaic cells, Applied Energy, Vol. 248, 2019, Pages 688-701, ISSN 0306-2619, https://doi.org/10.1016/j.apenergy.2019.04.147.
[75] R. Bjørk, K.K. Nielsen, The maximum theoretical performance of unconcentrated solar photovoltaic and thermoelectric generator systems, Energy Conversion and Management, Vol. 156, 2018, Pages 264-268, ISSN 0196-8904, https://doi.org/10.1016/j.enconman.2017.11.009.
[76] D.N. Kossyvakis, G.D. Voutsinas, E.V. Hristoforou, Experimental analysis and performance evaluation of a tandem photovoltaic–thermoelectric hybrid system, Energy Conversion and Management, Vol. 117, 2016, Pages 490-500, ISSN 0196-8904, https://doi.org/10.1016/j.enconman.2016.03.023.

[77] P. Niemann, G. Schmitz, Air conditioning system with enthalpy recovery for space heating and air humidification: An experimental and numerical investigation, Energy, Vol. 213, 2020, 118789, ISSN 0360-5442, https://doi.org/10.1016/j.energy.2020.118789.
[78] J. Jia, W.L. Lee, Y. Cheng, Q. Tian, Can reversible room air-conditioner be used for combined space and domestic hot water heating in subtropical dwellings? Techno-economic evidence from Hong Kong, Energy, Vol. 223, 2021, 119911, ISSN 0360-5442, https://doi.org/10.1016/j.energy.2021.119911.
[79] A. Martinez, S. Díaz de Garayo, P. Aranguren, M. Araiz, L. Catalán, Simulation of thermoelectric heat pumps in nearly zero energy buildings: Why do all models seem to be right?, Energy Conversion and Management, Vol. 235, 2021, 113992, ISSN 0196-8904, https://doi.org/10.1016/j.enconman.2021.113992.
[80] A. Martinez, S. Díaz de Garayo, P. Aranguren, D. Astrain, Assessing the reliability of current simulation of thermoelectric heat pumps for nearly zero energy buildings: Expected deviations and general guidelines, Energy Conversion and Management, Vol. 198, 2019, 111834, ISSN 0196-8904, https://doi.org/10.1016/j.enconman.2019.111834.
[81] S. Díaz de Garayo, A. Martínez, D. Astrain, Annual energy performance of a thermoelectric heat pump combined with a heat recovery unit to HVAC one passive house dwelling, Applied Thermal Engineering, Vol. 204, 2022, 117832, ISSN 1359-4311, https://doi.org/10.1016/j.applthermaleng.2021.117832.
[82] Z.B. Liu, L. Zhang, G.C. Gong, Experimental evaluation of a solar thermoelectric cooled ceiling combined with displacement ventilation system, Energy Conversion and Management, Vol. 87, 2014, Pages 559-565, ISSN 0196-8904, https://doi.org/10.1016/j.enconman.2014.07.051.
[83] H. Sun, B. Lin, Z. Lin, Y. Zhu, H. Li, X. Wu, Research on a radiant heating terminal integrated with a thermoelectric unit and flat heat pipe, Energy and Buildings, Vol. 172, 2018, Pages 209-220, ISSN 0378-7788, https://doi.org/10.1016/j.enbuild.2018.04.054.
[84] M.S. Oh, J.H. Ahn, D.W. Kim, D.S. Jang, Y. Kim, Thermal comfort and energy saving in a vehicle compartment using a localized air-conditioning system, Applied Energy, Vol. 133, 2014, Pages 14-21, ISSN 0306-2619, https://doi.org/10.1016/j.apenergy.2014.07.089.
[85] A. Attar, H.S. Lee, Designing and testing the optimum design of automotive air-to-air thermoelectric air conditioner (TEAC) system, Energy Conversion and Management, Vol. 112, 2016, Pages 328-336, ISSN 0196-8904, https://doi.org/10.1016/j.enconman.2016.01.029.
[86] M.Z. Yilmazoglu, Experimental and numerical investigation of a prototype thermoelectric heating and cooling unit, Energy and Buildings, Vol. 113, 2016, Pages 51-60, ISSN 0378-7788, https://doi.org/10.1016/j.enbuild.2015.12.046.
[87] Y. Lyu, A.R.M. Siddique, S.H. Majid, M. Biglarbegian, S.A. Gadsden, S. Mahmud, Electric vehicle battery thermal management system with thermoelectric cooling, Energy Reports, Vol. 5, 2019, Pages 822-827, ISSN 2352-4847, https://doi.org/10.1016/j.egyr.2019.06.016.
[88] Y. Ran, Y. Deng, T. Hu, C. Su, X. Liu, Energy Efficient Thermoelectric Generator-Powered Localized Air-Conditioning System Applied in a Heavy-Duty Vehicle. ASME. J. Energy Resour. Technol. July 2018; 140(7): 072007, https://doi.org/10.1115/1.4039607.
[89] R. Ji, T. Pan, G. Peng, J. Ma, N. Yang, Q. Hao, An integrated thermoelectric heating-cooling system for air sterilization— a simulation study, Materials Today Physics, Vol. 19, 2021, 100430, ISSN 2542-5293, https://doi.org/10.1016/j.mtphys.2021.100430.

[90] O. Yeler, M.F. Koseoglu, Energy efficiency and transient-steady state performance comparison of a resistance infant incubator and an improved thermoelectric infant incubator, Engineering Science and Technology, an International Journal, Vol. 31, 2022, 101055, ISSN 2215-0986, https://doi.org/10.1016/j.jestch.2021.09.001.
[91] S.H. Zaferani, M.W. Sams, R. Ghomashchi, Z.G. Chen, Thermoelectric coolers as thermal management systems for medical applications: Design, optimization, and advancement, Nano Energy, Vol. 90, Part A, 2021, 106572, ISSN 2211-2855, https://doi.org/10.1016/j.nanoen.2021.106572.
[92] S. Alshehri, Cooling Microprocessors with Commercial Thermoelectric Module Powered by Pulsed Current, International Journal of Advanced Trends in Computer Science and Engineering, Vol. 9, No.4, 2020, ISSN 2278-3091, https://doi.org/10.30534/ijatcse/2020/185942020.
[93] M.P. Gupta, M. Sayer, S. Mukhopadhyay, S. Kumar, Ultrathin Thermoelectric Devices for On-Chip Peltier Cooling, IEEE Transactions on Components, Packaging and Manufacturing Technology, Vol. 1, No. 9, pp. 1395-1405, September 2011, doi: 10.1109/TCPMT.2011.2159304.
[94] L. Shen, H. Chen, F. Xiao, Y. Yang, S. Wang, The step-change cooling performance of miniature thermoelectric module for pulse laser, Energy Conversion and Management, Vol. 80, 2014, Pages 39-45, ISSN 0196-8904, https://doi.org/10.1016/j.enconman.2014.01.003.
[95] M. Maaspuro, Experimenting and Simulating Thermoelectric Cooling of an LED Module, International Journal of Online and Biomedical Engineering (iJOE), Vol. 11, No. 4, 2015, eISSN: 2626-8493, https://doi.org/10.3991/ijoe.v11i4.4692.
[96] A. Gabriel-Buenaventura, B. Azzopardi, Energy recovery systems for retrofitting in internal combustion engine vehicles: A review of techniques, Renewable and Sustainable Energy Reviews, Vol. 41, 2015, Pages 955-964, ISSN 1364-0321, https://doi.org/10.1016/j.rser.2014.08.083.
[97] R. Saidur, M. Rezaei, W.K. Muzammil, M.H. Hassan, S. Paria, M. Hasanuzzaman, Technologies to recover exhaust heat from internal combustion engines, Renewable and Sustainable Energy Reviews, Vol. 16, Issue 8, 2012, Pages 5649-5659, ISSN 1364-0321, https://doi.org/10.1016/j.rser.2012.05.018.
[98] G. Li, J.G. Fernandez, D.A.L. Ramos, V. Barati, N. Pérez, I. Soldatov, H. Reith, G. Schierning, K. Nielsch, Integrated microthermoelectric coolers with rapid response time and high device reliability, Nature Electron 1, 555–561, 2018, https://doi.org/10.1038/s41928-018-0148-3.
[99] Z. Zhao, Z. Zuo, W. Wang, R. Liu, N. Kuang, Performance optimization for a combustion-based micro thermoelectric generator with two-stage thermoelectric module, Applied Thermal Engineering, Vol. 198, 2021, 117464, ISSN 1359-4311, https://doi.org/10.1016/j.applthermaleng.2021.117464.
[100] F. Zhang, L. Cheng, M. Wu, X. Xu, P. Wang, Z. Liu, Performance analysis of two-stage thermoelectric generator model based on Latin hypercube sampling, Energy Conversion and Management, Vol. 221, 2020, 113159, ISSN 0196-8904, https://doi.org/10.1016/j.enconman.2020.113159.
[101] F. Meng, L. Chen, F. Sun, Performance optimization for two-stage thermoelectric refrigerator system driven by two-stage thermoelectric generator, Cryogenics, Vol. 49, Issue 2, 2009, Pages 57-65, ISSN 0011-2275, https://doi.org/10.1016/j.cryogenics.2008.11.005.

[102] M.A. Olivares-Robles, F. Vazquez, C. Ramirez-Lopez, Optimization of Two-Stage Peltier Modules: Structure and Exergetic Efficiency, Entropy, 2012, 14, 1539-1552. https://doi.org/10.3390/e14081539
[103] T.H. Wang, Q.H. Wang, C. Leng, X.D. Wang, Parameter analysis and optimal design for two-stage thermoelectric cooler, Applied Energy, Vol. 154, 2015, Pages 1-12, ISSN 0306-2619, https://doi.org/10.1016/j.apenergy.2015.04.104.
[104] Y. Huang, Z. Chen, H. Ding, Performance optimization of a two-stage parallel thermoelectric cooler with inhomogeneous electrical conductivity, Applied Thermal Engineering, Vol. 192, 2021, 116696, ISSN 1359-4311, https://doi.org/10.1016/j.applthermaleng.2021.116696.
[105] H. Lv, X.D. Wang, J.H. Meng, T.H. Wang, W.M. Yan, Enhancement of maximum temperature drop across thermoelectric cooler through two-stage design and transient supercooling effect, Applied Energy, Vol. 175, 2016, Pages 285-292, ISSN 0306-2619, https://doi.org/10.1016/j.apenergy.2016.05.035.
[106] H. Sun, Y. Ge, W. Liu, Z. Liu, Geometric optimization of two-stage thermoelectric generator using genetic algorithms and thermodynamic analysis, Energy, Vol. 171, 2019, Pages 37-48, ISSN 0360-5442, https://doi.org/10.1016/j.energy.2019.01.003.
[107] J. Chen, Y. Zhou, H. Wang, J.T. Wang, Comparison of the optimal performance of single- and two-stage thermoelectric refrigeration systems, Applied Energy, Vol. 73, Issues 3–4, 2002, Pages 285-298, ISSN 0306-2619, https://doi.org/10.1016/S0306-2619(02)00120-4.
[108] D.D. Kamasi, M. Zainulloh, A. Nadhir, S.P. Sakti, Comparison between two-stage and three-stage Peltier thermoelectric coolers driven by pulse width modulation, J. Phys.: Conf. Ser. 1528, 012020, IOP Publishing, 2020, doi:10.1088/1742-6596/1528/1/012020
[109] E. Kanimba, M. Pearson, J. Sharp, D. Stokes, S. Priya, Z. Tian, A modeling comparison between a two-stage and three-stage cascaded thermoelectric generator, Journal of Power Sources, Vol. 365, 2017, Pages 266-272, ISSN 0378-7753, https://doi.org/10.1016/j.jpowsour.2017.08.091.
[110] T.J. Hendricks, Thermal System Interactions in Optimizing Advanced Thermoelectric Energy Recovery Systems, ASME. J. Energy Resour. Technol. September 2007, 129(3): 223–231, https://doi.org/10.1115/1.2751504.
[111] D.T. Crane, L.E. Bell, Design to Maximize Performance of a Thermoelectric Power Generator With a Dynamic Thermal Power Source, ASME. J. Energy Resour. Technol. March 2009, 131(1): 012401, https://doi.org/10.1115/1.3066392.
[112] G.B. Abdallah, S. Besbes, H.B. Aissia, J. Jay, Analysis of the effect of a pulsed heat flux on the performance improvements of a thermoelectric generator, Applied Thermal Engineering, Vol. 158, 2019, 113728, ISSN 1359-4311, https://doi.org/10.1016/j.applthermaleng.2019.113728.
[113] Y. Cai, A. Rezania, F. Deng, L. Rosendahl, J. Chen, Comprehensive experimental study of thermoelectric generators under transient boundary conditions, Energy Conversion and Management, Vol. 245, 2021, 114561, ISSN 0196-8904, https://doi.org/10.1016/j.enconman.2021.114561.
[114] D. Luo, Y. Yan, R. Wang, W. Zhou, Numerical investigation on the dynamic response characteristics of a thermoelectric generator module under transient temperature excitations, Renewable Energy, Vol. 170, 2021, Pages 811-823, ISSN 0960-1481, https://doi.org/10.1016/j.renene.2021.02.026.

[115] E. Yazdanshenas, A. Rezania, M.K. Rad, L. Rosendahl, Electrical response of thermoelectric generator to geometry variation under transient thermal boundary condition editors-pick, Journal of Renewable and Sustainable Energy, Vol. 10, 064705, 2018, https://doi.org/10.1063/1.5040166.
[116] W. Li, M.C. Paul, A. Montecucco, J. Siviter, A.R. Knox, T. Sweet, M. Gao, H. Baig, T.K. Mallick, G. Han, D.H. Gregory, F. Azough, R. Freer, Multiphysics simulations of thermoelectric generator modules with cold and hot blocks and effects of some factors, Case Studies in Thermal Engineering, Vol. 10, 2017, Pages 63-72, ISSN 2214-157X, https://doi.org/10.1016/j.csite.2017.03.005.
[117] E. Söylemez, E. Alpman, A. Onat, S. Hartomacıoğlu, CFD analysis for predicting cooling time of a domestic refrigerator with thermoelectric cooling system, International Journal of Refrigeration, Vol. 123, 2021, Pages 138-149, ISSN 0140-7007, https://doi.org/10.1016/j.ijrefrig.2020.11.012.
[118] J. Yu, H. Zhu, L. Kong, H. Wang, J. Su, Q. Zhu, Analysis of Nonlinear Transient Energy Effect on Thermoelectric Energy Storage Structure, Materials 13, no. 16: 3639, 2020, https://doi.org/10.3390/ma13163639.
[119] M. Nesarajah, F. Felgner, G. Frey, Modeling and simulation of a thermoelectric Energy Harvesting System for control design purposes, Proceedings of the 16th International Conference on Mechatronics, 2014, pp. 170-177, doi: 10.1109/MECHATRONIKA.2014.7018254.
[120] J.H. Meng, X.D. Wang, X.X. Zhang, Transient modeling and dynamic characteristics of thermoelectric cooler, Applied Energy, Vol. 108, 2013, Pages 340-348, ISSN 0306-2619, https://doi.org/10.1016/j.apenergy.2013.03.051.
[121] L.M. Shen, F. Xiao, H.X. Chen, S.W. Wang, Numerical and experimental analysis of transient supercooling effect of voltage pulse on thermoelectric element, International Journal of Refrigeration, Vol. 35, Issue 4, 2012, Pages 1156-1165, ISSN 0140-7007, https://doi.org/10.1016/j.ijrefrig.2012.02.004.
[122] J.N. Mao, H.X. Chen, H. Jia, X.L. Qian, The transient behavior of Peltier junctions pulsed with supercooling, Journal of Applied Physics, Vol. 112, Issue 1, 2012, https://doi.org/10.1063/1.4735469.
[123] G.J. Snyder, J.P. Fleurial, T. Caillat, Supercooling of Peltier cooler using a current pulse, Journal of Applied Physics, Vol. 92, Issue 3, 2002, https://doi.org/10.1063/1.1489713.
[124] M. Ma, J. Yu, A numerical study on the temperature overshoot characteristic of a realistic thermoelectric module under a current pulse operation, International Journal of Heat and Mass Transfer, Vol. 72, 2014, Pages 234-241, ISSN 0017-9310, https://doi.org/10.1016/j.ijheatmasstransfer.2014.01.017.
[125] M. Ma, J. Yu, J. Chen, An investigation on thermoelectric coolers operated with continuous current pulses, Energy Conversion and Management, Vol. 98, 2015, Pages 275-281, ISSN 0196-8904, https://doi.org/10.1016/j.enconman.2015.03.105.
[126] S.L. Wang, H.B. Liu, Y.W. Gao, Y. Shen, Y.R. Yang, X.D. Wang, D.J. Lee, Transient supercooling performance of thermoelectric coolers with a continuous double current pulse, Journal of the Taiwan Institute of Chemical Engineers, Vol. 120, 2021, Pages 127-135, ISSN 1876-1070, https://doi.org/10.1016/j.jtice.2021.02.030.
[127] Y.W. Gao, H. Lv, X.D. Wang, W.M. Yan, Enhanced Peltier cooling of two-stage thermoelectric cooler via pulse currents, International Journal of Heat and

Mass Transfer, Vol. 114, 2017, Pages 656-663, ISSN 0017-9310, https://doi.org/10.1016/j.ijheatmasstransfer.2017.06.102.
[128] J.H. Meng, H.C. Wu, D.Y. Gao, Z. Kai, G. Lu, W.M. Yan, A novel super-cooling enhancement method for a two-stage thermoelectric cooler using integrated triangular-square current pulses, Energy, Vol. 217, 2021, 119360, ISSN 0360-5442, https://doi.org/10.1016/j.energy.2020.119360.
[129] Y.W. Gao, C.L. Shi, X.D. Wang, Numerical analysis for transient supercooling effect of pulse current shapes on a two-stage thermoelectric cooler, Applied Thermal Engineering, Vol. 163, 2019, 114416, ISSN 1359-4311, https://doi.org/10.1016/j.applthermaleng.2019.114416.
[130] T.T. Lam, W.K. Yeung, Pulsed current effect on the performance of conical inhomogeneous thermoelectrics, Thermal Science and Engineering Progress, Vol. 22, 2021, 100747, ISSN 2451-9049, https://doi.org/10.1016/j.tsep.2020.100747.
[131] R. Yang, G. Chen, A.R. Kumar, G.J. Snyder, J.P. Fleurial, Transient cooling of thermoelectric coolers and its applications for microdevices, Energy Conversion and Management, Vol. 46, Issues 9–10, 2005, Pages 1407-1421, ISSN 0196-8904, https://doi.org/10.1016/j.enconman.2004.07.004.
[132] P.E. Ruiz-Ortega, M.A. Olivares-Robles, Peltier Supercooling in Transient Thermoelectrics: Spatial Temperature Profile and Characteristic Cooling Length, Entropy (Basel), 21(3):226, 2019, doi: 10.3390/e21030226.
[133] M.C. Torrecilla, A. Montecucco, J. Siviter, A. Strain, A.R. Knox, Transient response of a thermoelectric generator to load steps under constant heat flux, Applied Energy, Volume 212, 2018, Pages 293-303, ISSN 0306-2619, https://doi.org/10.1016/j.apenergy.2017.12.010.
[134] A. Montecucco, J. Siviter, A.R. Knox, Constant heat characterisation and geometrical optimisation of thermoelectric generators, Applied Energy, Vol. 149, 2015, Pages 248-258, ISSN 0306-2619, https://doi.org/10.1016/j.apenergy.2015.03.120.
[135] R.D. Pierce, R.J. Stevens, Experimental Comparison of Thermoelectric Module Characterization Methods, J. Electron. Mater. 44, 1796–1802, 2015, https://doi.org/10.1007/s11664-014-3559-6.
[136] E.A. Man, E. Schaltz, L. Rosendahl, A. Rezaniakolaei, D. Platzek, A High Temperature Experimental Characterization Procedure for Oxide-Based Thermoelectric Generator Modules under Transient Conditions, Energies 8, no. 11: 12839-12847, 2015. https://doi.org/10.3390/en81112341.
[137] R.D. Pierce, R.J. Stevens, Measuring thermal substrate resistance and impact on the characterization of thermoelectric modules, Measurement, Vol. 111, 2017, Pages 173-182, ISSN 0263-2241, https://doi.org/10.1016/j.measurement.2017.07.015.
[138] D. Luo, R. Wang, W. Yu, W. Zhou, Performance evaluation of a novel thermoelectric module with BiSbTeSe-based material, Applied Energy, Vol. 238, 2019, Pages 1299-1311, ISSN 0306-2619, https://doi.org/10.1016/j.apenergy.2019.01.139.

ABSTRACT

The dissertation addresses the issue of simulating the operation of systems equipped with thermoelectric modules. A distinctive quality of the research was consideration of the thermal resistance occurring between the thermoelectric junction and the heat exchanger. The theoretical basics of thermoelectric phenomena are shown and their characteristic features and mutual implications are discussed. The dissertation also presents their possible applications. The structure of the thermoelectric module is discussed, and the effect of the module geometric and material characteristics is described. Example simulations are presented of thermoelectric modules operating both as heat pumps and as electricity generators using the applied temperature gradient and the resulting heat flow.

A method was developed of determining parameters of the thermoelectric module and thermal resistance in the system using transient-state measurements that make use of the significant differences in the inertia of the thermal and the electric field. The developed methodology makes it possible to find the theoretical maxima of the system operating parameters and answers the question about the reasonableness of actions aiming to improve thermal contact in the system. The degradation of this contact can also be assessed over time. Also presented is the constructed test stand, which enables comprehensive evaluation of thermoelectric modules in any operating states and in a very wide range of parameters. The stand is fully automated, abundantly metered and computer-controlled using controllers.

In order to perform numerical simulations of the operation of systems using thermoelectric modules, multifunctional software based on developed analytical models was prepared. The software enables simulations of transient-state operation of one- and multi-stage systems. It is fitted out with procedures for designing and analysing the system geometrical features, as well as optimizing its operating conditions. The software was used to perform a number of numerical simulations of thermoelectric systems operating in the mode of both an electricity generator and a heat pump. The software was also validated experimentally on the aforementioned test stand.

First, the operation of the thermoelectric generator system was analysed for a wide range of contact thermal resistances. The effect of the resistance magnitude on the thermoelectric junction temperatures, maximum power and maximum efficiency was determined, and the optimal values of the electric current in terms of the maximization of the module power or efficiency were established.

The next step was to simulate the system of a two-stage thermoelectric cooler. The cooler operating characteristics and the ability to reach temperatures lower than those achievable in the steady state – the supercooling effect – were investigated. The system was optimized in terms of the selection of the number of thermoelectric legs for each stage to ensure temperature minimization and in terms of electric current shaping. The calculations were carried out for two different values of contact thermal resistance, and the performance of the optimized one- and two-stage system was compared.

Next, a concept of a thermoelectric air conditioner built using commercially available modules was presented. The parameters of the modules were determined independently on the

constructed test stand, and the results of the performed numerical simulations were validated experimentally. Economic analyses were also conducted of the proposed system, taking account of investment costs in the form of the purchase of modules and heat exchangers, along with the operating cost related to the consumption of electricity over the assumed lifetime of the device. The simulations in this regard were carried out with a varying number of thermoelectric modules, various dimensions of the heat exchangers and different values of the power supply so that the maximum cooling efficiency factor could be obtained. The efficiency related to the total cost was evaluated using the introduced $ETCC$ indicator. The calculations were performed in a wide range of electricity costs and a set difference between the outdoor temperature and the temperature of the air-conditioned room. Moreover, independent calculations were made assuming the possibility of modifying the geometry of the module internal elements. The possibility of increasing the cooling power at the expense of a reduction in the value of the economic cooling efficiency factor was investigated.

A thermoelectric device for waste heat recovery by means of electricity generation was simulated for a system installed at the exhaust of an internal combustion engine. The calculations were carried out using a specialist AVL BOOST software intended for modelling the operation of internal combustion engines, in which an own module analysing the operation of the thermoelectric heat recovery system was implemented. These tests were carried out for a motorcycle engine, where it was checked how the number of the proposed heat recovery segments affected the amount of the produced electricity depending on the internal combustion engine operating parameters. Next, calculations were performed for a passenger car engine during simulated driving cycles. The calculations took account of the thermal capacity of the heat exchanger placed between the thermoelectric modules and the flowing exhaust gas. Tests were performed to establish the impact of the heat exchanger thermal capacity on the amount of recovered energy, and the capacity optimal value was determined for assumed criteria.

STRESZCZENIE

Dysertacja podejmuje zagadnienie symulacji pracy układów wyposażonych w moduły termoelektryczne. Cechą przeprowadzonych badań było uwzględnienie oporu termicznego pomiędzy złączem termoelektrycznym, a wymiennikiem ciepła. Pokazano podstawy teoretyczne zjawisk termoelektrycznych, umówiono ich cechy oraz wzajemne implikacje. Przedstawiono również ich możliwe zastosowania. Omówiono budowę modułu termoelektrycznego wraz z opisem wpływu jego cech geometrycznych i materiałowych. Zaprezentowano przykładowe symulacje zarówno modułów termoelektrycznych pracujących w trybie pompy ciepła, jak również generatora energii elektrycznej z wykorzystaniem przyłożonego gradientu temperatury i wynikającego z tego przepływu ciepła.

W ramach badań opracowano sposób wyznaczania parametrów modułu termoelektrycznego oraz oporu termicznego w układzie z użyciem pomiarów stanów przejściowych, wykorzystujących znaczne różnice w bezwładności pól: termicznego i elektrycznego. Opracowana metodologia pozwala na wyznaczenie teoretycznych maksimów parametrów pracy układu oraz odpowiada na pytanie o zasadność działań zmierzających do poprawy kontaktu termicznego w układzie. Można także ocenić degradację tego kontaktu w czasie. Przedstawiono również wykonane stanowisko badawcze, które umożliwia kompleksową ocenę modułów termoelektrycznych w dowolnych stanach pracy i bardzo szerokim zakresie parametrów. Jest ono w pełni zautomatyzowane, bogato opomiarowane i sterowane komputerowo z wykorzystaniem regulatorów.

Do prowadzenia symulacji numerycznych pracy układów wykorzystujących moduły termoelektryczne przygotowano wielofunkcyjne oprogramowanie bazujące na opracowanych modelach analitycznych. Umożliwia ono symulacje pracy układów w warunkach nieustalonych dla układów jedno- i wielostopniowych. Oprogramowanie wyposażono w procedury analizy i projektowania cech geometrycznych układu, jak i optymalizacji warunków jego pracy. Za jego pomocą przeprowadzono szereg symulacji układów termoelektrycznych pracujących zarówno w trybie generacji elektryczności, jak i pompy ciepła. Oprogramowanie zostało również zwalidowane eksperymentalnie na opisanym stanowisku badawczym.

W pierwszej kolejności, przeprowadzono analizy pracy układu generatora termoelektrycznego dla szerokiego spektrum kontaktowych oporów termicznych. Określono wpływ wielkości oporu na temperatury złączy termoelektrycznych, maksymalne wartości mocy i sprawności oraz optymalne wartości prądu w obwodzie i oporu elektrycznego odbiornika mocy.

Następnie zasymulowano układ dwustopniowej chłodziarki termoelektrycznej. Zbadano jej charakterystyki pracy oraz zdolność do osiągania temperatur niższych niż osiągalna w stanie ustalonym – supercooling. Przeprowadzono optymalizację układu polegającą na doborze liczby słupków termoelektrycznych dla każdego stopnia ze względu na minimalizację temperatury oraz kształtowaniem przebiegów prądu. Obliczenia przeprowadzono dla dwóch różnych wartości kontaktowego oporu termicznego oraz porównano wskaźniki pracy zoptymalizowanych układów jedno- i dwustopniowego.

Dalej, zaprezentowano także koncepcję klimatyzatora termoelektrycznego zbudowanego w oparciu o dostępne na rynku moduły. Parametry modułów wyznaczono samodzielnie na

zbudowanym stanowisku badawczym, a wyniki symulacji numerycznych zwalidowano eksperymentalnie. Przeprowadzono również analizy ekonomiczne zaproponowanego układu uwzględniające koszty inwestycyjne w postaci zakupu modułów i wymienników ciepła oraz koszt eksploatacyjny związany ze zużyciem energii elektrycznej w założonym okresie życia urządzenia. Przeprowadzone w tym zakresie symulacje obejmowały zmienną liczbę modułów termoelektrycznych, wymiary wymienników ciepła oraz wartość mocy zasilającej tak, aby uzyskać maksymalny wskaźnik efektywności chłodniczej. Oceny efektywności odniesionej do kosztów całkowitych dokonywano za pomocą wprowadzonego wskaźnika $ETCC$. Obliczenia prowadzone były w szerokim zakresie kosztów energii elektrycznej oraz zadanej różnicy temperatury zewnętrznej i klimatyzowanego pomieszczenia. Ponadto, wykonano niezależne obliczenia przy założeniu możliwości modyfikacji geometrii wewnętrznych elementów modułu. Zbadano możliwość zwiększenia mocy chłodzącej kosztem zmniejszenia wartości wskaźnika ekonomicznej efektywności chłodniczej.

Symulacje urządzenia termoelektrycznego służącego do odzysku ciepła odpadowego poprzez produkcję elektryczności przeprowadzono dla urządzenia zabudowanego w układzie wylotowym silnika spalinowego. Obliczenia prowadzono za pomocą specjalistycznego oprogramowania służącego do modelowania pracy silników spalinowych - AVL Boost, w którym zaimplementowano własny skrypt służący do analizy pracy termoelektrycznego układu odzysku ciepła. Badania te przeprowadzono dla silnika motocyklowego, gdzie sprawdzono jak liczba zaproponowanych segmentów odzysku ciepła wpływa na ilość produkowanej energii elektrycznej w funkcji parametrów pracy silnika spalinowego. Następnie, obliczenia przeprowadzono dla silnika samochodu osobowego w znormalizowanych cyklach jazdy. Uwzględniono w takim wypadku także pojemność cieplną wymiennika znajdującego się pomiędzy modułami termoelektrycznymi a przepływającymi spalinami. Zbadano wpływ tej pojemności cieplnej na ilość odzyskiwanej energii oraz określono jej optymalną wartość przy założonych kryteriach.

APPENDICES

Applied Energy 293 (2021) 116943

Contents lists available at ScienceDirect

Applied Energy

journal homepage: www.elsevier.com/locate/apenergy

Mathematical model of a thermoelectric system based on steady- and rapid-state measurements

Ryszard Buchalik [a,*], Grzegorz Nowak [a], Iwona Nowak [b]

[a] Department of Power Engineering and Turbomachinery, Silesian University of Technology, Konarskiego 18, 44-100 Gliwice, Poland
[b] Department of Applications of Mathematical and Artificial Intelligence Methods, Silesian University of Technology, Kaszubska 23, 44-100 Gliwice, Poland

ARTICLE INFO

Keywords:
Thermoelectric generator
Heat transfer
Thermal resistance
Rapid measurement

ABSTRACT

The paper presents the development of a complete analytical model of a thermoelectric generator (TEG). Based on data coming from a small number of easily obtainable measurements, the model makes it possible to determine basic parameters of the TEG. Owing to measurements performed in the steady state and immediately after a rapid change of the TEG electrical state, the following quantities can be established analytically: the Seebeck coefficient, thermal conductivity and thermal resistance between heat exchangers and the TEG. The applied *rapid* method is based on the large difference in inertia between the electric and the thermal field. A rapid change from the short-circuit to the open-circuit electrical state makes it possible to record the voltage for the system thermal state corresponding to the short circuit. Experimental tests were carried out on a commercially available thermoelectric generator and the results proved the developed model usefulness. The simulation results show that the thermal resistance of the contact layers between the heat exchangers and the thermoelectric generators caused a loss of the temperature difference of the junctions from 30% at the recommended mechanical load to even over 50% if the clamping force was too low. Due to that, the determined power ratio, being an indicator of the utilization of the theoretical power capacity of a system burdened with thermal resistance, reaches values lower than 40% for the required clamping force and is below 20% for improper contact conditions The impact of the accuracy of the measurements on the values of the system parameters obtained from the model is evaluated by means of sensitivity analysis.

1. Introduction

The intensive development of civilization in recent decades has resulted in enormous demand for energy. This relates not only to electricity but also to heat and, to a large extent, to energy needed to drive vehicles. Nowadays, most of the energy is generated by firing fossil fuels [1], which results in high emissions of pollutants into the environment and causes alarming climate changes. The situation is serious enough to require decisive actions, such as increasing the share of renewable energy sources in the energy mix [2]. Obviously, conventional power generation plants cannot be replaced with zero-emission sources overnight, but any improvement in the energy conversion process can substantially reduce pollution. This especially relates to harvesting waste heat, which is irretrievably lost to the environment in a great number of different thermal processes. The energy can be considered free since it is not utilized and can be used successfully if only its exergy potential is sufficient. One of the methods is to use thermoelectric generators (TEGs), which convert heat directly into electricity. Eldesoukey and Hassan [3] concentrated on investigating a system where flow itself is the heat source for the system and the flow parameters affect the system performance. Thermoelectric modules can be easily used bidirectionally, to harvest waste heat and perform as a heater, or cooler when necessary [4]. Many recent works investigate issues related to the TEG application in the automotive industry, where hot exhaust gases are released into the environment. Some works analyse the whole system installed in the exhaust system of a road vehicle driven by a gasoline [5] or a diesel [6] engine, as well as a hybrid one [7]. The difference lies in the different level of the exhaust gas temperature. Further efforts to improve the heat transfer by changing the heat exchanger geometry are presented in [8]. More detailed studies involving an analysis of operating conditions of the TEM itself in the whole system with the exhaust from a combustion engine as the source of waste heat are presented in [9]. Zaher et al. [10] developed a numerical model of a TEG-integrated

* Corresponding author.
E-mail address: ryszard.buchalik@polsl.pl (R. Buchalik).

https://doi.org/10.1016/j.apenergy.2021.116943
Received 18 December 2020; Received in revised form 3 April 2021; Accepted 9 April 2021
Available online 24 April 2021

Nomenclature

$\dot{Q}$	heat flux,W
EMF	electromotive force,V
I	current intensity,A
P	power,W
R	electrical resistance,Ω
T	temperature,K
V	voltage,V
ZT	thermoelectric figure of merit, -
k	thermal conductivity,$\frac{W}{K}$
r	thermal resistance,$\frac{K}{W}$
α	Seebeck coefficient,$\frac{V}{K}$
π	Peltier coefficient,$\frac{W}{A}$
π_r	power ratio , -
ρ	electrical resistivity,Ωm

Subscripts

c	cold side of TEG
ca	cold heat exchanger
eff	effective
env	environment
h	hot side of TEG
ha	hot heat exchanger
int	internal
oc	open circuit
rs	rapid state
sc	short circuit
ss	steady state

heat exchanger for waste heat recovery from gas-fired appliances in the food industry. They evaluate the effect of axial heat conduction in a multi-row heat exchanger. Memon and Tahir [11] also analysed utilization of lens-concentrated thermal radiation energy of a heating stove. The more and more common use of photovoltaic panels has also prompted researchers to analyse hybrid PV-TEG systems, where the PV module is the TEG upper heat source. Paper [12] presents a combination of a concentrated photovoltaic cell (CPV) and a TEG, together with a numerical analysis of such a system. It is found that fluctuations in the solar radiation intensity have a substantial impact on the temperatures of the system individual elements. An increase in radiation involves a drop in the efficiency of the CPV and a rise in the efficiency of the TEG. Moreover, Darkawa et al. [13] suggest using phase change materials (PCM) on the TEG cold side to improve the efficiency of solar energy conversion. In this way an increase of a few percent was achieved in the power of the PV/TEG system and the temperature peak in the initial phase of the system operation was reduced due to heat accumulation. Bjørk and Nielsen [14] consider a tandem PV-TEG system where short-wave radiation is directed onto the photovoltaic cell and long-wave radiation – onto the TEG module. However, the authors point to a rather insignificant impact of such an extension on the system efficiency. Hybrid PV-TEG systems were investigated from a slightly different perspective in [15], where the authors focused on the assessment of the impact of the geometry of TEGs on efficiency. The results of the studies show that integration of dye-sensitized cells with TEGs can be a financially attractive solution.

Numerous descriptions and analyses of thermoelectric elements can be found in the literature. However, they are usually made assuming ideal boundary conditions of the TEG itself [16], which means perfect contact (no thermal resistance) between the thermoelectric module, the heat source and the heat sink. In fact, there is usually (as the thermoelectric module integral part) a layer of a material at the edges of the TEG that keeps the module together mechanically, then a heat-conducting layer followed by a heat exchanger and a cooling/heating medium. Each component of the system has its own thermal resistance characteristics (the temperature drop due to heat conduction). Pierce and Stevens [17] carried out experimental testing of the TEG thermal resistance using various methods and showing differences in the obtained values. They also indicated the most reliable ways of determining this quantity for TEGs. Most analyses presented in the literature ignore this resistance, so the heat exchanger temperature is taken as the temperature of the thermoelectric module respective side in relation to both the entire system [18] and an individual TEG [19]. This is also how Wera et al. [20] investigate commercially available thermoelectric modules and assess them in terms of the compliance of the parameters specified by the manufacturer with the results obtained on a test rig. As emphasized by the authors, the lack of generally accepted standards of presenting TEG characteristics makes them very difficult to compare. Therefore, the paper presents effective thermoelectric parameters of the analysed thermoelectric elements derived based on measurements and the manufacturer's data. They can be expressed as real parameters of thermoelectric materials or as effective values for the entire thermoelectric module [21]. Similarly, effective thermal conductivity was used in [22], where a model of the TEG operation under a constant heat flux was developed. The authors take account of the response of the thermoelectric module to temperature changes, and in order to achieve optimal operating conditions, they implement an algorithm for tracking the maximum power point. The key element deciding about the efficiency of the TEG operation will be thermal resistance of the layers in between the heat sources and the thermoelectric couple junctions. This resistance is taken into account in Kim [23]. The author derived the real difference in the temperature of thermoelectric junctions at known, symmetrical resistances on both sides of the element. It depends on the TEG parameters (thermal conductivity and electrical resistance, the Seebeck coefficient) and operating conditions (flowing current and the difference in the temperature of heat sources). In no-current conditions, the temperature difference of the junctions is only a function of the temperature difference of the heat sources and thermal contact conductivity (resistance) and internal conductivity. In their paper, Lv et al. [24] analyse all paths of the heat transfer between the sources focusing on limiting convective and radiative heat losses inside the generator. For this purpose, they investigate the impact of the filling of the space between the semiconductors and the insulation material. The measurement results indicate an improvement in efficiency of about 8% for thermoelectric generators modified in this way. The authors also show that this solution makes it possible to achieve an improvement in the TEG efficiency of no more than about 9%, and the share of the reduction in the radiative heat transfer in this respect does not exceed 2% of efficiency. A theoretical description of heat conduction in a thermoelectric couple but with a cylindrical structure (the so-called annular thermoelectric couple (ATEC)) is presented in [25]. The analysed system includes a constant-temperature heat source inside a cylinder with convective cooling on the cold side. The developed mathematical model makes it possible to find the temperature distribution in this structure of the TEG, knowing the conductivity of individual layers. A spatial numerical model of the TEG is presented in [26]. The authors focus on the impact of the Peltier effect on the effective temperature difference of the junctions using the convective heat transfer in the exchanger. In such situations, especially involving waste heat recovery from hot process gases, one more issue emerges – the convective heat transfer in the hot heat exchanger [27]. This additionally complicates the heat transfer model, especially in view of the fact that the flow on the hot gas side can

hardly be considered stationary.

For practical applications, it would be beneficial to have a mathematical model describing the performance of the entire thermoelectric system and not just its idealized elements. The thermal resistance important substrate is the layer of thermal grease which attaches the thermoelectric generator to heat exchangers. It is usually responsible for a relatively large part of the total thermal resistance between the heat source/sink and the thermoelectric junctions. The thermal resistance in the heat exchanger material (and other solid elements of the system) is relatively simple to determine, either analytically or numerically. However, it is difficult to predict the resistance of a thermally conductive layer (thermal grease, contact thermal resistance), even if its pure material parameters are known. The resistance depends on the system application method, humidity, surface finish, age, temperature and, most importantly, the clamping force. From the practical point of view, in order to simulate the system behaviour, it usually does not matter which component is the thermal resistance source. The key issue is that additional thermal resistance exists.

The Seebeck effect is responsible for the electromotive force (*EMF*) generated in a circuit composed of various types of conductors or semiconductors if their junctions are in different temperatures. A single thermoelectric generator is presented in Fig. 1. Because the voltage generated by one such element is slight and directly proportional to the temperature difference $V = \alpha\Delta T$, the practice is to use dozens or hundreds of them connected in series. In this paper, the Seebeck coefficient (α) for junctions is understood as the total coefficient for all thermocouples making up the module. The operating temperature of state-of-the-art TEGs is usually included in the range of 300–400 °C, but some products available on the market can operate in temperatures of up to 600 °C. Further research in this field should aim to find new materials characterized by higher Seebeck coefficients (α), smaller thermal conductivity (k), smaller electrical resistivity (ρ) and higher permissible operating temperatures defining the dimensionless figure of merit:

$$ZT = \frac{\alpha^2}{k\rho}T$$

Because the electromotive force of a thermocouple generator is linearly dependent on α and ΔT, a rise in their values has a positive influence on the element performance. The TEG energy conversion efficiency is generally rather low [28]. Therefore, studies should be taken up to utilize the potential of the thermoelectric phenomenon in full. A certain improvement can be achieved by geometrical optimization of the TEG structure [29].

One of the key issues related to the TEG operation is appropriate selection of electrical resistance of the connected power receiver. This parameter decides whether work is performed with the maximum possible power or maximum possible efficiency in given conditions, or at a different point [30]. Due to a change in the receiver electrical resistance, the current in the circuit changes and the amount of heat absorbed and released in the thermoelectric junction changes due to the Peltier effect. These phenomena involve the flow of heat and a change in the temperature distribution, which affects the system performance.

This paper presents a proposal for a method of relatively fast determination of quantities relevant for the simulation and description of the operation of the whole TEG system, with particular emphasis on the influence of additional thermal resistance in the system, between the generator and the heat exchangers.

The method consists in carrying out measurements both in steady states and in what is referred to as *rapid states*. The measurement results provide additional information about real operating conditions of thermoelectric junctions.

The paper contribution to the present state of knowledge is to offer an in-depth mathematical description of the phenomena occurring within the TEG and to use the relations to assess the TEG parameters and operating conditions. Firstly, the developed model will make it possible to predict the behaviour of the entire system (heat exchangers and the thermoelectric module). Secondly, it will enable determination of the characteristics of the TEG itself, together with a quantitative description of the thermoelectric phenomenon occurring in the material. Thirdly, it will enable evaluation of the potential for improvement in the entire system operation by determining theoretical maxima for a given thermoelectric couple and their distance from the current state of work. For this reason, a new parameter that makes it possible to assess the TEG system performance is introduced. Such an assessment can successfully be applied mainly in waste heat recovery systems, both at the stage of their design and use. The developed analytical model, due to the low computational cost of its application, can still serve as a convenient tool for the optimization of TEG systems.

2. Materials and methods

The elements constituting resistance, such as conduction in the heat exchanger material, conduction in the material of the TEG casing, conduction of the layer on the two materials interface together with thermal grease, are treated collectively. A schematic diagram of the system under consideration is shown in Fig. 2. T_{ha} and T_{ca} denote the temperature of the hot and the cold constant-temperature ideal heat source/sink, respectively. T_h and T_c denote the temperature of the TEG thermoelectric junctions. Due to the thermal grease layer, the air gap, the ceramic coating, etc., there is thermal resistance between the heat source/sink and the generator, which is marked schematically in the figure below using a wavy line.

For the steady-state open-circuit condition (zero current), the heat flux through the thermoelectric module is only due to simple conduction in the material, i.e. conduction through all layers located between the heat exchangers. At the steady-state current, the thermoelectric module itself absorbs and emits a greater heat flux due to the Peltier effect.

$$\frac{dQ}{dt} = \Pi \cdot I \tag{1}$$

where Π stands for the Peltier coefficient, and I is the circuit current

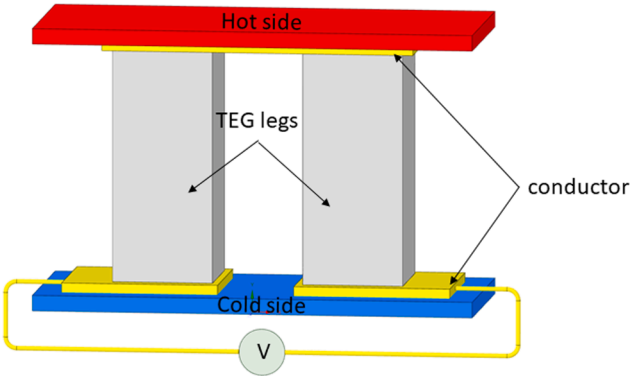

Fig. 1. Diagram of a thermoelectric generator.

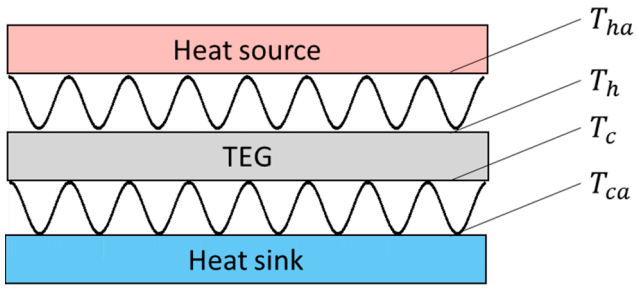

Fig. 2. Schematic diagram of the analysed thermoelectric system.

intensity. Because heat is absorbed on the hot side and emitted on the cold one, the phenomenon leads to a reduction in the effective temperature difference between the junctions ($T_h - T_c$). Being a function of temperature, the Peltier coefficient on the two sides of the thermoelectric generator is different. Additionally, Joule heat is also generated due to the flow of the electric current, increasing the cold heat flux and diminishing the hot one. A detailed description of the energy balance can be found in [23]. Both phenomena cause a reduction in the electromotive force because the force depends directly on the effective temperature difference between the junctions.

2.1. Measuring procedure

The measuring procedure proposed for the needs of the present work makes use of two kinds of measurements – one realized in the steady state and the other performed in the transient state (and known as the *rapid state* measurement). In the first case, at a set difference between the temperature of the upper and the lower heat source, the measurement is made after the system has achieved a steady thermal state, i.e. after the difference in the temperature of the TEG junctions and all other elements of the system has stabilized. After a change in the temperature of the heat sources, it takes at least several minutes to reach the steady state, due to the heat capacity. This is related to stabilization of the temperature gradient between the heat sources and the TEG junctions, and between the TEG hot and cold junction. The former depends on contact resistance and conductivity of the (usually ceramic) screens of the thermoelectric module. The latter is related to thermal conductivity of the legs (Joule heat) and Peltier effect.

The rapid state measurement is based on utilizing the system thermal inertia and consists in performing a measurement immediately that a change occurs in the current flowing through the module. In this situation, the measurement is performed for the temperature difference of the thermoelectric junctions not yet affected by the Peltier effect. If the results of the two measuring methods are plotted in a chart illustrating voltage generated at the TEG output depending on the current intensity ($V = f(I)$), straight lines with different slopes will be obtained.

In the steady state, according to Ohm's law, a rise/drop in the current intensity causes a rise/drop in voltage. What is more, the process direction (the TEG current increase/decrease) does not matter because in both cases the process runs along the same straight line, the location of which in the (I, V) system is defined by the temperature difference of the junctions.

Assuming that the thermoelectric junction temperature is exactly the same as the temperature of the corresponding heat exchanger, i.e. in the situation when the temperature is constant on both sides, the electromotive force generated by the junction has a constant value. The inclination angle of the straight line corresponding to *steady states* in the chart in Fig. 3 would then depend exclusively on the TEG internal electrical resistance. Keeping a constant temperature of the heat sources the *steady* line would coincide with *rapid* lines. In other words, the measured parameters would be independent of the measurement method. However, in real conditions the thermoelectric junction is not in direct contact with the heat exchanger. In terms of the heat transfer, there is contact resistance and thermal resistance of the materials in between. The resistance decreases the temperature of the hot thermoelectric junction compared to the temperature of the hot exchanger. The same phenomenon occurs on the cold side, leading to a rise in the temperature of the cold junction.

The thermal resistance of the layers is thus responsible for the reduction in the effective temperature difference between the thermoelectric junctions. As the current intensity increases, the quantitative share of the Peltier effect in the circuit rises. Due to that, the heat flux conducted by each layer gets bigger, causing a rise in the temperature difference between the junctions and the exchangers.

From the point of view of the measuring practice, two extreme electrical states are very convenient: the open-circuit (*oc*) state and the short-circuit (*sc*) state. In these points the measurements are the least difficult to perform. In the first situation the circuit is open, i.e. there is no current flow and Peltier heat is not generated. Voltage arises due to the Seebeck effect only. In the short-circuit state, current with the maximum intensity flows through the TEG and voltage drops to zero. Maximum Peltier heat is also produced. The effect of a violent change in the electrical load during the testing in the *rapid* state, e.g. transition from the *oc* to the *sc* state, is that for a short while there is a new state on the electrical side for the still unchanged temperature of the TEG junctions (still corresponding to the previous state, i.e. to zero current). After a while, due to the Peltier and Joule effects mentioned above, the system heads for a new thermal state, and – consequently – for the steady state.

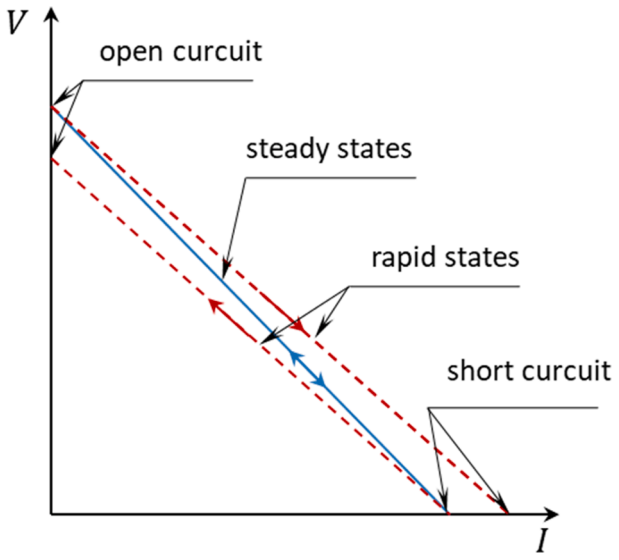

Fig. 3. I-V chart in steady and rapid states.

Very quick measurements (performed a fraction of a second after a change in the electrical state) of the current intensity and voltage make it possible to obtain the values of the two quantities for the yet unchanged thermal state of the system. The effect of the transition from the *sc* to the *oc* state is that for a fraction of a second voltage is measured that corresponds to the temperature difference occurring in the short-circuit state. Opening the circuit results in an immediate drop of the current intensity to zero and a rise in voltage depending on the present temperature difference between the TEG junctions. Similarly, the effect of a sudden transition from the open-circuit to the short-circuit state is that the current intensity is measured at a temperature difference of the junctions still corresponding to the open circuit (with no Peltier heat).

Such measurements will suffice to determine the total thermal resistance between the heat source and the TEG junctions because the temperature difference between the junctions decides about generated voltage. And this voltage, together with the TEG internal resistance, will determine the value of the current flowing through the thermoelectric module.

A schematic illustration of changes in the current intensity and voltage at a change in the electric circuit state is presented in Fig. 4. The chart on the left illustrates the history of the voltage on the TEG terminals at the transition from the *sc* state (steady state) to the *oc* state. Considering that at the short circuit the temperature of the TEG junction is lower (the Peltier effect), opening the circuit results in the creation of an electromotive force corresponding to the state – this is the level marked as *rapid state voltage*. If the current flow is stopped and the Peltier effect fades away, the temperature difference of the junctions rises, which is followed by a rise in voltage. Due to the non-zero thermal resistance (r) between the exchangers and the junctions, the process is not instantaneous. The same situation occurs at the circuit closing. A jump is first observed in the current intensity to the value corresponding

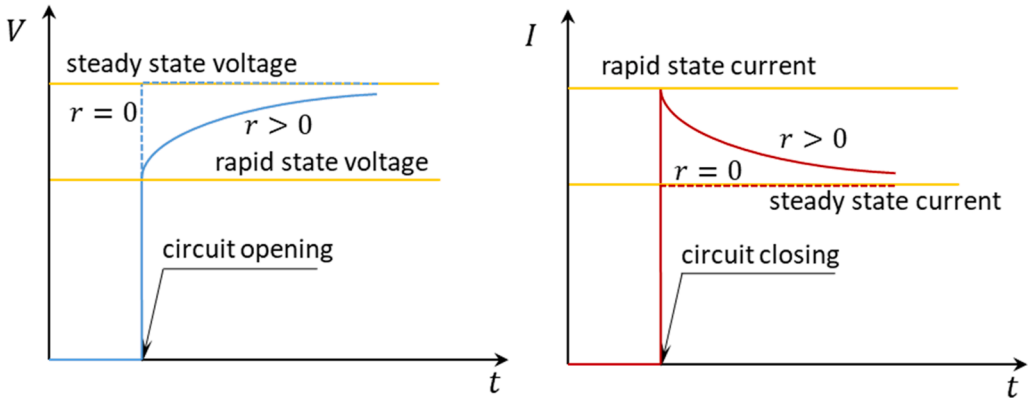

Fig. 4. Time-dependent changes in voltage during the circuit opening (left) and in the current intensity during the electric circuit closing (right).

to the temperatures in the open-circuit state (no Peltier effect and no Joule heat). Then, a decrease follows in the temperature difference of the junctions, which involves a reduction in the current intensity to the *steady state current* level.

The open circuit and the short circuit are the only states where values of the heat flux entering and leaving the thermoelectric generator are equal. This is due to the fact that the power generated by the TEG $P = V{\cdot}I$ is zero (either voltage or the current intensity is zero). This feature can be used to simplify the calculations where the *rapid* state measurement is performed focusing on the two states.

It should also be noted that the change in thermal resistance, being a result of a change in the temperatures of the thermoelectric junctions during the transition from the *sc* state to the *oc* state and vice versa, can be omitted. This is due to the fact that the change in the temperature of the junctions caused by the change of state is slight compared to the TEG absolute temperatures. Moreover, assuming the symmetry of thermal resistances on the two sides of the TEG, the mean temperature of the TEG inside is constant. Resistance can thus be established easily using the slope factor of the lines obtained from the *rapid* measurements (dashed lines in Fig. 3).

2.2. Mathematical model

The starting point for the mathematical description of the process considered herein is the energy balance of the system presented in Fig. 5. The TEG system is made of two heat exchangers (the hot one and the cold one) with a high heat transfer coefficient. The thermoelectric generator is placed in between. Heat $\dot{Q}_h$ delivered to the upper heat exchanger by electric heaters flows through the TEG creating a temperature gradient. Consequently, power P_{TEG} is generated. Heat $\dot{Q}_c$ leaving the system is collected in the cold exchanger and carried outside. The energy balance must additionally take account of heat losses. These are heat losses ("not indicated" in the measurements) to the environment through insulation ($\dot{Q}_{env}$) and the heat flowing through the insulation between the exchangers on the sides of the TEG ($\dot{Q}_{cond}$). It should be noted that the latter loss is a part of the heat carried out of the system $\dot{Q}_c$. Heat losses on the cold side are negligibly small because the exchanger temperature is close to ambient.

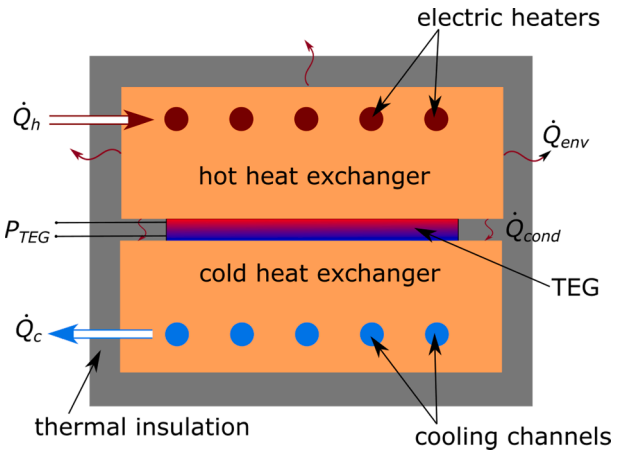

Fig. 5. Cross-section through the TEG system.

The balance takes the following form:

$$\dot{Q}_c = \dot{Q}_h - \dot{Q}_{env} - P_{TEG} \tag{1}$$

Writing a separate energy balance equation for the hot side and the cold side of the thermoelectric generator in the steady state, the following is obtained:

$$k(T_h - T_c) + \alpha I T_h - \frac{I^2 R_{int}}{2} = \frac{(T_{ha} - T_h)}{r} = \dot{Q}_h \tag{2}$$

$$k(T_h - T_c) + \alpha I T_c + \frac{I^2 R_{int}}{2} = \frac{(T_c - T_{ca})}{r} = \dot{Q}_c \tag{3}$$

The left side of the equations describes as follows: heat conducted by the TEG, Peltier heat and Joule heat. The right side represents the heat delivered to/carried away from the source, taking account of thermal resistance on the path from the heat source to the thermoelectric junction.

Solving the system of Eqs. (2) and (3) with respect to the temperature difference, a relation is obtained that defines the difference as dependent on the TEG parameters (r, α, R_{int}), the current intensity in the circuit in the steady state and the temperatures of the heat sources [23]:

$$T_h - T_c = \frac{(T_{ha} - T_{ca}) - \alpha I r (I^2 R_{int} r + T_{ca} + T_{ha})}{1 - (\alpha I r)^2 + 2kr} \tag{4}$$

It should be remembered that in the above formulae temperature is expressed in kelvins.

If all parameters of the thermoelectric generator are known, the temperature difference expressed by formula (4) can be used to find the electromotive force:

$$EMF = \alpha(T_h - T_c) \tag{5}$$

The same electromotive force can be expressed using the easily measurable temperature difference of the heat exchangers. In such a case, instead of the real Seebeck coefficient for the junctions, the so-called effective Seebeck coefficient for the entire TEG should be used:

$$EMF = \alpha_{eff}(T_{ha} - T_{ca}) \tag{6}$$

The current generated by the TEG in the short-circuit state can be expressed as the ratio between *EMF* and internal resistance R_{int}:

$$I_{sc} = \frac{\alpha(T_h - T_c)}{R_{int}} \tag{7}$$

Taking account of Eq. (4) for $I = I_{sc}$, this leads to:

$$I_{sc} = \frac{\alpha(T_{ha} - T_{ca})}{r\alpha^2(T_{ha} + T_{ca}) + R_{int}(1 + 2kr)} \tag{8}$$

It follows from Eq. (4) that temperatures of thermoelectric junctions vary with a change in the current intensity in the circuit. This is due to the Peltier effect, which – by absorbing and giving up varied amounts of heat on the junctions (depending on the current intensity) – causes a change in the temperature distribution. This in turn changes the heat fluxes conducted by each layer.

The voltage generated on the TEG terminals can be written as a function of the current intensity:

$$V(I) = EMF - IR_{int} \tag{9}$$

Although *EMF* is a quantity depending on I non-linearly (cf. formulae (4) and (5)), it may be assumed with sufficient accuracy that the dependence of V on I is linear. Example $V(I)$ distributions for the TEG analysed further below and expressed by formula (9) and the relative error resulting from the assumption of linear dependence are presented in Fig. 6.

Linear approximation of function (9) is realized easily based on the knowledge of the *EMF* for the open circuit ($I = 0$) and the short-circuit current I_{sc}, when $V = 0$.

The slope factor of the approximating line, expressed by Eq. (10), is practically the effective internal resistance of the system under consideration:

$$R_{eff} = \frac{V_{oc}}{I_{sc}} \tag{10}$$

Substituting (5) and (7) in (10) for $I = 0$, the result is as follows:

$$R_{eff} = \frac{r\alpha^2(T_{ha} + T_{ca})}{1 + 2kr} + R_{int} \tag{11}$$

which means that effective resistance is the effect of the TEG internal electrical resistance and the worsening of the heat transfer conditions (a higher temperature gradient on subsequent layers) between the sources and the thermoelectric junctions, expressed in formula (11) by the fraction on the right side of the equation. It should be noted that if there is no thermal resistance ($r = 0$), the formula takes the form of $R_{eff} = R_{int}$, which corresponds to the situation where the temperatures of the junctions are equal to the temperatures of the heat sources corresponding to them.

Using Eqs. (3), (5) and (8), an analytical relation can be derived that describes the Seebeck and the contact resistance coefficient (17) and (18), respectively, based on measurable quantities only:

$$\alpha = \frac{V_{oc}}{2(T_{ha} - T_{ca})} + \frac{\sqrt{I_{sc}(T_{ha} + T_{ca})\left[I_{sc}(T_{ha} + T_{ca})V_{oc}^2 + 8k(T_{ha} - T_{ca})^2(V_{oc} - I_{sc}R_{int})\right]}}{2I_{sc}(T_{ha}^2 - T_{ca}^2)} \tag{12}$$

$$r = \frac{\alpha(T_{ha} - T_{ca}) - V_{oc}}{2kV_{oc}} \tag{13}$$

The above equations can be used to establish α and r for a known value of the TEG thermal conductivity k.

It should be noted that the Seebeck coefficient determined in this manner is a property of the thermoelectric junction. In real conditions, where thermal contact resistance occurs, it is impossible to determine the real value of the Seebeck coefficient as a function of the temperature gradient by finding only the value of the TEG electromotive force for an open circuit. It is only possible to find its effective value for the entire thermoelectric generator

$$\alpha_{eff} = \frac{V_{oc}}{(T_{ha} - T_{ca})}. \tag{14}$$

Because the effective value is determined for a bigger temperature difference, the obtained effective coefficient is lower than the real one.

The TEG maximum power occurs for half the short-circuit current and totals

$$P_{max} = \frac{V_{oc}}{2}\frac{I_{sc}}{2}. \tag{15}$$

For set temperatures of the heat exchangers and with zero thermal resistance ($r = 0$), the maximum power can be used as the reference value for real TEG systems.

$$P_{max,r=0} = \frac{(0.5V_{oc})^2}{R_{int}} = \frac{\alpha^2(T_{ha} - T_{ca})^2}{4R_{int}}. \tag{16}$$

The real system maximum power ratio obtained by substituting (4) and (5) in (15), compared to power from (16), will be an indicator of the quality of the system operation (π_r). The relation will take the following form:

$$\pi_r = \frac{P_{max}}{P_{max,r=0}} = \frac{4I_{sc}R_{int}(I_{sc}(R_{int}(1 + 2kr) + \alpha^2 r(T_{ha} + T_{ca})) - 2\alpha(T_{ha} - T_{ca}))}{\alpha^2\left(\alpha^2 I_{sc}^2 r^2 - 4(1 + 2kr)\right)(T_{ha} - T_{ca})^2} \tag{17}$$

where I_{sc} is the short-circuit current obtained from measurements or determined from (8).

2.3. Sensitivity analysis

As already mentioned, to find the TEG parameters, it is necessary to

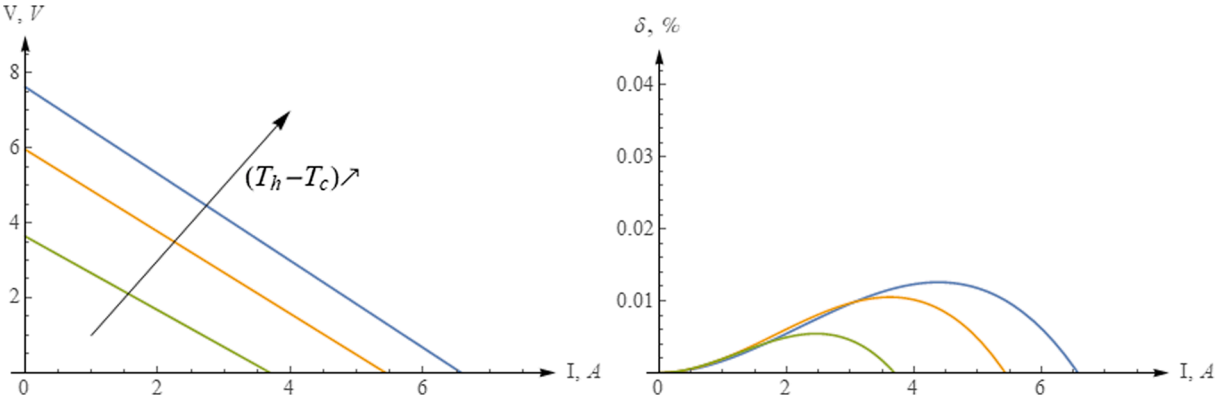

Fig. 6. V(I) chart for three different temperature differences ($T_h - T_c$) and the linear approximation relative error.

carry out appropriate measurements of temperature and selected electrical quantities. Measurements always involve a certain level of uncertainty as to the results, which is due to the quality and accuracy of the testing apparatus and conditions of the testing. It is therefore worthwhile to assess the impact of the inaccuracy of the measurement result on the value of the quantity determined based on it, i.e. to determine the tested system sensitivity to potential measuring errors. One of the tools used for this purpose is sensitivity analysis. As generally understood, it investigates the impact of the change in the independent variable on the change in the value of the dependent variable/variables. The basic notion used in the sensitivity analysis is the sensitivity coefficient – a quantity describing the impact of a parameter on the system performance. It is defined as the derivative of the observed (or sought) quantity depending on the variable (which is measured for example) with respect to which sensitivity is investigated:

$$Z_i = \frac{\partial Y(X_1, \cdots, X_n)}{\partial X_i} \tag{18}$$

It can be easily noticed that the sensitivity coefficient appears in the classic definition of the differential. This means that based on (18) it is possible to assess the effect of a change/disturbance in the ∂X_i measurement on the entire ∂Y system.

In the case of the phenomena investigated for the needs of this study, the important matter is the assessment of the impact of measured quantities on sought parameters, such as α and r. Because the parameters can be determined directly as functions of the measured quantities, the assessment of their sensitivity to uncertain quantities is relatively easy. It can be given in the form of a function because formulae (12) and (13) are differentiable in physically sensible ranges of changes.

Usually, the system sensitivity is not constant and varies as a function of the measured quantity. Knowing for which values of the measured quantity the measuring error is of marginal importance and for which the error impact has enormous significance is a valuable hint as to when the researcher has to take extra care of the measurement quality. The measuring error estimation is therefore important because this information specifies to what extent the parameters determined based on measured quantities can be trusted.

2.4. Test stand

In order to determine the tested system performance characteristics and test the procedure proposed in this paper, a test rig was built as shown in the diagram in Fig. 7.

The thermoelectric generator is heated/cooled using 10x10x5 cm copper blocks. The upper block (the hot heat source) is heated by electric heaters with a fully adjustable power supply equipped with a parameter monitoring system (voltage, current and true power). The bottom block is cooled by tap water passing through five circular channels. To control the operation of the heat exchangers, PID controllers (software implemented) are used. The cooling water temperature is also adjusted. An electric heater is installed at the cooling water inlet into the cold block to make it possible to adjust the water temperature to a set value (equal to or higher than the tap water temperature). This solution makes it possible to maintain the set temperature with an accuracy better than $0.5^{\circ}C$ both on the hot side and on the cold side of the TEG. Due to that, measurements can be performed assuming a constant temperature of the (upper and lower) heat source; the only quantity that changes is the heat flux. The heat flow released on the cold side is determined based on the measurement of the water mass flow using a Coriolis flow meter (0.15% accuracy with 95% confidence); the temperature of water flowing in and out is measured using PT100 resistance thermometers (accuracy according to class A, PN-EN 60751 – $0.25^{\circ}C$ at $50^{\circ}C$, the data logger accuracy – $0.015^{\circ}C$). To measure the temperature distribution in the copper blocks, one resistance thermometer and 9 thermocouples (type J, relative accuracy according to Class 1, PN-EN 60584-2 – $0.15^{\circ}C \pm 0.004|T|$) were used for each block. Both the copper blocks and the cooling water connections are thermally insulated with an insulating mat and insulating boards. The clamping force during the testing was applied using a purpose-designed structure. The force was measured by a piezoelectric force transducer. All thermal elements were covered with insulation materials to reduce heat losses to the environment.

2.5. Experimental measurements

The tests were performed on the TEP1-12656-0.6 thermoelectric generator manufactured by Termo-Gen AB. The thermoelectric module surface was factory-covered with a graphite-based material. The module was brand new and assembled for the first time. The experiments were performed for two different values of the clamping force. In the first case, the clamping force is made up only of the weight of the upper heat exchanger, the force sensor and the mounting bar. Its total value is estimated at up to 110N. This situation may reflect inappropriate installation, too small a clamping force or lack of thermal grease. The second test was carried out for the clamping force of about 3000N. The steady-state measurements covered the full allowable range of the electric current in the circuit – starting from the open-circuit condition almost to the short-circuit condition. In the case of rapid tests, voltage was measured at a violent *sc*-to-*oc* transition. The decision to measure voltage resulted from the fact that voltage measurements are much simpler to perform and the results are usually more accurate compared to current measurements. The measurements were recorded using a 16-

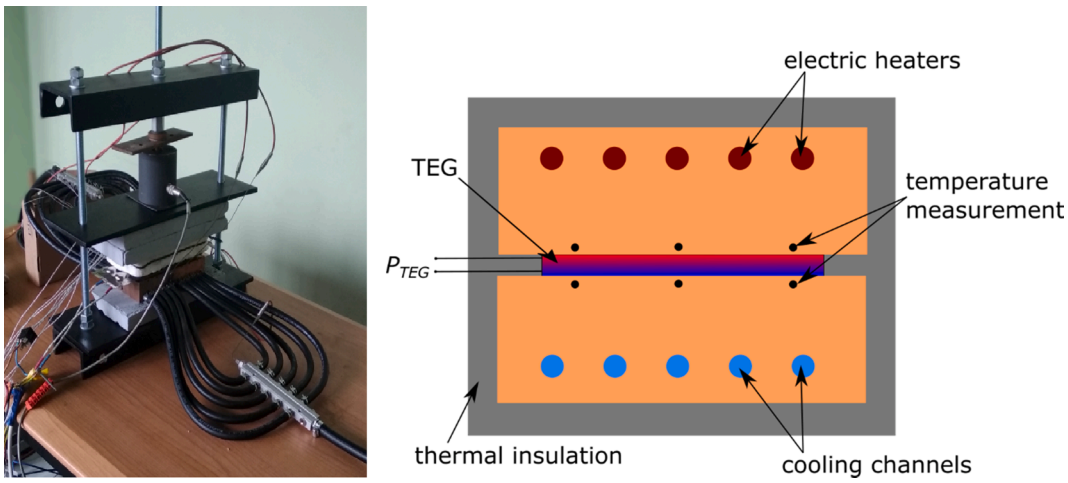

Fig. 7. Photo and schematic diagram of the test rig.

bit, $25kS/s$ voltage transducer, and a quick interrupter (switching time much shorter than $1ms$) was used to make a break in the electrical circuit.

The TEG was measured in operating temperatures, i.e. at a relatively high temperature gradient. During the tests, using a precise control system, constant temperature of the upper heat source was maintained. The heat flux of the cold exchanger was determined by the cooling water mass flow and the temperature difference. Resistance was measured using the *rapid* method for 4 different sets of temperatures of the heat exchangers. Apart from the basic measurements (numbered from 1 to 4), one additional measurement was performed (2a) in the same conditions as measurement (2) but after a few days' break, during which the system was under the load of $3000N$. The measurement results are listed in Table 1.

Fig. 8 presents the voltage-current characteristics obtained for measurements performed in the steady state and shown in Table 1 (the markings of the lines correspond to the data set number). The dashed lines represent the transition from the *sc* to the *oc* state; their intersection with the V axis shows the voltage value in the *rapid* state. The figure indicates that a rise in the temperature of the exchangers (and thereby – of the thermoelectric junctions) involves an increase in the distance between the characteristic and the origin of the system of coordinates. The lack of parallelism of lines 2, 3 and 4, which is difficult to notice but still present, results only from changes in the TEG parameters occurring with changes in the operating temperature.

The slope of the dashed lines depends only on the internal electrical resistance of the thermoelectric generator. The real steady-state operation line (solid) has a bigger slope, which is due to bigger resistance. It also clearly indicates the existence of thermal resistance on the heat source-thermoelectric element interface. It can also be seen that this resistance is bigger if there is hardly any clamping force (line 1). The results of the above-presented measurements and the model developed will be used to determine the TEG parameters following the procedure proposed earlier.

An example measurement is shown in Fig. 9, which presents the voltage vs. time characteristic, where the zero time corresponds to the point right before the circuit break. The left-hand side chart shows the entire process, while the right-hand side one presents the zoomed range ($10ms$) at the circuit brake.

In the described model and with the presented configuration of the test stand, the essential items are only the levels of the electromotive force for the *sc* and *oc* states represented in the figure by horizontal lines. It can be seen that the electric circuit was broken in the 4th *ms* of the test. Before the circuit was opened, the system was brought to the steady state for temperatures T_{ha} and T_{ca} according to Table 1 for a given measuring point. The important voltage level is the one recorded immediately after the circuit is opened (lower line in Fig. 9). After that, voltage approaches the value corresponding to V_{oc} for the steady state. The rate of the process is not important in the analysed example, but it depends indirectly on the system thermal capacity. It usually took several minutes to achieve the steady state. Then it was possible to make a measurement for the *oc* state.

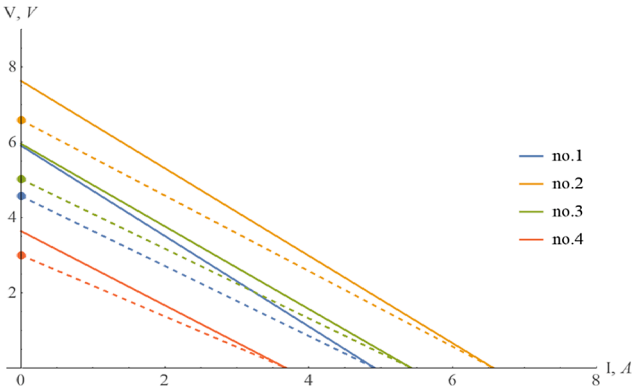

Fig. 8. Voltage-current chart for the measurement sets (solid lines: steady states, dashed lines: rapid states).

3. Results and discussion

Based on the measurements of the TEP1-12656-0.6 thermoelectric generator, its basic technical parameters were determined using the presented mathematical model. The calculations were performed for the TEG thermal conductivity of $k = 2.55W/K$, which results from the conductivity of typical thermoelectric materials and from the geometry of the internal structure of the tested thermoelectric generator.

In the sensitivity analysis, apart from checking the influence of the inaccuracy of the adoption of thermal conductivity k, the focus was also on the evaluation of the impact of the measurement of the circuit voltage on the Seebeck effect and contact resistance determined in the mathematical model. The voltage measurement, though very accurate itself, in the proposed procedure is performed for fast-changing (rapid) states, which creates the risk of producing bigger measuring errors.

The sensitivity analysis results presented in the charts in Figs. 10 and 11 show that the thermal conductivity has a very small effect both on α and on r, particularly if the TEG operation is analysed in operating conditions (curves 2–4). The 10% inaccuracy of the estimation of coefficient k leads to an error in the determination of the Seebeck coefficient at the level of $0.2mV/K$; for resistance, the uncertainty is of the order of $0.04K/W$. Voltage has a litle more significant impact, especially on the sought value of thermal resistance. Still, the sensitivity is too small to create mistrust in the used measurements because voltage is a quantity measured directly and with high accuracy ($10mV$). Moreover, the application of very fast voltage transducers to record *rapid* states minimizes the inaccuracies related to simulating the change in the system state (cf. Fig. 4). Measurements of the temperature of heat sources are realized with the accuracy of less than $0.5^{\circ}C$ in the analysed range of the system operation. It should be noted here that the presented sensitivity curves concern a specific state of the system operation allowing variability of the parameters with respect to which the sensitivity of the system is evaluated. The points marked with dots correspond to the estimated and adopted for further calculations value of k and the measured values of V obtained in the analysed states of the TEG operation. It should also be noted that all the measurements were recorded using a computer control and measurement system eliminating

Table 1
Results of the thermoelectric generator measurement performed in different operating conditions.

No.	Temperature hot /cold exchanger °C	Clamping force *N*	*oc* voltage *steady* *V*	*sc* current *steady* *A*	Heating power *oc* / *sc* *W*	*sc* voltage *rapid* *V*	Electrical resistance Ω
1	250/32.7	110	5.91	4.92	286/335	4.57	0.92
2	250/35.2	3000	7,63	6,57	378/467	6.59	1.00
3	190/33.2	3000	5.96	5.43	262/337	5.02	0.92
4	120/27.7	3000	3.64	3.69	153/196	3.00	0.81
2A	250/37.5	3000	7.95	6.89	392/494	6.97	1.01

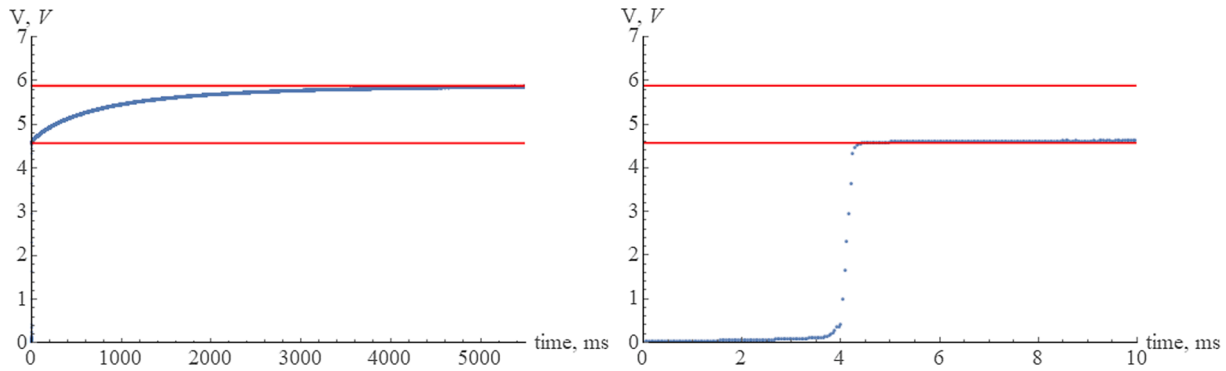

Fig. 9. Time-dependent changes in voltage at a rapid-state change from the short-circuit to the open-circuit condition. The right chart shows zoomed process of circuit break.

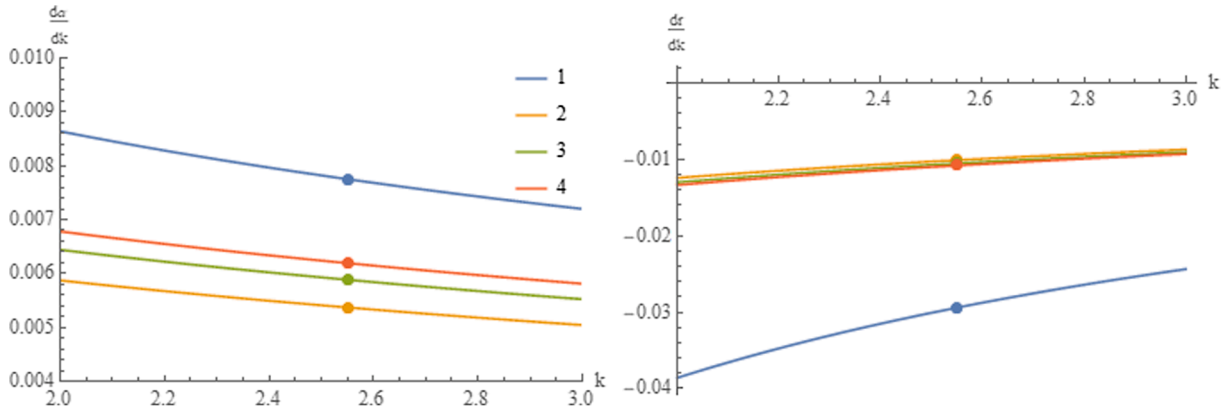

Fig. 10. Sensitivity of the Seebeck coefficient (left) and of contact resistance (right) to the accuracy of k estimation. Dots mark the assumed value of k for the TEG.

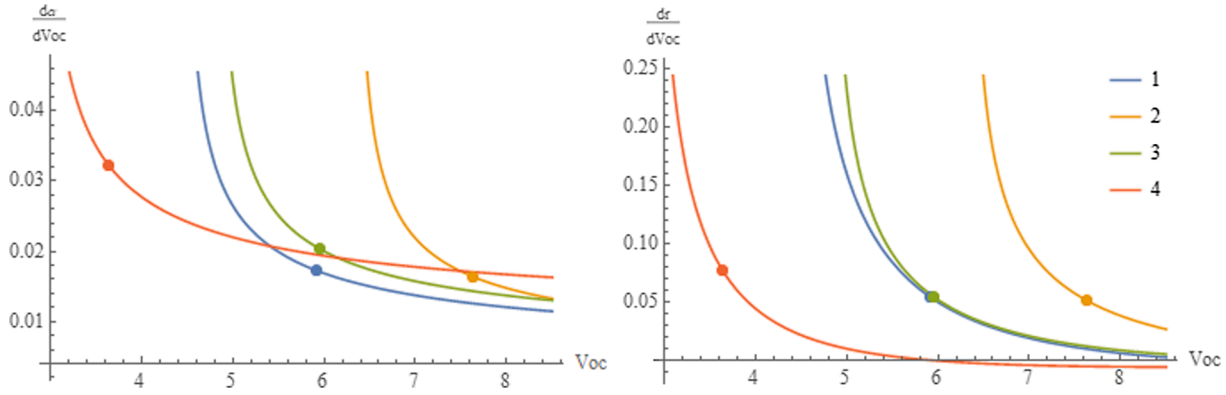

Fig. 11. Sensitivity of the Seebeck coefficient (left) and of contact resistance (right) to the accuracy of the voltage measurement. Dots mark the measured value of voltage for the TEG operating parameters.

accidental errors in readouts or data processing.

Using the results of voltage measurements realized in operating temperatures (2 to 4) and the adopted value of $k = 2.55W/K$ the TEG parameters (α, r and π_r) were determined. The results of the calculations are presented in Figs. 12 and 13 as functions of the temperature difference between the heat exchangers ($T_{ha} - T_{ca}$). The results obtained for measurements 2, 3 and 4 are marked in orange, and the results for measurements 1 and 2a – in blue and green, respectively.

It can be seen that if measurements were realized at a high clamping force (close to the maximum allowable clamping force for the module), resistance is less than half the resistance obtained for a small clamping force. It should be noted that measurement 2a, realized a few days after the other measurements and, therefore, on a non-unloaded element, gave a slightly lower resistance value. The observed change probably results from the heat-conducting paste on the TEG surface fitting the micro irregularities of the heat exchangers.

The Seebeck coefficients determined from the model in the analysed range of temperature differences differ from each other by less than 10% (Fig. 12). For a small clamping force, the higher value of α results from the lower temperature difference of the junctions, which can be noticed in Fig. 13, showing the mean temperature differences between the thermoelectric junction and the heat exchangers corresponding to it and determined at the maximum power generated by the TEG. It can be seen that the measurement performed at a small clamping force and at the highest operating temperature results in a decrease in the temperature difference of the junctions by over 120 K (about 60 K per each),

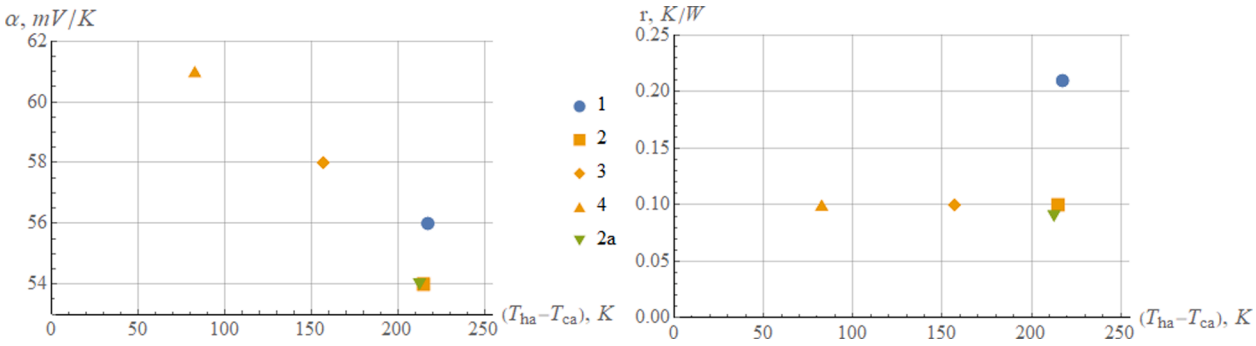

Fig. 12. Seebeck coefficient and thermal resistance obtained from the mathematical model based on the performed measurements.

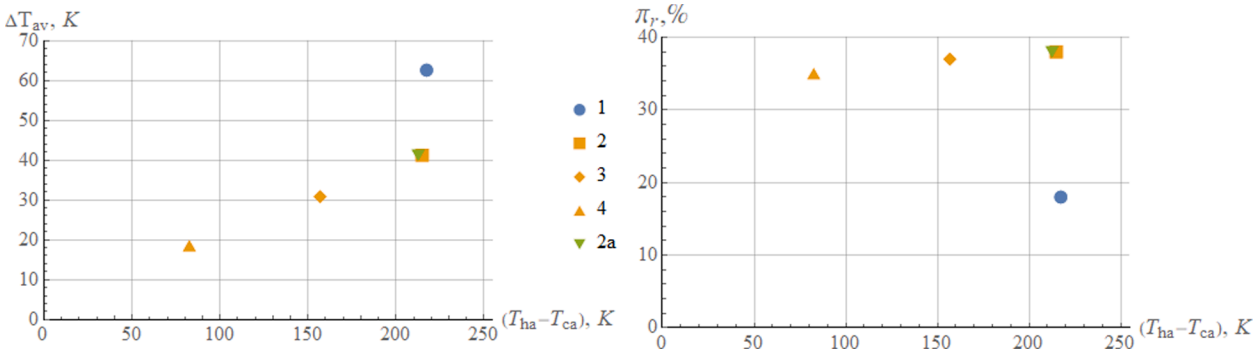

Fig. 13. Temperature "loss" on the TEG cold and hot side and the power ratio at the TEG maximum power.

compared to the temperature difference of the heat exchangers. This is by about 40 K more than in the case of a big clamping force. This "loss" of the temperature difference of the junctions decreases linearly with the operating temperature value. It should be remembered that the drops/rises are the effect of thermal resistance on the one hand and Peltier heat and Joule heat on the other. There is a slight difference (less than 1.6*K*) in these values on the two sides of the thermoelectric module, which results from the different heat flux through the two surfaces at the point of maximum power.

Due to the nature of the thermoelectric phenomenon and the limitations imposed by the second law of thermodynamics, even a slight drop in the useful temperature gradient on the electric junction involves a significant drop in power compared to the ideal situation when no thermal resistance occurs between the exchangers. Higher thermal resistance translates into a smaller power ratio, which is shown in the right chart in Fig. 13. Due to the occurrence of contact resistance, the achieved power can never come even close to 40% of the theoretical maximum value for given module and given temperatures. It may therefore be concluded that, considering the occurrence of resistance, heat sources could ensure a higher temperature difference. However, it is not clear whether the maximum operating temperature specified in the TEG data sheet relates to the temperature of the upper source or to the temperature of the junction.

4. Conclusions

The paper presents a complex mathematical model of thermoelectric phenomena that can be used to determine basic parameters of thermoelectric generators based on relatively simple measurements of electrical quantities and temperature of the TEG heat sources. A method is proposed that makes use of classic measurements realized in the steady state and *rapid* measurements performed in a fraction of a second after the TEG state changes but when the thermal state is still as before the change. In this work, considering the ease and accuracy of voltage measurements, a decision was made to perform *rapid* measurements of voltage during the short-circuit-to-open-circuit transition. Such voltage measurements make it possible to determine the electromotive force generated by the TEG, in a thermal state corresponding to the short-circuit current. A great advantage of the developed testing procedure is the possibility of finding real quantities describing the junction and the material which are much more useful than the effective values for the entire thermoelectric module.

The presented complete analytical model of the thermoelectric generator enables determination of the total Seebeck coefficient of thermoelectric junctions and contact resistance for a known value of the TEG thermal conductivity. The model also makes it possible to establish the practically unmeasurable real temperature difference between the junctions in specific operating conditions.

Because measurements always involve the risk that their results will be affected by measuring inaccuracy, a decision was made in this work to establish the impact of potential measuring errors and of errors in the estimation of the mathematical model main input quantities on the results of the calculations. For this purpose, an analysis was conducted of the sensitivity of determination of the Seebeck coefficient and thermal resistance to thermal conductivity and voltage. The sensitivity analysis results show a very small impact of the TEG thermal conductivity on the two parameters. At the same time it was noticed that the impact of the voltage measurement inaccuracy on their values is by an order higher. The system high sensitivity to such measurements does not compromise their usefulness because the quantities are determined with very high accuracy, which means that the effect of potential inaccuracies on their values is negligibly small.

To assess the effectiveness of the heat transfer between the heat exchangers and the TEG junctions, an indicator was introduced in the form of the power ratio. It shows what fraction of the TEG maximum theoretical power at zero thermal resistance is maximally achieved by the thermoelectric generator in given operating conditions. This indicator could therefore be used as a quality measure in the process of optimizing contact conditions and contact layers of newly designed thermoelectric modules, and also as a quantity evaluating the contact

quality for the same type of operated systems.

To sum up, the developed measuring method makes it possible, in terms of both calculations and measurements, to determine in a relatively simple way the TEG characteristic quantities and, thereby, establish theoretical maxima for set temperatures of heat sources. The procedures proposed in the paper can be used to define standardized tests enabling assessment of devices equipped with thermoelectric modules. Knowing the parameters characterizing the thermoelectric generator, it is also possible to perform diagnostic testing to identify a faulty element of the system, which can be very useful in the operational practice and quality control of devices.

The possibility of assessing the device operating conditions gives an answer to the question of how much the system can possibly be improved and where the theoretical maxima are. The thermal resistance and the power ratio calculations can be useful if thermal grease is to be replaced or changed or if surface finishing or clamping force modifications are considered.

It should be emphasized that if the thermal resistance value is adopted for the calculations as zero, noticeable differences in the assessment of the quality of the thermoelectric generator operation can arise, and this should be avoided.

CRediT authorship contribution statement

Ryszard Buchalik: Conceptualization, Methodology, Writing - original draft, Investigation, Resources. **Grzegorz Nowak:** Writing - review & editing, Supervision, Funding acquisition, Project administration, Validation. **Iwona Nowak:** Software, Formal analysis.

Declaration of Competing Interest

The authors declare that they have no known competing financial interests or personal relationships that could have appeared to influence the work reported in this paper.

Acknowledgements

The research was funded by the Polish National Science Centre (NCN Poland), Grant 2016/23/B/ST8/03133.

References

[1] Brutschin E, Fleig A. Innovation in the energy sector – The role of fossil fuels and developing economies. Energy Policy 2016;97:27–38.
[2] Hansen K, Breyer C, Lund H. Status and perspectives on 100% renewable energy systems. Energy 2019;175:471–80.
[3] Eldesoukey A, Hassan H. 3D model of thermoelectric generator (TEG) case study: Effect of flow regime on the TEG performance. Energy Convers Manage 2019;180:231–9.
[4] Kwan TH, Wu X, Yao Q. Complete implementation of the combined TEG-TEC temperature control and energy harvesting system. Control Eng Pract 2020;95.
[5] Su CQ, Wang WS, Liu X, Deng YD. Simulation and experimental study on thermal optimization of the heat exchanger for automotive exhaust-based thermoelectric generators. Case Stud Therm Eng 2014;4:85–91.
[6] Eid SM. Development and performance analysis of a TEG system using exhaust recovery for a light diesel vehicle with assessment of fuel economy and emissions. Appl Therm Eng 2019;147:661–74.
[7] Wang R, Yu W, Meng X. Performance investigation and energy optimization of a thermoelectric generator for a mild hybrid vehicle. Energy 2018;162:1016–28.
[8] Wang Y, Li S, Xie X, Deng Y, Liu X, Su C. Performance evaluation of an automotive thermoelectric generator with inserted fins or dimpled-surface hot heat exchanger. Appl Energy 2018;218:391–401.
[9] Tang ZB, Deng YD, Su CQ, Shuai WW, Xie CJ. A research on thermoelectric generator's electrical performance under temperature mismatch conditions for automotive waste heat recovery system. Case Stud Therm Eng 2015;5:143–50.
[10] Zaher MH, Abdelsalam MY, Cotton JS. Study of the effects of axial conduction on the performance of thermoelectric generators integrated in a heat exchanger for waste heat recovery applications. Appl Energy 2020;261.
[11] Memon S, Tahir KN. Experimental and Analytical Simulation Analyses on the Electrical Performance of Thermoelectric Generator Modules for Direct and Concentrated Quartz-Halogen Heat Harvesting. Energies 2018;11:3315.
[12] Mahmoudinezhad S, Rezania A, Rosendahl LA. Behavior of hybrid concentrated photovoltaic-thermoelectric generator under variable solar radiation. Energy Convers Manage 2018;164:443–52.
[13] Darkwa J, Calautit J, Du D, Kokogianakis GA. numerical and experimental analysis of an integrated TEG-PCM power enhancement system for photovoltaic cells. Appl Energy 2019;248:688–701.
[14] Bjørk R, Nielsen KK. The maximum theoretical performance of unconcentrated solar photovoltaic and thermoelectric generator systems. Energy Convers Manage 2018;156:264–8.
[15] Kossyvakis DN, Voutsinas GD, Hristoforou EV. Experimental analysis and performance evaluation of a tandem photovoltaic–thermoelectric hybrid system. Energy Convers Manage 2016;117:490–500.
[16] Nolas GS, Sharp J, Goldsmid HJ. Thermoelectrics, Basic Principles and New Materials Developments. Heidelberg, New York, Berlin: Springer-Verlag; 2001.
[17] Pierce RD, Stevens RJ. Measuring thermal substrate resistance and impact on the characterization of thermoelectric modules. Measurement 2017;111:173–82.
[18] Ji D, Wei Z, Mazzoni S, Mengarelli M, Zhao J, Pou J, et al. Thermoelectric generation for waste heat recovery: Application of a system level design optimization approach via Taguchi method. Energy Convers Manage 2018;172:507–5016.
[19] Wei-Hsin C, Chen-Yeh L, Chen-I H, Wei-Lun H. Experimental study on thermoelectric modules for power generation at various operating conditions. Energy 2012;45:874–81.
[20] Weera S, Lee H, Attar A. Utilizing effective material properties to validate the performance of thermoelectric cooler and generator modules. Energy Convers Manage 2020;205.
[21] Lee H, Sharp J, Stokes D, Pearson M, Priya S. Modelling and analysis of the effect of thermal losses on thermoelectric generator performance using effective properties. Appl Energy 2018;211:987–99.
[22] Compadre Torrecilla M, Montecucco A, Siviter J, Knox AR, Strain A. Novel model and maximum power tracking algorithm for thermoelectric generators operated under constant heat flux. Appl Energy 2019;256.
[23] Kim S. Analysis and modelling of effective temperature differences and electrical parameters of thermoelectric generators. Appl Energy 2013;102:1458–63.
[24] Lv S, Liu M, He W, Li X, Gong W, Shen S. Study of thermal insulation materials influence on the performance of thermoelectric generators by creating a significant effective temperature difference. Energy Convers Manage 2020;207.
[25] Tan Q, Chen G, Sun Y, Duan B, Li G, Zhai P. Performance of annular thermoelectric couples by simultaneously considering interface layers and boundary conditions. Appl Therm Eng 2020;174.
[26] Liao M, He Z, Jiang C, Fan X, Li Y, Qi F. A three-dimensional model for thermoelectric generator and the influence of Peltier effect on the performance and heat transfer. Appl Therm Eng 2018;133:493–500.
[27] Li W, Peng J, Xiao W, Wang H, Zeng J, Xie J, et al. The temperature distribution and electrical performance of fluid heat exchanger-based thermoelectric generator. Appl Therm Eng 2017;118:742–7.
[28] Luo D, Wang R, Yu W, Zhou W. Performance evaluation of a novel thermoelectric module with BiSbTeSe-based material. Appl Energy 2019;238:1299–311.
[29] Royale A, Simic M, Lappas P, Schiffer P, Palaniswamy R. Novel, shape-optimised, TEG subsystem design. Proc Comput Sci 2019;159:2607–15.
[30] Buchalik R, Nowak I, Rogozinski K, Nowak G. Detailed Model of a Thermoelectric Generator Performance. ASME J Energy Resour Technol 2020;142(2).

Ryszard Buchalik
Institute of Power Engineering and Turbomachinery,
Silesian University of Technology,
18 Konarskiego St, 44-100 Gliwice, Poland
e-mail: ryszard.buchalik@polsl.pl

Iwona Nowak
Institute of Mathematics,
Silesian University of Technology,
23 Kaszubska St, 44-100 Gliwice, Poland
e-mail: iwona.nowak@polsl.pl

Krzysztof Rogozinski
Institute of Power Engineering and Turbomachinery,
Silesian University of Technology,
18 Konarskiego St, 44-100 Gliwice, Poland
e-mail: krzysztof.rogozinski@polsl.pl

Grzegorz Nowak
Institute of Power Engineering and Turbomachinery,
Silesian University of Technology,
18 Konarskiego St, 44-100 Gliwice, Poland
e-mail: grzegorz.nowak@polsl.pl

Detailed Model of a Thermoelectric Generator Performance

The paper deals with mathematical modeling of heat transfer phenomena occurring in a system containing thermoelectric elements. The main focus was on creating a useful computational tool for designing, validating, testing, controlling, and regulating the energy harvesting system with a thermoelectric cell. The model widely described in the literature, assuming a constant temperature level on both sides of the cell, has been modified to take into account the thermal resistance of heat exchangers that are inseparable parts of nearly every device of this kind. The results and conclusions from the solutions of equations forming a formalized record of the proposed method, the assumed approach to modeling, used physical phenomena and sensitivity analysis of the impact of the tested parameters on the system operation was presented. The calculations were made for the data of a selected thermoelectric generating cell available on the market.
[DOI: 10.1115/1.4044367]

Keywords: alternative energy sources, energy conversion/systems, energy systems analysis, thermoelectric modules, TEG, energy harvesting, thermal resistance

1 Introduction

The following discussion addresses the use of thermoelectric effects for energy harvesting from waste heat. This situation may take place in the internal combustion engines, where hot gases are discharged from the system, and a significant amount of thermal energy contained in them is, in conventional solutions, lost to the environment [1]. Typically, the exhaust gas has a relatively high temperature, so the energy flux lost in this way is a substantial contribution to the engine energy balance [2]. The basic component of the energy recovery system can be a thermoelectric generator (TEG) which converts heat into electric power on the basis of the Seebeck effect [3]. Such devices may have many advantages, such as simplicity of use, failure-free operation, noiselessness, lack of moving parts, low production cost, small dimensions, low mass, and others [4]. However, there are methods to achieve greater efficiency of the energy harvesting system but with a significant level of complication and other technical problems [5]. Thermoelectric modules have many different applications and potential applications in various fields of science and technology [6]. Considering the construction of an energy harvesting device, the design of a heat exchanger is in contact with the fumes on one side and with the hot end of the thermoelectric cell on the other side becomes a key issue. Its characteristics, and in particular the thermal resistance, modify the operating conditions of the module itself. Many efforts have been made to achieve lower thermal resistance of heat exchangers [7,8]. There are many methods to determine thermoelectric module characteristics [9]. Some of them are based on measurement collected at steady state (direct measurements) while the others focus on the transient conditions. Operation parameters of the coworking heat exchanger, in particular, the heat flux transferred, depend on thermal properties of the system components, mainly the thermoelectric cell, which generates the useful effect in the form of electric power. Thermal conditions, such as the heat flux entering the thermoelectric cell, vary due to the magnitude of electric current in a circuit, which in turn affects temperature and heat flux distribution in the whole arrangement. In order to model the occurring phenomena and simulate the whole system, the temperature of exhaust gases, their chemical composition, pressure pulsations, e.g., wave and acoustic phenomena, should be taken into account. The literature describes the proposed method of modeling, optimization, and analyzing of the whole thermoelectric cell system, taking into account the thermal resistance of many elements, including heat exchangers, the heat transfer (between surfaces in contact and related to a liquid medium), conduction, and so on [10]. Also, the design arrangement of thermoelectric material inside the module is important [11]. Air-filled areas modify the heat flux by convection, conduction, and radiation [11,12]. A lot of effort and work is required to design the hot side heat exchanger being in contact with the hot gas. Usually, its surface must be much larger than the thermoelectric cell surface in order to ensure optimum working conditions [13]. The design process of heat exchanger is strongly influenced by the convective heat transfer from the heat source [14] and/or transfer through radiation [15]. Another extremely important issue is the unsteadiness of these parameters in time. What is more, they can vary in a very wide range. In Sec. 2, a description of the most essential parameters of the thermoelectric module operation set is proposed. It was decided to analyze the influence of usually neglected phenomena on the thermoelectric generator performance and their mutual interaction. There are some works available that also address this issue [16,17]. These works, despite the fact that they coincide in some parts with the results presented below, are made for different materials, thermoelectric modules, and parameters of the analyzed object. However, the main difference and novelty introduced in this work is that the following analysis expands earlier works especially in terms which is useful in the practical application of the thermoelectric module and control of the electric load system (power receiver, useful effects). In the past, the influence of, among others, the cell's geometrical parameters has been studied (e.g., assuming constant resistance of power receiver). But this kind of parameter cannot be modified when the module is already manufactured and installed, though electrical resistance can be very easily set (manually or

Contributed by the Advanced Energy Systems Division of ASME for publication in the Journal of Energy Resources Technology. Manuscript received December 30, 2018; final manuscript received July 20, 2019; published online July 29, 2019. Assoc. Editor: Wojciech Stanek.

automatically) during the operation with programable DC/DC converter. Some of the following relationships, dependencies, and charts were made based on the assumption that the power receiver's resistance is always (constantly) adjusted to the optimum value due to the adopted criterion (maximum power or efficiency). The question was also asked about the quantitative impact of the obtained results and the legitimacy of including them in the design of the entire system. Conclusions from this analysis may be useful in planning experiments aimed at determining thermoelectric module characteristics or testing a whole heat recovery system, for example, coupled with an internal combustion engine. Recently, a lot of such research has been conducted in various arrangements [3,18–23]. The possibility of controlling heat fluxes and temperatures of junctions by the electric current in the circuit was also analyzed. The idea, with minor modifications, can also be used in thermoelectric refrigeration and cooling.

2 Modeling Approach

Plenty of mathematical models of thermoelectric cells and their ideal benchmarks can be found in the literature. However, the vast majority of them are based on an assumption of constant temperature or constant heat flux at both sides of the module [4,16,24]. In the first case, almost always an error of varying the temperature of the hot and cold end of the cell is unavoidable. A situation, when ideal heat source (constant temperature) is connected without thermal resistance to the generator, is obviously impossible. This discrepancy results from the fact that the existence of temperature gradient and magnitude of the heat flux is inextricably linked together [25]. The amount of heat supplied to the cell and released from it varies with the resistance of the connected electric power receiver, i.e., the electric current in the circuit. This current, through the existence, among others, of the Seebeck voltage and the Joule effect, affects the heat flow through the module [4].

Considering the cell's surface, its temperature results from supplying and releasing appropriate amount of heat. If the heat flux entering and leaving the cell changes, then the flux passing through the heat exchangers (in contact with the cell and the contact layers of the elements that are integral parts of the system) also change. As a result, the temperature gradient in the heat exchanger and other components changes. Assuming that the temperature of heat source is constant, it causes a change in the temperature of the hot side of the thermoelectric cell. Analogous considerations can be made for the cold end of the cell, whose temperature will be slightly higher than the temperature of the heat sink (also constant). The proposed method extends the standard approach by taking into account the heat exchangers (heat source and heat sink) that are in contact with TEG and relevant heat resistance factor. In this case, we assume constant temperatures of both heat exchangers (instead of TEG surfaces), while TEG surface temperatures result from heat transfer intensity. Heat transfer resistance may represent conduction in the material layer, as well as contact resistance between the elements, conduction within coating of the module, etc. In practice, it is usually impossible to maintain the temperature of both ends of the cell at a constant level because of their connection to heat exchangers (hot and cold) through elements with thermal resistance. Usually, due to technical difficulties, the temperature of the cell surface is not directly measured. The measuring sensor is located at a certain distance, and its indication is the value between the actual temperature of the cell's side and the heat exchanger (hot or cold, depending on the side considered). The proposed method of modeling can be used, among others, to answer the question regarding the measurement error and inaccuracy of relevant calculations. First of all, this model will allow determining how the working conditions of the cell change depending on the thermal resistance of the coupled heat exchangers. Due to the marginal significance of the Thompson effect, it was neglected in the analyses.

2.1 Phenomena Description. The main purpose of this work is to build a precise mathematical model of the thermoelectric generator assembly which can be used to perform thermal calculations of the whole system, without considering the internal structure of the thermoelectric cell itself (Fig. 1). The following considerations relate to the steady-state operation. First of all, the thermoelectric cell consists of a solid material and therefore conducts heat according to Fourier's law [25]. This phenomenon is relatively easy to model in the case where no electrical power is generated. The thermal conductivity of the entire cell (calculated on the basis of external geometrical dimensions and the temperature difference between the hot and cold sides, only) is one of the crucial parameters. Closer analyses should take into account the dependence of variations in thermal conductivity and other parameters with temperature. This phenomena (thermal conductivity) is sufficient to describe a cell when no electric load is applied (no current flow—open circuit). The voltage measurement between the cell leads allows calculating the equivalent Seebeck coefficient for the entire cell on the basis of the temperature difference between the hot and cold sides. Voltage arises at materials' connections (pairs) with different Seebeck coefficients. The value results from the product of the difference of these coefficients for contacting materials used to build the cell, the temperature difference, as well as the number of electrically connected pairs in series [4].

However, as mentioned above, this description is intended to describe the cell as a whole, so for the sake of further consideration, an equivalent Seebeck coefficient is adopted (1). The eqv index refers to the values determined for the entire cell. This method is described in the literature, is widely used, and is useful when detail analysis of the thermoelectric cell interior is not needed or not possible [26].

$$V_{OC} = \alpha_{eqv} \cdot \Delta T \tag{1}$$

Allowing the flow of current in the circuit, i.e., connecting a receiver of electric power to the cell, significantly changes the energy balance of the cell. The first important element is that the heat flux supplied to the cell is not equal to the released one. Their difference is the work done by the electric current in the external part of the circuit (power receiver). Second, which is even more important, the flowing current is a reason for the Peltier effect. The current flowing in the cell passes through a thermoelectric connector on which there is a difference in electrical potentials (Seebeck voltage), so the product of this voltage and current is the thermal power generated (or received) at each end of the cell. This effect counteracts the temperature gradient applied to the cell and, thus, increases both heat fluxes—entering and exiting the cell.

In a particular case, if the external resistance is equal to 0 Ω (short-circuit), the power is not fed outside the cell. Therefore, the heat flux entering the cell is equal to the released one. In this case, the factors that increase and decrease the heat flow resulting from the Peltier effect will not be equal because of the same electric current and different absolute temperatures. Thus, the flux resulting from them will not also be equal, which apparently violates the first law of thermodynamics. The missing factor is generated in the cell's internal volume due to the electric resistance of the cell

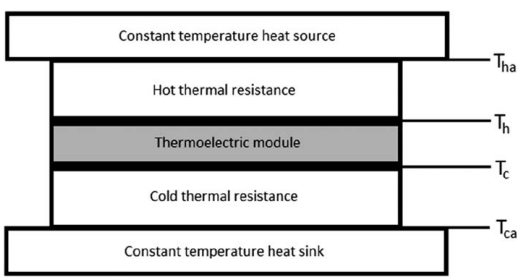

Fig. 1 Schematic diagram

material—Joule heat. This effect reduces the heat flux at the hot side of the module and increases it at the cold one. The equivalent resistance occurring in the following equation stands for the electrical material resistance of the entire cell, and it results from the product of the number of posts and joints (solders), respectively, their resistance, and connections type.

2.2 Mathematical Model. The output power (useful effect) of the thermoelectric module can be expressed as (2)

$$P = V \cdot I = (\mathcal{E} - IR_{\text{int}}) \cdot I = (\alpha \cdot (T_h - T_c) - IR_{\text{int}}) \cdot I \tag{2}$$

Quantities like α_{eqv}, K_{eqv}, and R_{int} refer to the properties of the entire module, resulting internal structure and composition (number of connections, dimensions, etc.).

The total heat flux entering the thermoelectric module is a sum of heat absorbed due to the Peltier effect and heat conducted through the module and Joule heat (3). Other phenomena (Thomson effect, conduction and convection in air, sealing between thermoelectric legs, etc.) are much less important and have not been taken into account.

$$\begin{aligned} Q_h &= Q_{\text{Peltier}} + Q_{\text{Conduction}} + Q_{\text{Joule}} \\ &= \alpha_{\text{eqv}} I T_h + K_{\text{eqv}} \Delta T - \frac{1}{2} I^2 R_{\text{int}} \end{aligned} \tag{3}$$

Therefore, the overall efficiency can be expressed as

$$\eta = \frac{P}{Q_h} = \frac{(\alpha \cdot \Delta T - IR_{\text{int}}) \cdot I}{\alpha_{\text{eqv}} I T_h + K_{\text{eqv}} \Delta T - (1/2) I^2 R_{\text{int}}} \tag{4}$$

The relation between the constant temperature heat source or heat sink and temperature of the thermoelectric module surface can be expressed in the following way for conduction (Eqs. (5) and (6)) and/or radiation (Eqs. (7) and (9))

$$T_c = T_{ca} + Q_c \cdot r_c \tag{5}$$

$$T_h = T_{ha} - Q_{(\text{conv})h} \cdot r_h \tag{6}$$

$$T_h^4 = T_{ha}^4 - Q_{(\text{rad})h} \cdot r_{(\text{rad})h} \tag{7}$$

$$Q_h = Q_{(\text{conv})h} + Q_{(\text{rad})h} \tag{8}$$

In the above equations, the factor r (with h or c index, corresponding to the hot and cold sides of the cell, respectively) represents the total linear thermal resistance (conducting in a solid material and contacts at the boundary, e.g., thermal grease) of the heat exchanger. It is the proportionality factor between the temperature difference and the heat flux via conduction at each side of the exchanger. Factor $r_{(\text{rad})h}$ represents the thermal resistance for radiation in a similar way like r for conduction. All of them, r_h,r_c and $r_{(\text{rad})h}$, were assumed to be constant (independent of temperature and other variables).

As for the radiation heat transfer, the level of heat resistance comes from the Stefan–Bolzmann relation (9)

$$Q_{(\text{rad})h} = \sigma A F \left(T_1^4 - T_2^4\right) \tag{9}$$

where F is in the range 0–1 and represents the view factor, emittance. In order to solve the problem, the first law of thermodynamics should also be taken into account, combining the heat fluxes (entering and leaving the thermoelectric module) and the electrical power.

3 Sample Calculation, Result, and Discussion

Sample calculations of equivalent conduction thermal resistance were done for a 10 cm thick layer of copper (its area is equal to the surface contact area of the sample thermoelectric module described below). In this case, r is equal to 0.065 K/W. To compare, the resistance of 2.6 K/W corresponds to a 5 mm thick Plexiglas.

In order to illustrate the behavior of the actual module, data for a commercially available thermoelectric generator TECTEG MFR, TEG1-PB12690 were assumed. Thus (from manufacturer data sheet), $R = 2.05\ \Omega$, $K = 0.3912$ W/K, the contact surface area $A = 62 \times 62$ mm^2, $\alpha_{\text{eqv}} = 0.0233$ V/K, and the hot side temperature $T_h = 873$ K (max). Therefore, $T_{ha} = 873$ K and $T_{ca} = 303$ K.

The calculations were made using WOLFRAM MATHEMATICA software.

3.1 Thermoelectric Generator Performance for Fixed Temperatures. In order to determine the efficiency and electric power of the cell as a function of current in the circuit for the given constant temperatures of the upper and lower heat sources (T_{ha}, T_{ca}), Eqs. (2) and (4) were used. In practical implementation, various points of this graph can be obtained by changing the electrical resistance of the power receiver connected to the system.

Calculations were done by numerical optimization because use of Eq. (4), with T_h and T_c expressed by (5) and (6), does not lead to a closed-form solution. Although the curves resemble parabolas, they actually are not. Radiation does not occur in the situations considered, which correspond to an opaque material of heat exchanger and other thermal resistances (e.g., thermal grease).

As can be seen in the graphs (Figs. 2 and 3), as the thermal resistance of the heat exchangers accompanying the module increases, the maximum efficiency of the cell, maximum power and short-circuit current, decreases. This not only negatively affects the operation of the system by reducing the useful effect—electric power—but also reduces the temperature difference between both sides of the cell and in consequence, the heat flux. Therefore, the drop in electric power is higher than the fall in efficiency. Thermoelectric effects influence the thermal characteristics of the entire system (heat flux at constant T_{ha} and T_{ca}). It obviously changes the heat flux supplied to the system and released from it and in consequence, the temperatures of both hot and cold sides (T_h and T_c), which should be taken into account when designing other components of the system. Most importantly, both the resistance of the power receiver and the electric current, which correspond to maximum efficiency or maximum power, change.

With the increase of r, the temperature variation of both surfaces of the cell, along with the varying current intensity, increases (Fig. 4). The variation is highest for current close to zero (in particular, $r > 0$) and decreases as the current is close to the short-circuit one. Varying only the receiver's electrical resistance, i.e., the current in the circuit, the temperature (of cell's surfaces) can vary in some range. For $r = 0.065$ K/W, temperature at the hot side can vary from 854 K to 859 K depending only on the electric current. For $r = 1$, it can vary from 724 K to 748 K (24 K difference). For $r = 2.6$, the variation is from 662 K to 682 K (20 K difference). It can be seen that the potential to change the temperature by the receiver resistance is the highest for $r = 1$ (considering only the cases presented in Fig. 4). For the lower values of r, the temperature is much closer to the temperature of the heat source, which is constant according to the assumption. For the higher values of r, the temperature gradient on the thermoelectric cell is significantly lower, so the short circuit current is also smaller, and the potential of the temperature variation is lower. The length of the curves in Fig. 4 is the result of the possible electric current intensity under given conditions (see Fig. 1). Lowering the temperature gradient on the cell (by applying greater electric current) is the reason for shifting the maximum power and efficiency points (Figs. 2 and 3) toward the lower value of electric currents with the increase of the thermal resistance r_h, r_c.

Figure 5 shows the temperature change of the cold and hot sides of the cell for the electric current intensity selected at each point to achieve the highest possible power. It has to be taken into account that these temperatures may be higher or lower depending on the electric load of the cell (for nonoptimum electrical resistance) and

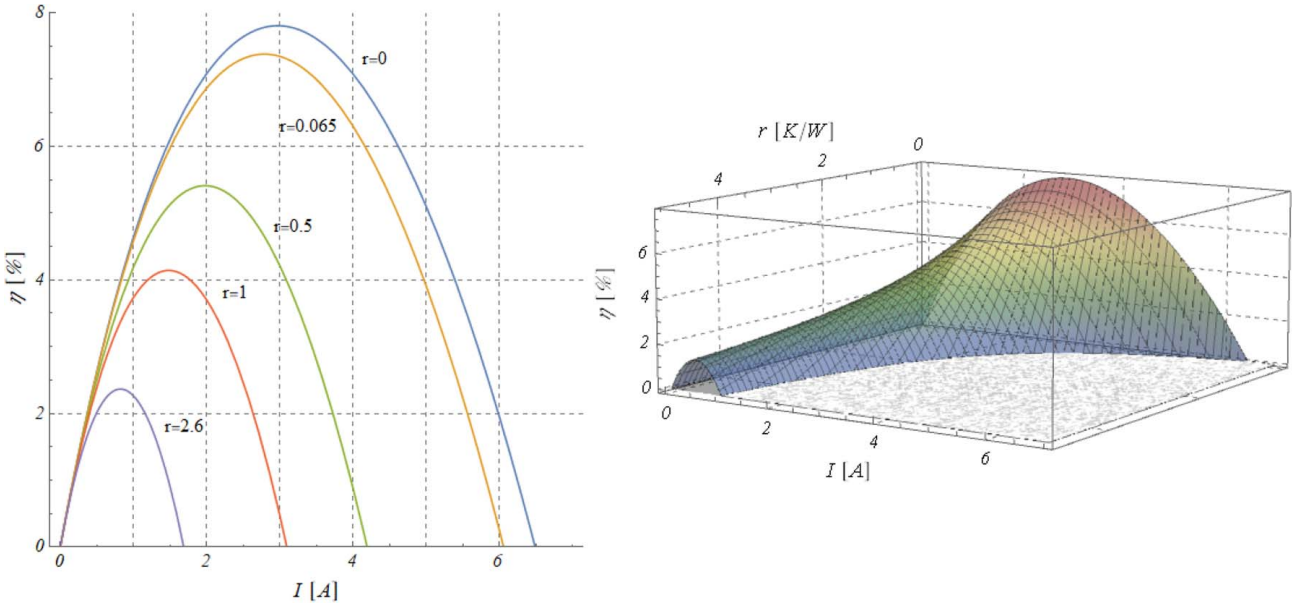

Fig. 2 Efficiency as a function of current at $T_{ha} = 873$ K and $T_{ca} = 303$ K for different r ($r = r_h = r_c$)

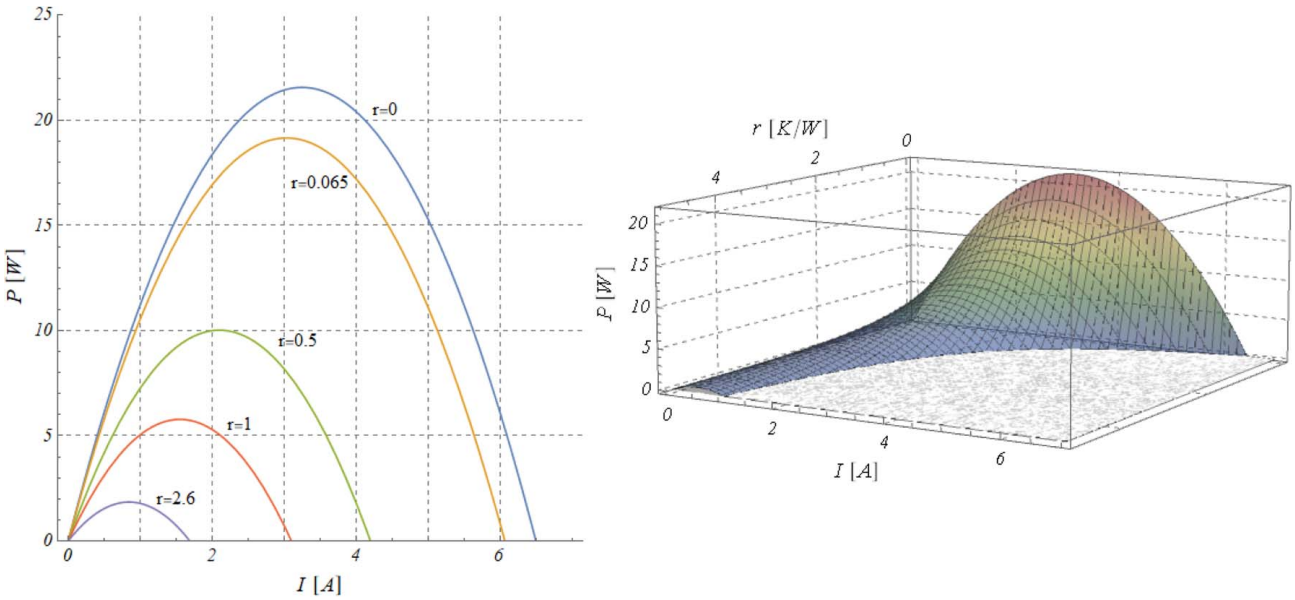

Fig. 3 Power (external) as a function of current at $T_{ha} = 873$ K and $T_{ca} = 303$ K for different r ($r = r_h = r_c$)

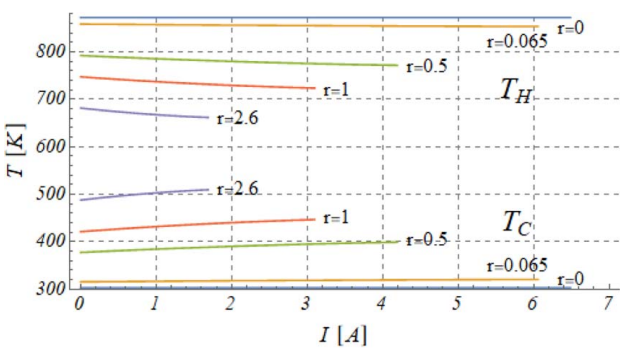

Fig. 4 Module side temperatures as a function of current at $T_{ha} = 873$ K and $T_{ca} = 303$ K for various r ($r = r_h = r_c$)

changes in the electric current in the circuit. This graph presents usable temperature difference (ΔT) in a direct way, and, for a given resistance of the heat exchanger (r), it is an indicator describing the work of the cell and deviation from heat source temperatures (ideal model). Similar results are obtained for the highest efficiency, and the diagrams look alike.

Figure 6 presents the values of the external resistance which should be connected as the output power to achieve the desired magnitude of current for different values of r. The plotted black lines represent the optimum value to achieve the best efficiency (solid line) and the highest power (dashed line). There is a statement in electric engineering for idealized battery (electromotive source and constant internal resistance) that in order to achieve the highest electrical power of the external receiver, its resistance should be equal to the inner resistance of the power source ($R_{\text{ext}} = R_{\text{int}}$). However, this is valid only in the case of constant

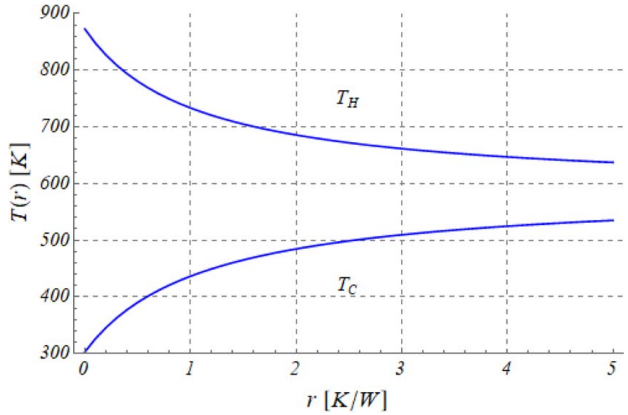

Fig. 5 Temperature of module sides at $T_{ha} = 873$ K and $T_{ca} = 303$ K for different r ($r = r_h = r_c$), for maximum power

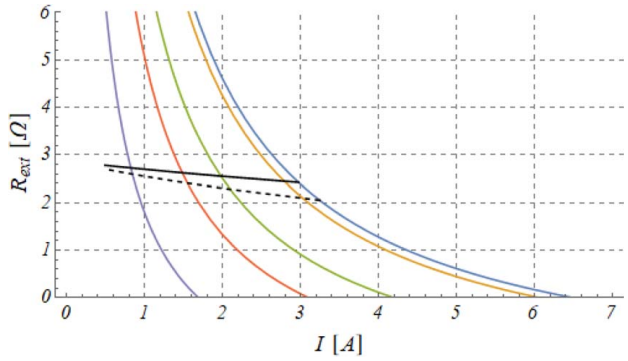

Fig. 6 Selected aspects of the external resistance value at $T_{ha} = 873$ K and $T_{ca} = 303$ K for different r ($r = r_h = r_c$)

electromotive force. In the case of thermoelectric generator with a constant Seebeck coefficient, it is only true at constant temperature difference between both sides of the cell—ΔT. In most real situations, heat transfer takes place through conduction and convection (resistance r_h and r_c), so increasing the heat flux supplied and released from the cell as a result of increasing the current in the circuit leads to lowering the temperature of the hot side and increasing the cold one. The electrical resistance of the receiver, in order to achieve maximum power and maximum efficiency, should be 2.05 Ω and 2.455 Ω, respectively.

This is obviously true for $r = 0$. In fact, for the $r_h = r_c = 1.2$, this resistance is 2.44 Ω and 2.64 Ω, respectively. Resistance changes (increases) in relation to the idealized model (assuming $r_c = r_h = 0$ K/W). This phenomenon reduces the current flowing in the system (for the points of maximum power and efficiency); at the same time, the occurring decrease in temperature difference ΔT (resulting from nonzero r_c and r_h) reduces the electromotive force and thus also lowers down current in the circuit. The same phenomenon, i.e., decreasing ΔT, also reduces the short-circuit current, most intensively from all possible working points (electric current values). The statement quoted above is retained in every analyzed condition, so the point of maximum achievable power can be obtained by setting the electric current value to half of the short circuit current with satisfactory accuracy.

It seems reasonable to accept the rule that to obtain the maximum power, the current should be set to half the value of the short-circuit. The relative deviation in power magnitude is not higher than 0.00001 in the range of r from 0 K/W to 5 K/W. It practically does not exist, so the statement is true. The situation is a little bit more complicated for achieving the best possible efficiency. Figure 7 presents the difference between efficiency in both situations. First, for the electric current corresponding to the best

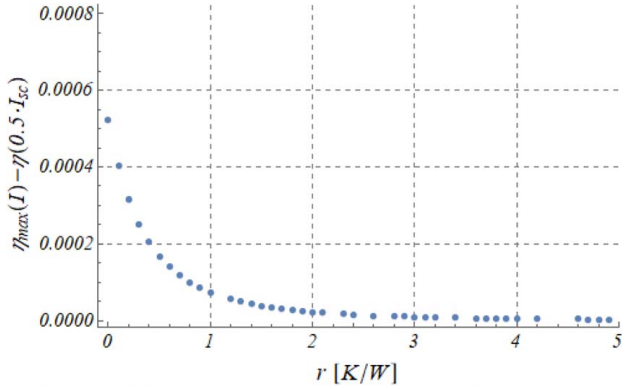

Fig. 7 Difference between best possible efficiency and efficiency when electric current equals half short circuit current for given r

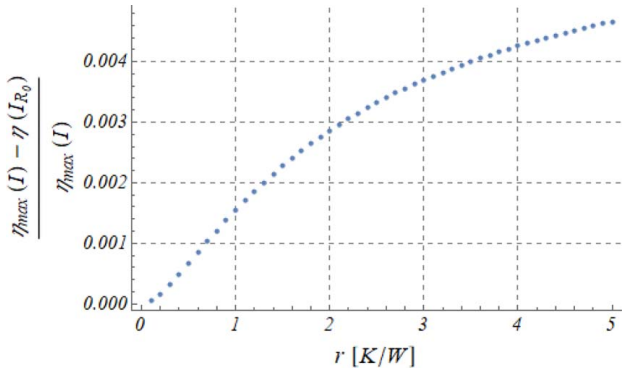

Fig. 8 Difference between best possible efficiency and efficiency when resistance of the power receiver is fixed (R_0) for given r

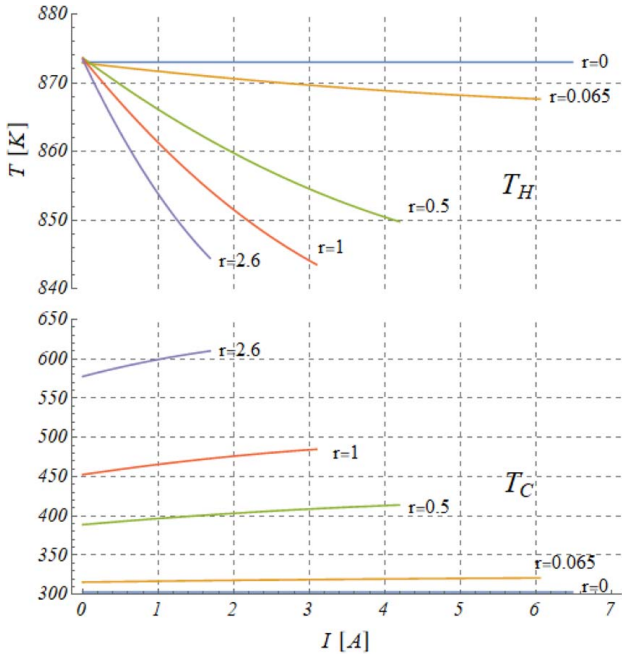

Fig. 9 Module side temperatures as a function of current at selected T_{ha} and $T_{ca} = 303$ K for various r ($r = r_h = r_c$)

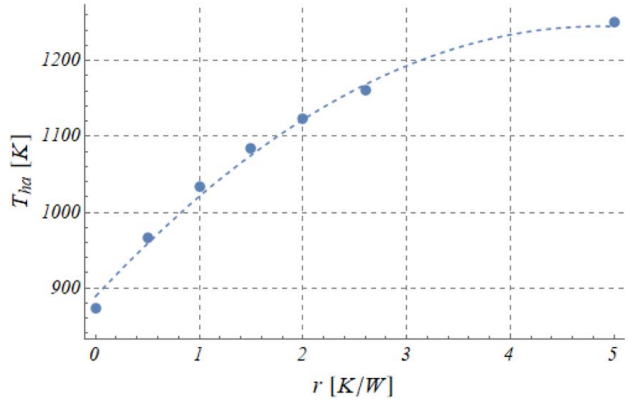

Fig. 10 Optimal value of T_{ha} for different heat exchanger resistance (description in text)

possible efficiency for given r, and second, for any r, the current is set to a half of the short-circuit current. Figure 8 shows the relative deviation of efficiency when constant external resistance of 2.05 Ω is applied. This case would give a vertical line (constant resistance) when imposed in Fig. 6. This is the value for best efficiency if $r = 0$ (this is the point, where dashed line crosses the curve for $r = 0$).

3.2 Determination of the Heat Source Temperature. In the above considerations, the temperature of the heat source (T_{ha}) was determined based on the maximum allowable temperature of the hot side of the thermoelectric cell. When designing a test bench for thermoelectric cell, it is completely a safe solution, but it can be seen that for working conditions with a significant thermal resistance of heat exchangers ($r > 0$), the temperature of the cell (T_h) does not approach the permitted maximum. Therefore, the temperature of the heat source (T_{ha}) can be risen up.

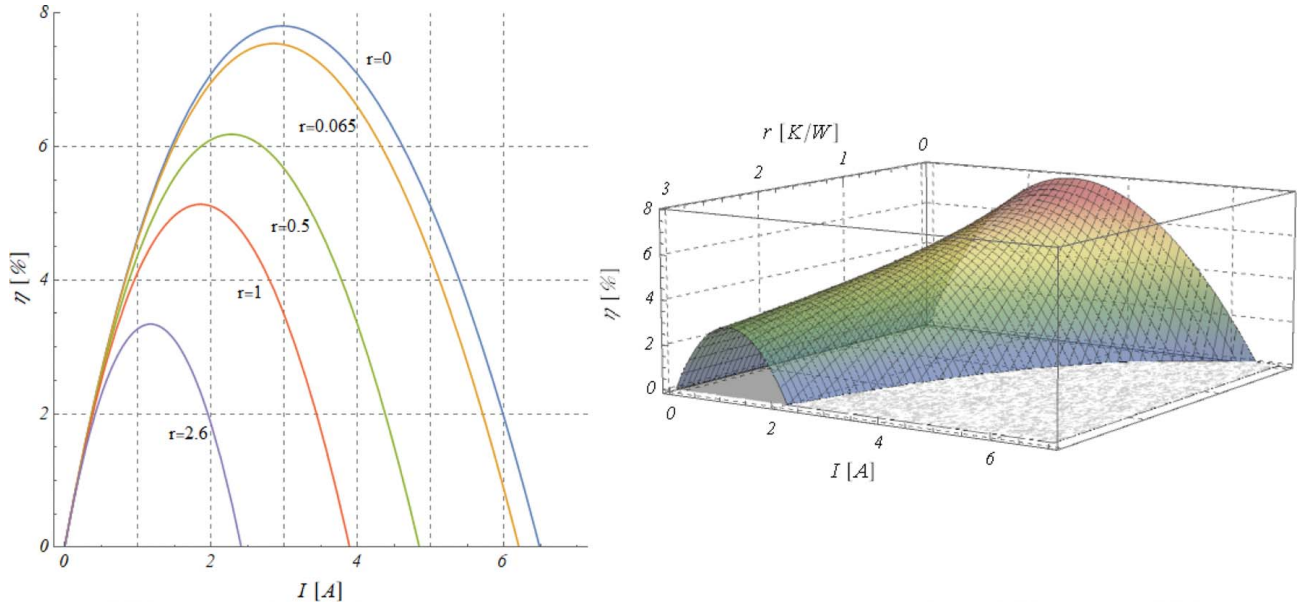

Fig. 11 Efficiency as a function of current at variable T_{ha} and $T_{ca} = 303$ K for different r ($r = r_h = r_c$)

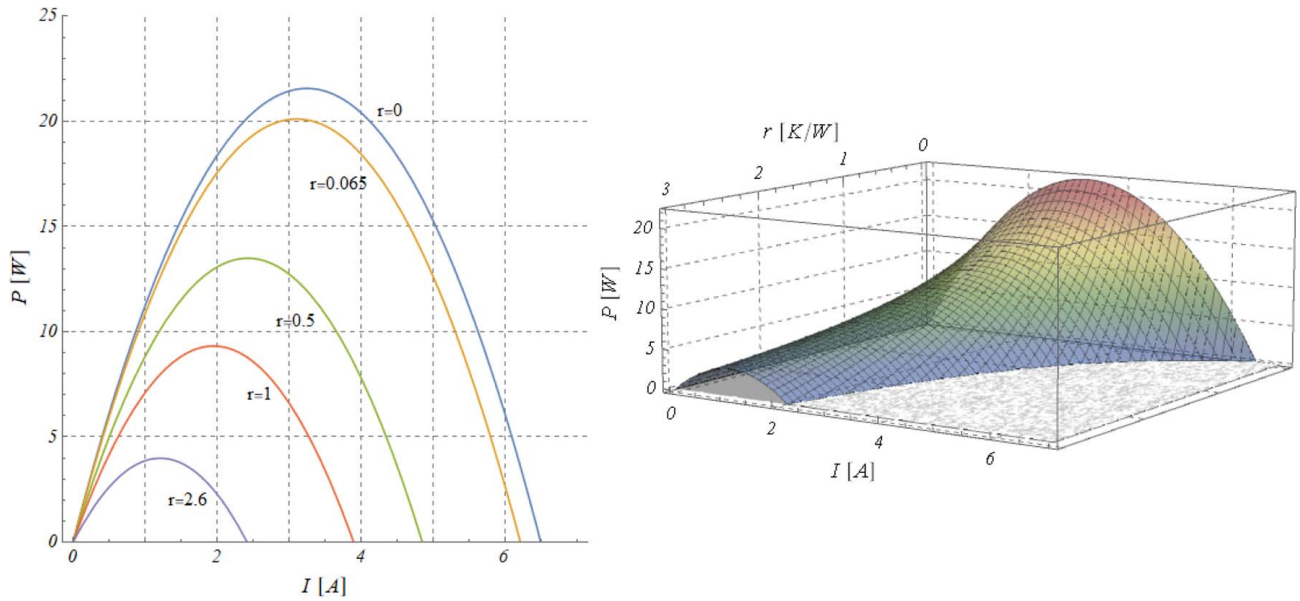

Fig. 12 Power (external) as a function of current at variable T_{ha} and $T_{ca} = 303$ K for different r ($r = r_h = r_c$)

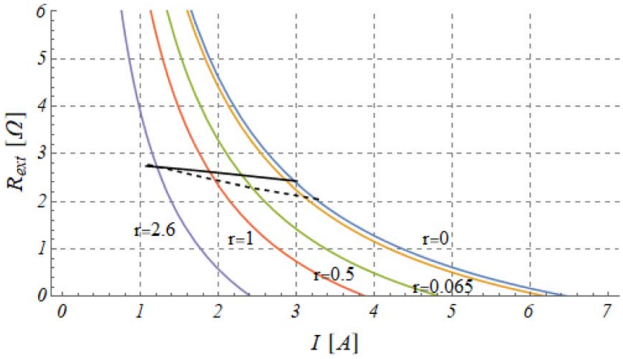

Fig. 13 Selected aspects of the external resistance value at variable T_{ha} and $T_{ca} = 303$ K for different r ($r = r_h = r_c$)

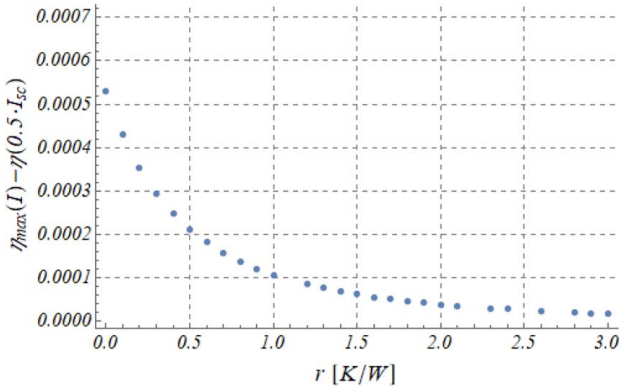

Fig. 14 Difference between the best possible efficiency and efficiency when electric current equals half short-circuit current for given r for variable T_{ha}

The situation in which the value of T_{ha} is independently selected for every value of r was considered. It was done in such a way that T_{ha} is as high as possible but not exceeding the allowed working conditions of the thermoelectric cell, regardless of the current in the circuit. The temperature of the module sides is presented in Fig. 9 in a similar way to Fig. 4.

For the same reasons as in the previously considered situation, the greatest potential for temperature regulation by changes in the electric current in the circuit is observed for $r = 1$. For lower values of r, temperature of the module is relatively close to the temperature of the heat source. For the higher values of r, the temperature drop is more significant for operational parameters, so the short circuit current is smaller, which affects the potential temperature variation. The T_{ha} temperature in this case obviously increases with the rise of thermal resistance of the exchanger, as shown in Fig. 10.

Calculation of efficiency and electrical power of the thermoelectric cell was also made for the situations with variable T_{ha}, like described above (highest possible, without violating the permissible temperature limit for thermoelectric cell regardless of the electric current), in the same way as in Figs. 2 and 3. Results are presented in Figs. 11 and 12.

Figure 13 presents the relation between the electrical resistance of the power receiver connected to the thermoelectric module in a similar way to Fig. 6 but for variable T_{ha} (according to Fig. 10). Figures 14 and 15 show the difference between the best possible efficiency and efficiency when electric current equals half short-circuit current and respectively the difference between the best possible efficiency and efficiency when resistance of power receiver is fixed (R_0). This fixed resistance corresponds to the optimum efficiency working condition when no extra thermal resistance is imposed ($r = 0$).

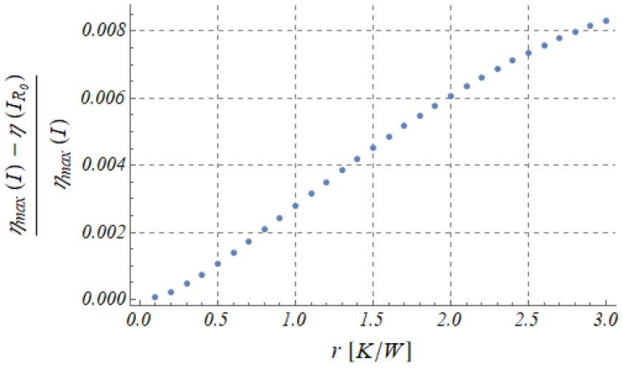

Fig. 15 Difference between the best possible efficiency and efficiency when resistance of the power receiver is fixed (R_0) for given r for variable T_{ha}

4 Conclusions

The proposed method of modeling thermoelectric generators taking into account the thermal resistance gives the results of calculations in line with the predictions. Calculations were made for different magnitudes of thermal resistance of heat exchangers. In the majority of practical implementations, this value is or should be minimized, so usually it is not greater than one ($r < 1$). Simulations carried out for $r = 0.065$ K/W (corresponding to the conductivity in the copper layer with a thickness of 10 cm) showed that the maximum achievable efficiency of the cell decreased from 7.80% to 7.38% and the power decreased from 21.57 W to 19.16 W. The optimum value of the electrical resistance of the power receiver (due to the maximization of power or efficiency) changes as the thermal resistance of the associated elements increases. These changes are very small, which implies the practical unprofitability of taking them into account in the design of a real system. Popular DC/DC voltage converters capable of varying the input resistance have an efficiency clearly below 1, which will not allow achieving the desired profit resulting from their use in considered cases. For the analyzed cell model, it can be stated, with a fairly good approximation for most applications, that the working points with maximum efficiency and maximum power overlap. For $r = 0$, their difference is about 9% of the current value, which results in a relative efficiency deviation of no more than 0.7%. This value decreases with the increase of r for both cases (constant and variable T_{ha}), so the relative difference in the current intensity between the point of maximum power and the point of maximum efficiency is smaller. If the thermal resistance is maintained at a low level, it does not significantly affect the performance of the whole thermoelectric system. When considering 10 cm copper layer ($r = 0.065$ K/W), differences in operational parameters are below the level which can be measured by vast majority of popular equipments, so they are practically insignificant. These differences have usually no influence on laboratory tests of appropriately designed systems with the thermoelectric cell. Another important issue which should be taken into account is thermal resistance at the contact between the thermoelectric cell and the heat exchanger. It strongly depends on the clamping force, the thermal grease used, and smoothness of the surfaces. It is very hard to estimate the correct value of r in such a case. The final r value should be a sum of r for conduction within the material (0.065 K/W for 10 cm copper) and r for the contact between materials. A small value of r is already introduced in most of the commercially available thermoelectric cells, because of the ceramic layer or coating.

The scope of these investigations was to assess the influence of the heat exchanger thermal resistance without considering the internal structure of thermoelectric cells. Proposed method and behavior of the entire system can be used to assess thermal contact quality (e.g., thermal grease quality) by finding correct value of r, which matches the model. For both presented situations (constant and

variable T_{ha}), the potential of varying the temperature of the thermoelectric module hot side (and accompanying heat exchanger) is the biggest for the value of $r = 1$. This observation can be useful when designing a system in which a fine control of temperature is essential. Doing it in this way can be faster and more accurate than controlling the heat source. For different arrangements of the thermoelectric cell system, it may be also necessary to consider the heat transmitted by radiation. It will probably have much more intensive effect on the deviations from the ideal model analyzed above ($r = 0$, constant surface temperature of the cell) due to stronger changes in heat flux along with changes in radiant surface temperatures.

Funding Data

- National Science Centre (Grant No. 2016/23/B/ST8/03133; Funder ID: 10.13039/501100004281).

Nomenclature

I = electric current, A
W = work of electricity in external resistance, J
r_c = heat resistance of the heat exchanger behind the cold side, K/W
r_h = heat resistance of the heat exchanger behind the hot side (conduction), K/W
$r_{(\mathrm{rad})h}$ = heat resistance of the heat exchanger behind the hot side (radiation), K/W
K_{eqv} = equivalent thermal conductivity (for the entire cell), W/(mK)
Q_c = heat flux at the module cold side, W
Q_h = heat flux at the module hot side, W
R_{int} = internal electric resistance (for the entire cell), Ω
T_c = module cold side temperature, K
T_h = module hot side temperature, K
T_{ca} = temperature of the heat sink (constant), K
T_{ha} = temperature of the heat source (constant), K
V_{OC} = voltage (open circuit, electromotive force), V
α_{eqv} = equivalent Seebeck coefficient, V/K
ΔT = temperature difference at the module, equal to $T_h - T_c$, K
$\mathcal{E}$ = electromotive force, V

References

[1] Schock, H., Brereton, G., Case, E., D'Angelo, J., Hogan, T., Lyle, M., Maloney, R., Moran, K., Novak, J., Nelson, C., Panayi, A., Ruckle, T., Sakamoto, J., Shih, T., Timm, E., Zhang, L., and Zhu, G., 2013, "Prospects for Implementation of Thermoelectric Generators as Waste Heat Recovery Systems in Class 8 Truck Applications," ASME J. Energy Res. Technol., **135**(2), p. 022001.

[2] Rychter, T., and Teodorczyk, A., 2006, *Theory of Piston Engines*, WKL, Warsaw (in Polish).

[3] Buchalik, R., Buczkowski, D., Przybyla, G., and Nowak, G., 2016, "Investigation of Waste Heat Recovery for Automobile Application Based on a Thermoelectric Module," J. KONES Powertrain Transp., **23**(4), pp. 25–32.

[4] Nolas, G. S., Sharp, J., and Goldsmid, H. J., 2001, *Thermoelectrics, Basic Principles and New Materials Developments*, Springer-Verlag, New York.

[5] Zhu, G., Liu, J., Fu, J., and Wang, S., 2017, "A Combined Organic Rankine Cycle With Double Modes Used for Internal Combustion Engine Waste Heat Recovery," ASME J. Eng. Gas Turbines Power, **139**(11), p. 112804.

[6] Champier, D., 2017, "Thermoelectric Generators: A Review of Applications," Energy Convers. Manage., **140**(Part 2), pp. 167–181.

[7] Amini, A., Ekici, O., and Yakut, K., 2019, "Investigating the Effect of Medium Liquid Layer Circulation on Temperature Distribution in a Thermoelectric Generator Heat Exchanger Assembly," ASME J. Energy Res. Technol., **141**(4), p. 041902.

[8] Mansouri, N., Timm, E. J., Schock, H. J., Sahoo, D., and Kotrba, A., 2016, "Development of a Circular Thermoelectric Skutterudite Couple Using Compression Technology," ASME J. Energy Res. Technol., **138**(5), p. 052003.

[9] Pierce, R. D., and Stevens, R. J., 2017, "Measuring Thermal Substrate Resistance and Impact on the Characterization of Thermoelectric Modules," Measurement, **111**(Dec.), pp. 173–182.

[10] He, W., Wang, S., Li, Y., and Zhao, Y., 2016, "Structural Size Optimization on an Exhaust Exchanger Based on the Fluid Heat Transfer and Flow Resistance Characteristics Applied to an Automotive Thermoelectric Generator," Energy Convers. Manage., **129**(Dec.), pp. 240–249.

[11] Siddique, A. R. M., Kratz, F., Mahmud, S. J., and Heyst, B. V., 2019, "Energy Conversion by Nanomaterial-Based Trapezoidal-Shaped Leg of Thermoelectric Generator Considering Convection Heat Transfer Effect," ASME J. Energy Res. Technol., **141**(8), p. 082001.

[12] Gao, J., Du, Q., Chen, M., Li, B., and Zhang, D., 2015, "Assessing the Accuracy of Mathematical Models Used in Thermoelectric Simulation: Thermal Influence of Insulated Air Zone and Radiation Heat," Appl. Therm. Eng., **82**(May), pp. 162–169.

[13] Wang, Y., Shuai, L., Zhang, Y., Deng, Y., and Su, C., 2016, "The Influence of Inner Topology of Exhaust Heat Exchanger and Thermoelectric Module Distribution on the Performance of Automotive Thermoelectric Generator," Energy Convers. Manage., **126**(Oct.), pp. 266–277.

[14] Ying, X., Ye, F., Liu, R., and Bao, H., 2018, "Design and Optimization of Thermoelectric Cooling System Under Natural Convection Condition," ASME J. Therm. Sci. Eng. Appl., **10**(5), p. 051008.

[15] Liu, T., and Yang, Z., 2018, "Performance Assessment and Optimization of a Thermophotovoltaic Converter—Thermoelectric Generator Combined System," ASME J. Energy Res. Technol., **140**(7), p. 072010.

[16] Chen, M., Lu, S., and Liao, B., 2005, "On the Figure of Merit of Thermoelectric Generators," ASME J. Energy Res. Technol., **127**(1), pp. 37–41.

[17] Chen, L., Gong, J., Sun, F., and Wu, C., 2002, "Effect of Heat Transfer on the Performance of Thermoelectric Generators," Int. J. Therm. Sci., **41**(1), pp. 95–99.

[18] Mohamed, E. S., 2019, "Development and Performance Analysis of a TEG System Using Exhaust Recovery for a Light Diesel Vehicle With Assessment of Fuel Economy and Emissions," Appl. Therm. Eng., **147**(Jan.), pp. 661–674.

[19] Mahmoudinezhad, S., Rezaniakolaei, A., and Rosendahl, L. A., 2017, "Experimental Study on Effect of Operating Conditions on Thermoelectric Power Generation," 9th International Conference on Applied Energy, ICAE2017, Cardiff, Aug. 21–24, pp. 558–563.

[20] Hendricks, T. J., 2007, "Thermal System Interactions in Optimizing Advanced Thermoelectric Energy Recovery Systems," ASME J. Energy Res. Technol., **129**(3), pp. 223–231.

[21] Crane, D. T., and Bell, L. E., 2009, "Design to Maximize Performance of a Thermoelectric Power Generator With a Dynamic Thermal Power Source," ASME J. Energy Res. Technol., **131**(1), p. 012401.

[22] Ran, Y., Deng, Y., Hu, T., Su, C., and Liu, X., 2018, "Energy Efficient Thermoelectric Generator-Powered Localized Air-Conditioning System Applied in a Heavy-Duty Vehicle," ASME J. Energy Res. Technol., **140**(7), p. 072007.

[23] Tang, Z. B., Deng, Y. D., Su, C. Q., Shuai, W. W., and Xie, C. J., 2015, "A Research on Thermoelectric Generator's Electrical Performance Under Temperature Mismatch Conditions for Automotive Waste Heat Recovery System," Case Stud. Therm. Eng., **5**(Mar.), pp. 143–150.

[24] Montecucco, A., Siviter, J., and Knox, A. R., 2015, "Constant Heat Characterisation and Geometrical Optimisation of Thermoelectric Generators," Appl. Energy, **149**(July), pp. 248–258.

[25] Lienhard IV, J. H., and Lienhard V, J. H., 2017, *A Heat Transfer Textbook*, Phlogiston Press, Cambridge, MA.

[26] Ji, D., Wei, Z., Mazzoni, S., Mengarelli, M., Rajoo, S., Zhao, J., Pou, J., and Romagnoli, A., 2018, "Thermoelectric Generation for Waste Heat Recovery: Application of a System Level Design Optimization Approach Via Taguchi Method," Energy Convers. Manage., **172**(Sept.), pp. 507–516.

Energy Conversion and Management 259 (2022) 115587

Contents lists available at ScienceDirect

Energy Conversion and Management

journal homepage: www.elsevier.com/locate/enconman

Comparative analysis and optimization of one- and two-stage cooling systems with thermoelectric cells with respect to supercooling

Ryszard Buchalik [a], Grzegorz Nowak [a,*], Iwona Nowak [b]

[a] Department of Power Engineering and Turbomachinery, Silesian University of Technology, Konarskiego 18, 44-100 Gliwice, Poland
[b] Department of Applications of Mathematical and Artificial Intelligence Methods, Silesian University of Technology, Kaszubska 23, 44-100 Gliwice, Poland

ARTICLE INFO

Keywords:
Thermoelectric cooler
Supercooling
Thermal resistance
Current shaping

ABSTRACT

The paper discusses issues related to the modelling of a cooling system equipped with thermoelectric modules to achieve the lowest possible temperature of the cooled space. Considerations were made for both the steady state and the momentary capability to reach the lowest possible temperatures. The analysis concerns modules arranged as the in-series thermal connection in a sandwich configuration and the parallel connection in a single layer. It was assumed that in each case the modules worked with identical heat exchangers. Optimal sizes were found for the modules in each of the analysed configurations, both considering and omitting in the model the thermal resistance between the system elements. Taking resistance into account results in an almost 50% increase in the module dimensions to 90/250, compared to 60/170, and also in the minimum temperature rise by even up to 20*K*. Inducing higher currents in the circuits of the modules can cause momentary supercooling of the cold heat reservoir significantly below the temperature achievable in the steady state. The highest values of momentary drops in temperature can be achieved through current pulse in the circuits, and also for higher thermal capacities of the upper and additional internal reservoir in a sandwich system. To determine optimal supply currents for the modules, optimization was carried out. In the considered configurations this made it possible to achieve momentary supercooling temperatures by about 18*K* lower compared to the steady state. The most essential design variables are the number of thermoelectric legs, the shape of the thermal capacity of the current pulse shape and the internal reservoir.

1. Introduction

This paper deals with the simulation of a system using thermoelectric modules operating in the cooling mode (thermoelectric cooler -TEC). The use of this type of devices is now becoming increasingly common in various branches of technology. One typical application is the use of thermoelectric cells in consumer refrigerators [1], to maintain a constant temperature of electronic components [2] or in systems preventing the formation of thermal stresses [3]. The advantage of thermoelectric cells is their universality. Apart from the heat pump-mode operation, they can also work as electricity generators using a temperature gradient and converting part of the heat flux into electrical energy [4]. The main downsides limiting an even wider use of thermoelectric modules are their relatively low energy-conversion efficiency when they operate as a generator and a low coefficient of performance (COP) when they operate as a heat pump. The need to improve efficiency is evident in the intensive development, both in the search for new thermoelectric materials and in the shaping of the thermoelectric cell properties [5,6]. An improvement in the efficiency of systems using thermoelectric cells can be achieved by minimizing thermal resistance in the system, which can be realized by ensuring proper conditions of contact between individual modules and heat exchangers [7], proper shaping of the heat sink exchanging heat with the environment (especially in the case of air cooling), and the use of phase-change materials (PCMs) with appropriately selected temperature [8]. A non-standard application of thermoelectric cells is power generation based on the heat released due to nuclear reactions [9], which is mainly used in space technology. Another application inspired by the current Covid-19 pandemic is the need for air disinfection. Ji et al. [10] proposed a solution to inactivate potential viruses by heating air to a high temperature and then administering it to the patient after prior cooling using TEC modules. More and varied applications of thermoelectric materials, together with the latest findings are presented in [11].

TECs can also be used to produce the so-called supercooling phenomenon [12], which involves achieving a momentary drop in the

* Corresponding author.
E-mail address: grzegorz.nowak@polsl.pl (G. Nowak).

https://doi.org/10.1016/j.enconman.2022.115587
Received 7 November 2021; Received in revised form 17 March 2022; Accepted 4 April 2022
Available online 11 April 2022

Nomenclature

Latin symbols

A	leg surface area, m^2
c	thermal capacity, J/K
HTF	heat transfer coefficient,W/K
h	leg height,m
I	current intensity,A
m	mass,kg
n	number of the module legs
P	power,W
$\dot{Q}$	heat flux,W
r	contact thermal resistance,Km^2/W
R	electrical resistance,Ω
t	time,s
T	temperature,K

Greek symbols

λ	thermal conductivity,$W/(mK)$
ρ	resistivity,Ωm
α	Seebeck coefficient,V/K

Subscripts

al	lower ambient
au	upper ambient
l	lower
m	internal heat reservoir
TEM	thermoelectric module
u	upper

cooled space temperature below the minimum value achievable in the steady state. This issue was analysed in [13], discussing the use of different current pulses to achieve the lowest possible temperature of the cooling system cold side. It may be also possible to obtain a lower cooling temperature than in the steady state by using modules thermally connected in series (a multi-stage system) or modules in a thermally parallel configuration (a one-stage system). Considering the possibility of optimizing the height of the thermoelectric leg, which would lead to lowering the minimum adiabatic temperature of the thermoelectric cooler and, using an appropriately selected current at the same time, the use of multi-stage cooling would be more effective than a one-stage system [14,15]. There are works dealing with the phenomenon of supercooling in a multi-stage system. Gao et al. [16] showed a possible configuration along with a comprehensive description of such a system, but in their study they limited themselves to an arbitrary number of legs in both layers. In [17] attention is drawn to different parameters of the internal structure of the cell due to the optimization performed for both layers of the two-stage system, assuming variations in their parameters. Some researchers use advanced parameter optimization methods, such as the genetic algorithm (GA) [18,19]. The authors of [20] present an analysis of the variability in the performance of a multi-stage cooler due to the heterogeneity of the material parameters. Chen et al. [21] analysed the COP and the cooling capacity of a two-stage refrigerator system and presented its mathematical model. The authors of [22] show an example of the application of a PCM in a heat exchanger accompanying a multi-stage system of thermoelectric cells and the utilization of the phase-change phenomenon when supercooling conditions are reached. Meng et al. [23] investigated the operation of a multi-stage system considering the supercooling phenomenon induced by triangular and square current waveforms in the circuit. In Gao et al. [24] the authors focused on analysing the impact of current shaping in the circuit, this time – in a multi-stage system. Multi-stage systems can be useful not only in the case of the classical design of cells with a flat shape, but also for other geometrical configurations [25]. There are many works devoted to the thermoelectric cell system co-operation with photovoltaics [26] and also to multi-stage thermoelectric modules [27]. Min and Rowe [28] showed the concept of a domestic refrigeration device whose cooling capacity could be increased due to the application of multi-stage thermoelectric cells. The authors of [29] discuss an experiment performed to investigate the impact of the shape of the current pulses on the TEC module characteristics.

The multi-stage configuration can also be useful when thermoelectric cells are used as an electricity generator (thermoelectric generator – TEG). Such a case was studied by Zhao et al. [30], who optimized the number of the TEG legs. The authors of [31] addressed the problem of optimizing the dimensions of the TEG legs in a multi-stage configuration, taking into account the dependence of the system parameters on temperature. The study of Zhang et al. [32], on the other hand, is an example of multi-parameter optimization of a multi-stage system. Thermoelectric cells can also be used in combination with fuel cells. An example use of a multi-stage thermoelectric module co-operating with a membrane fuel cell is described in Guo et al. [33]. The literature includes works indicating that using a multi-stage configuration (with more than 2 stages) is beneficial both in the case of heat pumps [34] and electricity generation [35]. Like in one-stage modules, the device efficiency can be improved by shaping the legs in a way that deviates from their fixed cross-section [36].

The novelty and originality of the approach presented herein consists in:

- analysing supercooling in a two-stage system;
- taking account of the thermal capacity of the internal heat reservoir in the in-series configuration and determining the impact of its value on the system operation and characteristics;
- taking account of contact thermal resistance between the system elements in the modelling;
- optimizing the TEC size (number of legs) in each layer independently;
- independent modelling of the current curves in the circuits of thermoelectric cells;
- optimizing supply current curves to obtain the maximum supercooling effect;
- analysing the supercooling potential for each of the tested configurations and comparing them.

The results of the calculations performed in transient conditions, for the examples investigated in this work, show that one of the most significant parameters deciding about the quality of the TEC circuit operation is the thermal resistance arising between the elements [37]. If this resistance is omitted in the calculations, the cooled space minimum temperature gets substantially overestimated, and the optimization process carried out for such operating conditions gives much smaller sizes of the module than the dimensions which are actually required. It should be noted that for the system in-series configuration, each cooling stage of the TEC introduces additional thermal resistances. Taking them into account is thus an essential element of the TEC model.

2. Mathematical model

The analyses carried out in this paper concern the operation of a thermoelectric cooler system with a single and a double thermoelectric module. In the two-module system, the modules are arranged in series; the sandwich configuration is separated by a layer of a solid material. The separating layer has a specific value of thermal capacity. Contact

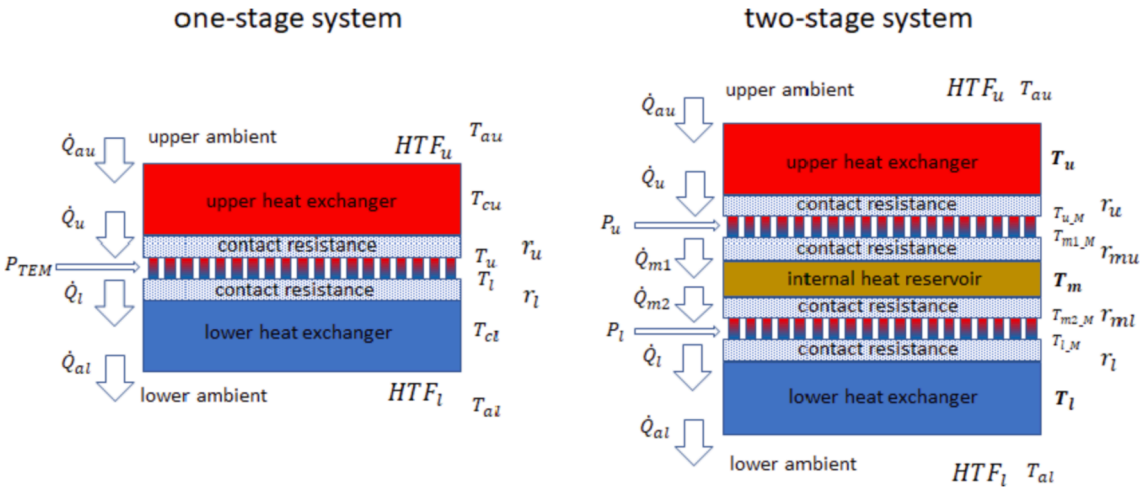

Fig. 1. One- and two-stage TEC system.

resistance is assumed to exist between each element of the system (Fig. 1), which increases the effective temperature difference at the thermoelectric cell junctions. The contact layer resistance was assumed as constant per unit area, therefore the thermal resistance value varies in proportion to the number of legs in each case under consideration.

The energy balance for the heat exchangers and the cell separating layer in the two-module mode is written as:

$$\dot{Q}_u = \dot{Q}_{au} - m_u c_u \frac{dT_u}{dt} \tag{1a}$$

$$\dot{Q}_l = \dot{Q}_{al} + m_l c_l \frac{dT_l}{dt} \tag{1b}$$

$$\dot{Q}_{m2} = \dot{Q}_{m1} - m_m c_m \frac{dT_m}{dt} \tag{1c}$$

where $\dot{Q}_{au}$ and $\dot{Q}_{al}$ are the heat fluxes collected and given to the environment by the upper (u) and lower (l) heat exchangers. The separating layer (m) can be treated as the internal heat reservoir. It is assumed in the model that both the exchangers and the separating layer in between the modules have temperatures levelled over their entire volume. Naturally, only balance equations (1a) and (1b) will occur for the one-module system.

The heat flux transferred between the heat exchanger and the environment is the product of the temperature difference in the two mediums and the heat transfer coefficient between them (HTF), i.e.:

$$\dot{Q}_{au} = HTF_u(T_{au} - T_u) \tag{2a}$$

$$\dot{Q}_{al} = HTF_l(T_l - T_{al}) \tag{2b}$$

The heat transfer coefficient is defined as the amount of heat transferred at a unit temperature difference (W/K), putting the system geometry aside.

Considering the relations describing heat conduction in the thermal resistance layers between the modules and the heat exchangers, it can also be noticed that the heat flux in that area is the product of the difference in temperature on the two sides of the contact layer (the heat exchanger and the thermoelectric junction) and the layer conductivity. This conductivity is the inverse of thermal resistance. To determine this resistance, r_i, describing the layer independently of its surface area (where i is u, mu, ml, l, respectively), should be used and then divided by the surface area of the layer. The layer surface area is understood as the total surface area of the legs multiplied by factor f_{Ai} determining the part of the cell surface that is not occupied by the legs. It follows that:

$$\dot{Q}_u = \frac{(T_u - T_{u\_M}) n_u A_u f_{A,u}}{r_u} \tag{3a}$$

$$\dot{Q}_{m1} = \frac{(T_{m1\_M} - T_m) n_u A_u f_{A,u}}{r_{mu}} \tag{3b}$$

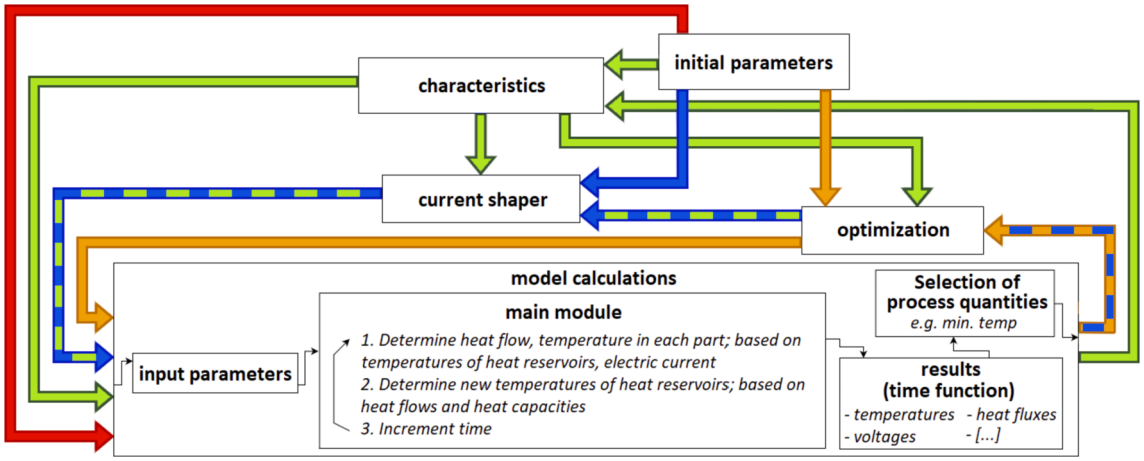

Fig. 2. Structure of calculations in the program.

Fig. 3. Stand for experimental testing of the TEC in the sandwich configuration.

$$\dot{Q}_{m2} = \frac{(T_m - T_{m2\_M})n_l A_l f_{A,l}}{r_{ml}} \tag{3c}$$

$$\dot{Q}_l = \frac{(T_{l\_M} - T_l)n_l A_l f_{A,l}}{r_l} \tag{3d}$$

Due to the rapid heat transfer in the thermoelectric element legs, which is the effect of their relatively small thermal capacity compared to the exchangers, the transfer can be treated as a quasi-steady state which depends on the temperature of the exchangers at time t and current I, i.e.:

$$T_u(t, I_u, I_l) = T_u(T_u(t), T_m(t), T_{au}, I_u) \tag{4a}$$

$$T_l(t, I_u, I_l) = T_l(T_l(t), T_m(t), T_{al}, I_l) \tag{4b}$$

$$T_m(t, I_u, I_l) = T_m(T_m(t), T_u(t), T_l(t), I_u, I_l) \tag{4c}$$

The boundary conditions to solve the above model are the ambient temperatures (upper and lower) and the currents in the thermoelectric module circuits, while the initial conditions are the temperatures of the heat exchangers and of the separating layer material. A detailed description of the thermoelectric module model is presented in [38]. To solve a problem formulated in this way, it is still necessary to determine the conditions for the heat transfer between the environment and the exchangers, the contact resistance between the system elements, the material parameters and the system geometrical features.

2.1. Computational software

The presented model has been implemented in the developed *ThermoelectricCalc* program. The program is used for comprehensive analyses of systems equipped with thermoelectric modules. A flowchart illustrating the system operation is presented in Fig. 2.

Basic model calculations based on the presented equations (1–4) supplemented with the equations described in [38] are realized in the *model calculations* module, where using input data (the system parameters, the time step and simulation time), time-dependent histories of the quantities that characterize the system operation (temperatures, voltage, current, heat flux, etc.) are determined. The main method is to trigger one-off calculations manually with preset parameters (the red path). The orange path calls the calculation model to determine the value of the objective function for each analysed variant of the solution. If the path of the algorithm operation goes through the *current shaper* module (the blue or green path), a procedure for shaping varied current pulses is incorporated into the optimization process. The green path with the *characteristics* module controls the automation of the process of determining full characteristics of the impact of the selected parameters on the system performance, e.g. the impact of thermal capacity of a selected reservoir on the system minimum temperature.

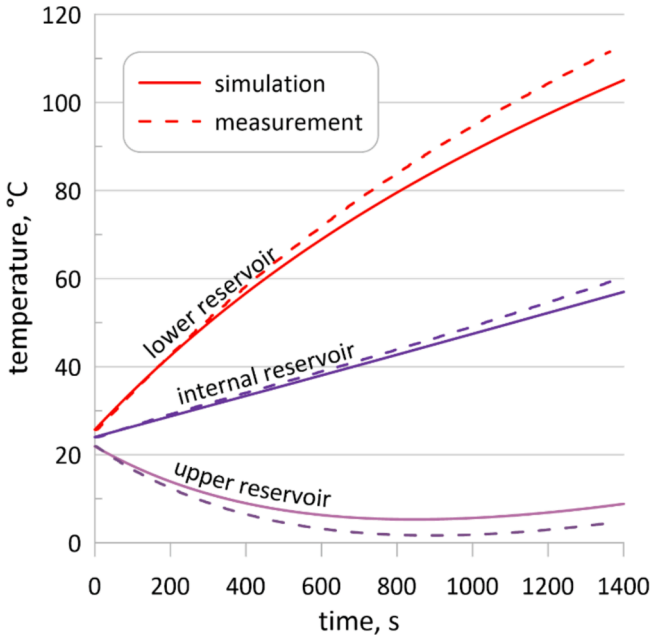

Fig. 4. Comparison between simulation and measurement results for constant currents in the circuits of the TEC modules.

2.2. Experimental validation

The applied software tool prepared based on the presented model was validated experimentally using a measuring system made of two thermoelectric modules and three heat reservoirs arranged in a sandwich configuration (cf. Figs. 1 & 3). The heat reservoirs were made as $100x100x50mm$ copper blocks. The testing was performed using two identical thermoelectric modules (MCTE1-19913L-S), the parameters of which were established using the testing stand and the procedures described in [38]. The *HTF* coefficients were also found experimentally by investigating the course of the process of the cooling of the heat reservoirs from the steady state and also by measuring the power needed to maintain a constant temperature. The tested system data are listed in Table A1 in the Appendix.

The first stage of the testing was experimental determination of the minimum temperature achievable in the steady state. For this purpose, simulations were performed using the *ThermoelectricCalc* program to find this quantity. In this way, the values of the current supplying the thermoelectric modules were also obtained. The applied automation of the measurements enabled a parallel experimental search for the minimum temperature. In order to reduce the time of the measurements, the current variability area was narrowed down to values close to the simulation results. The current was changed with the step of $0.01A$. This resulted in the temperature of $15.7^{\circ}C$ obtained for the upper and the lower module currents of $0.67/0.6A$, respectively. The corresponding values obtained from the simulations are $15.1^{\circ}C$ and $0.62/0.71A$, respectively.

In the next step, simulations were performed to determine constant

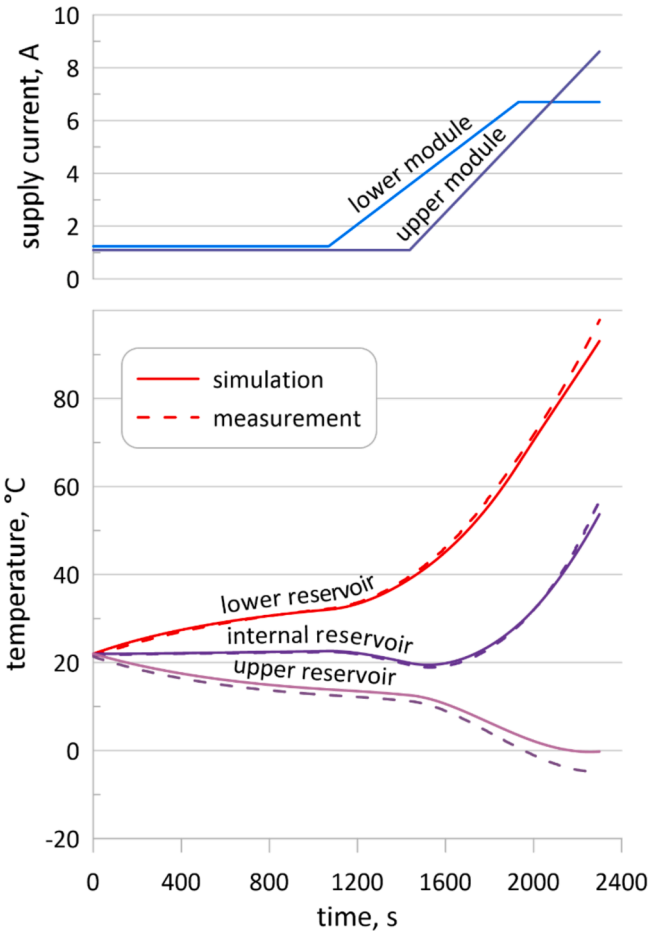

Fig. 5. Comparison between simulation and measurement results for varied currents.

magnitudes of the supply current that ensured achieving the minimum temperature of supercooling. The currents (4.78/5.49*A*) were then set on the testing stand and temperature measurements were carried out. In the case of the simulation, the minimum temperature was reached at the level of $4.5^{\circ}C$, whereas for the measurements the value was $2^{\circ}C$. Fig. 4 presents a comparison between time-dependent changes in temperatures obtained from the simulations and from the measurements performed on the testing stand.

It can be seen that the simulation results agree with the results of the measurements quite well. The differences in the temperature of the cooled and the internal reservoir do not exceed $3K$. Slightly bigger differences are observed for the heat sink, which is in direct contact with the environment.

In the next step of the validation process, the system response to a pulse of electric currents in the circuits of the TEC modules was examined. For this purpose, optimization simulations were first performed to establish such a history of the pulse, defined by the initial current, the rate and the time of the rise in the current and the current final value, that ensured achieving the minimum temperature of the upper reservoir. The simulation results and the results of measurements performed for such a pulse are presented in Fig. 5.

Based on the comparisons presented above, it can be seen that the results obtained from the simulation process run using the developed program correspond well to the results of real measurements and also guarantees reaching significantly lower supercooling temperature. The slight differences may be due to errors in the estimation of the TEC parameters, differences between individual modules, as well as the adopted simplifications.

Table 1
Parameters of the thermoelectric system operation.

Parameter	Value
Upper heat reservoir initial temperature T_{u0}, °C	20
Lower heat reservoir initial temperature T_{l0}, °C	20
Ambient upper temperatureT_{ua}, °C	20
Ambient lower temperature T_{la}, °C	20
Upper heat reservoir thermal capacity $c_u, J/K$	300
Lower heat reservoir thermal capacity $c_l, J/K$	450
Internal heat reservoir thermal capacity $c_m, J/K$	300
Heat resistances of contacts $r_i, \mu Km^2/W$	1 or 100
$HTF_u, W/K$	0.5
$HTF_l, W/K$	10
Number of legs n	100
Surface filling factor f_A	1
Electrical resistivity $\rho, \mu\Omega m$	53
Thermal conductivity $\lambda, W/K/m$	6.3
Seebeck coefficient $\alpha, mV/K$	1.6
Leg height h, mm	3
Leg cross-sectional area A, mm^2	10

The performed experiment proved the correctness of the formulated mathematical model and the usefulness of the model implementation in the *ThermoelectricCalc* program, in conditions of both constant currents and current pulsations.

3. Numerical examples

The numerical examples analysed in this work were based on a virtual TEC module whose parameters reflected data obtained from measurements of commercial thermoelectric modules intended for refrigeration applications. The tests were carried out on a purpose-made stand described in [38]. The only quantity that was not directly reflected in the simulations was the number of the legs, as it was a configuration parameter of the modelled and optimized system. As the reference case, it was assumed that the applied module consisted of 100 legs, and all the parameters utilized in the calculations were determined based on this assumption. For the testing purposes, it was further assumed that fractions of a single module could be used, i.e. that the number of legs in a single layer did not need to be a multiple of 100.

The values of the other data used for the calculations and characterizing the tested system were assumed based on a several-litre cooler adapted for commercial applications. In the model, the temperature of the environment is given independently on the system two sides. In the cases under analysis, its value was assumed as identical and equal to the ambient temperature. The initial temperature of all elements of the system was also assumed to be equal to the ambient temperature. The heat exchange with the cooled space (HTF_u) represents its thermal insulation from the environment, while HTF_l reflects the heat transfer to the environment by the heat sink. A complete list of parameters is presented in Table 1.

3.1. Analysis of the two-module cooling system

To evaluate the effect of combining thermoelectric modules to achieve better cooling performance, simulations were performed of in-series and parallel thermal connections of the two cells (Fig. 6). The results were compared with those obtained for a one-module system ($n = 100$). The simulations were based on the assumption that in all the cases the thermoelectric cells operated with identical exchangers (identical heat transfer coefficients *HTF*, i.e. the same heat sink giving up heat and the same cooled space insulation).

The difference between the system with two modules connected in parallel and the one-module configuration was the different number of thermoelectric couples ($n = 200$ instead of $n = 100$). The calculations were carried out in the transient state for a levelled initial temperature of the system equal to the ambient temperature.

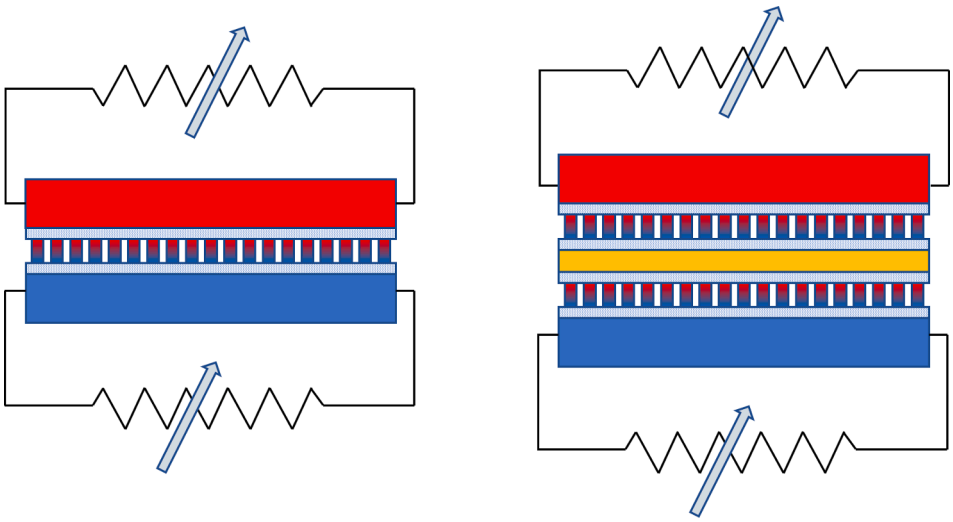

Fig. 6. System with a single module or with two modules connected in parallel (left) and a two-module system connected in series (right).

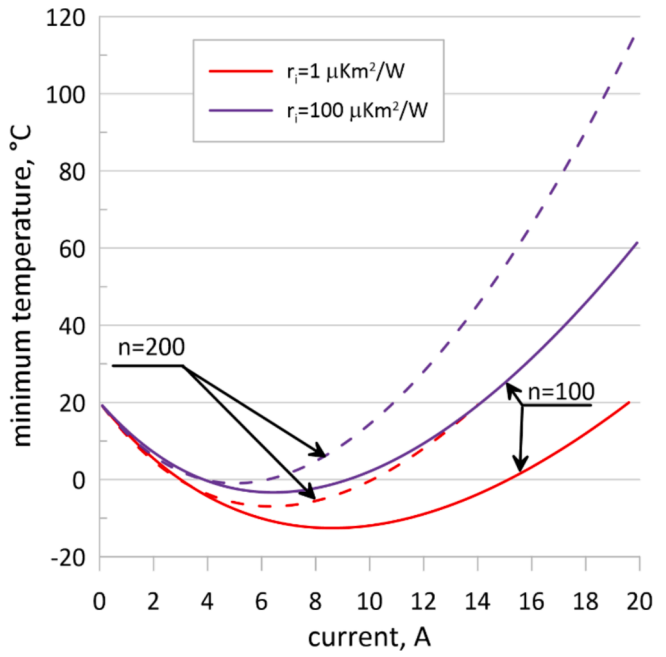

Fig. 7. Minimum temperature of the cold exchanger in steady-state conditions depending on the current for the one- and the two-module parallel configuration; solid lines represent the single TEC case (n = 100) and dashed lines represent two thermally connected TECs in parallel (n = 200); in both cases the heat sink is the same; the red lines show the minimum temperature for close-to-zero thermal contact resistance and the purple lines – for realistic contact resistance.

3.2. Parallel connection of TECs

The first step was to simulate the one-module system and the system with two modules connected in parallel. In this case, the number of the legs was doubled in the simulations of the two-module system, while the other parameters were left unchanged. Then the system static characteristics were determined, running the calculations until the steady state was obtained for each trial.

Figure 7 shows the minimum temperature of the cold exchanger achieved in the steady state for the two systems under consideration. The results were obtained for models in which contact thermal resistance was and was not taken into account (in the latter case – a very small but non-zero value of $r_i = 1\mu Km^2/W$ was assumed). In the former case, the resistance was assumed as the same on both sides of the module, totalling $r_i = 100\mu Km^2/W$. The graphs indicate that in all the analysed cases there is an optimum value of the electric current for which the cooled space temperature is the lowest. In situations where contact resistance of the layers is taken into account, this temperature is higher and its optimum is reached for smaller currents. This phenomenon is due to the higher total heat conduction resistance and lower cooling efficiency. The lower efficiency is due to the fact that the heat-absorbing junction is to some extent isolated from the cooled space (thermal resistance), which causes a bigger temperature gradient in the thermoelectric element.

It may come as a surprise that for two thermoelectric cells connected in parallel, the minimum temperature is higher than for a single cell. This results from the adopted assumption that the heat sinks exchanging heat (described by *HTF*) are characterized by identical parameters in both cases. Hence, adding another cell, firstly increases thermal conductivity between the two sides of the cells (a bigger number of legs) and, secondly, increases the amount of heat that has to be given up by the heat sink to the environment (Joule and Peltier heat), which raises the temperature of the hot side. This phenomenon would not occur if each cell had its own heat sink to dissipate heat. Then adding another module would always lower the cold side temperature. In such a situation there is no optimal number of cells, and an increase in their number will cause an asymptotic decrease in the cooled space temperature up to the adiabatic temperature of the cell with the defined heat sink for the set current. It should also be remembered that the power delivered to the cell varies not only with the current but also with the generated electromotive force, which increases with the temperature gradient. Furthermore, in the case of two modules connected in parallel, Ohm's voltage for a given current is twice higher than for a one-module configuration (when the modules are electrically connected in series), which also leads to a drop in cooling performance in case of limited power supply.

3.3. Series connection of TECs

In the next step, a two-module system was simulated with the cells thermally connected in series (according to the diagram presented in Fig. 6). It was assumed that the system was built of two identical modules with the same parameters as in the simulations discussed above. Moreover, equal values of contact resistance were assumed between each individual layers of the system sandwich structure. It is worth noting here that in such a system there are four layers of contact

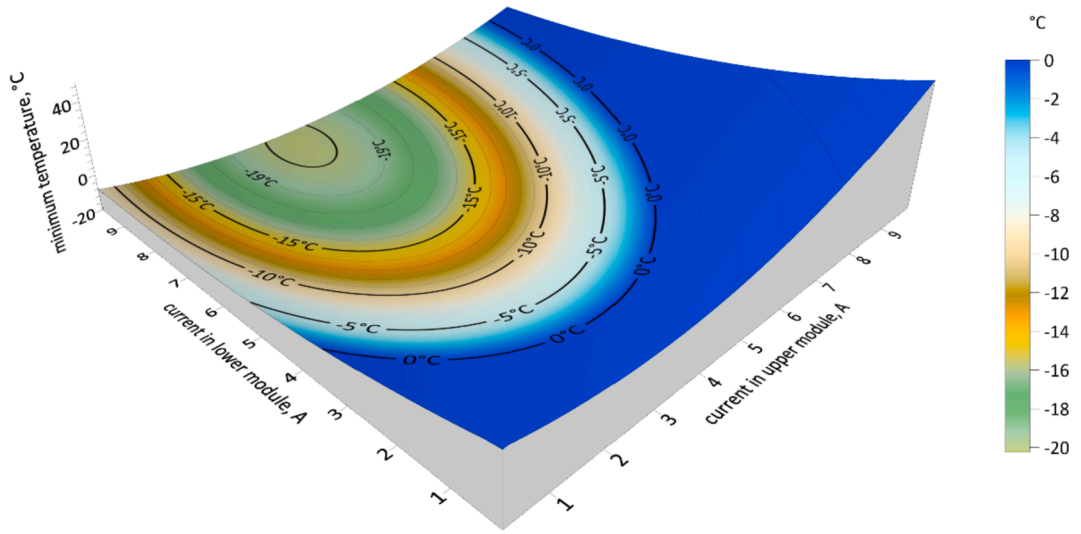

Fig. 8. Minimum temperature of the cold reservoir in the steady state depending on currents in the modules – thermal resistance of the layers omitted; the surface depth (minimum temperature) is enhanced with the colour scale.

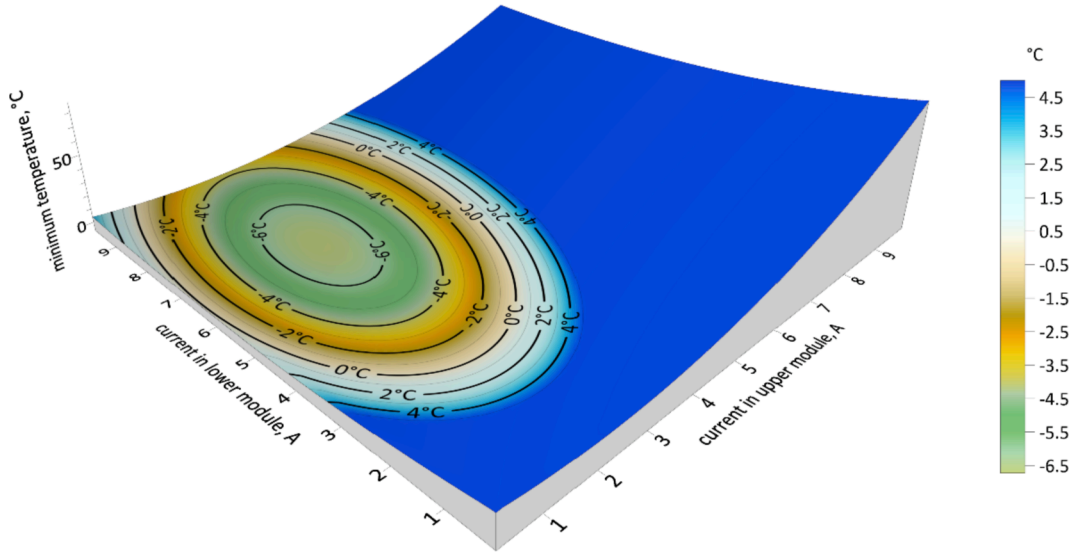

Fig. 9. Minimum temperature of the cold reservoir in the steady state depending on currents in the modules – thermal resistance of the layers taken into account; the surface depth (minimum temperature) is enhanced with the colour scale.

resistance between the upper and the lower heat reservoir.

To determine the minimum temperature of the cold heat reservoir, calculations were performed for different combinations of the values of the current flowing in the circuits of the modules. It was assumed that the currents varied in the range of $0-10A$ with the $0.1A$ step. The calculations were carried out for cases with contact thermal resistances both omitted and taken into account ($r_i = 100\mu Km^2/W$).

Analysing the graph illustrating the minimum temperature of the reservoir in the steady state, for the case omitting contact resistance (Fig. 8), it can be seen that the temperature minimum of $-20.24^{\circ}C$ is reached for the current of $9.2A$ for the lower cell (located farther from the cooled space) and $3.9A$ for the upper cell (located closer to the cooled space). Moreover, it can be concluded from the graph that the current in the upper cell has a stronger influence on the achieved minimum cooling temperature. The heat produced at the hot end of the lower module is released via the heat sink to the constant-temperature environment, while the heat produced by the upper cell must travel a much longer path, consisting additionally of conduction in the lower cell and thermal resistances (if taken into account) arising on the contact surfaces. Both of the determined current optima are positive because the upper cell cools the cooled space directly and the lower cell provides a lower temperature for the upper cell hot side (internal heat reservoir). This improves the entire system cooling capacity understood as the ability to reach the lowest possible temperature. Furthermore, it can be observed that for relatively high currents, especially in the upper cell, the heat generation due to the Joule heat effect significantly exceeds the cooling related to the Peltier phenomenon. As a result, the cooled reservoir temperature achieved in the steady state is higher than the ambient temperature.

For the analysis of the two-stage system taking account of the contact thermal resistance of $r_i = 100\mu Km^2/W$ (Fig. 9), the minimum temperature of the system cold side is by far higher than in the case of no resistance, totalling $-6.72^{\circ}C$. This occurs for currents $I_u = 2.6A$ in the upper cell and $I_l = 6.7A$ in the lower cell. The electric currents are by almost 30% lower in this case, which is related to lower Peltier and Joule heat. The reasons for which the determined currents are lower and the minimum temperature is higher are the same as for the one-module configuration. It is worth noting, however, that if evaluated

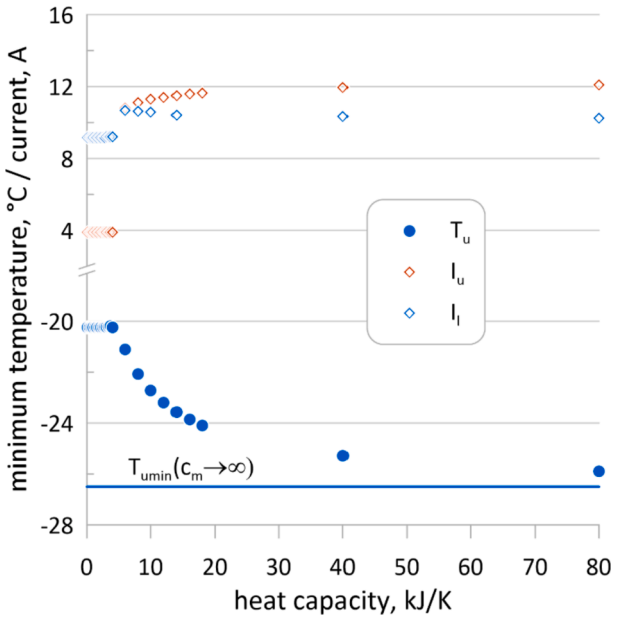

Fig. 10. Impact of the thermal capacity of the internal reservoir on the minimum temperature in the reference system, and the currents in the circuits of the modules corresponding thereto.

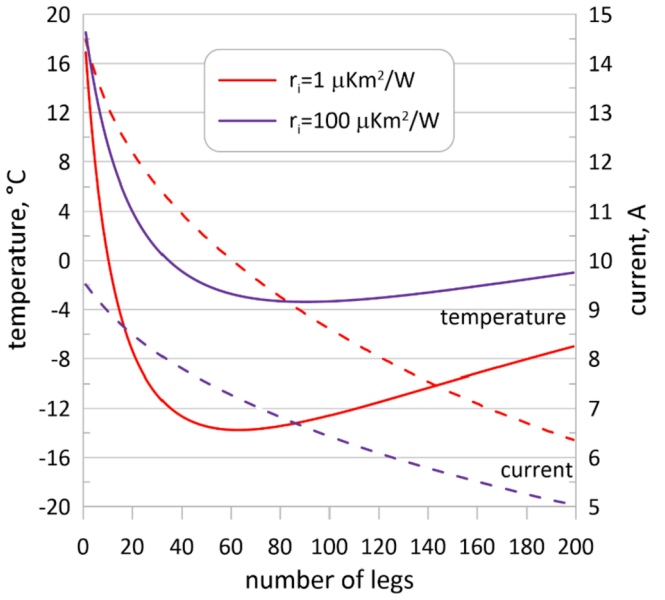

Fig. 11. Minimum temperature of the system cold end, and the corresponding value of the current in the circuit depending on the number of thermoelectric legs in the steady state.

qualitatively, the results are consistent with the observations made for the case with no contact resistance. It can also be seen that, whether or not contact resistance is taken into account, the minimum temperature achieved in the cooled space is lower for the two-stage configuration. The relative decrease in the temperature difference is of course related to the inclusion of contact resistance in the analysis and it is bigger for the two-stage configuration because in such a system the number of resistance layers is doubled, which results in doubled total thermal resistance.

3.4. Thermal capacity impact

In the steady-state analysis the heat capacity of the system individual components is irrelevant. This subsection presents a discussion of the conditions in which the lowest possible temperature of the cooled (upper) reservoir is obtained, regardless of whether it is reached in the steady state or whether it occurs only momentarily, even before reaching the steady state. The value of the minimum temperature in the latter case strongly depends on the initial conditions. In the examples under analysis it is assumed that the initial temperature is equal to the ambient temperature. The possibility of obtaining a low temperature of the cooled reservoir even before reaching the steady state is related to the thermal capacities in the system and to the temperatures of the system components at the moment that the minimum is reached.

The thermal capacity of the internal heat reservoir in the TEC sandwich structure will determine the thermal characteristics of the system. Consequently, it will affect the history of the cold reservoir temperature in transient states. To analyse this influence, a number of simulations were performed for various thermal capacity values (c_m), assuming a constant current for each circuit. The value of those currents was determined (independently for the two circuits) in a way that ensured the minimum momentary temperature of the cooled reservoir. The results for the reference case, i.e. a system with two identical modules with 100 legs each and with the assumption of no contact resistance, are shown in Fig. 10.

The graph indicates that if the thermal capacity of the internal heat reservoir is relatively small, comparable to the thermal capacity of the upper and the lower exchanger in analysed case (cf. Table 1), it has no impact on the minimum temperature achieved. In such a situation the minimum temperature of the cold reservoir is achieved in the steady state. As the thermal capacity rises, here from about $6kJ/K$, a systematic decrease in the minimum temperature is observed. The temperature asymptotically approaches the value marked by the horizontal line. The asymptote corresponds to an infinitely large thermal capacity of the internal reservoir. This result was obtained by setting a constant temperature of the internal reservoir at the initial level. For capacities for which a drop in the minimum temperature is observed, the lowest temperatures are no longer obtained in the steady state but only in a momentary thermal state of the system. For different values of the internal reservoir thermal capacity, different currents are obtained in the circuits of the thermoelectric modules ensuring the existence of the temperature global minimum before reaching the steady state. It is worth noting that the moment that thermal capacity starts to affect the system thermal inertia, an abrupt rise in the current is observed in both circuits. In the module closer to the upper reservoir the rise is a few times higher. This phenomenon appears for the thermal capacity value, above which the lowest temperature is no longer achieved in the steady state, but before the steady state is actually reached. Still visible is a rise in the current flowing in the upper module circuit and a slight drop in the circuit of the lower module. The histories of the currents, like in the case of temperature, have an asymptotic nature. This leads to the conclusion that the phenomenon of reaching the minimum momentary temperature (lower than in the steady state) is possible due to the relatively high thermal capacity of the internal heat reservoir and appropriate selection of the current. Owing to that, despite the heat supplied by the upper module, the internal reservoir temperature changes slowly. At the same time, the cooled reservoir capacity is relatively small, which causes fast changes in its temperature. Therefore, in the time when the internal reservoir temperature is still lower than the steady state value, a possibility arises of achieving the minimum temperature of the cooled chamber. For this reason, the temperature momentary minimum occurs between the system activation and the moment of reaching the steady state. This effect also occurs for small thermal capacities c_m, but it is then so insignificant that it does not cause a temperature drop below the minimum temperature of the steady state.

3.5. Cooling system optimization

Based on the observed phenomena described above, a question was

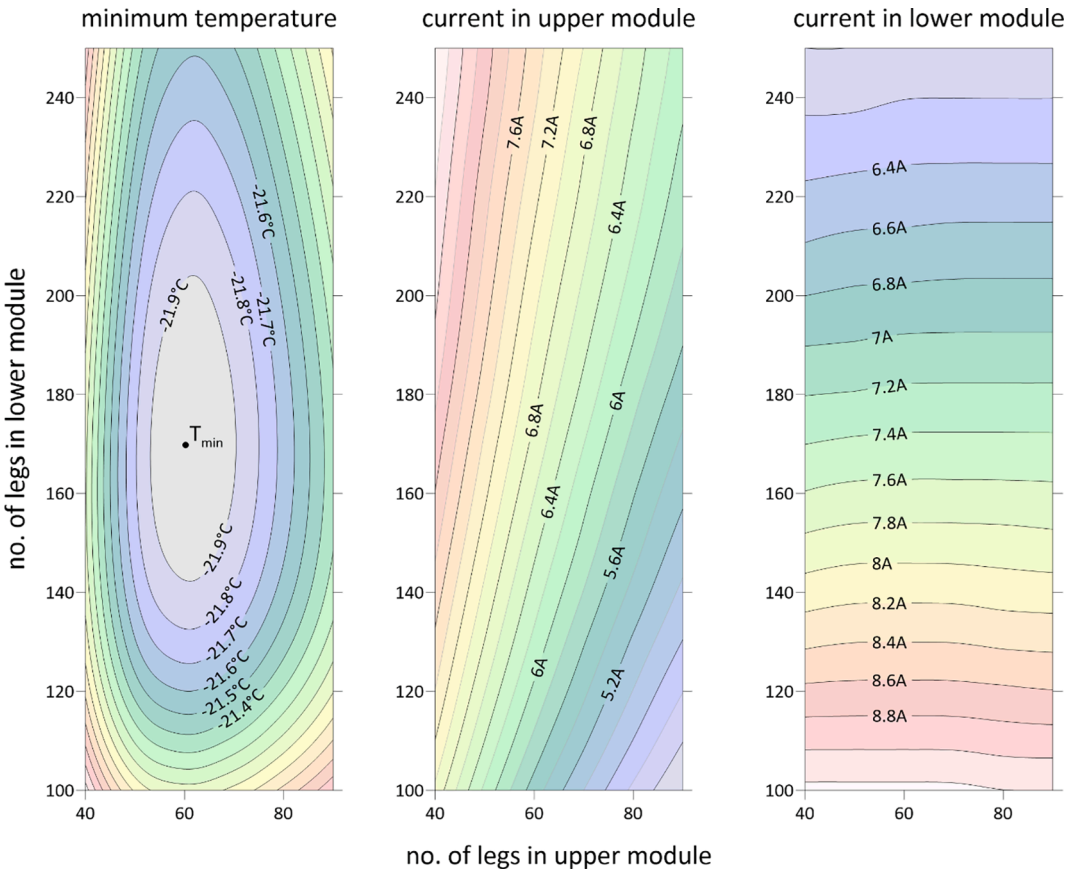

Fig. 12. Minimum steady-state temperature of the cold reservoir, and the currents corresponding thereto in the upper and in the lower module – contact resistances not taken into account.

posed regarding the optimal number of the couples of thermoelectric legs with defined parameters. Depending on the available thermoelectric modules, the desired number of thermoelectric couples can be obtained by using an appropriate number of modules. In the presented study, however, it is assumed that the number of the leg couples is a design variable and does not have to be a multiple of the number of legs in a specific available module. The first to be optimized were one-stage systems of thermoelectric couples/modules connected thermally in parallel and co-operating, like before, with identical heat sinks.

Figure 11 presents the system optimization results taking no account of contact resistance ($r_{si} = 1\mu Km^2/W$) and, like in previous analyses, with the resistance layers of $r_{si} = 100\mu Km^2/W$. The curves illustrate the minimum temperature reached for a set number of legs and the electric current that guarantees this temperature level. It can be seen here that there is a clear temperature minimum that varies depending on the existence of contact resistance. In the case of perfect contact, the optimum number of legs is 62. The minimum temperature obtained for this solution is $-13.75^{\circ}C$ at the current of 9.9A. If thermal resistance (with a set pre-determined value) is taken into account, the optimum number of legs increases to 90, and the minimum temperature to $-3.37^{\circ}C$. The current in this situation is 6.6A. The histories shown in the figure indicate that the presence of contact resistance caused a flattening of the temperature curve and a relatively wide range of the number of legs (from 67 to 122) to ensure that temperatures below $-3^{\circ}C$ are achieved. It is therefore should be easier to find suitable commercial modules with the required number of legs.

It can also be seen in the graph that the current optimal value decreases with a rise in the number of legs. Up to a certain point, raising the number of legs is beneficial because the Peltier heat (the cooling effect) is increased. When increasing the number of legs, it is also possible to decrease the current in the module circuit keeping the same total Peltier heat, and decreasing the Joule heat at the same time. The former is proportional to the current, while the latter increases with the current square. However, the opposite effect has to be remembered. Increasing the number of legs increases the amount of heat conducted by the thermoelectric couples, leading to heat conduction opposite to the direction of the cooling Peltier effect and a decrease in the temperature gradient. This has an unfavourable effect on the system operation efficiency, and for this reason the optimal number of the thermoelectric couples can be determined.

In the next step similar simulations were performed for the two-stage system. In this case the optimization was carried out for both modules simultaneously. Compared to the previous one, the problem is more difficult, because here there are two design variables to deal with (the number of legs is determined separately for each module). It is important to note at this point that changes made in one module directly affect the operating conditions of the other and vice versa. This in turn will affect the optimal number of thermoelectric couples for them. Therefore, a complete Design of Experiment (DoE) was carried out over a reasonable range of the number of legs to determine the entire field of possible solutions. For the sake of clarity, the results are shown in a range of the number of legs narrowed down to the surroundings of the optimal point.

The contour graphs shown in Fig. 12 illustrate the impact of a change in the number of legs in the two thermoelectric modules on the minimum temperature obtained in the cooled heat reservoir and the currents needed to reach the temperature. The results concern the situation where the contact resistance between the system layers is not taken into account. In such a case, the lowest temperature of the cooled space, with the value of $-22.0^{\circ}C$, is obtained using 170 and 60 legs in the lower and in the upper cell, respectively. It is achieved for the current of 6.75A in the upper cell and 7.45A in the lower cell. In these conditions the

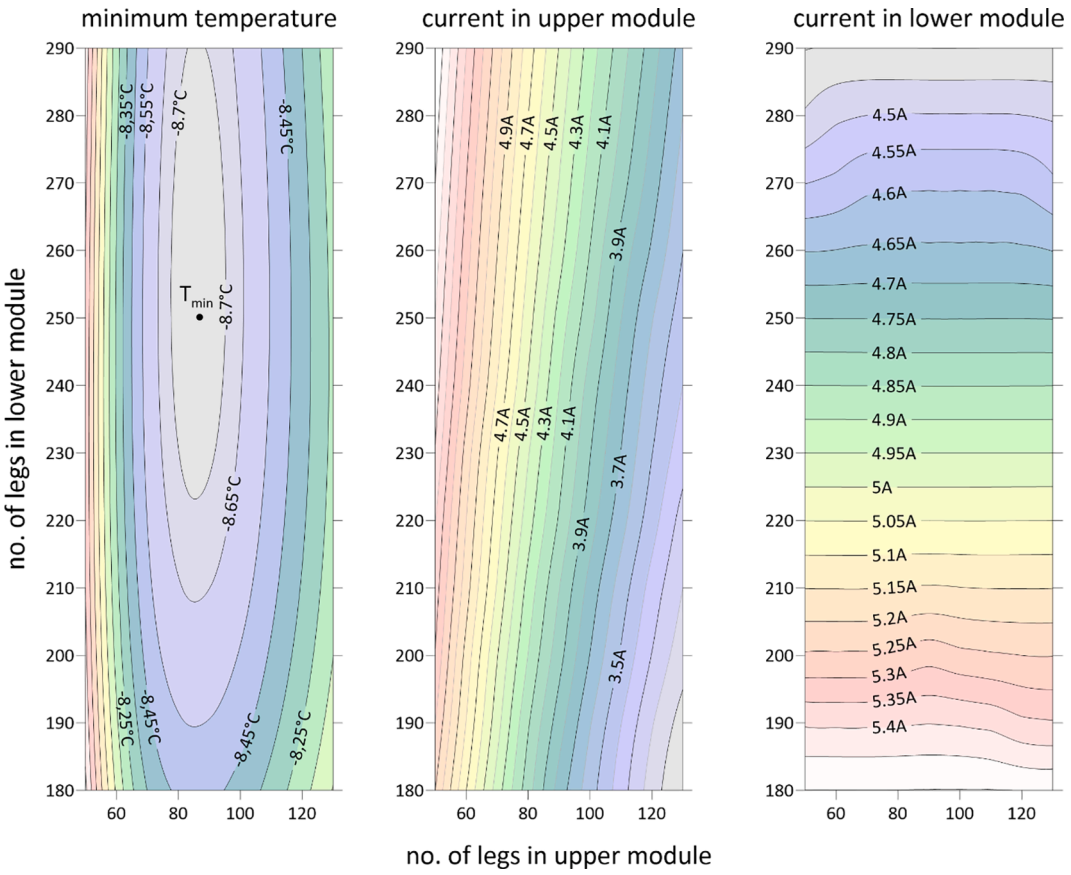

Fig. 13. Minimum steady-state temperature of the cold reservoir, and the currents corresponding thereto in the upper and in the lower module – contact resistances taken into account.

temperatures of the internal heat reservoir and of the hot exchanger are $T_m = 8.47^{\circ}C$ and $T_l = 46.29^{\circ}C$, respectively. Similar calculations were performed for the case where thermal contact resistance $r_i = 100\mu Km^2/W$ is taken into account. The results are shown in Fig. 13.

This time, the lowest temperature of $-8.72^{\circ}C$ is obtained for much larger thermoelectric modules, i.e. those with 90 legs in the upper module and 250 legs in the lower module. In this optimal configuration the currents for the upper and for the lower module are $I_u = 4.25A$ and $I_l = 4.75A$, respectively.

In both analysed cases of the thermal path in-series connection of the

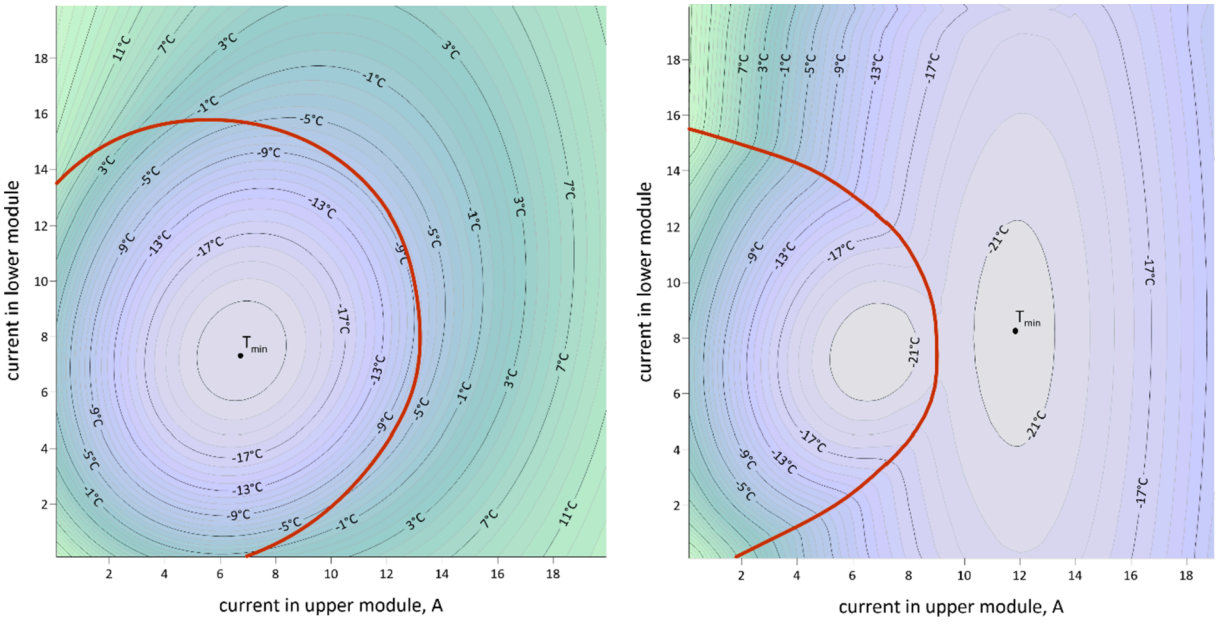

Fig. 14. Minimum temperature of the upper reservoir depending on the currents in the module circuits in the 60/170 configuration for small (300 J/K) and large (20 kJ/K) thermal capacities of the internal reservoir.

modules, omitting and taking contact resistance into account, similar patterns can be observed. The effect, both relative and absolute, of a change in the number of legs (and the magnitudes of the current) is greater for the upper module and significantly smaller for the lower module. This again shows that in the entire cooling process, the module located closer to the cooled space is more important. The minimum temperature isolines take on an elliptical shape with a substantially longer axis in the direction of changes in the number of the lower cell legs, which indicates that for the optimal size of the upper module there is a relatively wide range of sizes for the lower one, still ensuring temperature close to the minimum. A change in the number of the lower module legs results in nearly linear changes in the current flowing through the module, at an almost constant current in the upper module circuit. Analysing the graphs, it can also be seen that the optimal value of the current in the upper circuit is affected not only by the number of legs in the upper module but also in the lower one.

In the next step, for the optimally selected structure of each module in the in-series configuration (60/170 for the variant without contact resistance), the impact was determined of the current flowing through the modules on the system minimum temperature. As the calculations were carried out as transient-state ones, for each combination of currents the global minimum temperature over time and the temperature after the system reached the steady state were determined. It was assumed that the initial conditions were identical temperatures of the environment and of all elements of the system.

Figure 14 shows the results of determining the system global lowest temperature, for constant currents in the circuits of both thermoelectric modules, with the initial condition $T_0 = 20^{\circ}C$. The charts include additional lines drawn around the areas in which the steady-state temperature is at the same time the lowest temperature during the entire cycle of the system operation, i.e. from the start-up to the steady state. Outside this area, in the transient state, shortly after the device is turned on, a temperature lower than the steady-state temperature occurs momentarily.

The graph on the left, corresponding to heat capacity $c_m = 300J/K$, shows clearly that the minimum achievable temperature is the value that occurs in the steady state. The global minimum achieved for $n = 60/170$ coincides with the currents in Fig. 12. It should not be forgotten that large currents, in addition to the beneficial Peltier phenomenon, intensify the Joule heat, which leads to an increase in the system temperature. The Joule heat depends on the square of the current in contrast to the linear dependence of the Peltier effect. Nevertheless, as it was observed, a large current can temporarily produce a temperature lower than that obtained in the steady state, but still exceeding the value corresponding to the optimal configuration of currents. Therefore, supercooling is impossible to occur using a constant current in the $c_m = 300J/K$ configuration.

The situation is changed for thermal capacity $c_m = 20kJ/K$. In this case the steady-state values are the same as for smaller capacities, but the transient-state minimum temperatures vary. In Fig. 14 the global minimum is beyond the area surrounded by the line, which means that the minimum temperature is achieved momentarily in the transient state. This global minimum temperature is reached for currents for which the steady-state temperature is far from optimal. This is due to the much larger thermal capacity of the internal reservoir compared to the other ones, which results in slow changes in its temperature, and reaching the steady state takes a relatively long time. During that time it is possible to achieve the minimum temperature of the cooled chamber owing to the internal reservoir temperature lower than in the steady state.

For low thermal capacities of the internal reservoir, the global minimum temperature, as a function of the current, is reached in the steady state. As the thermal capacity is increased, an additional local minimum is formed in the temperature history (occurring before the temperature becomes steady). This minimum, after a certain boundary value of thermal capacity is exceeded, takes over the role of the global minimum. This is the same phenomenon that can be observed in Fig. 10.

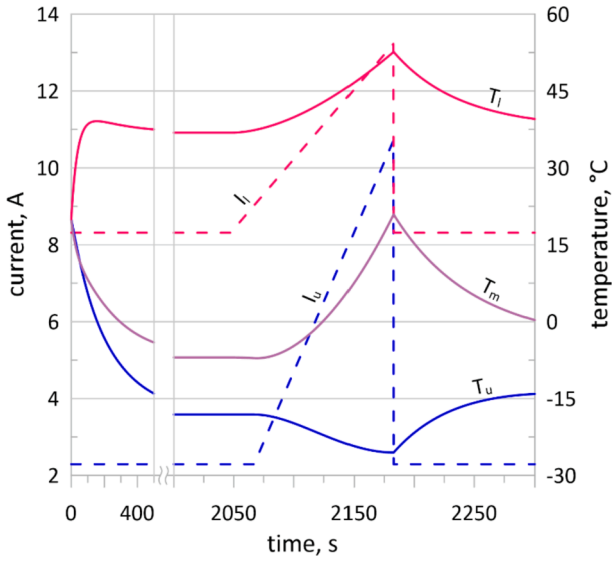

Fig. 15. Optimized current characteristics and the temperatures of the heat reservoirs corresponding to them for the reference system.

3.6. Shaping the electric current characteristic of the modules

In the next stage of the testing, the behaviour of the system was simulated at the profile of the electric current varying over time. The aim of those simulations was to obtain the cold reservoir momentary temperature as low as possible, with a value below the temperature obtained in the steady state, and also below the temperature obtained momentarily at constant supply currents.

In the first step an initial system was assumed. It is made of two identical modules with the number of legs $n = 100$. The modules are separated by a layer of a solid material with thermal capacity $c_m = 300J/K$. Moreover, no contact resistance between the system layers is taken into consideration. The data for the calculations were taken as presented in Table 1. It is assumed that the electric current changes linearly with a specific slope (rate of increment in the current), a determined initial current and the moment when the current starts to rise. For each module these 3 parameters created a set of 6 design variables of the optimization task, whose objective was to achieve the lowest possible temperature of the cold reservoir at any instant of the cycle. The calculations were performed using the optimization module of the *ThermoelectricCalc* program. In parallel, an optimization process was carried out using an evolutionary algorithm where the model of the phenomenon was represented by an appropriate set of differential equations. Very similar results in the concurrent runs of optimization confirmed the correctness of the histories of the currents flowing in the thermoelectric cells determined as optimal in terms of the system temperature minimization.

The optimization resulted in two independent histories of the current (I_u,I_l) for respective circuits of the thermoelectric modules. It can be seen in the chart in Fig. 15 that the initial current in the upper module is almost four times lower than in the lower module (2.3*A* vs. 8.3*A*). The rate of the increment in the upper module current is twice higher, totalling $72.7mA/s$. A rise in the current in the upper module involves a sharp rise in the Peltier effect and, consequently, momentary cooling of the upper reservoir down to $-25.5^{\circ}C$.

A similar optimization process, related to shaping the current characteristic, was run for the optimal structure (determined for minimum steady-state temperature) of the thermoelectric modules (number of legs: 60 and 170) determined previously for constant currents. The results concern the case where the system contact resistances were not

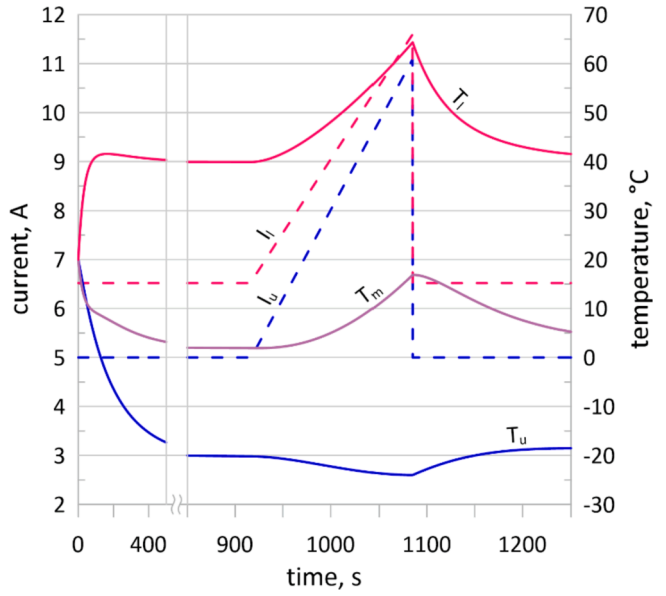

Fig. 16. Optimized current characteristics and the temperatures of the heat reservoirs corresponding to them for the 60/170 system.

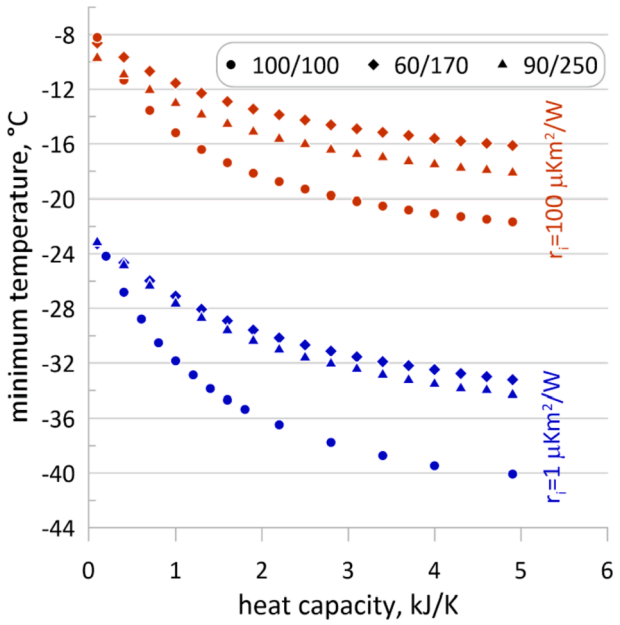

Fig. 17. Minimum temperature of the system depending on thermal capacity.

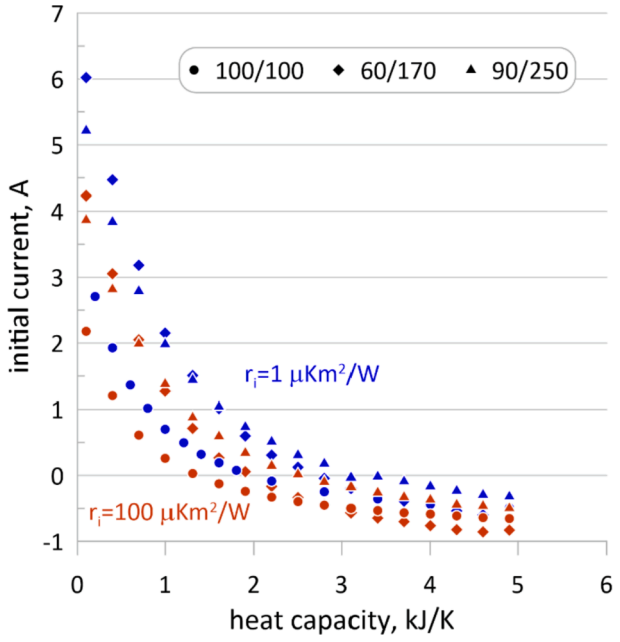

Fig. 18. Thermal capacity impact on the optimal value of the initial current of the upper module.

taken into account.

At constant currents flowing in the module circuits, the analysed system ensured the cold reservoir temperature at the level of $-22^{\circ}C$. Optimizing the current curve, the minimum temperature can be momentarily lowered to $-24^{\circ}C$ (Fig. 16).

This is due to lower currents in the initial phase of the system operation, and – after the temperatures of all reservoirs become relatively steady – the fast rate of the increment in the current. The final value of the current is practically insignificant because the minimum temperature is achieved in the phase of the linear increase in the current, and the only objective of the performed optimization is exactly the minimum temperature. Because further raising of the current after the minimum temperature is achieved would heat up the entire system, the current should be reduced to the initial value after the minimum temperature is achieved.

Supercooling can thus be achieved by cooling down the internal heat reservoir in the initial phase from the start-up and at a constant current. As the current rises linearly, the Peltier effect increases, and the contact between the module hot side and the relatively cool internal heat reservoir momentarily neutralizes the effects related to the release of the Joule heat and help to achieve minimum temperature.

In this case, it is the ratio of the thermal capacity of the internal reservoir to the capacity of the cooled reservoir that is of key importance. The described effect can vitally be observed if the thermal capacity of the internal or lower heat reservoir is relatively large. Comparing Fig. 15 with Fig. 16, it can be seen that in the structurally optimized system, unlike in the reference case, the heating of all three heat reservoirs, due to the increase in the current, proceeds at a similar rate. When comparing the two cases, it can be seen that the reference structure is characterized by a minimum temperature that is approximately $1.5^{\circ}C$ lower. This is the effect of the much larger dimensions of the upper module. In the reference case, in the first phase, when the system is striving to reach the minimum temperature of the internal reservoir, the current in the upper cell is smaller, and therefore there is a potential to increase the current without excessively enhancing the Joule effect at the same time. In the optimal case, the current is higher, which narrows the range of its variation. It can thus be concluded that a different curve illustrating changes in the values of the current ensuring the minimum temperature corresponds to different configurations of the size of the thermoelectric cells.

The above-presented procedure for the optimization of the current characteristic was then used to determine the relationship between the minimum temperature achieved by the system and the thermal capacity of the internal heat reservoir. Fig. 10 shows such a relationship for constant currents flowing in the modules. In the problem discussed here, where the current changes linearly, the reference case (100/100) and two optimal structures (60/170 and 90/250) determined for the model without and with contact resistance ($r_i = 100\mu Km^2/W$) were investigated. For each case, an independent optimization procedure was carried out to select the initial currents, the rate of the increment in the currents and the instant at which the linear rise in the current begins.

The results presented in Fig. 17 show the minimum temperature of the upper reservoir as a function of the internal reservoir thermal capacity, for the case with and without contact resistance taken into

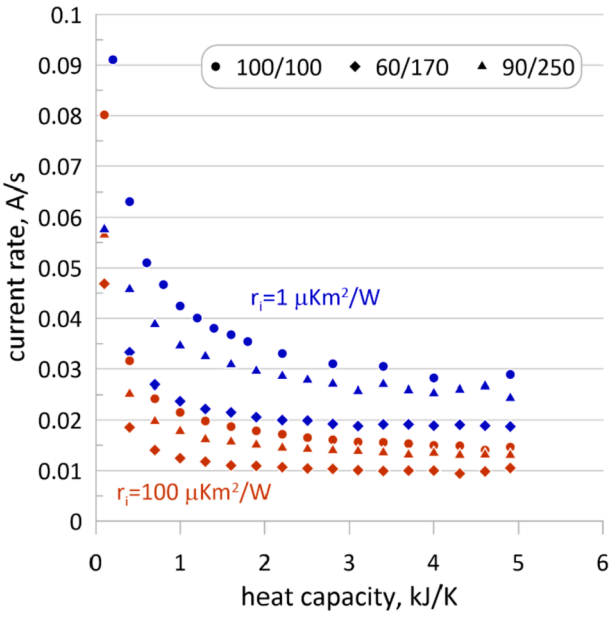

Fig. 19. Thermal capacity impact on the optimal value of the rate of the increment in the current of the upper module.

account (red and blue points, respectively). It should be noted that each point in the graph represents individually optimized curves of the currents flowing in the circuits of the thermoelectric modules, obtained for individual capacities. The presented graphs indicate that an increase in the internal reservoir thermal capacity makes it possible to achieve a lower minimum temperature. At the same time, as the thermal capacity rises, the minimum temperature tends asymptotically to reach a certain boundary value. The largest gain in temperature is obtained for the reference case, which is not optimized in any way.

Fig. 18 and Fig. 19, respectively, show the values of the initial current in the upper module and the rate of the rise in the current leading to achieving the temperature minimum depending on the system thermal capacity. The two relations are similar in character to the history of the minimum temperature. The value of the initial current is similar, both with and without contact resistance taken into account. However, if the resistance is taken into consideration, the rate of the increment in the current is lower. The biggest changes in the two quantities are observed at small thermal capacities ($< 1kJ/K$) of the system. It should be mentioned here that the other optimized quantities (concerning the electric current in the lower module) are less essential, and a change in their value has a smaller impact on the achieved minimum temperature of the cooled chamber. The lower module does not affect the cooled space directly, and its role is limited exclusively to ensure better operating conditions (a bigger difference in temperature) of the module located closer to the cooled chamber via moderating internal reservoir temperature. It can be seen in Fig. 18 that for high thermal capacity values, the initial current is negative. This proves that in the initial phase both cells cause the internal reservoir cooling to make it possible, after a while, for the lowered temperature of the reservoir together with the reservoir large thermal inertia to obtain a low temperature of the cooled space. It was noticed during the optimization that the main parameters having an impact on the achieved minimum temperature were as follows: the initial current of the upper cell, the initial current of the lower cell and the rate of the increment in the upper current.

The above-presented method of defining the current curve was characterized by 6 degrees of freedom – for each stage (upper and lower) these were: the initial value, the increment rate and the beginning of the increment. Optimization attempts were also made for other methods of defining the current characteristic. One of them was the method of a jump change in the current (square waveform), where the initial value, the final value and the time of the jump are set. Using this method, it was possible to obtain lower temperatures than with a constant current, but still they were significantly higher than the temperatures obtained for histories with a linear phase of the increment.

Another approach was an attempt to increase the number of the degrees of freedom of the electric current characteristic, in the hope of obtaining lower temperatures. For this purpose, the phase of the current rise was changed from linear to parabolic. This increases the number of the degrees of freedom by four (for each curve, the weight of the coefficient at the square and the location of the apex of the parabola). Yet another way to describe the current characteristic was to use a broken line composed of two linear functions. In this case, each current curve had 10 degrees of freedom, which made the optimization process even more difficult and time-consuming. Unfortunately, for neither of the current shaping methods, increasing the number of the degrees of freedom made it possible to obtain results better than those from defining the current curve rise linearly.

The results obtained for different configurations of the system at a very high thermal capacity of the internal reservoir are listed in Table 2. The differences between the minimum temperature achieved in the steady state and the momentary cooling in the transient state obtained for a constant and a pulse with linearly varying current are clearly seen here. The importance of contact resistance is also very evident. The results indicate that the resistance should be reduced as much as possible for the best cooling ability. As it cannot be eliminated completely, taking it into account in the calculations is important both from the point of view of the determined operating parameters of the system and in relation to the optimization of the thermoelectric module configuration. Moreover, it can be seen that compared to constant currents, the pulse with linear current increase makes it possible to obtain a much lower temperature. For the sake of comparison, Table 3 presents the minimum temperatures achieved using one layer of thermoelectric modules.

Comparing the results obtained for the two- and one-stage system, it can be noticed that the use of two-stage cooling brings essential advantages in the form of a lower temperature. The cases optimized taking resistance into account (Table 2 and Table 3 columns with 100 $\mu Km^2/W$ thermal contact resistance) point to a difference of $6^{\circ}C$ in the steady state. In the transient state, where the internal reservoir thermal capacity plays an important role, the difference can reach up to $18^{\circ}C$. It is also worth emphasizing that for a one-stage system with an optimal size of the module, the achieved minimum temperature is close to the temperature in the steady state. This means that the supercooling effect is

Table 2
Minimum temperature of the cold reservoir for various configurations of the system for $c_m = 20kJ/K$.

Number of legs n_u/n_l	100/100	100/100	60/170	60/170	90/250	90/250
Thermal contact resistance r_i, $\mu Km^2/W$	1	100	1	100	1	100
Steady state T_{min}, °C	−20.2	−6.7	−22.0	−8.0	−20.9	−8.7
Constant current T_{min}, °C	−26.5	−11.3	−22.6	−8.0	−25.8	−10.6
Current shaper T_{min}, °C	−44.1	−24.2	−36.7	−18.6	−37.8	−21.1

Table 3
Minimum temperature of the cold reservoir at a single thermoelectric layer.

Number of legs n	100	100	90	90	62	62
Thermal contact resistance r_i, $\mu Km^2/W$	1	100	1	100	1	100
Steady state T_{min}, °C	−12.6	−3.3	−13.1	−3.4	−13.8	−2.8
Constant current T_{min}, °C	−12.6	−3.3	−13.1	−3.4	−13.8	−2.8
Current shaper T_{min}, °C	−13.6	−3.6	−13.8	−3.6	−14.1	−2.9

substantially reduced. It has to be also remembered that the optimal system structure is different whether the resistance is or is not taken into account.

4. Summary and conclusions

The presented research deals with the modelling of transient states of a cooling system with thermoelectric modules. Various configurations of the TEC system were tested with a view to obtaining the lowest temperature of the cooled space. The research was conducted assuming a constant surface of the heat source/sink on the system two sides exchanging heat with the environment. For this reason, the difference in the heat exchange with the surroundings between the analysed cases was only the effect of the temperature difference between the hot and the cold sides of the system. As part of the study, using an own program – *ThermoelectricCalc*, and based on the presented mathematical model of the system, simulations were carried out of various configurations of thermoelectric modules, considering their parallel and in-series thermal connection. The parallel system was made of thermoelectric modules laid side by side, co-operating with a common hot and cold heat exchanger. In the case of the in-series connection, two modules in a sandwich configuration were analysed. The modules were separated by an internal heat reservoir with a set thermal capacity. The simulations covered the time from switching on the current in the circuits of the thermoelectric cells to reaching the steady state. The accuracy of the simulation program was experimentally validated with a dedicated test stand on commercially available thermoelectric modules.

The impact of the current value in the thermoelectric module circuit on the minimum temperature of the cooled space was investigated in the first place. The results indicate that for a given geometrical configuration of the system, the current value that ensures reaching the temperature minimum can be specified unequivocally. This is true for both the parallel and the in-series configuration. In the latter case, two different currents supplying the modules occur. The testing results demonstrate that for lower currents the temperature minimum is achieved in the steady state, whereas for higher currents, the phenomenon referred to as supercooling can be observed. Supercooling means that during transient-state operation, the system temperature can reach lower values compared to the steady state. The supercooling effect also depends on the magnitude of the internal reservoir thermal capacity. It was observed that for thermal capacities of up to a certain value (here $6kJ/K$), the minimum temperature corresponds to the steady state, while above this value supercooling occurs and is stronger with the increase in thermal capacity.

Better effects can be obtained through optimal selection of geometrical configurations of thermoelectric modules. For this purpose, the number of thermoelectric couples was optimized for the two considered methods of the arrangement of the cells. In the case of the sandwich structure, the two modules are characterized by a substantially different number of legs, and the module in contact with the cold exchanger is smaller. The results of the study also indicate that the achieved temperature minimum and the optimal size of the thermoelectric modules are strongly affected by the thermal contact resistance arising between the system elements.

At a constant current, supercooling is achieved at its relatively high values, leading to high temperatures in the steady state. This can be avoided by shaping the current in the circuits of the modules. As proved by the research results, bringing the system to a quasi-steady state at a constant initial current, and then using an appropriately selected current pulse, produces the effect of a momentary reduction in the cold side temperature. The minimum is reached at a certain moment of the phase of the current rise. To avoid excessive heating of the system, the current raising process should be broken, and the current should be returned to its initial value. It was found that for the optimally selected system configuration, the supercooling can reach as much as $18^{\circ}C$ compared to the steady-state operation. An important factor that affects the minimum temperature of the system is the thermal capacity of the internal heat reservoir. An increase in this quantity makes it possible to lower the minimum temperature.

CRediT authorship contribution statement

Ryszard Buchalik: Conceptualization, Methodology, Software, Writing – original draft. **Grzegorz Nowak:** Supervision, Funding acquisition, Writing – review & editing. **Iwona Nowak:** Writing – review & editing.

Declaration of Competing Interest

The authors declare that they have no known competing financial interests or personal relationships that could have appeared to influence the work reported in this paper.

Acknowledgements

The research was funded by the Polish National Science Centre (NCN Poland), Grant 2016/23/B/ST8/03133.

Appendix A

Table A1
Parameters of the experimental thermoelectric system.

Parameter	Value
Ambient upper temperature T_{ua}, °C	22
Ambient lower temperature T_{la}, °C	22
Upper heat reservoir initial temperature T_{u0}, °C	22
Internal heat reservoir initial temperature T_{m0}, °C	22
Lower heat reservoir initial temperature T_{l0}, °C	22
Upper heat reservoir thermal capacity $c_u, J/K$	1300
Lower heat reservoir thermal capacity $c_l, J/K$	1350
Internal reservoir thermal capacity $c_m, J/K$	1300
$HTF_u, W/K$	0.01
$HTF_l, W/K$	0.32
Number of legs n	100
Electrical conductivity $\rho, \mu\Omega m$	53
Thermal conductivity $\lambda, W/K/m$	5.7
Seebeck coefficient $\alpha, mV/K$	1.44
Leg height h, mm	3
Leg cross-sectional area A, mm^2	10
Contact resistance $r, \mu Km^2/W$	45
Clamping force N	700

.

References

[1] Söylemez R, Alpman E, Onat A, Hartomacıoğlu S. CFD analysis for predicting cooling time of a domestic refrigerator with thermoelectric cooling system. Int J Refrig 2021;123:138–49.
[2] Lyu Y, Siddique AR, Majid SH, Biglarbegian M, Gadsden SA, Mahmud S. Electric vehicle battery thermal management system with thermoelectric cooling. Energy Rep 2019;5:822–7.
[3] Yu J, Hongji Z, Li K, Haoqing W, Jiawen S, Qingshan Z. Analysis of nonlinear transient energy effect on thermoelectric energy storage structure. Materials 2020; 13(16):3639.
[4] Nesarajah M, Felgner F, Frey G. Modelling and simulation of a thermoelectric Energy Harvesting System for control design purposes. In: Proceedings of the 16th International Conference on Mechatronics; 2014. p. 170–7.
[5] Tian Z, Lee S, Chen G. Heat transfer in thermoelectric materials and devices. ASME J Heat Transfer 2013;135(6):061605.
[6] Eivari HA, Sohbatzadeh Z, Mele P, Assadi MHN. Low thermal conductivity: fundamentals and theoretical aspects in thermoelectric applications. Mater Today Energy 2021;21:100744.
[7] Wang S, Xie T, Xie H. Experimental study of the effects of the thermal contact resistance on the performance of thermoelectric generator. Appl Therm Eng 2018; 130:847–53.

[8] Selvam C, Manikandan S, Vijay Krishna N, Lamba R, Kaushik SC, Mahian O. Enhanced thermal performance of a thermoelectric generator with phase change materials. Int Commun Heat Mass Transfer 2020;114:104561.
[9] Fleith P, Cowley A, Canals Pou A, Valle Lozano A, Frank R, López Córdoba P, González Cinca R. In-situ approach for thermal energy storage and thermoelectricity generation on the Moon: modelling and simulation. Planet Space Sci 2020;181:104789.
[10] Ji R, Pan T, Peng G, Ma J, Yang N, Hao Q. An integrated thermoelectric heating-cooling system for air sterilization — a simulation study. Mater Today Phys 2021; 19:100430.
[11] He W, Zhang G, Zhang X, Ji J, Li G, Zhao X. Recent development and application of thermoelectric generator and cooler. Appl Energy 2015;143:1–25.
[12] Yang R, Chen G, Ravi Kumar A, Snyder G, Fleurial JP. Transient cooling of thermoelectric coolers and its applications for micro devices. Energy Convers Manage 2005;46(9–10):1407–21.
[13] Wang SL, Liu HB, Gao YW, Shen Y, Yang YR, Wang XD, et al. Transient supercooling performance of thermoelectric coolers with a continuous double current pulse. J Taiwan Inst Chem Eng 2021;120:127–35.
[14] Meng F, Chen L, Sun F. Performance optimization for two-stage thermoelectric refrigerator system driven by two-stage thermoelectric generator. Cryogenics 2009;49(2):57–65.
[15] Olivares-Robles MA, Vazquez F, Ramirez-Lopez C. Optimization of two-stage peltier modules: structure and exergetic efficiency. Entropy 2012;14:1539–52.
[16] Gao YW, Lv H, Wang XD, Yan WM. Enhanced Peltier cooling of two-stage thermoelectric cooler via pulse currents. Int J Heat Mass Transf 2017;114:656–63.
[17] Wang TH, Wang QH, Leng C, Wang XD. Parameter analysis and optimal design for two-stage thermoelectric cooler. Appl Energy 2015;154:1–12.
[18] Cheng YH, Shih C. Maximizing the cooling capacity and COP of two-stage thermoelectric coolers through genetic algorithm. Appl Therm Eng 2006;26(8–9): 937–47.
[19] Sun H, Ge Y, Liu W, Liu Z. Geometric optimization of two-stage thermoelectric generator using genetic algorithms and thermodynamic analysis. Energy 2019;171: 37–48.
[20] Huang Y, Chen Z, Ding H. Performance optimization of a two-stage parallel thermoelectric cooler with inhomogeneous electrical conductivity. Appl Therm Eng 2021;192:116696.
[21] Chen J, Zhou Y, Wang H, Wang JT. Comparison of the optimal performance of single- and two-stage thermoelectric refrigeration systems. Appl Energy 2002;73 (3–4):285–98.
[22] Ruiz-Ortega PE, Olivares-Robles MA, Enciso-Montes de Oca OY. Supercooling in a new two-stage thermoelectric cooler design with phase change material and Thomson effect. Energy Convers Manage 2021;243:114355.
[23] Meng JH, Wu HC, Gao DY, Kai Z, Lu G, Yan WM. A novel super-cooling enhancement method for a two-stage thermoelectric cooler using integrated triangular-square current pulses. Energy 2021;217:119360.
[24] Gao YW, Shi CL, Wang XD. Numerical analysis for transient supercooling effect of pulse current shapes on a two-stage thermoelectric cooler. Appl Therm Eng 2019; 163:114416.
[25] Asaadi S, Khalilarya S, Jafarmadar S. A thermodynamic and exergoeconomic numerical study of two-stage annular thermoelectric generator. Appl Therm Eng 2019;156:371–81.
[26] Li G, Shittu S, Diallo T, Yu M, Zhao X, Ji J. A review of solar photovoltaic-thermoelectric hybrid system for electricity generation. Energy 2018;158:41–58.
[27] Zhao Q, Zhang H, Hu Z, Hou S. Achieving a broad-spectrum photovoltaic system by hybridizing a two-stage thermoelectric generator. Energy Convers Manage 2020; 211:112778.
[28] Min G, Rowe DM. Experimental evaluation of prototype thermoelectric domestic refrigerators. Appl Energy 2006;83(2):133–52.
[29] Lv H, Wang XD, Meng JH, Wang TH, Yan WM. Enhancement of maximum temperature drop across thermoelectric cooler through two-stage design and transient supercooling effect. Appl Energy 2016;175:285–92.
[30] Zhao Z, Zuo Z, Wang W, Liu R, Kuang N. Performance optimization for a combustion-based micro thermoelectric generator with two-stage thermoelectric module. Appl Therm Eng 2021;198:117464.
[31] Yin T, Li ZM, Peng P, Liu W, Shao YY, He ZZ. Performance analysis of a novel two-stage automobile thermoelectric generator with the temperature-dependent materials. Appl Therm Eng 2021;195:117249.
[32] Zhang F, Cheng L, Wu M, Xu X, Wang P, Liu Z. Performance analysis of two-stage thermoelectric generator model based on Latin hypercube sampling. Energy Convers Manage 2020;221:113159.
[33] Guo X, Zhang H, Wang J, Zhao J, Wang F, Miao H, Yuan J, Hou S. A new hybrid system composed of high-temperature proton exchange fuel cell and two-stage thermoelectric generator with Thomson effect: energy and exergy analyses. Energy 2020;195:117000.
[34] Kamasi DD, Zainulloh M, Nadhir A, Sakti SP. Comparison between two-stage and three-stage Peltier thermoelectric coolers driven by pulse width modulation. J Phys: Conf Ser 2020;1528(1):012020.
[35] Kanimba E, Pearson M, Sharp J, Stokes D, Priya S, Tian Z. A modeling comparison between a two-stage and three-stage cascaded thermoelectric generator. J Power Sources 2017;365:266–72.
[36] Lin S, Yu J. Optimization of a trapezoid-type two-stage Peltier couples for thermoelectric cooling applications. Int J Refrig 2016;65:103–10.
[37] Beltrán-Pitarch B, Maassen J, García-Cañadas J. Comprehensive impedance spectroscopy equivalent circuit of a thermoelectric device which includes the internal thermal contact resistances. Appl Energy 2021;299:117287.
[38] Buchalik R, Nowak G, Nowak I. Mathematical model of a thermoelectric system based on steady- and rapid-state measurements. Appl Energy 2021;293:116943.

Energy & Buildings 268 (2022) 112168

Contents lists available at ScienceDirect

Energy & Buildings

journal homepage: www.elsevier.com/locate/enb

Technical and economic analysis of a thermoelectric air conditioning system

Ryszard Buchalik *, Grzegorz Nowak

Department of Power Engineering and Turbomachinery, Silesian University of Technology, ul. Konarskiego 18, Gliwice 44-100, Poland

ARTICLE INFO

Article history:
Received 8 February 2022
Revised 28 April 2022
Accepted 9 May 2022
Available online 13 May 2022

Keywords:
Thermoelectric cooler
Air conditioning
Economic analysis
Thermal resistance
TEC

ABSTRACT

The paper presents simulations of an air conditioning system based on thermoelectric modules. The proposed system is of a very simple structure, easy to control, scalable, noiseless, and harmless to the environment. The most important parameters that were to be changed were the number of modules, the electric current, and the size of the heat exchangers. The analyses were carried out for a commercially available thermoelectric module whose parameters were determined experimentally. The air conditioning system was analysed in terms of its cooling capacity and *COP*. Furthermore, it was optimized with economic criteria to achieve the highest cooling capacity of 1 dollar of total cost (electricity and investment) in a set period of device lifetime (*ETCC* – economic total cooling capacity). For 2400 h of device operation, at a temperature difference of 5 K and the average electricity cost in the EU, the optimized *ETCC* totals about 0.58 W/$. With the possibility of altering the inner geometry of the thermoelectric modules, the factor increased to 0.64 W/$. The test results showed that the device optimized in terms of *ETCC* did not operate with maximum cooling power and could be overloaded by about 30% in the reference working conditions.

1. Introduction

The climate in many regions of the world results in air temperatures that substantially exceed human comfort levels. Providing comfortable living and especially working conditions in such environments requires air conditioning of the rooms where people spend their time. Maintaining the temperature of thermal comfort has a positive impact on human well-being and productivity [1,2]. Climate control is also very important in heavy machinery and transportation where staff are exposed for a long time to extreme weather conditions. For staff comfort, the climate control system should generally be compact, portable and noiseless, which can be achieved using a thermoelectric cooler (TEC). The same requirements come from the electric car industry.

As indicated by relevant reports, in many countries the costs of air conditioning in the room contribute significantly to household electricity expenditures [3]. The impact of the use of air conditioners on global warming is also important [4]. Climate damage is caused not only by electricity consumption for refrigeration and air conditioning purposes, but also by refrigerants, such as chlorofluorocarbons [5] or hydrochlorofluorocarbons [6], which enhance the greenhouse effect. The study [7] shows that higher energy consumption is observed in cities and is much more affected by the number of households than by the size of the population. This leads various institutions, including the United Nations, to take action to reduce electricity usage [8]. In parallel, work is conducted to quantitatively estimate the demand for cooling power and rationalize its utilization, especially taking comfort indicators into account [9]. Some sophisticated control strategies and algorithms can be profitable in obtaining a better cooling efficiency [10]. The same applies not only to stationary applications but also to passenger vehicles [11].

The classical solutions applied in room cooling (portable or wall-mounted) are compressor-based air conditioning systems that work in the refrigeration cycle. Using thermoelectric modules can be a promising alternative. In an electrically powered thermoelectric module, the temperature difference is generated by absorbing the Peltier heat at one end of the thermoelectric junction and releasing it at the other end. Thermoelectric modules are usually made of two different materials with appropriate properties connected electrically in series-parallel; thermally they are connected in parallel. The module is composed of legs made of two different materials placed in between ceramic surfaces of the cover. The application of thermoelectric devices in zero-emission buildings, including the role of air conditioning, is described in [12].

* Corresponding author.
E-mail address: ryszard.buchalik@polsl.pl (R. Buchalik).

https://doi.org/10.1016/j.enbuild.2022.112168
0378-7788/

Nomenclature

$\dot{Q}$	heat flow, W
I	electric current, A
P	power, W
R	electrical resistance, Ω
T	temperature, K
V	voltage, V
HTF	heat transfer factor, W/K
N	unit cost
n	number of module legs
D	unit cost of cooling power,$\$/W_{el}$

Subscripts

j	thermoelectric junction
l	lower (heated)
out	outdoor
u	upper (cooled)
in	indoor
el	electric
h	leg height, m
k	thermal conductivity, $\frac{W}{K}$
r	thermal resistance, $\frac{K}{W}$
α_m	Seebeck coefficient for a thermocouple, $\frac{V}{K}$
α	Seebeck coefficient, $\frac{V}{K}$
n	number of legs, -
ρ	electrical resistivity, Ωm
$ETCC$	economic total cooling capacity, $W/\$$
tot	total
r	rapid state
s	steady state
op	operation
R	radiator

Its reliability is, in turn, discussed in [13]. In [14] an experimental study of a solar thermoelectric air conditioner with hot water supply is presented. The system shows quite a high *COP* (coefficient of performance) in combined space cooling and water heating. Dongxu et al. [15] presented the issue of simulating and optimizing the internal structure of thermoelectric elements in an air conditioning system. A similar problem is presented in [16] for transient conditions. Analyses that combine thermoelectric modules integrated into the ceiling with ventilation and airflow inside the room are presented in [17], as well as those that combine thermoelectric modules with solar powered systems. Yilmazoglu [18] discussed experimental research on a prototype thermoelectric HVAC system composed of a thermoelectric module with radiators located in ventilation ducts. The test system consists of a single TEC and observations of the flow and thermal conditions are taken.

The internal structure of the thermoelectric module can also be optimized [19] and such optimization can include nonstandard geometries of the legs [20,21]. Various non-planar concepts of the thermoelectric module design are presented in [22]. The authors of [23] analysed multistage refrigeration systems based on thermoelectric coolers (TECs). Attar and Lee [24] presented a concept of thermoelectric air conditioning with air-to-air heat exchangers for use in automobiles together with optimization by changing the electric current and the number of modules. Sun et al. [25] showed a novel radiant heating terminal integrated with a TEC and analysed its operation under real conditions. It turned out to be more efficient and faster than the conventional system.

Remarkable development can be observed nowadays in the search for thermoelectric materials, which may result in more efficient thermoelectric modules available on the market [26,27]. A broad overview of thermoelectric modules and their applications is presented in [28].

The heat transferred by a thermoelectric module has to be taken from the cooled space and carried to the outside. This is usually achieved using fan-assisted radiators, with the potential participation of a liquid medium that transports heat between the TEC and the radiator. The required level of heat transfer can only be ensured by radiators with an adequate capacity [29]. The medium carrying heat can be in the form of liquid water [30] or in the form of phase-change materials utilizing transition heat [31].

An air conditioning system suitable for a specific application should be selected based not only on the *COP* of the device itself and the demand for cooling power at a set temperature, but also on the operating characteristics and energy consumption over a 24-hour cycle, as well as the investment cost. The point here is to determine the peak power, taking into account the thermal capacity of the building in the analyses [32]. In multi-chiller integrated systems, the algorithms controlling each device to achieve the desired optimum parameters can be very sophisticated [33]. Rationalizing energy consumption, the heat generated by the air conditioner heat sink (outdoor radiator) can be used, for example, to heat domestic water rather than being released into the environment [34]. The possibility of partial energy recovery in an air conditioning system and control of humidity in the room is described in [35]. Another useful idea to utilize the air conditioning system to produce clean water is described by Luqman and Al-Ansari [36]. The presented method can be applied regardless of the type of air conditioner.

Most currently used air conditioners are driven by mechanical energy supplied to the compressor, which is usually driven by an electric motor. This concerns the equipment in vehicles, large professional systems for cooling industrial rooms, as well as household appliances. This paper focuses on smaller devices intended for home use, with a special emphasis on the so-called portable air conditioners, which are entirely enclosed in a single, stand-alone casing. The basic problem in this type of equipment is the need to carry away heat to the outside of the cooled room. This is usually realized by blowing hot (heated) air out of the room through a connected ventilation duct (concertina pipe). In addition, such air conditioners are characterized by an uncomfortable level of operating noise, considerable weight, and quite large casings.

The negative features of the compressor-based air conditioner can be eliminated by using a thermoelectric system. Such a system can be successfully used in buildings, heavy machinery (e.g. cranes), and electric cars for both cabin climate control and seat cooling. Also, in applications where precisely controlled temperature is required, a thermoelectric system could be a solution. Its design is very simple and no environmentally harmful refrigerants are required for its operation. Moreover, the system is easy to control smoothly by changing the supply current.

This paper presents a proposal for a thermoelectric air conditioning system. In the considered configuration the role of the heat pump is played by a set of thermoelectric modules, while heat is collected from the cooled space and discharged into the environment owing to an environmentally inert liquid (e.g. water) and radiators on the two sides of the system. The operation of such a system was analysed from technical and economic points of view, and the structure of the system was optimized in terms of the eco-

nomic efficiency of the solution. Since *COP* provides only information on the system efficiency, a new indicator called *ETCC* (economic total cooling capacity) was introduced to involve the investment and operational cost in a given period of time. The analyses were based on commercially available thermoelectric modules whose operational parameters were determined experimentally. No such analysis has been published so far, and the research results give an idea as to the rationality of constructing and operating the proposed air conditioning system based on TECs.

2. Mathematical model

The analysis concerns an air conditioning system equipped with thermoelectric modules. It is assumed that there are heat reservoirs on both sides of the modules and heat is supplied and carried away by a liquid to and from the radiators exchanging heat with the environment.

The analysed air conditioning system is illustrated schematically in Fig. 1.

Based on the diagram presented in Fig. 1, a mathematical model of the air conditioning system was proposed. Due to thermoelectric Peltier phenomena, the heat with indoor temperature T_{in} is transferred to the environment with outdoor temperature T_{out}. The heat absorption from the cooled space and the heat transfer to the outside are controlled through heat transfer factors HTF_{in} and HTF_{out}, respectively. In practice, the two factors characterize the size and efficiency of the radiators. The heat absorbed on the upper side is then expressed as:

$$\dot{Q}_{in} = HTF_{in}(T_{in} - T_u) \tag{1}$$

and the heat released to the outdoor environment is:

$$\dot{Q}_{out} = HTF_{out}(T_l - T_{out}) \tag{2}$$

Assuming no heat losses in the liquid pipeline, the energy balance for the thermoelectric part is given by (3) and (4). Fig. 1 shows a single couple of thermoelectric legs at magnification.

A typical thermoelectric module is made of many such cells connected electrically in series. The cells are made of two semiconductors connected electrically is series and thermally in parallel. A current flowing through such a thermoelectric couple causes absorption of heat $\dot{Q}_{in}$ on the top surface and a release of heat $\dot{Q}_{out}$ on the bottom.

There are three main phenomena in the thermoelectric modules that influence the heat pumping between the upper and lower sides: the Peltier effect, Joule heat and heat conduction. But only the first is the heat pumping driving process. Since the Peltier heat absorbed at the upper thermoelectric junction is released in the lower one, a temperature gradient occurs at the legs that is responsible for the Seebeck effect (voltage generation) and opposes the Peltier effect. The thermal gradient is also directly proportional to heat conduction through the legs, which in consequence acts against the pumping of heat. Moreover, the current flowing through the legs causes a release of Joule heat (caused by electrical resistance) in their entire volume, which also has a negative impact on the module performance. All the above-mentioned processes gathered in balance equations for the upper and the lower part of the module are defined as:

$$\alpha I T_{ju} - \frac{I^2 R}{2} + k(T_{ju} - T_{jl}) = \frac{(T_u - T_{ju})}{r_u} = \dot{Q}_{in} \tag{3}$$

$$\alpha I T_{jl} + \frac{I^2 R}{2} + k(T_{ju} - T_{jl}) = \frac{(T_{jl} - T_l)}{r_l} = \dot{Q}_{out}, \tag{4}$$

where T_{ju}, T_{jl} are the upper and lower temperatures of the thermoelectric junctions, respectively, k is the leg thermal conductivity, α stands for the Seebeck coefficient, R is electrical resistance, and I is electric current.

3. Experimental determination of the system parameters

This section describes the methods of determining the parameters of the TEC and the conditions of thermal contact between the cells needed to model the operation of the air conditioning system under consideration. Since the manufacturer's documentation of the thermoelectric modules usually does not contain all the information needed for the calculations, and because experience shows that the parameters specified in the manufacturers data sheets do not always correspond to reality, experimental tests were carried out to determine the module parameters and the conditions of the module cooperation with heat exchangers.

3.1. Test stand

The analyses of air conditioning systems performed further below are based on the use of thermoelectric modules with parameters achieved under real conditions by commercially available devices. In this case, the MCTE1-19913L-S modules [37] intended for refrigeration systems were used. Because the internal structure of the tested module is unknown for the current study, it was assumed that a single module consisted of $n = 100$ with the leg

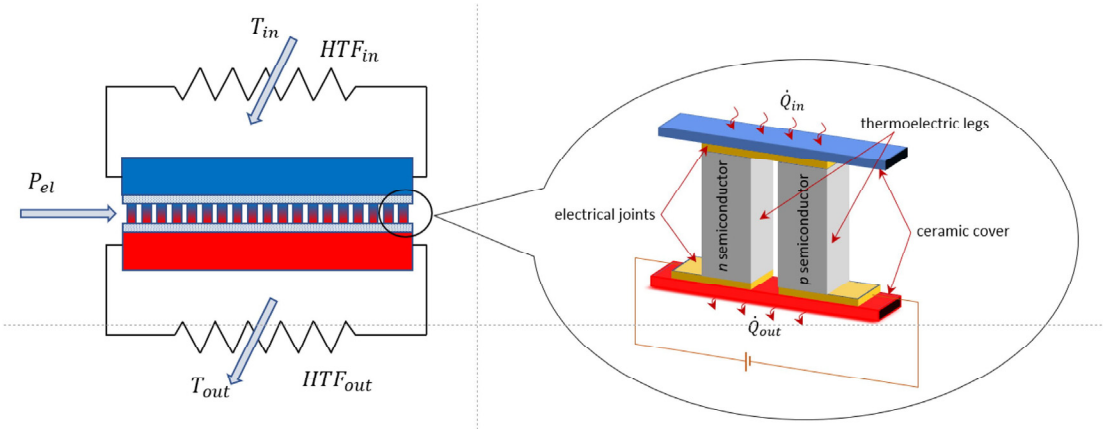

Fig. 1. Diagram illustrating the air conditioning system. The thermoelectric module is supplied with electricity to pump heat from the indoor (in) to the outdoor (out) environment. The intensity of the heat exchange between the system and the environment is controlled via HTFs. A single thermoelectric couple is presented on the right.

height $h_{ref} = 3mm$; all the parameters used in the calculations were determined based on this assumption. This assumption does not influence the results.

The TEC parameters were established using a purpose-made test stand (Fig. 2), described in detail in [38]. It is equipped with two heat exchangers in the form of copper blocks with a thermoelectric module placed and clamped between them using controlled force. Electric heaters are installed in the upper block (where heat is absorbed), whereas in the lower heat exchanger (where heat is released to the environment) there are cooling channels with water flowing at a precisely controlled flow rate. The stand is abundantly metered to record both thermal and electric quantities. The measuring stand design enables, among others, operation in the mode of a set temperature difference, when the heaters, located in the upper block and controlled by a program PID controller, maintain a constant temperature difference between the blocks at a set level.

The contact conditions between the exchangers and the module determine the thermal resistance on the interface of these elements, and thus significantly affect the achieved operating parameters. Therefore, during the system assembly, a layer of copper grease was applied to the surface of the modules and the whole was compressed with a force of $1kN$ and heated to $80^{\circ}C$; it was then left for 24 h. The force was maintained ($\pm 5\%$) for all the described test cases.

3.2. Thermal contact resistance

The first stage of the testing was to determine the magnitude of thermal resistance between the heat exchangers and the TEC thermoelectric joints using the dedicated test stand described above in subsection 3.1. For this purpose, the lower exchanger was cooled with a stream of tap water to keep its temperature in the range of $19 - 22^{\circ}C$. The direction of the current of $I = 5A$ flowing in the TEC circuit was set to ensure the cooling of the upper heat exchanger and the heating of the lower one. The following quantities were measured during the testing: the temperature of the blocks, the heat supplied by the heaters (to maintain the set temperature difference between the blocks ΔT), the steady-state voltage V_s and the voltage immediately after breaking the cell electrical circuit V_r. The testing method is based on a large difference in the inertia in the thermal and electrical fields. Shortly after the change in the electrical state (from short-circuit to open-circuit), for several milliseconds the temperature can still be considered unchanged, so it corresponds to the previous electrical state. The V_r is directly proportional to the temperature difference in the thermoelectric joints at the steady state. The results of the measurements and the parameters determined based on them are shown in Table 1. All the presented measurements relate to the steady state, except the measurement of V_r, which is the voltage value at the TEC terminals right after (milliseconds) the circuit is broken in the thermal steady state of the TEC (the so-called *rapid measurement* [38]).

The three measurements (first three rows in Table 1) were performed for a slight (or zero) difference between the temperature of the blocks from $-5K$ to $5K$, while the last raw presents data resulting from their linear approximation. It was assumed that the changeability of the investigated parameters in the range under analysis was a linear function of the difference between the temperatures of the blocks. This suggests that the TEC properties may be treated as temperature independent. This assumption was confirmed by the measurement results. Therefore, based on linear approximation, it is possible to determine the value of the temperature difference between the blocks for which voltage (rapid measurement) $V_r = 0$. This corresponds to an equal temperature of the thermoelectric junctions. Under such conditions, it is possible to determine the mean value of the contact resistance because, due to no heat conduction through the thermoelectric module, the difference between the temperature of the heat exchangers (ΔT) arises only on the contact layers. The determined total heat flowing through the module two surfaces.

$$\dot{Q}_{tot} = \dot{Q}_u + \dot{Q}_l \tag{5}$$

divided by the temperature difference makes it possible to calculate thermal resistance,

$$r = \frac{\Delta T}{\dot{Q}_{tot}} \tag{6}$$

totalling $r = 0.070K/W$. It is assumed that the thermal resistance is identical on both sides of the module. The calculated value defines thermal resistance of one of the layers. The $\dot{Q}_u$ value is known because it is equal to the electric power supplied to electric heaters. $\dot{Q}_l$ can be calculated on the basis of the energy balance using the joule heat produced in the TEC, P_{el} and $\dot{Q}_u$. The P_{el}, can be calculated by multiplication of current ($5A$) and the voltage V_s.

$$P_{el} = IV_s \tag{7}$$

so,

$$\dot{Q}_l = \dot{Q}_u + P_{el}. \tag{8}$$

3.3. Module parameters

Based on the averaged voltage difference ($V_s - V_r$) and current, it is easy to determine internal electrical resistance of the TEC circuit ($R = 1.59\Omega$).

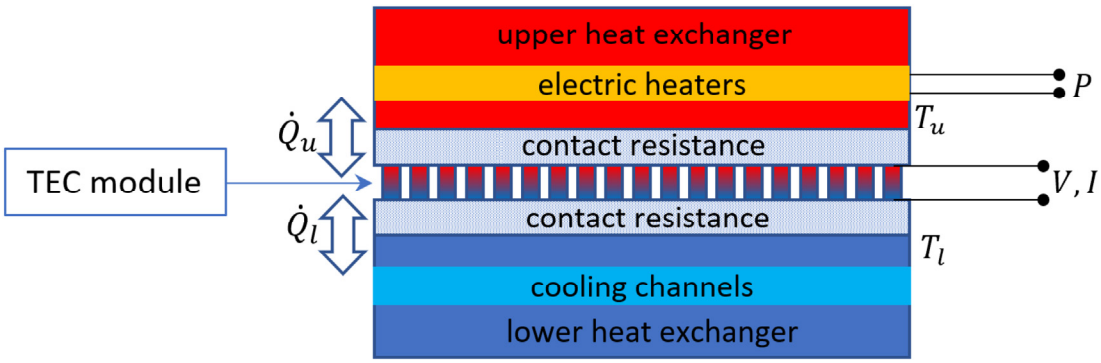

Fig. 2. Diagram of the measuring system consisting of the upper heat exchanger with temperature (T_u) with installed electric heaters, the lower heat exchanger with temperature (T_l) with the cooling channels. The thermoelectric module is mounted between the heat exchangers and supplied with electricity (V, I). Heat resistance occurs on the contact surfaces between the module and the exchangers.

Table 1
Results of the TEC module measurements.

I, A	$\Delta T, K$	V_s, V	V_r, V	P_{el}, W	$\dot{Q}_l, W$	$\dot{Q}_u, W$	$\dot{Q}_{tot}, W$
5	−5	9.45	1.56	47.3	59	106	165
5	0	9.24	1.29	46.2	72	118	190
5	5	9.00	0.96	45.0	84	129	213
5	21	7.96	0	41.5	123	165	288

Subsequent measurements were then made for the upper block temperature set to $35^{\circ}C$ to establish the Seebeck coefficient and the thermal conductivity of the module. In this case, the focus was only on the steady-state voltage generated by the module at a zero current in the TEC circuit. The zero current condition guarantees that there is no Peltier heat. The measurements were carried out for two different mass flow rates of the cooling water. Due to that, different temperatures of the lower block were obtained (Table 2).

The ambient temperature during all the measurements was constant: $T_a = 24^{\circ}C$. The measurements first make it possible to establish the coefficient of heat loss to the environment. The upper block temperature is kept constant all the time by the electric heaters, and the temperature of the lower block changes due to the change in the water flow rate. In such a situation, in the steady state, no heat is used for electricity generation, so the input and output heats are equal $\left(\dot{Q}_u = \dot{Q}_l\right)$. Like above, due to the linear dependence of the heat flow on the temperature difference, a linear approximation makes it possible to find the power supplied to the heaters in the situation when the lower exchanger temperature is equal to the temperature of the upper one $(T_u = T_l)$. This leads to the value of $\dot{Q}_{loss} \approx 5W$. Dividing it by the temperature difference between the upper block and the environment $(T_u - T_a)$, the coefficient of heat loss to the environment $HTF_{loss} = 0.45W/K$ was determined for the testing on the measuring stand. Next, it is possible to calculate the heat conducted by the module $(\dot{Q}_{TEC} = \dot{Q}_u - \dot{Q}_{loss})$, which is the difference between the heat supplied by the heaters and the heat loss to the environment. This loss value is used to correct $\dot{Q}_{tot}$ and the previously determined contact resistance. The correction is made by changing the values of heat $\dot{Q}_u$ in Table 1 by a correction factor calculated using the current temperature of the upper block and the above-mentioned HTF_{loss} value, i.e. $\dot{Q}'_{tot} = \dot{Q}_{tot} - 2(T_u - T_a)HTF_{loss}$ Now the value of $\dot{Q}_{tot}$ from Table 1 corresponding to $V_r = 0$ can be corrected down by about $20W$ due to the loss, and this results in a correction of r to $0.076K/W$.

The measurements were repeated using a different, high-quality thermal grease (Thermal Grizzly Kryonaut) on the interface between the module and the exchangers. In this way, the value of the temperature difference for $V_r = 0$ was obtained at the level of about $7K$ (instead of $21K$). As a result, the final contact resistance determined decreased to $r = 0.027K/W$. This indicates a closely three times greater ability to carry heat for high-quality grease than for standard copper grease, and it was adopted for the calculations.

Knowledge of contact thermal resistance and the heat flow through the cell allows us to determine the temperature difference deviation $(\delta_{\Delta T})$, i.e. the deviation between the measured temperature difference of the blocks (ΔT) and the unknown temperature difference on the thermoelectric junction (ΔT_{TEC}). This provides the basis for the determination of the real temperature difference on the thermoelectric junction.

The values presented above make it possible to find the Seebeck coefficient as the ratio between the generated voltage and the temperature difference at the thermoelectric junction $(\alpha = V/\Delta T_{TEC})$, as well as the thermal conductivity of the thermoelectric legs as the ratio between the heat conducted by the cell and the temperature difference at the junction ($k = \dot{Q}_{TEC}/\Delta T_{TEC}$).

In the case of thermal analyses conducted for an air conditioning system, due to its operating temperature range, the impact of thermal radiation can be omitted [39]. For the same reasons, it is also justified to assume the module parameters as temperature-independent [12], which was proven experimentally.

The analysis presented further below is conducted using the TEC parameters listed in Table 3. All the quantities are calculated for the assumed number of legs $n = 100$, leg height $h = 3mm$ and $A = 10mm^2$.

4. Validation

The analytical model and the software developed based on it to perform the analyses were validated experimentally on a purpose-built specialist measuring stand. The details of the stand structure and its testing potential are presented in [38]. The stand is made of two copper blocks acting as the heat sink and the cooled space. The former has cooling channels with water flowing inside and the latter includes electric heaters (cf. Fig. 2). The tested thermoelectric module is placed in between the blocks.

The validation testing was carried out using another specimen of the MCTE1-19913L-S module type adopted for the analyses. The surfaces of the module contact with the blocks were covered with high-quality thermal paste (Thermal Grizzly Kryonaut).

The first to be established were the parameters of the tested module specimen and the operating conditions of the thermoelectric system. This was done using the same procedure as the one described in section 3. The measurement results indicate that almost none of the parameters listed in Table 3 differs by more than 2–3% compared to the tested specimen. The only quantity for which the difference between the TEC specimens was noticeable was the Seebeck coefficient. It was up to 10%.

The validation tests consisted in bringing the system to a steady state at a given mass flow rate of water cooling the lower block. The upper block was heated with electric heaters controlled by a PID controller to maintain the block constant temperature equal to the temperature of the environment. Such a state ensures that there is no heat loss to the environment. In the steady state, the power supplied to the heaters is equal to the cooling power gener-

Table 2
Measurements for a constant value of T_u

$T_u, ^{\circ}C$	$T_l, ^{\circ}C$	$\dot{Q}_u, W$	V_s, V	$\dot{Q}_{TEC}, W$	$\delta_{\Delta T}, K$	$\Delta T_{TEC}, K$
35	19.1	26	1.02	21	1.6	14.3
35	25.3	17	0.64	12	0.9	8.8

Table 3
TEC module parameters.

$\alpha_m, mV/K$	$\rho, \mu\Omega m$	$\lambda, W/(Km)$	$n, -$	h, mm	A, mm^2
1.44	53	5.7	100	3	10

ated by the module for a set supply current and a set temperature difference of the modules. Therefore there is no need to measure the cooling water mass flow rate; only the lower block temperature has to be measured. Such measurements were carried out for several different values of the cooling water mass flow rate and the module supply current. It should also be stated here that the measurement of currents and temperatures poses no challenge and the results are burdened with a slight error only. In this case, temperature was measured using PT100 resistance thermometers with high absolute measuring accuracy (less than 0.5%). Power was measured using an EA-PSI 9200–25 T lab power supply with the accuracy of 0.4%.

Very good agreement was observed between the measurement ($\dot{Q}_{exp}$) results and the results of the simulations $\dot{Q}_{sim}$ (Table 4). The determined cooling power differs by about 6% maximum. On average the difference is less than 4%. Despite the one-dimensional nature of the model, the measurement results appear to confirm that the impact of the phenomena occurring spatially is slight.

5. Performance simulations of the system

5.1. TEC module characteristic curves

First, the characteristics of the analysed single stand-alone thermoelectric module were made. For this purpose, it was assumed that the temperature of the radiators was steady and set in advance for each point of the characteristic determination. The upper radiator temperature was constant and equal to $25^{\circ}C$ in each case. It is also assumed that at the interface between the thermoelectric junction and the liquid transporting heat, the thermal resistance per unit area is estimated at the level of $r_{su} = r_{sl} = 42\mu Km^2/W$, for which $27\mu Km^2/W$ is the contribution of thermal resistance on the contact surface of TEC (Section 3.3) and another 15 $\mu Km^2/W$ involves heat resistance between the exchanger and the liquid stream. This value was also adopted for further simulations. The cooling power and the *COP* were calculated for a wide range of currents in the circuit supplying the ther-

Table 4
Validation results.

Test no.	I, A	$\Delta T, K$	$\dot{Q}_{sim}, W$	$\dot{Q}_{exp}, W$	Error %
1	3	4.78	54.5	52.9	2.9
2	3	−1.04	64.6	63.3	2.0
3	6	3.74	105.2	101.5	3.6
4	6	23.36	70.6	66.3	6.1
5	9.8	8.89	133.4	130.6	2.1
6	6	3.47	101.9	101.9	0.0
7	2	−0.74	42.9	43.9	2.3

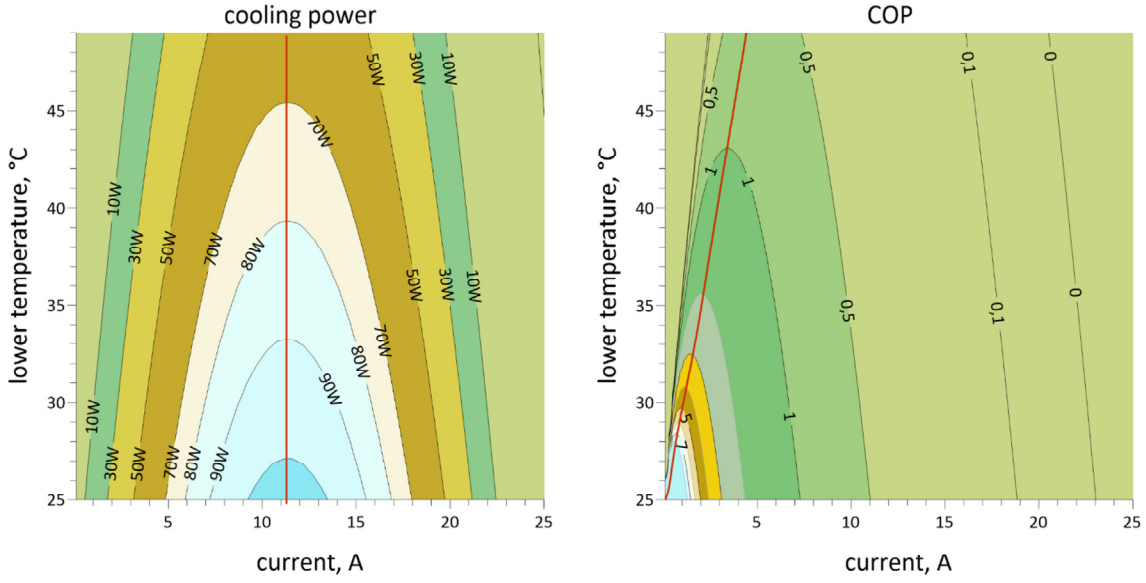

Fig. 3. Cooling power and COP depending on the module current and on the discharge heat exchanger radiator (lower) temperature for the constant upper radiator temperature of $25^{\circ}C$. The red lines pass through the maxima. The maximum power for each lower temperature occurs almost along a line of constant current. (For interpretation of the references to colour in this figure legend, the reader is referred to the web version of this article.)

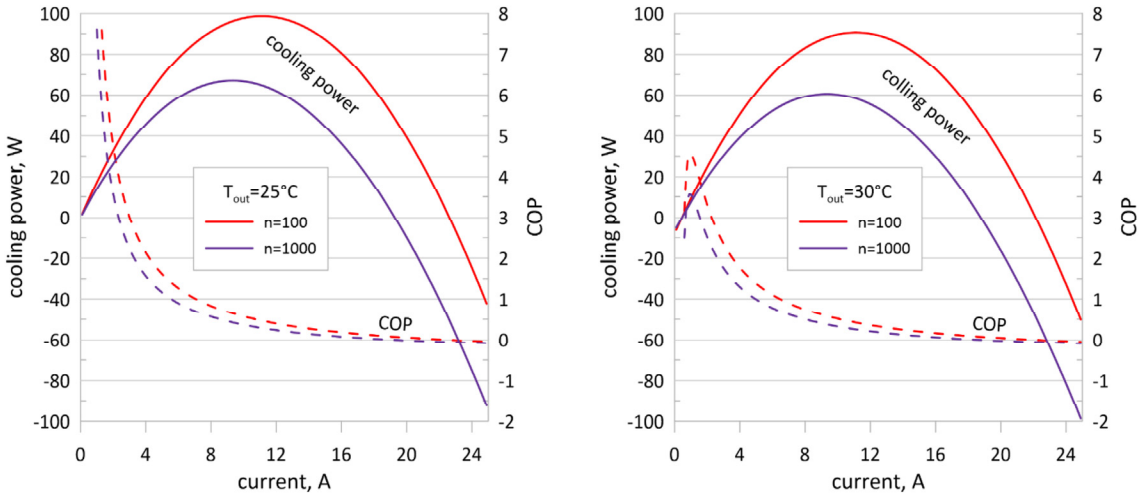

Fig. 4. Cooling power and COP values for the outdoor temperature of 25 °C and 30 °C. Indoor temperature is constant (25 °C) for the system presented in Fig. 1. Lines marked as n = 100 show the results for a single module system, while those marked with n = 1000 represent one of the modules in the 10-module system. $HTF_{in} = 100W/K$, $HTF_{out} = 200W/K$.

moelectric module at different temperatures of the lower radiator. This made it possible to plot the charts presented in Fig. 3, which show the results of the performed steady-state simulations.

Fig. 3 indicates that the useful effect in terms of cooling power decreases with a rise in the temperature difference between the exchangers. An increase in the difference also involves a reduction in the range of currents for which the positive level of cooling power can be achieved. It can be seen that the red line that passes through the cooling power maxima for a given temperature difference corresponds to an almost constant current value, which is slightly higher than 11*A*. Analysing the maximum *COP* curve (red line passing through maxima), where the *COP* is defined as the cooling-to-electric power ratio, it can be found that the maxima are shifted towards low currents, and *COP* values higher than 3 can only be obtained for a temperature difference smaller than 8*K* at currents of less than 3*A*.

Based on the presented results, it can be observed that, for a single thermoelectric module (n = 100), the operation of the system at the difference in the temperature of the heat exchangers at the level of 10*K* with the *COP* value of at least 1 (right graph) makes it possible to achieve a cooling power of the order of $30 - 50W$(left graph).

5.2. Characteristics of the air conditioning system

At this stage radiators characteristics were taken into account. It was initially assumed that on the heat discharge side (outdoor), the radiator is twice as large as on the heat absorption side (indoor). Both radiators are additionally assisted by fans. Therefore, the heat transfer conditions are estimated at the levels of $HTF_{in} = 100W/K$ and $HTF_{out} = 200W/K$, where $100W/K$ is equivalent to a single computer cooler[1].

The analysis focused on the steady-state operation of an air conditioning system (described in section 2) using the TEC tested above under specific heat transfer conditions ($HTF_{in} = 100W/K$ and $HTF_{out} = 200W/K$). Simulations were carried out to investigate the achieved cooling power and *COP* depending on the current supplying the thermoelectric module for two selected temperatures of the lower (outdoor) heat reservoir of $T_{out} = 25^{\circ}C$ (0*K* difference) and $30^{\circ}C$ (5*K* difference), while the temperature of the upper (indoor) heat reservoir is constant ($T_{in} = 25^{\circ}C$). The results presented above point to the rather low cooling power of a single thermoelectric module. For this reason, another option was analysed, with a parallel thermal connection of 10 modules ($n = 1000$).

The curves in Fig. 4 illustrate the cooling power and the *COP* for a thermoelectric system with a single module ($n = 100$) and for a system with ten identical modules ($n = 1000$). For the latter case, the results are presented for one module of the 10-module system. The cooling power curves demonstrate that, in each case, there is a maximum for a specific value of the current. The curves plotted for the 10-module system show a lower maximum cooling power. Moreover, this maximum occurs for a lower current. This is due to the amount of heat exchanged with the environment at the same radiators applied for both situations, with one and ten modules. In the latter case, the radiators cannot ensure sufficient heat exchange to fully utilize the cooling potential of such a number of thermoelectric modules. This results in an excessive rise in the temperature gradient between both sides of the modules. Lower heat dissipation means a lower supply current of the TEC, which is due to the trade-off between Peltier and Joule heat. A further increase in the number of modules would enhance the observation and would follow with a continuous drop in *COP*. It should be remembered that a larger total surface of modules translates into a drop in overall contact thermal resistance, and thereby in a drop in the temperature difference (at constant heat flow) between the thermoelectric junction and the corresponding heat reservoir. Additionally, an increase in the number of TECs leads to a rise in heat conduction via the modules and hence may reduce the temperature difference between the junctions.

What makes the cooling power of 10 thermoelectric modules (normalized to a single module) lower also results in a lower efficiency of the system. At a zero-temperature gradient, *COP* increases with a decrease in the current flowing in the circuit. If there is a temperature gradient, the situation is different. For low current values, *COP* is negative, which is due to the reversed heat flow direction. Only a higher current value ensures that the Peltier effect is strong enough to reverse the heat flow direction and cause the cooling of the upper heat reservoir.

5.3. Impact of the number of thermoelectric modules in the system

In the next step, the impact of the number of TEC modules applied in the system on the cooling characteristic was evaluated.

[1] 360mm type; 15 FPI; fan-assisted.

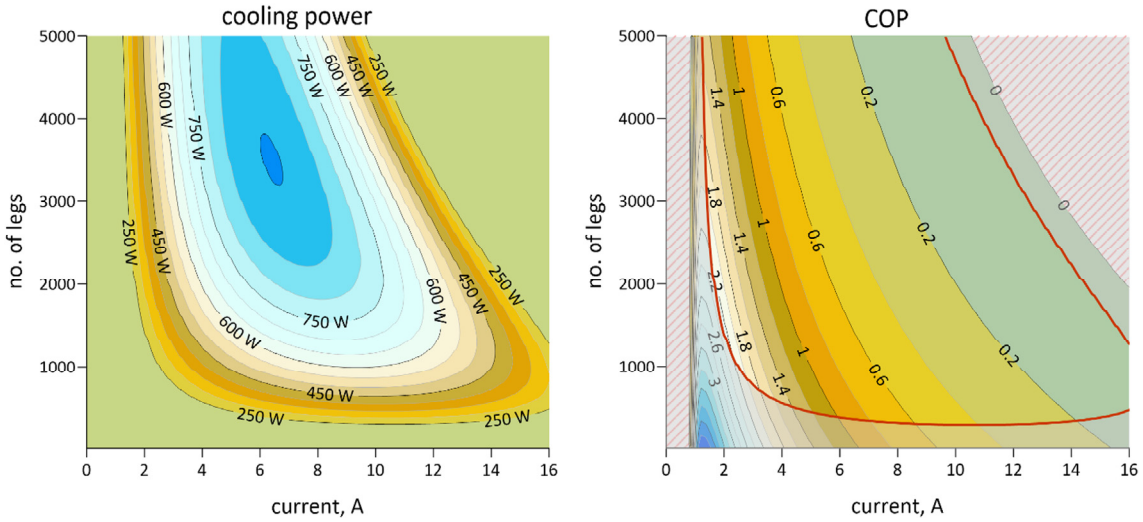

Fig. 5. Cooling power (left) and COP (right) as a function of the number of legs and currents. The dashed area (right) represents the COP below zero (reverse heat flow), and the red line shows the cooling power of 250 W. $HTF_{in} = 100W/K$, $HTF_{out} = 200W/K$. (For interpretation of the references to colour in this figure legend, the reader is referred to the web version of this article.)

The parameters of the module used in the calculations are listed in Table 3. Like in the previous step, constant heat transfer conditions are still assumed as $HTF_{out} = 200W/K, T_{out} = 30^{\circ}C$ (outdoor) and $HTF_{in} = 100W/K, T_{in} = 25^{\circ}C$ (indoor). To obtain a large enough coverage of the search space, it is assumed that the variable will be the number of thermoelectric legs (with a step of 20). The electric current of the TECs was the other parameter. Searching the space in the useful range of currents and dimensions of the thermoelectric system (the number of legs), contour maps were created to represent cooling power and the *COP*. It is assumed that only configurations with cooling power values greater than 250*W* are of any interest. The contour maps obtained are presented in Fig. 5.

The maximum power of the system analysed under the adopted assumptions is 913*W*. This corresponds to the number of legs $n = 3580$, which means 35–36 reference modules supplied with the current of 6.3*A*. Successive levels of cooling power have oval shapes, with stronger elongation in the direction describing the number of legs. This implies that for a relatively wide range of the number of thermoelectric modules, a similar maximum cooling capacity can be obtained. It can also be concluded from the chart that the smaller the size of the thermoelectric part, the greater the range of the current changeability for similar power values. For bigger systems, the current should be selected with higher precision to achieve the set power.

The maximum *COP* reaches the value of 2.28 for $n = 1680$, with a current of 1.8*A*. This value is located at the edge of the domain and results directly from the adopted limitation of the solution space (minimum cooling power of 250*W*). For the maximum cooling power point, *COP* totals 0.42. Higher *COP* values can be noticed in the graph, but they correspond to a very low cooling power, which puts them beyond the area of solution of interest. We can again see that there is a trade-off between cooling power and *COP* in the respected domain.

Because the maximum *COP* depends on the minimum assumed cooling power of the system, the next graph (Fig. 6) presents the relation between these indicators. In addition, for each of the presented cases, the number of TEC modules required by the system and their supply current are specified.

Fig. 6 indicates that a rise in the system minimum power causes a drop in the cooling efficiency. More co-operating thermoelectric modules (marker size and number) are also required, and a higher current is necessary to supply them.

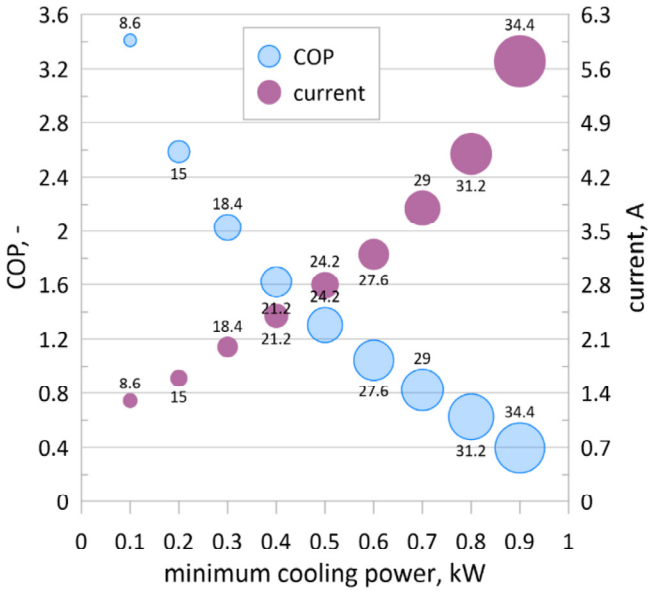

Fig. 6. Maximum COP, number of 100-leg modules and current (both optimized for maximum COP) depending on the system minimum cooling power. The values at the markers denote the corresponding number of modules. For the required minimum cooling power the respective size of the thermoelectric part, the COP and the optimum supply current can be determined. $HTF_{in} = 100W/K$, $HTF_{out} = 200W/K$.

6. Economic optimization of the air conditioning system

The next stage of the air conditioning system analysis is the system economic evaluation. Based on available commercial information, the real cost of a thermoelectric leg is adopted at the level of $N_{TEC} = 0.3\$$ (1% of the reference 100-leg module price). The unit cost of the radiators, estimated in the same manner on the basis of 360 mm 15 FPI cooler, is assumed at $N_R = 0.75\$/(W/K)$. It is based on commercially available computer radiators. The price of electricity needed to supply the thermoelectric module totalled

in the EU[2] $N_{el} = 0.2484\$/kWh = 69n\$/J$ on average, and this value is adopted for the calculations presented below. It is further assumed that the device operates 8 h per day on 60 days of the year, which gives the total of 480 h of operation per year. The calculations are performed for 5 years of service (2400 h). These data were used to determine the cost related to unit cooling power (D) of electricity consumption by the device during its life (N_{op}):

$$N_{op} = DP_{el} = N_{el}P_{el}t \tag{9}$$

where N_{el} is the unit price of electricity, P_{el} – the system electric power and t is the device service life. For the assumptions made above $D = 0.6\$/W_{el}$. It should be noted that the P_{el} value includes the number of the thermoelectric modules, electric current in the circuit and, indirectly, the temperatures at both sides.

The total cost of heat pumping between indoor and outdoor environments and investments in related devices can be expressed as a sum of costs of electricity, radiators, and thermoelectric modules:

$$F = N_{op} + HTF_{in} \cdot N_R + HTF_{out} \cdot N_R + N_{TEC} \cdot \left(0.8 + 0.2\frac{h}{h_{ref}}\right) \tag{10}$$

It is assumed that heat exchange on the two sides of the system proceeds with the use of radiators with the same unit cost N_R. The cost of thermoelectric modules was assumed to consist in 80% of manufacturing costs and in 20% in the used thermoelectric material, which is included in the last term of (10) as the ratio between the heights of legs (h/h_{ref}). To minimize the costs, the system was optimized. The design variables of the optimization process were the dimensions of the radiators described by the *HTF* and the current that supplies the modules, which is included in the N_{op} (electricity cost). The objective function was built in the following form:

$$G = ETCC - \frac{g}{\dot{Q}_{in}} = \frac{\dot{Q}_{in}}{F} - \frac{g}{\dot{Q}_{in}} \tag{11}$$

where:

$$g = \begin{cases} 10 & for\ i \le 0.8\ i_{max} \\ 1 & for\ i > 0.8\ i_{max} \end{cases} \tag{12}$$

and i is the iteration number. *ETCC* stands for *economic total cooling capacity* and indicates cooling power achieved from 1$ of the total cost of the system. The total cost consists of the electricity cost (assumed 5 years) and the device purchase cost. The aim of the task was to maximize *ETCC*. The objective function includes two factors, the first of which (*ETCC*) is the directly maximized quantity, while the role of the second ($g/\dot{Q}_{in}$) is to introduce some pressure related to the system cooling power. During the optimization process using only the first term of the objective function, it turned out that it gave a few similar extrema for different values of the design variables. Therefore, another term was introduced into the function that slightly (the impact on G is of up to 1%) favours solutions with a higher cooling power value. Due to a jump change in the g parameter, more pressure on the optimization process is introduced at the first stage, which improves convergence. Then, the solutions are stable and repeatable. Moreover, in the case of two identical configurations with the same value of *ETCC*, the one with a higher cooling power will be considered better. Such a device (at the set number of modules or cooling power) will have a higher power-to-size factor, which also means reduced secondary costs not taken into account in the optimization and related to the making of the casing, packaging, transport, ease of use, etc.

Using conditions formulated in this way, calculations were performed for an air conditioning system made of 10 basic TEC modules ($n = 1000$) with the thermoelectric leg height of $h = h_{ref} = 3mm$. Supply current and both HTF values were the design variables. In this situation, the last term of function F (10) is constant. The results are shown in the form of a contour map, the creation of which required optimizing the *ETCC* for each pair (D, T_{out}). The optimization results are shown in Fig. 7.

The contour map presented shows the cooling power achieved at the investment of the device and the total operating cost per unit (1$) depending on the cost of electricity and the outdoor temperature. For the reference data ($T_{out} = 30^{\circ}C$ and $D = 0.6\$/W_{el}$), the result is $ETCC = 0.58W/\$$. For low electricity prices and at a small difference between the cooled space and the environment, the indicator is equal to $1W/\$$, whereas at a high outdoor temperature and expensive electricity in the analysed range, it can drop even to about $0.12W/\$$. It has to be emphasized that the device can be scaled proportionally to achieve different cooling power at the same *ETCC*.

6.1. A device with the design cooling power of 2 kW

The results of the optimization presented above put aside the cooling power provided by the system under specific operating conditions. Therefore, it was decided in the next step to determine the required number of basic thermoelectric modules to ensure a reliable cooling power of $2kW$, which is a power level typical of portable air conditioning devices for small rooms. The device is assumed to operate at the maximum value of *ETCC*. At this stage, an additional variable of the objective function is the number of legs n, while further calculations are still based on the reference and constant height of the leg ($h = h_{ref} = 3mm$).

Fig. 8 presents the required number of thermoelectric modules needed to achieve the cooling capacity of $\dot{Q}_{in} = 2kW$ in maximum *ETCC* conditions and the corresponding electric current. Naturally, the cooling power can also be increased in a certain range by

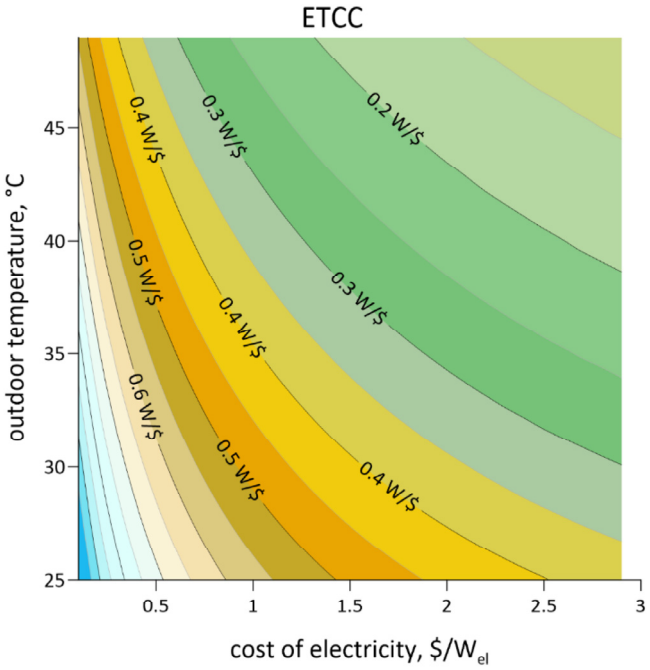

Fig. 7. ETCC as a function of the cost of electricity (D) and outdoor temperature (T_{out}) for constant $T_{in} = 25^{\circ}C$. For a given cost of electricity, an increase in outdoor temperature makes air conditioning more expensive (drop in *ETCC*). (For interpretation of the references to colour in this figure legend, the reader is referred to the web version of this article.)

[2] Price as of September 2021.

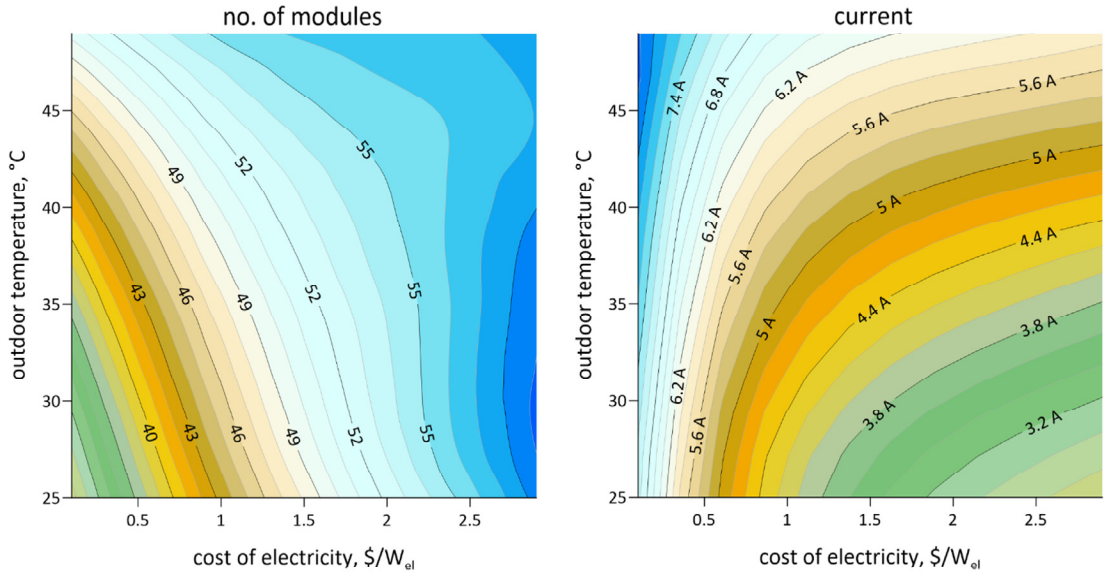

Fig. 8. Number of thermoelectric modules for 2 kW of cooling power (left) and respective current in the circuit (right) at optimal operating conditions (maximum ETCC) depending on the cost of electricity and the outdoor temperature. If the cost of electricity grows the higher number of modules results from a lower share of investment in the total cost and a possible lower supply current.

increasing the current in the thermoelectric modules, but the system operation under such conditions proceeds beyond the optimum value of *ETCC* and is then less cost-effective. The results show that, for the reference point, reaching the required level of power involves the need to use 4140 legs, which means about 41 basic reference modules. The supply current for this number of cells is then almost 5 A.

In the analysed range of changeability of the parameters, the required number of modules varies from 30 to 60, which results in a different share of investment and operating costs in total expenditures. The required number of modules increases with increasing electricity cost, which means higher investment costs. It also rises with an increase in the temperature difference, but at a slower rate than in the case of operating costs. On the one hand, a larger number of modules allows for the desired cooling capacity by the Peltier effect for smaller current values. On the other hand, Joule heat (an undesirable phenomenon) is proportional to the current squared, while Peltier's effect is directly proportional. Therefore, it seems to be profitable to use many modules. However, it should be noted that a higher number of modules means a larger amount of heat conducted by the thermoelectric legs, and this deteriorates the effectiveness of the system operation. Additionally, the price of each module plays a role.

Other contour maps were also prepared for an analysed device with the cooling power of $2kW$. They show the *HTF* values of each radiator (indoor and outdoor) at various operating conditions (temperature) and at various levels of the cost of electricity. The coefficients have a direct impact on the size and/or quality of the radiators on the two sides of the system and thereby – on their cost.

The contour maps in Fig. 9 illustrate the rise in *HTF* s with a rise in the temperature difference between the indoor and outdoor environments. The rate of the rise is higher on the outside. The outdoor radiator is generally bigger, and the HTF_{out}/HTF_{in} ratio in the shown range is from 1.15 to 1.89. Attention should be drawn to the fact that the costs related to the purchase of the radiators are not negligibly small and were considered in the objective function (11) through the product of $HTF_{in/out}$ and N_R in (10).

So far, for each operating point of the system defined by cooling power, the difference between indoor and outdoor temperature, and the cost of electricity, the optimal design and operating parameters of the system have been selected. However, the question arises as to how a change in the system operating conditions, e.g., the outdoor temperature or the cost of electricity, will affect *ETCC*. Although it is relatively simple to control the system supply current, making structural changes to the existing system design seems irrational. To determine the level of changes in *ETCC* due to changes in the conditions mentioned above, calculations were performed for a system optimized for the reference parameters ($T_{out} = 30^{\circ}C$ and $D = 0.6\$/W_{el}$). In this case, the design characteristics determined design features of the system are $HTF_{out} = 741W/K$, $HTF_{in} = 567W/K$ and $n = 4150$, while the supply current was optimized for maximum *ETCC*.

Fig. 10 presents the percentage change in *ETCC* (left) and cooling power (right) of the device based on changes in both the cost of electricity and the outdoor temperature. The system is optimized at the reference point ($0.6\$/W_{el}, 30^{\circ}C$) for the maximum *ETCC*. It can be read from the graph that a rise in the outdoor temperature by less than $5K$ causes a drop in *ETCC* less than 1% and about 5% drop in cooling power. In the entire range presented above, the change does not exceed 10% for *ETCC* but reaches about 25% for cooling capacity.

6.2. Impact of a change in leg height

It should be noted that the leg height of the thermoelectric material of the module has an impact on both the TEC operating parameters and, to a certain extent, on the manufacturing costs. A change in leg height involves mainly a change in the amount of heat conducted by the module, in the generated Joule heat, and in the mass of the thermoelectric material used. Therefore, simulations were performed to assess the *ETCC* of the air conditioning system, considering the variability in leg height. Due to this, the objective function (10) operates now with an additional variable, h. Thermoelectric material is assumed to account for 20% of the manufacturing cost of the TEC module (factors of 0.2 and 0.8 in (10)). The leg reference height ($h_{ref} = 3mm$) concerns the basic model with a known purchase cost. The calculations were carried out in the same manner as those performed for a constant leg height, specifying for each point (D, T_{out}) the optimal dimensions of radia-

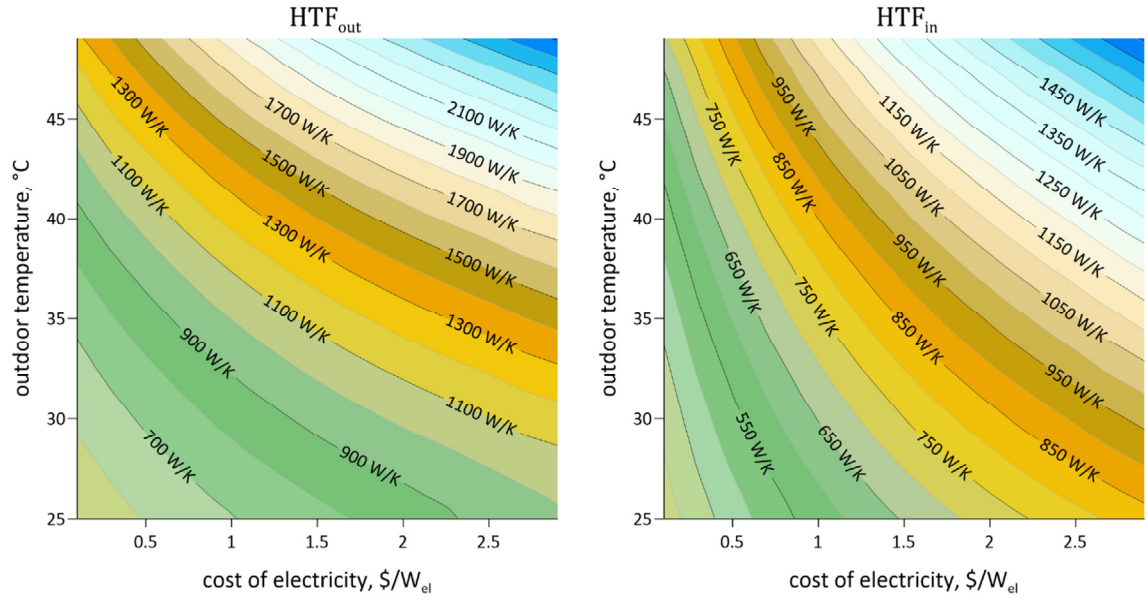

Fig. 9. Heat transfer coefficients at the 2 kW device optimized for ETCC optimal operating conditions as a function of the cost of electricity and the outdoor temperature. The indoor temperature is 25 °C. Higher HTF values mean a bigger and more expensive radiator.

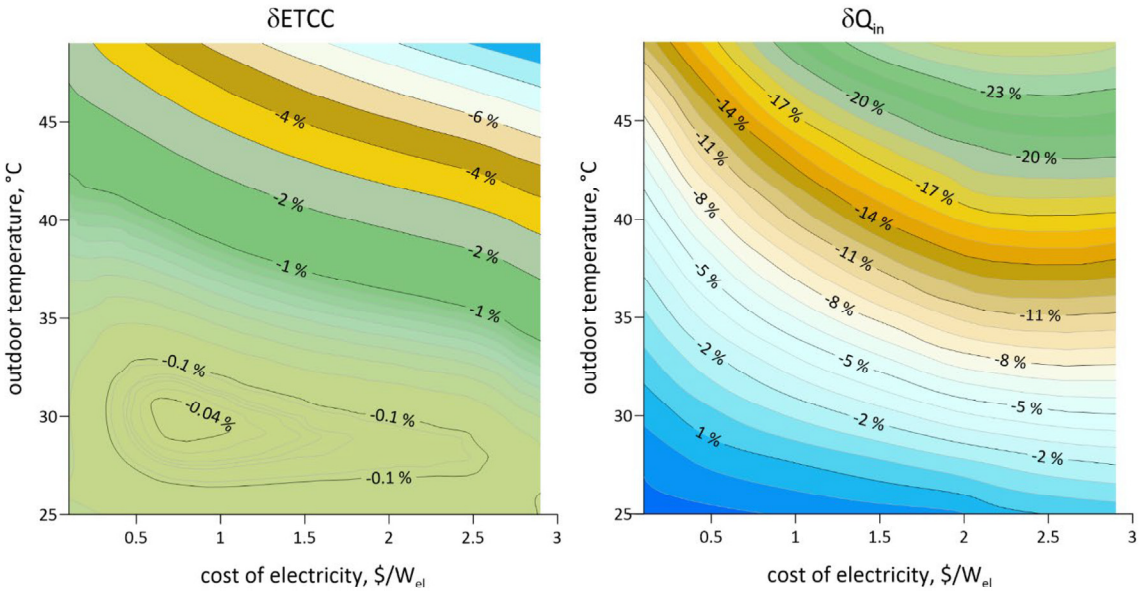

Fig. 10. Percentage deviation of ETCC and cooling power from the optimal value for the reference point for a change in the outdoor temperature and in the cost of electricity. No deviation in the reference point (0.6$/Wel, 30 °C). HTF factors and the number of modules were maintained the same as for the reference point, electric current was optimized each time. ETCC deteriorates beyond the reference point.

tors (both *HTFs*), the number of modules (n), the current (I), and additionally the leg height (h).

The graph on the left in Fig. 11 presents *ETCC* under the same operating conditions as previously (2400 h of operation). Because the leg height also varies in this case, its optimal value is shown on the right. When comparing the results for the reference point ($D = 0.6\$/W_{el}$ and $T_{out} = 30^{\circ}C$), the *ETCC* rises substantially from $0.58W/\$$ to $0.64W/\$$ (Fig. 7 vs. Fig. 11). This corresponds to the leg height by more than half lower compared to the reference case. A change in the leg height also involves changes in the system's other design features, i.e., the size of radiators, the number of modules (legs). The supply current will be different, too. Compared again to the reference point, for a device with a cooling power of $2kW$, the heat transfer factors are $HTF_{out} = 804W/K$ and $HTF_{in} = 605W/K$, respectively, and they are less than 10% higher than in the case of the fixed leg height of $h = h_{ref} = 3mm$. The number of modules required to achieve the set power is in this case about 32 ($n = 3220$).

The above calculations relate to a situation where a change in leg height involves a proportional 20% change in the cost of the thermoelectric module compared to the reference module (0.2 factor in (10)). If the module cost is assumed to be constant regardless of the leg height-

($F = N + HTF_{in} \cdot N_R + HTF_{out} \cdot N_R + N_L \cdot 1$), the *ETCC* will total $0.62W/\$$, whereas for a proportional increase in the module cost with the increase in the amount of the thermoelectric material.

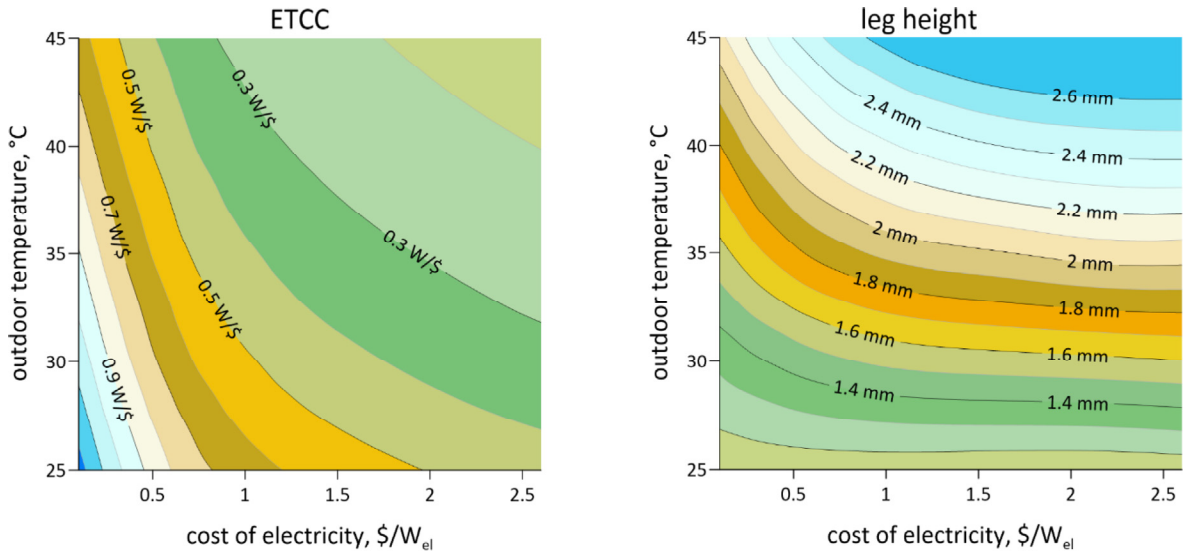

Fig. 11. Optimized ETCC and corresponding leg height as a function of the cost of electricity and outdoor temperature. Case for variable leg height.

$(F = N + HTF_{in} \cdot N_R + HTF_{out} \cdot N_R + N_L \cdot (h/h_{ref}))$ it would be $0.75W/\$$. In a way, these two values determine the range of *ETCC*, depending on the share of thermoelectric material cost within the TEC.

Fig. 12 shows the percentage deviation of *ETCC* (left) and cooling power (right) for a system designed for the reference point at an optimized height of the module legs. Comparing the presented results with those shown in Fig. 10, for cells with a leg reference height of $3mm$, it can be noticed that in this case the system is more sensitive to changes in both temperature and electricity cost. In the analysed range of changeability of temperature and costs, up to a 35% increase in *ETCC* and a 50% drop in cooling power can be expected. It follows that a system optimized for pre-determined operating conditions (reference point) is characterized by a better *ETCC* during design-state operation, but any deviation from that state causes an accelerated deterioration of the factor.

7. The maximum cooling power of the system

The optimization results were related to achieving the maximum *ETCC* under the given conditions. However, in each design configuration, the system is able to operate with a significantly higher cooling power than the value resulting from the *ETCC* optimum, provided that it is supplied by an adequately stronger current. To observe the control range of such a device, the impact of the supply current on the cooling power and *ETCC* related to operation in such conditions was investigated. Calculations were performed for a system optimized for the reference conditions. The test was carried out for the reference modules ($h = 3mm$) and for modules with leg optimized height ($h = 1.46mm$).

Fig. 13 illustrates the device cooling power and the corresponding *ETCC*, along with the *COP*, depending on the thermoelectric system supply power. Both the power and *ETCC* curves have a clear

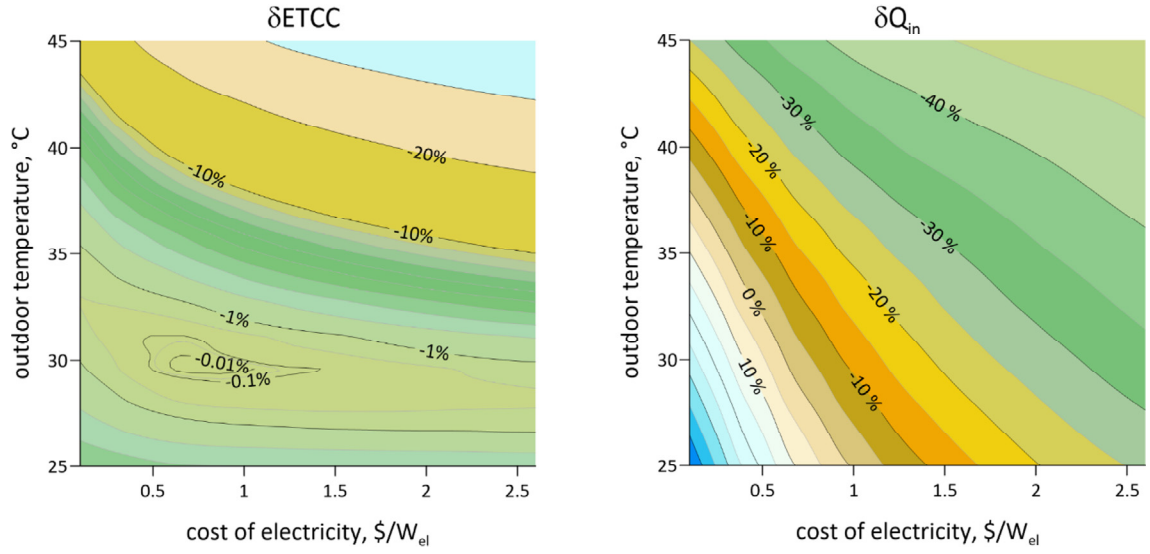

Fig. 12. Percentage deviation of ETCC and cooling power from the optimal value for the reference point for a change in the outdoor temperature and in the cost of electricity. No deviation in the reference point (0.6$/W$_{el}$, 30 °C). HTF factors and the number of modules were maintained the same as for the reference point, electric current was optimized each time. ETCC deteriorates beyond the reference point. Case for a variable leg height.

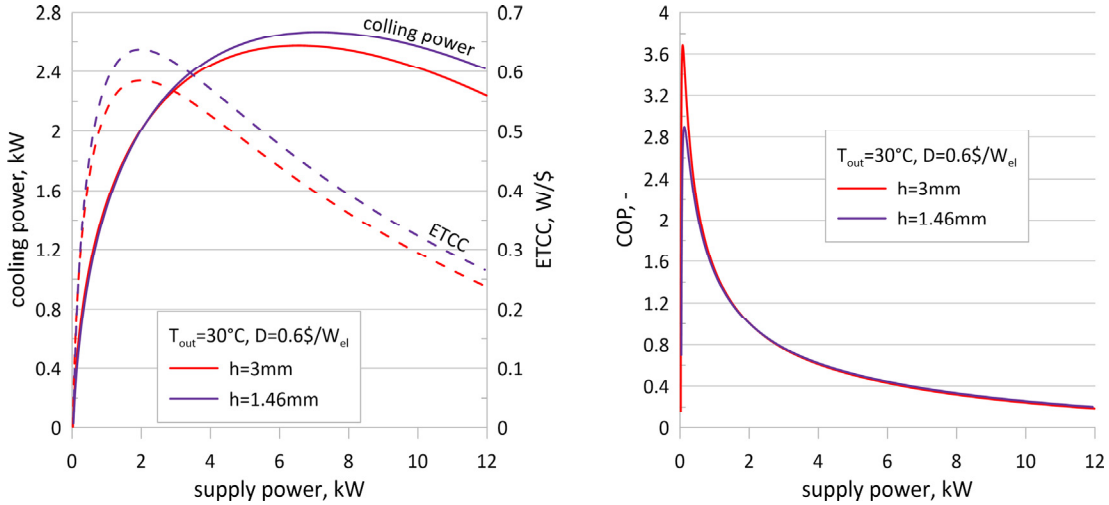

Fig. 13. Impact of supply power on the device (optimized for maximum ETCC) cooling power and ETCC (left) and COP (right). The graphs are for the outdoor temperature of 30 °C, the indoor temperature of 25 °C and for the cost of electricity of 0.6$/$W_{el}$ (reference point).

extremum, but a shift can be observed between them. The highest cooling capacity per 1 dollar of the total cost occurs for a lower supply power than the maximum of the cooling power. It is thus demonstrated that if the device is designed in terms of the economic optimum, there is still a cooling capacity margin, which in the case of a momentary increase in the demand for cooling, makes it possible to satisfy the demand. For a device with the reference height of the leg and 2 *kW* nominal cooling capacity, the maximum cooling power is 2.57*kW*. This means that it is possible to achieve a 28% increase in cooling power. When analysing the case with the optimized leg height, the maximum cooling power of 2.67*kW* can be observed. Clearly, this means a substantial increase in supply power, which translates into a drop in the *COP* from about 1 to 0.38. The device operation beyond the cost optimum involves an increase in the total cost.

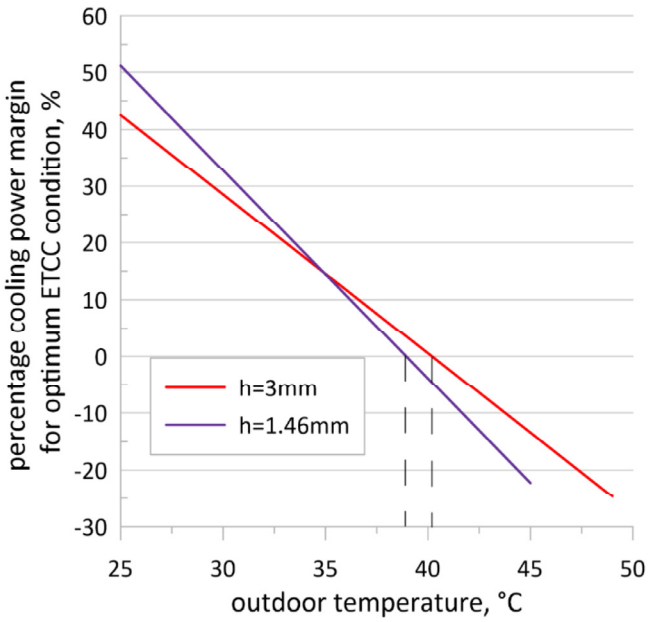

Fig. 14. Percentage cooling power margin for cooling power at optimum ETCC for the reference point as a function of the outdoor temperature. The dashed lines mark the outdoor temperature up to which an increase in cooling power is possible. Above these temperatures, the maximum cooling capacity is below the design level.

To what extent the cooling capacity can change with outdoor temperature regardless of the total cost is shown in Fig. 14. It can be seen that the change in cooling power is nearly linear with outdoor temperature. For a zero change, there is the highest outdoor temperature at which the system can achieve the design cooling capacity (at significantly lower *ETCC*). For higher temperatures, the maximum cooling power is lower than the design level. For the cases analysed, the temperature is slightly above $40^{\circ}C$ for the reference module height and about $39^{\circ}C$ for the optimized, respectively. The cooling power for the maximum *ETCC* in Fig. 13 and its possible increase (28% in the case of 3*mm* legs and 33% for the 1.46*mm* legs, respectively) is visible here for temperature $30^{\circ}C$.

It should be emphasized here that continuous operation of the device with a power higher than optimal is also possible. However, in such a situation, lower *ETCC* s must be considered. Another thing worth noting is the fact that *ETCC* does not fall at the same rate as the rise of supply power (in this case, for the power maximum – 2.5 times) because the cost of electricity is only one of the elements of the total cost and the cooling power does not change linearly with electric current or electric power.

8. Summary and conclusions

The paper presents a concept of a thermodynamic system of an air conditioner using thermoelectric modules. Analyses were based on commercially available modules intended for cooling purposes, and the performance parameters of the TECs were experimentally determined. In addition to the operating parameters of the module itself, the contact resistance between the module and the heat exchangers was also determined and included in the system simulations. The analysed system consisted of thermoelectric modules thermally connected in parallel, heat exchangers in contact with TECs, and radiators exchanging heat with the environments. It was assumed that heat was transported from the exchangers to the fan-assisted radiators by a liquid medium. The validity of the proposed mathematical model and the developed software was proven experimentally.

The concept of the air conditioning system was tested numerically in terms of the performance parameters. It was observed that increasing the size of the thermoelectric part resulted in lower cooling power and lower *COP* per module if the size of the radiators on both sides of the system were kept constant. This is, first of all, an effect of more heat being conducted by the modules. A larger

heat flux with the same radiators causes a larger temperature gradient between the thermoelectric junctions, and this results in a decrease in cooling capacity and *ETCC*.

The system was then optimized to maximize the cooling capacity achieved from 1$ of the total system cost in a set lifetime of the device. All calculations were performed taking account of both investment and operation costs. The calculations were run for two design variants of the thermoelectric modules, i.e. for the commercial system with the thermoelectric leg constant predetermined reference height and for the case where the height may vary.

For the set leg height and the assumed time of the device operation (2400 h) and for the average price of electricity in the EU, the *ETCC* of $0.58W$ per 1 dollar was obtained. To construct a device with a cooling power of $2kW$, 41 assumed TECs are required. By additionally optimizing the height of the module legs, and assuming that the cost of the thermoelectric material in the TEC total cost is 20%, the value of $ETCC = 0.63W/\$$ was obtained for legs by about 50% shorter than the reference ones. In this case, to generate $2kW$ of cooling power, 32 reference modules are needed and the radiators must be about $6 - 8\%$ bigger.

The system optimized in terms of economic efficiency can be overloaded by about 30%, which involves a 2.5-fold drop in *COP*. The device continuous operation (2400h) in the condition of maximum cooling power would cause about a 30% drop in *ETCC* in the entire assumed cycle of operation.

When comparing the presented air conditioning thermoelectric system with conventional compressor-based solutions, it can be seen that, at comparable cooling power, it is substantially more expensive and has a lower *COP* as well as *ETCC*. However, the thermoelectric system has a number of advantages: the simplicity of design, silent operation, lack of a compressor, and the possibility to use any (environmentally friendly/safe) liquid medium transporting heat. Such a system can also work as a room heater by reversing the direction of the current that supplies the TECs. Furthermore, the momentary reversal of the current can be used, for example, to heat up the exchanger to remove the accumulated liquefied humidity from the air and reduce the biological hazard. Moreover, the control system of such a device in the form of a regulated DC power supply seems to be very simple, and the thermoelectric cells can be electrically connected in series or in parallel to adapt the circuit to the voltage range of the power supply at a given power level.

Declaration of Competing Interest

The authors declare that they have no known competing financial interests or personal relationships that could have appeared to influence the work reported in this paper.

Acknowledgements

The research was funded by the Polish National Science Centre (NCN Poland), Grant 2016/23/B/ST8/03133

References

[1] N. Mao, D. Pan, Z. Li, Y. Xu, M. Song, S. Deng, A numerical study on influences of building envelope heat gain on operating performances of a bed-based task/ambient air conditioning (TAC) system in energy saving and thermal comfort, Applied Energy 192 (2017) 213–221.
[2] J. Mei, X. Xia, Energy-efficient predictive control of indoor thermal comfort and air quality in a direct expansion air conditioning system, Applied Energy 195 (2017) 439–452.
[3] T. Randazzo, E. De Cian, M.N. Mistry, Air conditioning and electricity expenditure: The role of climate in temperate countries, Economic Modelling 90 (2020) 273–287.
[4] Davis, L.W., Gertler, P.J. Air conditioning and global warming, Proceedings of the National Academy of Sciences of the United States of America. May 2015. 112 (19). 5962-5967.
[5] M. Lickley, S. Solomon, S. Fletcher, G.J.M. Velders, J. Daniel, M. Rigby, S.A. Montzka, L.J.M. Kuijpers, K. Stone, Quantifying contributions of chlorofluorocarbon banks to emissions and impacts on the ozone layer and climate, Nature Communications 11 (1) (2020).
[6] M.M. Hurwitz, E.L. Fleming, P.A. Newman, F. Li, E. Mlawer, K. Cady-Pereira, R. Bailey, Ozone depletion by hydrofluorocarbons, Geophys. Res. Lett. 42 (20) (2015) 8686–8692.
[7] A.M.R. Nishimwe, S. Reiter, Estimation, analysis and mapping of electricity consumption of a regional building stock in a temperate climate in Europe, Energy and Buildings 253 (2021) 111535.
[8] UNEP. 2011. HFCs: A Critical Link in Protecting Climate and the Ozone Layer. United Nations Environment Programme (UNEP). 36pp.
[9] D.K. Lim, B.H. Ahn, J.H. Jeong, Method to control an air conditioner by directly measuring the relative humidity of indoor air to improve the comfort and energy efficiency, Applied Energy 215 (2018) 290–299.
[10] J. Mei, X. Xia, M. Song, An autonomous hierarchical control for improving indoor comfort and energy efficiency of a direct expansion air conditioning system, Applied Energy 221 (2018) 450–463.
[11] M.S. Oh, J.H. Ahn, D.W. Kim, D.S. Jang, Y. Kim, Thermal comfort and energy saving in a vehicle compartment using a localized air-conditioning system, Applied Energy 133 (2014) 14–21.
[12] A. Martinez, S. Díaz de Garayo, P. Aranguren, M. Araiz, L. Catalán, Simulation of thermoelectric heat pumps in nearly zero energy buildings: Why do all models seem to be right?, Energy Conversion and Management 235 (2021) 113992
[13] A. Martinez, S. Díaz de Garayo, P. Aranguren, D. Astrain, Assessing the reliability of current simulation of thermoelectric heat pumps for nearly zero energy buildings: Expected deviations and general guidelines, Energy Conversion and Management 198 (2019) 111834.
[14] Z.B. Liu, L. Zhang, G.C. Gong, Y.Q. Luo, F.F. Meng, Experimental study and performance analysis of a solar thermoelectric air conditioner with hot water supply, Energy and Buildings 86 (2015) 619–625.
[15] J. Dongxu, W. Zhongbao, J. Pou, S. Mazzoni, S. Rajoo, A. Romagnoli, Geometry optimization of thermoelectric modules: Simulation and experimental study, Energy Conversion and Management 195 (2019) 236–243.
[16] P.E. Ruiz-Ortega, M.A. Olivares-Robles, C.A. Badillo-Ruiz, Transient thermal behavior of a segmented thermoelectric cooler with variable cross-sectional areas, Int J Energy Res. (2021) 1–11.
[17] Z.B. Liu, L. Zhang, G.C. Gong, Experimental evaluation of a solar thermoelectric cooled ceiling combined with displacement ventilation system, Energy Conversion and Management 87 (2014) 559–565.
[18] M.Z. Yilmazoglu, Experimental and numerical investigation of a prototype thermoelectric heating and cooling unit, Energy and Buildings 113 (2016) 51–60.
[19] S. Shittu, G. Li, X. Zhao, X. Ma, Review of thermoelectric geometry and structure optimization for performance enhancement, Applied Energy 268 (2020) 115075.
[20] A. Fabián-Mijangos, G. Min, J. Alvarez-Quintana, Enhanced performance thermoelectric module having asymmetrical legs, Energy Conversion and Management 148 (2017) 1372–1381.
[21] X. Wang, J.i. Qi, W. Deng, G. Li, X. Gao, L. He, S. Zhang, An optimized design approach concerning thermoelectric generators with frustum-shaped legs based on three-dimensional multiphysics model, Energy 233 (2021) 120810.
[22] X.-X. Tian, S. Asaadi, H. Moria, A. Kaood, S. Pourhedayat, K. Jermsittiparsert, Proposing tube-bundle arrangement of tubular thermoelectric module as a novel air cooler, Energy 208 (2020) 118428.
[23] A. Provensi, J.R. Barbosa, Analysis and optimization of air coolers using multiple-stage thermoelectric modules arranged in counter-current flow, International Journal of Refrigeration 110 (2020) 19–27.
[24] A. Attar, H.S. Lee, Designing and testing the optimum design of automotive air-to-air thermoelectric air conditioner (TEAC) system, Energy Conversion and Management 112 (2016) 328–336.
[25] H. Sun, B. Lin, Z. Lin, Y. Zhu, H. Li, H. Wu, Research on a radiant heating terminal integrated with a thermoelectric unit and flat heat pipe, Energy and Buildings 172 (2018) 209–220.
[26] Conrad, K.J. A physics-based compact model for thermoelectric devices. 2015. Open Access Theses. 539. https://docs.lib.purdue.edu/open_access_theses/539.
[27] H.A. Eivari, Z. Sohbatzadeh, P. Mele, M.H.N. Assadi, Low thermal conductivity: fundamentals and theoretical aspects in thermoelectric applications, Materials Today Energy 21 (2021) 100744.
[28] S.M. Pourkiaei, M.H. Ahmadi, M. Sadeghzadeh, S. Moosavi, F. Pourfayaz, L. Chen, M.A. Pour Yazdi, R. Kumar, Thermoelectric cooler and thermoelectric generator devices: A review of present and potential applications, modeling and materials, Energy 186 (2019) 115849.
[29] D. Luo, R. Wang, W. Yu, W. Zhou, Performance optimization of a converging thermoelectric generator system via multiphysics simulations, Energy 204 (2020) 117974.
[30] C. Junior, C. Richter, W. Tegethoff, N. Lemke, J. Koehler, Modeling and Simulation of a Thermoelectric Heat Exchanger using the Object-Oriented Library TIL, Modelica (2008).
[31] C. Selvam, S. Manikandan, N.V. Krishna, R. Lamba, S.C. Kaushik, O. Mahian, Enhanced thermal performance of a thermoelectric generator with phase

change materials, International Communications in Heat and Mass Transfer 114 (2020) 104561.
[32] R. Tang, S. Wang, K. Shan, H. Cheung, Optimal control strategy of central air-conditioning systems of buildings at morning start period for enhanced energy efficiency and peak demand limiting, Energy 151 (2018) 771–781.
[33] A. Beghi, L. Cecchinato, M. Rampazzo, A multi-phase genetic algorithm for the efficient management of multi-chiller systems, Energy Conversion and Management 52 (3) (2011) 1650–1661.
[34] J. Jia, W.L. Lee, Y. Cheng, Q.i. Tian, Can reversible room air-conditioner be used for combined space and domestic hot water heating in subtropical dwellings?, Techno-economic evidence from Hong Kong, Energy 223 (2021) 119911
[35] P. Niemann, G. Schmitz, Air conditioning system with enthalpy recovery for space heating and air humidification: An experimental and numerical investigation, Energy 213 (2020) 118789.
[36] M. Luqman, T. Al-Ansari, A novel integrated wastewater recovery, clean water production and air-conditioning system, Energy Conversion and Management 244 (2021) 114525.
[37] Multicomp pro. Thermoelectric device datasheet. MCTE1-19913L-S.
[38] R. Buchalik, G. Nowak, I. Nowak, Mathematical model of a thermoelectric system based on steady- and rapid-state measurements, Applied Energy 293 (2021) 116943.
[39] W. Li, M.C. Paul, A. Montecucco, J. Siviter, A.R. Knox, T. Sweet, M. Gao, H. Baig, T.K. Mallick, G. Han, D.H. Gregory, F. Azough, R. Freer, Multiphysics simulations of thermoelectric generator modules with cold and hot blocks and effects of some factors, Case Studies in Thermal Engineering 10 (2017) 63–72.

Article citation info:
BUCHALIK, R., ROGOZIŃSKI, K., NOWAK, G. The potential of thermoelectric energy harvesting in vehicles equipped with ICE. *Combustion Engines*. 2019, **179**(4), 70-74. DOI: 10.19206/CE-2019-411

Ryszard BUCHALIK
Krzysztof ROGOZIŃSKI
Grzegorz NOWAK

CE-2019-411

The potential of thermoelectric energy harvesting in vehicles equipped with ICE

The paper deals with an issue of waste heat recovery in a selected configuration of an internal combustion engine. A possibility of using thermoelectric cells (currently available on the market) for production of electricity with heat extracted from the exhaust gas was considered. The calculations were made using specialized software. Features and design assumptions of the heat recovery system were presented and their influence on parameters of the entire system was investigated (efficiency of the internal combustion engine, power, etc.). An assessment of the applicability of the energy recovery system based on thermoelectric effects and characteristic of the proposed configuration was performed. Some issues that require further research have been highlighted.

Key words: *combustion engine, heat recovery, thermoelectric module, heat transfer, exhaust system*

1. Introduction

Improvement in internal combustion engine performance is one of the main goals engineers deal with. There are many sophisticated solutions based, in some sense, on controlling the combustion process inside the combustion chamber and the piston motion. Some of them increase pressure, temperature, compression ratio, valve timing, etc. But in nearly every combustion engine system a significant part of the energy is lost due to the waste heat expelled to the surroundings [10]. Some heat is lost in the engine cooling system, via the central radiator, but this heat source has relatively low temperature. Much higher temperature occurs, however in the exhaust system. An attempt was made to analyse the possibilities, issues and selected problems of heat recovery from the exhaust gas. One of the possibilities discussed in this paper is the use of the thermoelectric modules, which convert heat into electricity. The basic principle of their operation is the Seebeck effect. A thermoelectric module is usually a flat sheet (thickness of a few millimetres) of semiconductors between ceramic (electrical insulator) plates. If a thermal gradient occurs throughout the module a voltage difference is generated [3, 9]. The thermoelectric modules have several advantages like the lack of moving parts, long lifetime, very small size and noiseless operation. On the other hand, their efficiency is rather low. There are, of course, some more efficient methods of waste heat recovery (Organic Rankine Cycle, turbine) but they are usually quite complex and difficult or unreasonable to use in mobile applications [4, 14]. The thermoelectric module can be easily retrofitted, e.g. by replacing genuine muffler with a modified one. Descriptions of experimental research systems, including modules assembled into vehicles can be found in the literature [2, 7, 11]. The following considerations were performed to make a coarse assessment of the amount of heat which can be recovered, overall characteristics of such heat recovery system and different working conditions that can occur in typical vehicle drivetrain. The result obtained can be useful in a design process of specific heat exchangers, identifying crucial issues and targets.

2. Modelling approach

The analysis of waste heat recovery was based on a 4 stroke, a spark ignited, 500 ccm motorcycle engine. A simplified model of immediate fuel combustion at a constant volume was used. Perfectly stoichiometric air to fuel ratio was assumed and friction inside the engine block between moving elements was neglected. The exhaust system in proposed configuration consists of, among the others, a thermoelectric module assembly unit. This assembly consist of a straight pipe, in which exhaust gases flow, a highly heat conductive material between inner pipe surface and the thermoelectric cells (hot side heat exchanger – heat source), the thermoelectric module and the cooling system. The hot side of the thermoelectric module can be attached directly to the heat source (a flat surface covered with thermal grease). The opposite side of the thermoelectric module should be attached to the water cooling system (cold side heat exchanger – heat sink). The remaining surfaces were assumed adiabatic. Figs 1 and 2 present both a cross-sectional and an isometric view of the heat recovery system proposed.

The specialized software – AVL Boost, was used to carry out the simulations.

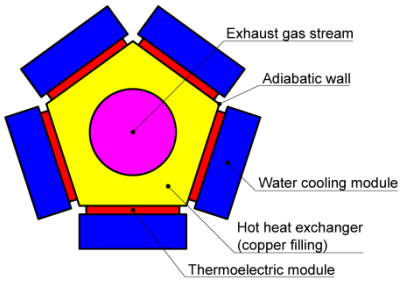

Fig. 1. A cross-sectional view of thermoelectric module assembly

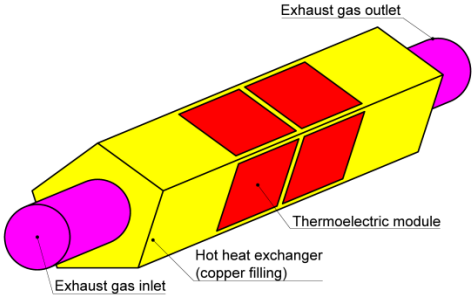

Fig. 2. Thermoelectric module assembly

The overall thermal resistance of this assembly can be calculated as the proportionality factor between heat transferred through the system (from the exhaust gas to cooling water) and temperature difference at both sides of the domain. One of them is the inner surface in contact with hot exhaust gas, whereas the second one is the thermoelectric module cold side (cooled with water flow from the cooling system). Due to a major difference in magnitudes of thermal resistance of the thermoelectric module and the heat exchangers the heat exchangers resistance can be neglected [1]. In other words, if constant heat flux is imposed to the system the temperature gradient is significant only across the thermoelectric module whereas within the hot heat exchanger the temperature distribution is nearly uniform. The same situation occurs at the cold side – the temperature of the heat exchanger and the module cold side is almost the same. This assumption is true for heat exchangers made of a highly heat-conductive material, e.g. copper. In such a case, the gas-wall temperature difference drop along the flow direction is not large. In the described configuration it is relatively small (not greater than 100 K), so the temperature of heat source for modules in one thermoelectric assembly was assumed to be constant. As a result, in one assembly the temperature of the inner wall (in contact with exhaust gases) and thermoelectric modules hot side is the same [1, 6].

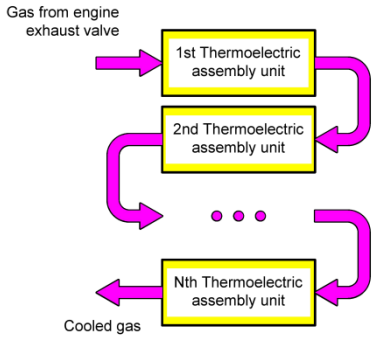

Fig. 3. General configuration of exhaust heat recovery system

Based on literature and the technical data of commercially available thermoelectric modules, the thermal conductivity of exemplary module (Tecteg TEG1-PB12690) was assumed as about 0.5 W/K (~ 273 W/570°C) for surface 62 mm × 62 mm [12] (0.5 W/K corresponds to 2 K/W thermal resistance). Thermal conductivity of the thermoelectric module is subjected to change with electrical load (electric current in a circuit results with the Peltier effect – phenomena related to the Seebeck effect). However, using a DC/DC converter within the system, whose aim is to provide optimal working conditions (electrical resistance of power receiver for the highest module power or the highest efficiency) immediately minimises the problem. So, the overall thermal conductivity can be assumed constant [1]. Proposed thermoelectric assembly unit consists of 10 mentioned thermoelectric modules attached to the exhaust pipe. The modules used have a maximum allowable working temperature of 600°C. To keep the constant temperature distribution within the heat source, the modules should be uniformly distributed on the heat source surface, e.g. if the cross section is pentagon-like showed on Fig. 1 it results in 2 thermoelectric modules (62 mm × 62 mm) on each wall. The temperature of the heat source was determined based on the 0.5 W/K thermal conductivity of the thermoelectric modules. For 10 thermoelectric modules (one assembly unit) the thermal conductivity (reverse of thermal resistance) is about 10 W/K. On this basis, a script in C language was developed and implemented in the software to calculate the temperature of the heat source. The module cold side temperature (resulting from water cooling) was assumed to be 50°C. To model the heat transfer coefficient between the stream of exhaust gas and the channel wall (heat source, with a temperature equal to module hot side) a Reynolds analogy have been used. It provides a rough approximation of a general heat exchanger. The amount of electric energy produced as useful result in thermoelectric module was calculated using the heat transferred from exhaust gas into the heat exchanger in assembly unit (heat recovered in a unit) multiplied by temperature gradient between hot and cold side of the thermoelectric module and then multiplied by factor (0.000128) corresponding to the datasheet of the thermoelectric module (~7% efficiency at 600°C/50°C). The efficiency of electric power generation can be assumed proportional to the temperature gradient, so it is adopted here.

An alternative method for efficiency assessment can be based on Carnot efficiency for given temperatures (heat source and heat sink) multiplied by an appropriate factor. This method corresponds to the assumption that the thermoelectric figure of merit (coefficient of performance) is constant over temperature for the thermoelectric module component materials (semiconductors, legs) [9].

3. Reference experimental setup

At the initial step of considerations, to avoid an influence of intensive wave phenomena, a large plenum (500 litres) have been added between the exhaust port and the thermoelectric module assembly(s). It was assumed adiabatic, so temperature and enthalpy changes were negligibly small. Its only task to stabilize the exhaust gas velocity to obtain reference data without the influence of pressure waves and cyclic motions. The plenum is connected with exhaust port via adiabatic, 31 mm – diameter and 500 mm – long pipe. The pressure waves within the pipe influence to some extent the exhaust gas discharge, but these phenomena are not analysed here. Dimensions of this pipe were chosen to reduce the unavoidable effects as much as possible. The variations in velocity due to the plenum over one engine cycle do not exceed 3%. Without the plenum, the changes are, not only bigger than 100%, but also a backflow is observed. So, the use of plenum justifies the assumption of a constant velocity flow. A total number of nine thermoelectric assembly units were simulated. Figure 3 presents the overall view of the AVL Boost model. These units are represented by pipe 8 and 10–17 (marked in red in Fig. 3). Restrictors between them are dummy elements with coefficients "1". The formula interpreters calculate wall temperatures for thermoelectric assembly unit (one pipe means one unit, each of the nine units is equivalent of 10 thermoelectric modules). All simulations were made to represent only the steady-state conditions and the calcula-

tions were conducted to achieve the convergence with the spatial resolution of 10 mm.

The heat flux throughout the assembly can be adjusted, within the software, with the heat transfer factor parameter. It is a ratio of real heat transfer coefficient and the value used in calculations. A value equal to one represents conduction in the simple pipe, as shown in Fig. 1. Values greater than 1 represent e.g. internally finned pipe or other changes in geometry which intensify the heat flow. This value was set to keep the maximum temperature at the allowable limit (exceeding 600°C of pipe wall temperature would damage the module). This condition results in heat transfer factor of 1.02. Particular solutions of heat exchangers for thermoelectric modules to provide the best heat exchange can be found in the literature [5, 8].

The calculations were made for a reference point - full throttle, 6000 rpm. The mechanical power of the engine is therefore 24.62 kW. Total enthalpy flow behind the plenum is 27.7 kW (reference zero: 1 atm; 25°C), which corresponds to temperature 1278 K, mass flow 24 g/s and velocity (mean) 69 m/s. Table 1 shows some selected results obtained for the thermoelectric module assembly units. Heat flux means heat recovered in particular assembly unit (heat flux through thermoelectric modules), electric power is generated by thermoelectric modules as described above, and it is the useful effect.

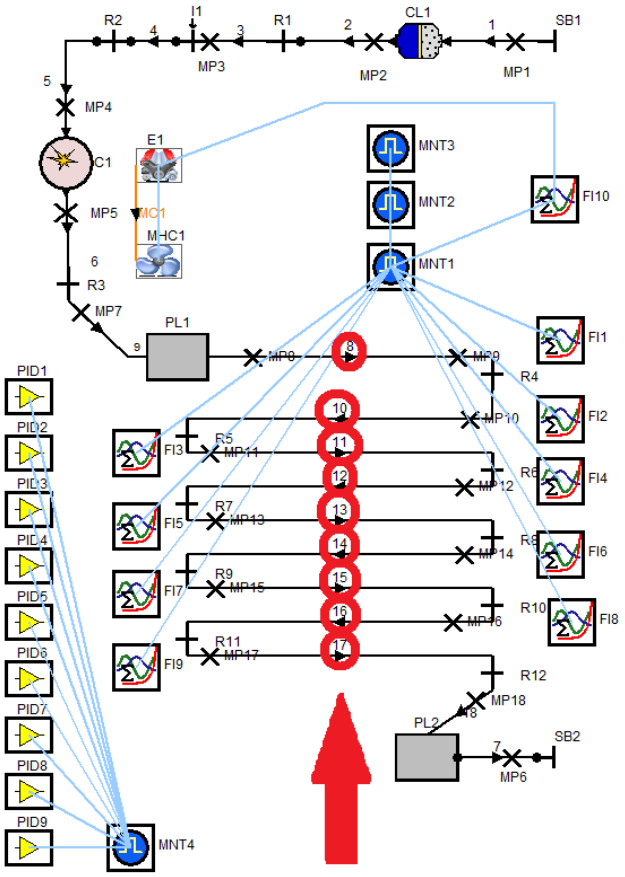

Fig. 4. Overall view of test bench in AVL Boost

It can be seen from Table 1, that efficiency of each next thermoelectric assembly unit decreases. This results from a reduction in the temperature of the exhaust gas which, in consequence, decreases the heat flux and efficiency of the thermoelectric modules due to a drop of temperature gradient.

Table 1. Selected parameters of nine units (heat transfer factor for every unit – 1.02) during operation in full throttle at 6000 rpm

Thermoelectric assembly unit	Inlet gas temp. [K]	Outlet gas temp. [K]	Wall temp. [K]	Heat flux [W]	Electric power [W]
1	1278	1191	873	2748	193
2	1191	1111	820	2483	158
3	1111	1038	771	2242	129
4	1038	972	728	2023	105
5	972	910	688	1823	85
6	910	855	651	1642	69
7	855	804	651	1478	56
8	804	758	589	1330	45
9	758	716	562	1196	37
Sum				16966	877

Table 2. Selected parameters of nine units for variable heat transfer factor during operation in full throttle at 6000 rpm

Thermoelectric assembly unit	Inlet gas temp. [K]	Outlet gas temp. [K]	Wall temp. [K]	Heat flux [W]	Electric power [W]	Heat transfer factor [-]
1	1278	1191	873	2751	194	1.02
2	1191	1102	873	2751	194	1.38
3	1102	1013	873	2751	194	2.10
4	1013	921	873	2751	194	4.49
5	921	836	827	2520	163	10
6	836	761	754	2154	119	10
7	761	697	754	1836	101	10
8	697	641	635	1561	62	10
9	641	593	588	1325	45	10
Sum				20400	1265	

In the next step, a PID regulator has been involved in the system and tuned to set the heat transfer factor for every thermoelectric module assembly independently. Obtained data are presented in Table 2.

As it can be noticed from Table 2, the total recovered energy in the form of electric power is about 1.27 kW. To provide the same heat flux, and in consequence, the same temperature of the module, greater heat transfer factors are required. This is because of the drop in enthalpy of the exhaust stream. Here, the heat transfer factor was arbitrarily limited to 10.

In the next stage, the plenum has been modified. Its volume changed from 500 l to 5 l. The variation of velocity during one engine cycle is now significant. Values of instantaneous velocity behind the plenum are in this case between 110 m/s forward and 10 m/s reverse. For this situation, similar analyses were made as described previously and presented in Table 2. The mean inlet and outlet gas temperatures are the same as before. For the first four thermoelectric module assemblies, the wall temperatures also must be the same because it is a criterion to tune the heat transfer coefficient and it is equal to the maximum allowable thermoelectric module temperature.

Table 3. Optimal heat transfer coefficient for each first four subsequent thermoelectric module assembly

Thermoelectric assembly unit	1	2	3	4
Heat Transfer Coefficient	1.06	1.44	2.26	5.34

Because of the amount of energy and reasonably small heat transfer factor, further considerations are limited to four thermoelectric module assemblies. The heat transfer factors are also similar. Table 3 presents the heat transfer coefficients for the 5 l plenum.

4. Experimental setup in different working conditions

For further considerations, the system consisting of four thermoelectric module assemblies (each assembly consists of 10 modules) were taken into account. Each of them has different heat transfer factor coefficient presented in Table 3, which is optimum for the reference point (6000 rpm, full throttle). The proposed system was analysed at different working conditions.

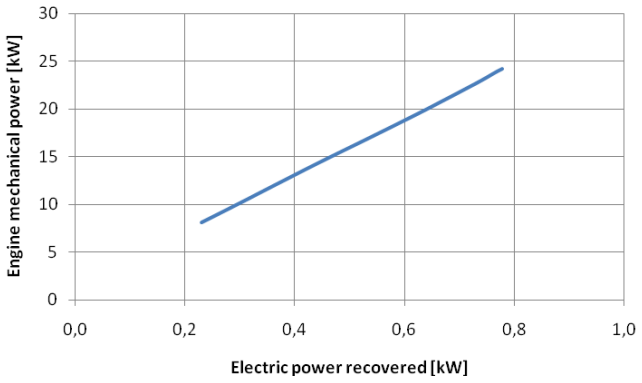

Fig. 5. Recovered power for 6000 rpm

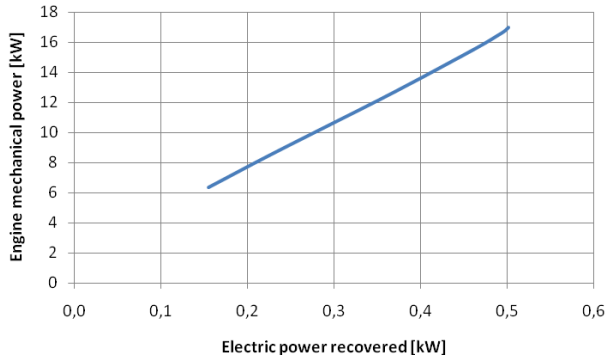

Fig. 6. Recovered power for 4000 rpm

Two rotational speeds of 6000 rpm and 4000 rpm were considered, with different throttle position, from 5% (flow coefficient restriction 0.05 in the intake manifold) to 100% (flow coeff. 0.98). Diagrams in Fig. 5 and Fig. 6 show the total amount of harvested electric energy in the four thermoelectric module assembly (40 thermoelectric modules in total).

5. Results discussion

The results of the proposed configuration have been presented above. In the first configuration, when nine thermoelectric module assemblies are identical, the recovered electric power was 877 W. It is about 3.5% of the engine mechanical output power. After modification of the thermoelectric module assembly assuming individual tuning of geometry (heat transfer factor) for every unit, the efficiency of more than 5% was achieved. But for units number 5 to 9 a high heat transfer factor is necessary. This value has been limited to 10 in this paper due to practical reasons. The highest possible amount of produced electric energy is achievable only in the first four units. The efficiency of the thermoelectric module becomes lower as the temperature of the heat source decreases. The influence of cyclic motion and pressure wave is relatively small in this case. It is hard to predict how this phenomenon influences the whole system. On one hand, the forward and reverse cyclic motion intensify the heat transfer factor, but on the other, some portion of the hot gases can be rapidly pushed through the heat exchanger. Some description and analysis of this phenomena can be found in [13]. The behaviour of the proposed system is nearly linear with decreasing load of the engine for both investigated rotational speeds.

6. Conclusion

Results obtained in the investigation can be useful for further analysis concerning the geometry of heat exchanger, economic profitability of waste heat recovery systems. It can also be helpful in rough estimation of the number of thermoelectric assemblies or simple modules. The geometry was assumed arbitrary. In the real arrangement, this can vary significantly and influence heat transfer phenomena due to cyclic pulsation in the exhaust system. It can enhance or lower the effective heat flux. The length of the heat exchanger can also have a different influence depending on the engine rotational speed and a ratio between gas pulse length and heat exchanger length. Some ways of enhancing the heat flux are the elongation of the heat exchanger, internal fins, turbulisers, etc. It has to be a subject of further investigation which one is more profitable. The acoustic phenomena have not been taken into account in this case and further investigation dealing with sound level and exhaust after treatment (3 W cat, DPF) should be also performed. The amount of energy possible to recover is not very large, Although it should be notified, that this is the electric energy – with high exergy level. In conventional solutions, the alternator is used to produce electricity and its efficiency, the amount of consumed mechanical power have to be also considered. In the pro-posed configuration, the power of alternator changes, it can possibly be switched off or working like an engine. The transient phenomena and heating period have to be also the subject of further investigation. Reasonability of using the thermoelectric solution strongly depends on the development of thermoelectric cells, materials and their cost.

Acknowledgements

This work was supported by the National Science Centre grant no. 2016/23/B/ST8/03133.

Bibliography

[1] BUCHALIK, R., NOWAK, I., ROGOZINSKI, K., NOWAK, G. Detailed model of a thermoelectric generator performance. *Proceedings of the 5th International Conference: Contemporary Problems of Thermal Engineering.* Gliwice, 18-21 September 2018.

[2] HENDRICKS, T. J. Thermal system interactions in optimizing advanced thermoelectric energy recovery systems. *Journal of Energy Resources Technology*. 2007, **129**. DOI: 10.1115/1.2751504

[3] IZIDORO, C.L., ANDO JUNIOR, O. H., CARMO, J.P., SCHAEFFER, L. Characterization of thermoelectric generator for energy harvesting. *Measurement*. 2017, 106, 283-290. DOI: 10.1016/j.measurement.2016.01.010

[4] KARVONEN, M., KAPOOR, R., UUSITALO, A., OJANEN, V. Technology competition in the internal combustion engine waste heat recovery: a patent landscape analysis. *Journal of Cleaner Production*. 2016, **112**, 3735-3743.

[5] KUMAR, S., HEISTER, S.D., XU, X. et al. Thermoelectric generators for automotive waste heat recovery systems part i: numerical modeling and baseline model analysis. *Journal of Electronic Materials*. 2013, **42**(4), 665-674.

[6] LIENHARD, J.H.IV., LIENHARD, J.H.V., A Heat Transfer Textbook. *Phlogiston Press*. Cambridge Massachusetts, 2017.

[7] LIU, X., DENG, Y.D., LI, Z., SU, C.Q. Performance analysis of a waste heat recovery thermoelectric generation system for automotive application. *Energy Conversion and Management*. 2015, 90, 121-127.

[8] LIU, X., DENG, Y.D., ZHANG, K. et al. Experiments and simulations on heat exchangers in thermoelectric generator for automotive application. *Applied Thermal Engineering*. 2014, **71**, 364-370.

[9] NOLAS, G.S., SHARP, J., GOLDSMID, H.J. Thermoelectrics; Basic Principles and New Materials. *Springer-Verlag*. Berlin-Heidelberg-New York 2001.

[10] RYCHTER, T., TEODORCZYK, A. Teoria silników tłokowych. *WKL*. Warszawa 2006.

[11] SCHOCK, H. et al. Prospects for implementation of thermoelectric generators as waste heat recovery systems in class 8 truck applications. *Journal of Energy Resources Technology*. 2013, **135**. DOI: 10.1115/1.4023097

[12] Tecteg TEG1-PB12690 Thermoelectric module datasheet: tecteg.com/wp-content/uploads/2017/04/TEG1-PB12690-Spec-sheet.pdf

[13] WENDLAND, D. Automobile exhaust-system steady-state heat transfer. *SAE 1993 Transactions: Journal of Materials & Manufacturing-V102-5*.

[14] ZHU, G., LIU, J., FU, J., WANG, S.A. Combined organic Rankine cycle with double modes used for internal combustion engine waste heat recovery. *Journal of Engineering for Gas Turbines and Power*. 2017, 139. DOI: 10.1115/1.4036955

Ryszard Buchalik, MEng. – Institute of Power Engineering and Turbomachinery, Silesian University of Technology.
e-mail: *ryszard.buchalik@polsl.pl*

Krzysztof Rogozinski, MEng. – Institute of Power Engineering and Turbomachinery, Silesian University of Technology.
e-mail: *krzysztof.rogozinski@polsl.pl*

Prof. Grzegorz Nowak, DEng., DSc. – Institute of Power Engineering and Turbomachinery, Silesian University of Technology.
e-mail: *grzegorz.nowak@polsl.pl*

Modelling the internal combustion engine waste heat recovery using thermoelectric modules

Ryszard Buchalik, Grzegorz Nowak, Krzysztof Rogozinski

Department of Power Engineering and Turbomachinery; Silesian University of Technology, Gliwice, Poland, ryszard.buchalik@polsl.pl (CA); grzegorz.nowak@polsl.pl; krzysztof.rogozinski@polsl.pl

Abstract:

This paper presents an analysis of the use of a thermoelectric energy recovering device in commercial vehicles equipped with a combustion engine. The efficiency of thermal engines is limited, especially in mobile solutions. A significant amount of heat is emitted to the environment at various temperature levels (cooling system and exhaust). An attempt was made to analyse the rationality and profitability of the implementation of thermoelectric modules in the internal combustion engine system, especially in the exhaust. A numerical model was created and implemented in a professional software. The vehicle itself was also modelled, which enables simulation of various driving conditions, cycles and vehicle specifications, both steady- and transient-state. An improvement can be observed in the overall efficiency of the vehicle due to the energy recovering system. Focus on the overall profitability was made. Profiles of velocity and temperature in the exhaust pipe were shown and analysed in terms of the heat exchange process. The heat capacity of the energy recovering system and its influence on the system performance were analysed.

Keywords:

thermoelectricity, combustion engine, energy recovering, driving simulation

Introduction

An analysis of the number of vehicles now operated worldwide points to a number of 1.1 billion, with a continuous upward trend. It is estimated that the number will increase by another several hundred thousand cars in the next years, especially in developing countries. Internal combustion engines, which are now the main source of drive for most of them, are globally responsible for huge emissions of carbon dioxide and other harmful pollutants into the atmosphere. Ongoing intensification of efforts can be observed in recent years aiming to mitigate the harmful environmental impact by stricter standards set out in relevant legal regulations and imposed on new cars launched into the market. The efficiency of internal combustion engines used in vehicles totals 30-40% at best [1]. In standard operating conditions it is usually a few times lower. The biggest energy loss is related to the high temperature of large amounts of exhaust gases emitted to the environment. Many works are now being carried out on the recovery of what is considered to be waste energy in conventional solutions. This paper deals with the issue of energy recovering in a vehicle equipped with an internal combustion engine. Some investigations [2-4] considering the use of the exhaust gas enthalpy have been made and can be found in literature. One of the most promising methods is the application of thermoelectric modules (TEMs) due to their advantages – they are a simple, low-cost solution which is maintenance-free, has no moving elements and enables direct production of electric power [5]. A thermoelectric module works on the basis of a temperature difference, and the heat flux passing through it is partially converted into electricity.

The main thermoelectric phenomenon is the Seebeck effect. It consists in generating an electromotive force in a conductor composed of two different materials (with different Seebeck coefficients), when their joints are kept at different temperatures. Second related phenomenon is the Peltier effect. It consists in absorbing heat at one junction and expelling it on the other. Magnitude of this heat is proportional to the electric current in the cell circuit and the temperature of the respective junction. There are current values for which maximum power or efficiency in heat energy to electricity conversion is achieved.

In this case, the hot side is heated with the exhaust gas, whereas the other has to be cooled. A system based on this phenomenon can also be easily retrofitted by replacing a part of a generic exhaust system. A lot of investigations have been made considering, for example, the system efficiency [6,7], the geometry of heat exchangers [8-10], the strategy of the exhaust gas stream control [11] and the configuration of heat exchangers

[12]. This paper describes the idea of using specialized AVL BOOST software to create a useful, comprehensive model to simulate the influence, behaviour and profitability of the exhaust energy recovering system made of thermoelectric modules. The software enables one-dimensional calculations of the exhaust gas dynamics and of the related processes occurring in internal combustion engines.

Modelling and system approach

The main idea of this paper is to provide a simulation tool for an assessment of the thermoelectric energy recovering module installed in a car exhaust system. The input data taken for the calculations represent a typical C-segment car with a four-cylinder 1.5L gasoline engine. The model consists of pipes, junctions, a pressure restrictor (also acting as a throttle), plenums at the gas stream inlet and outlet and an air filter. No additional elements are introduced at this stage – like forced charging, a turbine, pollution after-treatment, etc. Gases are modelled as real ones with the most important parameters taken as a function of temperature, pressure, and chemical composition. The general layout of the model of the investigated system presented in the software GUI is shown in Fig. 1. To simplify the simulation process, constant volume combustion is assumed to occur at the top dead centre. The air-to-fuel ratio is fixed at 0.85 compared to the stoichiometric ratio.

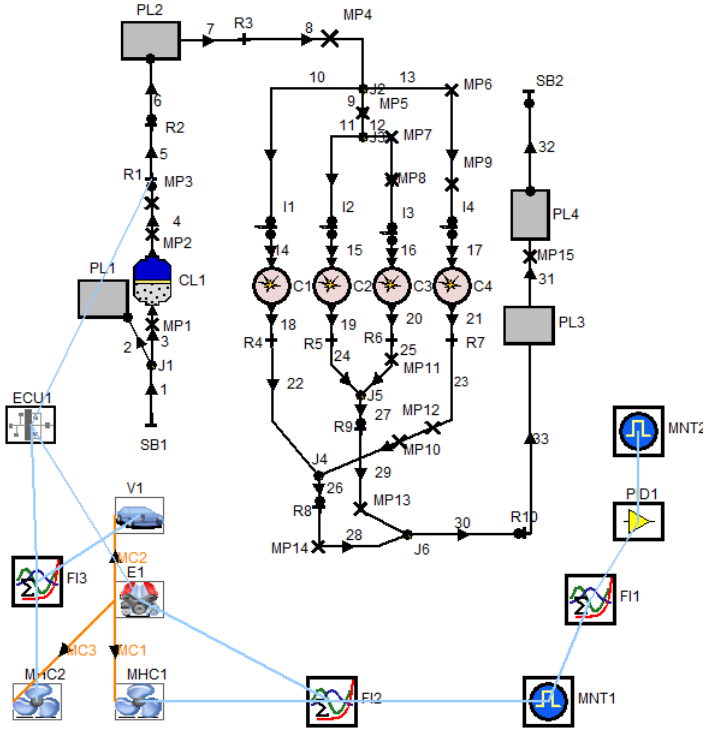

Fig. 1. General view of the model layout in AVL Boost

The resulting maximum mechanical brake power and torque of the engine in the selected range are presented in Fig. 2. The exhaust system is assumed to be thermally insulated from the surroundings all the way down from the cylinder outlet valve to the thermoelectric heat exchanger.

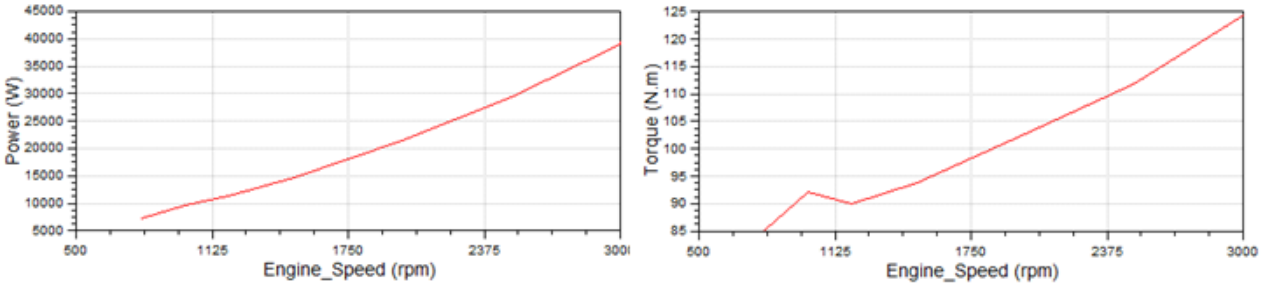

Fig. 2. Power and torque of the engine under investigation

Fig. 3 presents the mean velocity and temperature (averaging in time domain for the entire cycle) downstream the exhaust manifold for a fully open throttle corresponding to the data presented in Fig. 2.

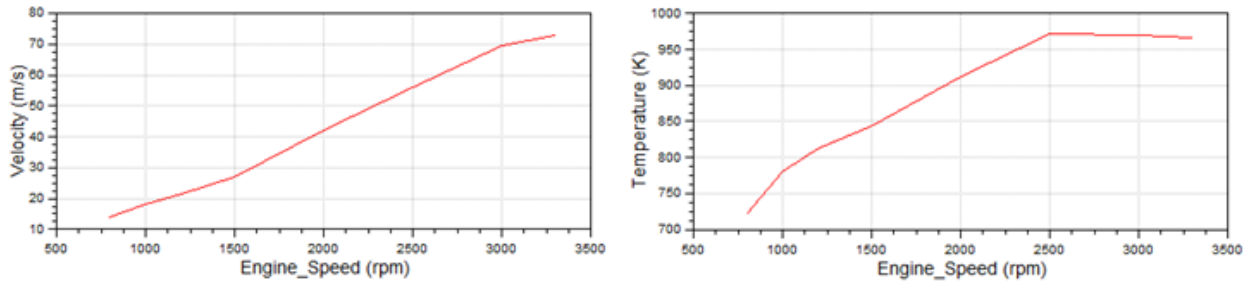

Fig. 3. Mean velocity and mean temperature

The analysed model of the recovery system consists of a hot heat exchanger (copper filling), thermoelectric modules and a cold heat exchanger in the form of a water cooling module. The heat capacity of the hot heat exchanger is taken into account. The harvesting system is schematically shown in Fig. 4. The heat exchanger is modelled as a pipe in the model layout of the engine. The solver included in the program uses the Reynolds analogy [13] to determine the heat transfer based on the distribution of the fluid flow parameters, such as temperature, velocity, pressure, mass fraction, etc. in each time step and each point along the pipe. A procedure in the C language was developed to calculate the operating parameters in the hot heat exchanger. The determined value of the instant heat transferred from the gas into the TEM system is processed to determine the temperature gradient (versus time) in the heat exchanger and the TEM generated power and efficiency. The TEM power and efficiency depend only on the hot heat exchanger temperature. The change in the temperature (in time) comes from the difference between the heat flowing through the TEM and the heat from the exhaust gas divided by the heat capacity. The initial length of the pipe is 500 mm and its diameter is 44 mm. The heat exchanger between the hot side of the thermoelectric cell and the exhaust gas has the same temperature throughout its volume. It is also assumed in this paper, that the resistance to heat conduction inside the exchanger is negligible comparing to the other heat-conducting components of the system.

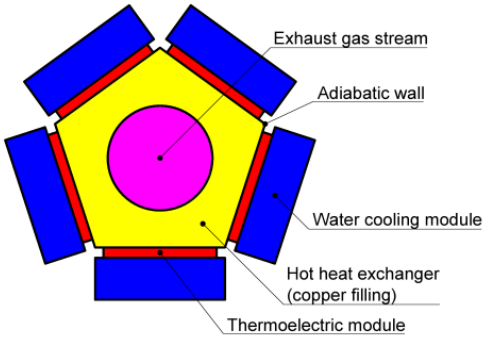

Fig. 4. Schematic diagram of the thermoelectric energy recovering system

Numerical simulations

The aim of the numerical simulations using the model presented in Fig. 1 was to assess the possibility of utilizing exhaust gas enthalpy by means of an energy-recovery system based on a system of thermoelectric modules. The calculations were performed first for the steady state and then for the transient-state conditions of the engine operation.

Steady-state conditions

The presented thermoelectric module is modelled based on the data of commercially available TEMs. For the calculations presented further below, a module is assumed with the hot side maximum temperature of 650°C, total thermal resistance of 2 K/W, efficiency of 7.5% at the 600K temperature difference (changing linearly with temperature) and the cold side constant temperature of 50°C. It is also assumed that the system consists of ten thermoelectric modules thermally connected in parallel. This results in 0.2 K/W total thermal resistance. The heat transfer coefficient inside the heat exchanger is set to 7.51, which can represent ribs inside the tube.

This specific value was set to make it possible to achieve maximum parameters of the thermoelectric modules (based on the maximum temperature) at 3300 rpm of the engine at full throttle at steady-state conditions. For this configuration, the engine working conditions corresponding to a higher heat transfer would result in damage to the thermoelectric system. In such a case, allowing higher rotational speed than 3300, a bypass system would be required to avoid damage of the system.

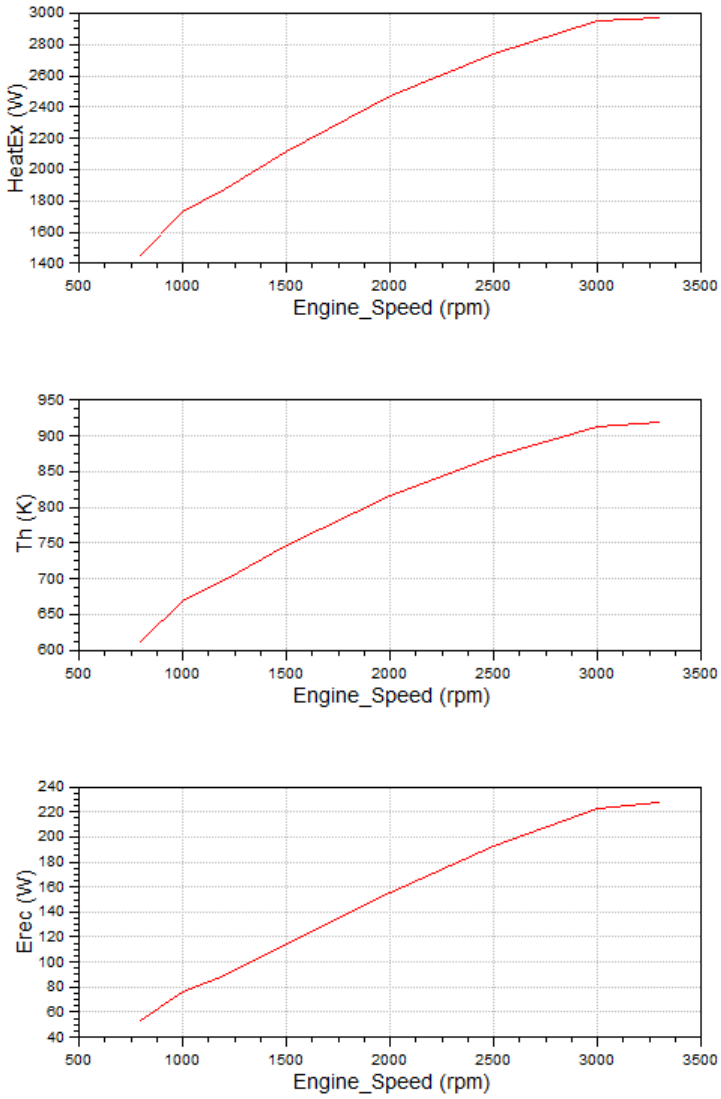

Fig. 5. Energy recovering parameters of the system of thermoelectric modules; heat flow through the system (HeatEx), heat exchanger temperature (Th) and electricity produced (Erec) in steady-state conditions

There are 10 modules placed on one heat exchanger which, as mentioned above, has uniform temperature throughout the entire volume. Consequently, all simulated thermoelectric modules have the same hot end temperature at all times, and therefore identical operating conditions. The heat entering the exchanger from the flue gas depends on the gas duct geometry, its position, length and diameter.

Fig. 5. presents the steady-state operating parameters for the simulated thermoelectric energy recovering system. *HeatEx* denotes heat conducted through the thermoelectric energy recovery system, Th is the TEM hot side temperature (simultaneously the gas duct inner surface temperature), *Erec* stands for useful electric energy extracted by the recovery system.

It can be seen that an increase in the engine rotational speed is accompanied by a rise in the mean values of the exhaust gas both velocity and temperature (averaged in time domain). Each of these two phenomena analysed independently causes an increase in the heat transfer being the effect of forced convection. Consequently, the relative increase in the heat transfer due to both these processes is more intense than the proportional increase in either of the two quantities analysed independently. The *HeatEx* and the Th curve

have an identical shape, which is due to the adopted way of modelling the thermoelectric module – where the TEM constant thermal conductivity and constant temperature of the cold end are assumed. The effective amount of the generated electrical energy (*Erec*) depends on the TEM efficiency and the recovered waste heat flux, so it is steeper.

All the above mentioned diagrams refer to the full throttle operation and steady-state conditions. During normal driving conditions a more important issue is how to estimate the mentioned parameters for a partial load. To represent it, three points corresponding to the engine speeds of 1000 rpm, 2500 rpm and 3300 rpm are chosen. Fig. 6 presents a drop in the mean temperature (averaged over time for entire engine cycle) and in the mean velocity in those points at the exhaust manifold outlet as a function of engine throttling – the results are shown with respect to the brake power. The right ends of the curves represent maximum power at respective rotational speeds, and the left side is the condition corresponding to a nearly closed throttle (pressure factor = 0.01, which explains power below zero at some states).

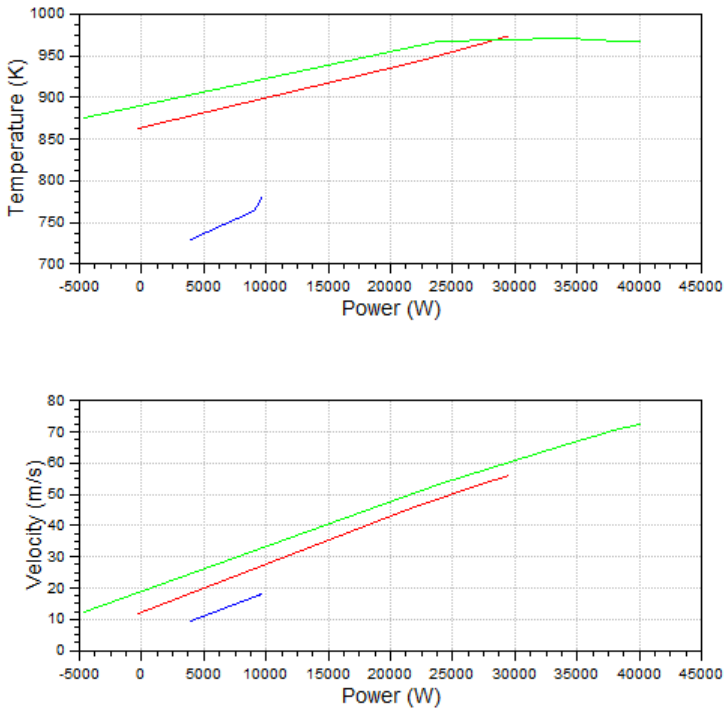

Fig. 6. Variation in the mean temperature (time average) and velocity under a partial load; blue – 1000 rpm, red 2500 rpm, green – 3300 rpm

For a set value of the engine rotational speed, both temperature and velocity vary monotonically with an increase in power. Obviously, the load-dependent variation is stronger for higher rpm values due to the wider range of power available for those rotational speeds. Velocity behaves in a linear manner because it is directly related to the mass flow through the system, which in turn is related to the amount of supplied fuel, and thus indirectly – to power. The simulations show that the dynamics of the temperature variation is the highest for the lowest of the analysed rotational speeds, i.e. 1000 rpm.

An important issue is the heat transfer in the exhaust system for the pulsations and repetitive movements coming from the exhaust valves. Fig. 7 presents the velocity profile during one cycle of the engine (two rotations) at the exhaust manifold outlet. The momentary values of both velocity and pressure differ significantly from the mean value during a single cycle of the engine operation. This is due to the strong unsteadiness of the phenomenon of the cylinder emptying and the related thermodynamic and gasodynamic phenomena. They come from the cyclic opening of the exhaust valve. The relative velocity fluctuations are much bigger compared to the relative fluctuations in temperature, which level off naturally due to thermal diffusion, gas mixing and the possible bidirectional exchange of heat with the collector elements. The green line represents zero brake power, so there is very little power generated by the combustion pressure in the cylinder. This results in the near sinusoidal shape of the curve due to cyclic emptying of the cylinder. As a result, a pressure wave is created and there is a periodic movement of gas in the exhaust duct. As for the other two curves, there is a clear deviation from a sinusoidal waveform due to the rapid expansion of hot gas immediately after the valve opening and formation of a shockwave.

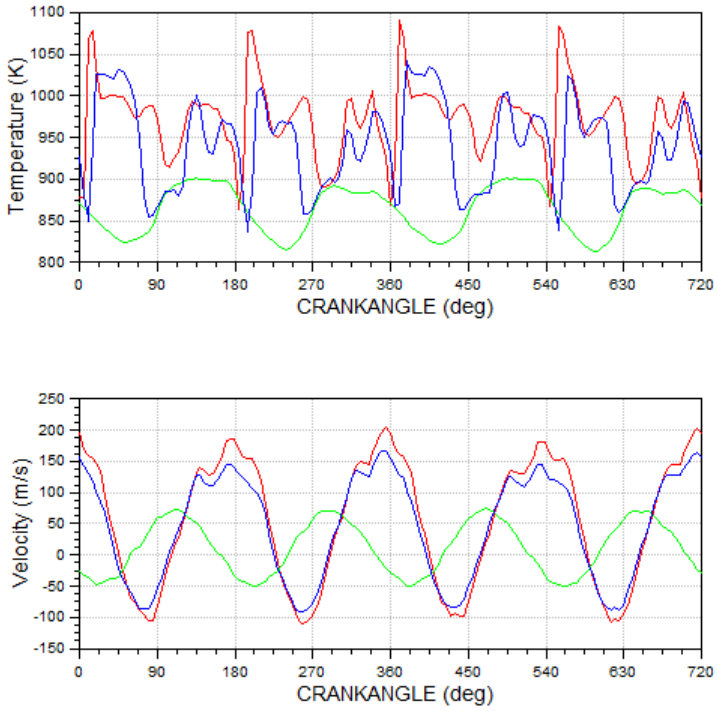

Fig. 7. Variation in temperature and velocity at 2500 rpm for different throttling; red – full power, blue – about 20 kW, green – zero brake power

Based on the above considerations a thesis can be proposed that by altering the position and dimensions of the heat exchanger, it is possible to significantly influence the heat transfer process and its characteristics. The rotational speed of 2500 rpm was chosen for the following analysis. The calculations shown above take into account a 50 mm-long pipe between the exhaust manifold (last junction connecting together all exhaust pipes from every cylinder) and the thermoelectric harvesting system (further on referred to as the connecting pipe). Four values of the thermoelectric heat exchanger length are considered – 200, 300, 400 and 500 mm. Several lengths of the connecting pipe are taken into consideration, starting from 50 mm up to 2300 mm. Fig. 8 shows the dependence of the recovered heat, i.e. the heat collected by the heat exchanger, on the exchanger length for three selected lengths of the connecting pipe (50, 1150 and 1600 mm). Due to the drop in the jet temperature, the amount of heat extracted from the exhaust gas along the exchanger decreases.

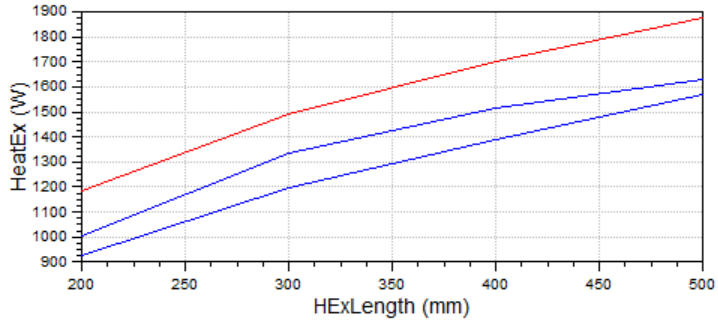

Fig. 8. Heat flowing through the thermoelectric system for 3 different connecting pipe lengths at 2500 rpm (from top to bottom – 50 mm, 1150 mm, 1600 mm) as a function of the heat exchanger length

To better illustrate the phenomenon, Fig. 9 presents the heat transferred through the 300 mm long heat exchanger as a function of the connecting pipe length. A periodical upswing in the heat value can be observed with local maxima at about 500 mm and 1600 mm. The local minimum is observed for an exchanger with the length of about 1200 mm.

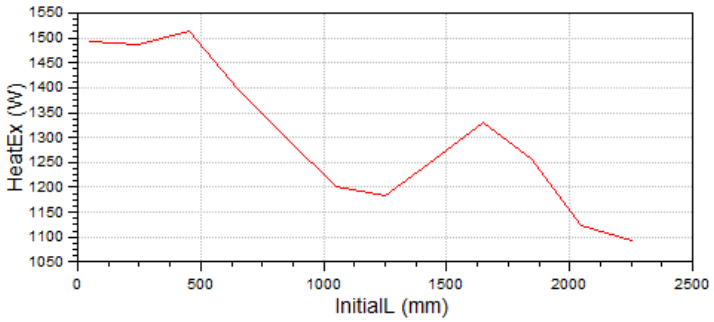

Fig. 9. Heat flowing through the thermoelectric system for different connecting pipe lengths at 2500 rpm for the 300 mm-long heat exchanger

The pulsating nature of the flow and the gas outflow through the valve from the cylinder cause a non-homogenous distribution of velocities and temperatures. They are averaged and slightly damped after manifold, but still present. As a result of pulsations, for some lengths of the connecting pipe and the heat exchanger a portion of hot gas is present in the heat exchanger longer than for other lengths – the hottest portion can either "fly through" the exchanger or reverse velocity (stays longer) while in the exchanger. The latter effect results in temperature averaging (alignment) associated with the turbulent flow. Therefore, despite the fact that the pipe is thermally insulated from the environment, an increase in its length causes temperature alignment and a lower temperature of the heat exchanger. For some combinations of the connecting pipe and the exchanger lengths, the average temperature of the heat exchanger is higher than for some configurations with longer exchanger. It can result in higher heat flow, despite smaller heat transfer area between heat exchanger and exhaust gas. This is a source of paradox, it is related to the pulsating nature of velocities and pressures and their relative phase shift, which is different at each point in the system. For this reason, less heat is transferred due to convection. The same phenomenon is probably responsible for the nonlinear increase in the heat flow if the heat exchanger is lengthened. The described phenomena can be vividly seen if animations of temperature, pressure and velocity are created. The pulsations seem to have a much stronger effect on the convective heat transfer than the mean velocity (time averaging).

Transient conditions

The above simulations enable a deeper understanding of the proposed system and its characteristics, but the most important problem is the simulation of the profitability of such a system in real driving conditions. A model taking account of transient phenomena is developed, with a special focus on the heat capacity of the investigated energy recovering system. The driver model changes gears at fixed rotational speeds of the engine – 1200 and 3300 rpm, and the process takes 0.8 s. The thermoelectric harvesting system is tuned to achieve the maximum allowable power at full throttle and 3300 rpm, as described above. The vehicle minimum speed is limited to 1.8 m/s (idle in first gear). The most important parameter in transient conditions is the heat capacity of the hot heat exchanger collecting heat from the exhaust gas and transferring it to the TEM. The assumed cycle takes 200 s and consists of idle standstill (5 s) at the beginning, rapid acceleration up to 120 km/h, mild braking (regenerative) and finally idle standstill again (150 s). The velocity profile is presented in Fig. 10 and the corresponding engine parameters – rotational speed and the load factor – are shown in Fig. 11.

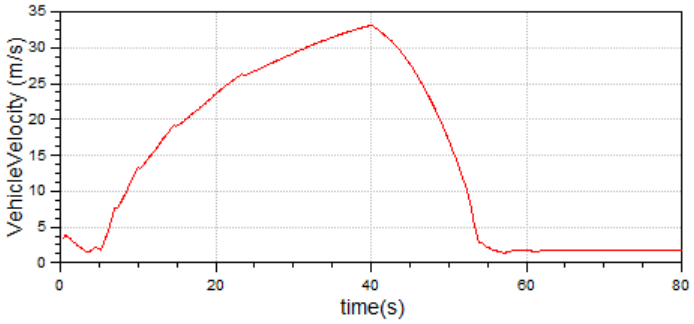

Fig. 10. Velocity profile of the vehicle for the investigated driving cycle

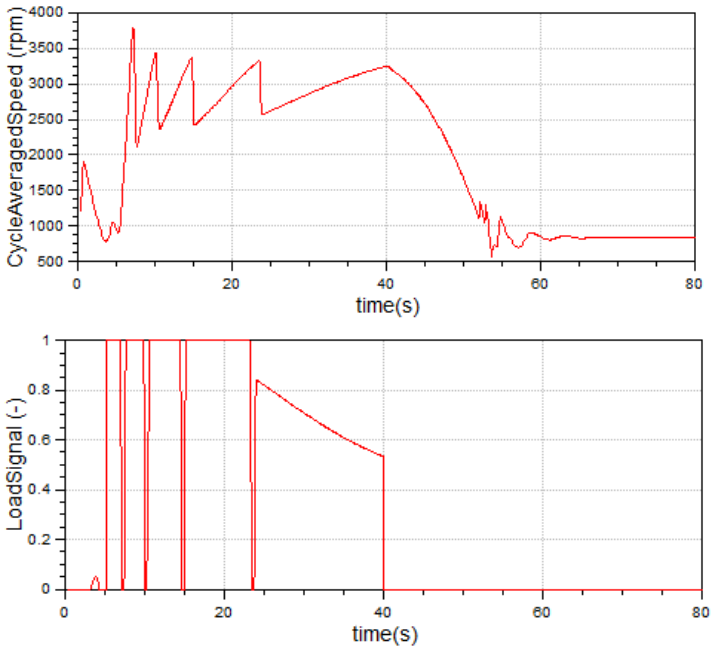

Fig. 11. Rotational speed and the load signal of the engine for the investigated driving cycle

The crucial parameters for the recovery of energy in the driving cycle in question are investigated for different heat capacity values of the heat exchanger – 76, 90, 380, 760, 1520 J/K.

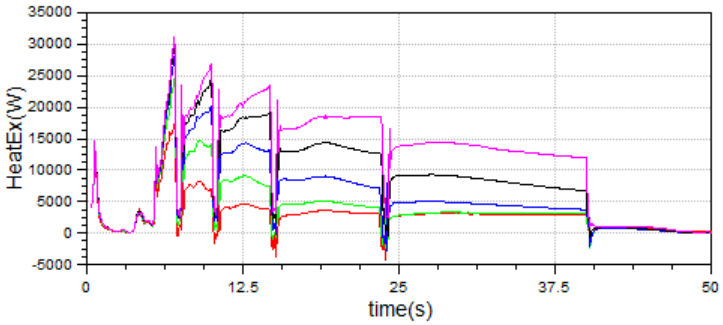

Fig. 12. Heat flow from gas to the heat exchanger for different heat capacity values; red – 76 J/K, green – 190 J/K, blue – 380 J/K, black – 760 J//K, pink – 1520 J/K in the "drive" part of the cycle

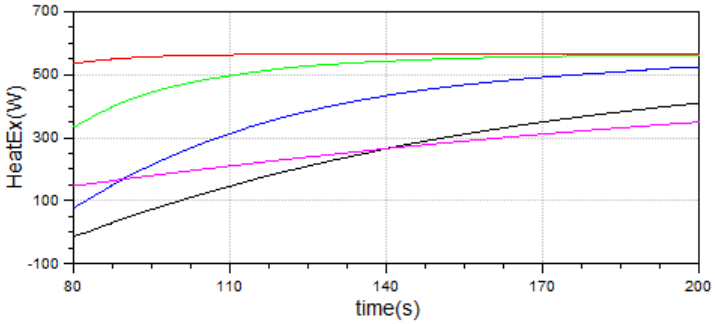

Fig. 13. Heat flow from gas to the heat exchanger for different heat capacity values () during the "standstill" part of the cycle

Fig. 12 illustrates distinct changes in the heat flux transferred by the exhaust gas during acceleration and gear changing. This is related to the significant differences in the exhaust gas temperature and mass flow. The higher the heat capacity of the heat exchanger, the more heat it absorbs at initial stages. Higher heat capacity means greater possibilities of heat accumulation in periods of intensive supplies of heat. It can be also observed, that during short periods of time during the gear change, the heat exchanger releases heat back to the exhaust gas. It is related to changes in a wide range of temperature and exhaust gas velocity along with changes in

engine operating parameters. During gear shifting the engine brake power is suddenly reduced to nearly zero. Fig. 13 presents the same process, but for idling. In this situation, at low heat capacity the system reaches thermodynamic equilibrium almost immediately. But the higher the heat capacity, the longer the process.

Fig. 14 presents the resulting temperature of the heat exchanger versus time in the "driving" part of the described cycle. It can be seen that the smaller the heat capacity of the heat exchanger, the faster the temperature changes in it, which is obvious. The heat exchanger temperature level will, in turn, influence the amount of heat recovered by the heat recovery system, as shown in Fig. 15.

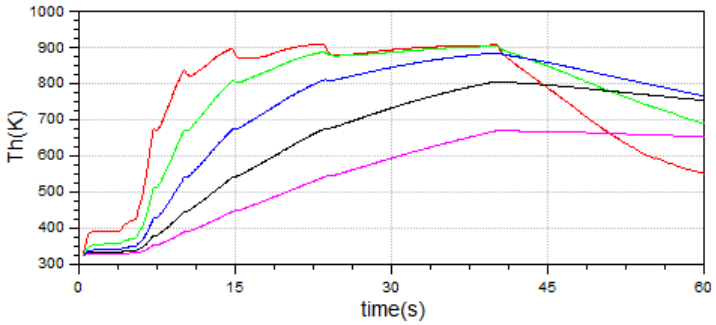

Fig. 14. Temperature of the heat exchanger for different heat capacity values; red – 76 J, green – 190 J/K, blue – 380 J/K, black – 760 J//K, pink – 1520 J/K

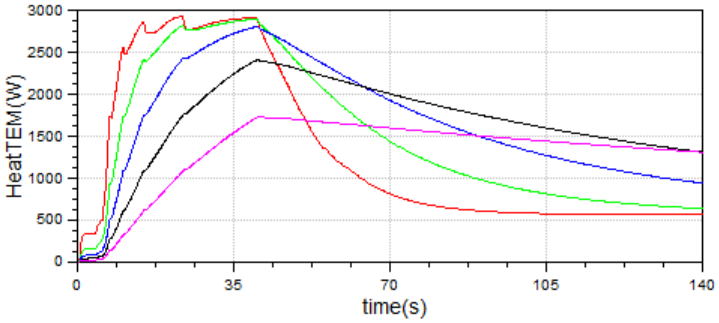

Fig. 15. Heat flow through the TEM for different heat capacity values; red – 76 J, green – 190 J/K, blue – 380 J/K, black – 760 J//K, pink – 1520 J/K

Because a constant temperature of the cold side of the TEM was assumed, the heat flux through the module is proportional to the temperature of the hot side of the heat exchanger. It can be seen that a rapid increase in temperature involves an equally fast rise in the amount of heat. Such a system with low heat capacity is characterized by high dynamics of variability, which will directly affect the dynamics of the TEM performance presented in Fig. 16 illustrating the electric power generated by the TEM.

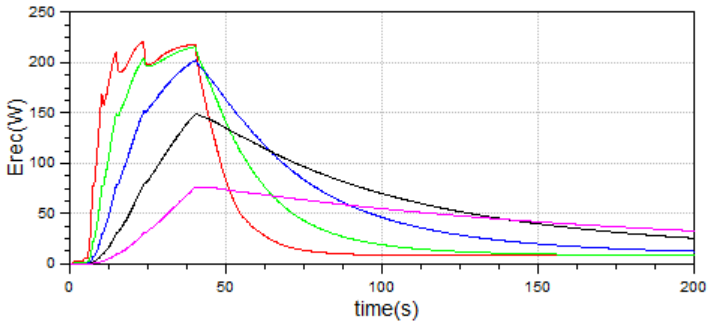

Fig. 16. Electric power generated by the TEM for different heat capacity values; red – 76 J, green – 190 J/K, blue – 380 J/K, black – 760 J//K, pink – 1520 J/K

The presented results show that low heat capacity of the recovery system can be disadvantageous due to the rapid rise in the heat exchanger temperature, which can reach levels exceeding the maximum operating temperature of the TEM. Such a situation would necessitate a partial bypass of the exhaust. On the other hand, high heat capacity limits the fast rate of the temperature rise and ensures considerable accumulation of heat

inside the heat exchanger. However, this may also result in the exchanger cooling down. This heat can be fully utilized to supply the TEM in a later phase of the cycle. However, in such a case the energy conversion may occur in lower temperature which generally results in lower TEM efficiency and consequently reduced level of recovery. The data presented in Fig. 17 are the effect of the electric power integration in time, so they represent the total amount of electricity produced from the beginning of the cycle.

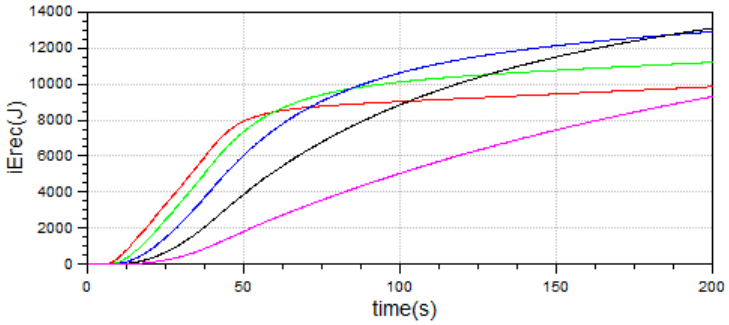

Fig. 17. Electric energy recovered by the TEM for different heat capacity values; red – 76 J, green – 190 J/K, blue – 380 J/K, black – 760 J//K, pink – 1520 J/K

Analysing Fig. 17, it can be concluded that the total output of the system depends on the time frame under analysis. For the smallest analysed heat capacity, the highest amount of generated energy is obtained if the analysis covers the initial time of movement. The case with the heat capacity of 380 J/K results in the largest amount of recovered energy in the interval from about 90 to 180 seconds. This is already the period of the engine idle operation, after the acceleration and the deceleration manoeuvres. However, there is no significant reason why the system using a thermoelectric module could not continue operation for some time even after the engine is shut down, using the accumulated heat to charge the battery or supply electric power to comfort equipment (ventilation, audio, infotainment, etc.) in the vehicle.

Real drive test

In the next step of the considerations, the velocity profile to be followed by the car is assumed. It is based on some parts of the WLTP cycle. The total covered distance is approx. 12.9 km. The calculation is performed for one selected heat capacity value: 76 J/K.

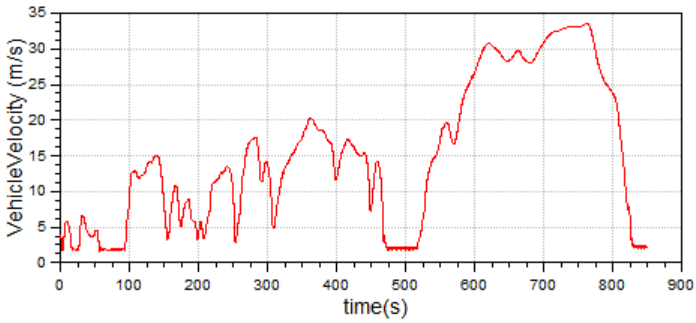

Fig. 18. Velocity profile of a simulated real driving cycle

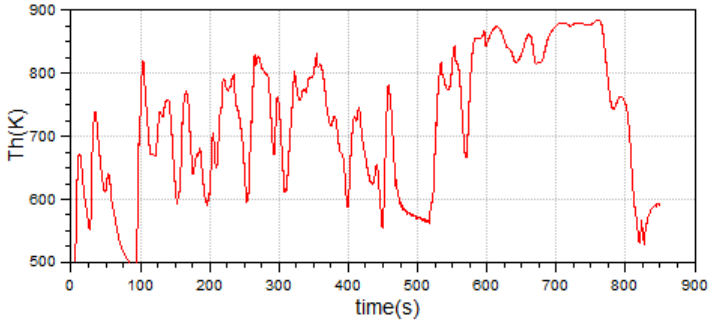

Fig. 19. Heat exchanger temperature profile of a simulated real driving cycle

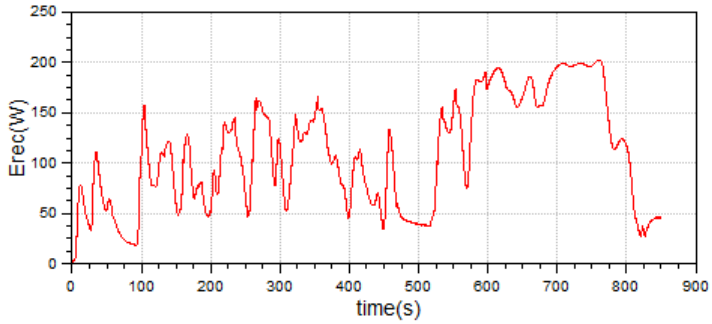

Fig. 20. Electric power harvested in a simulated real driving cycle

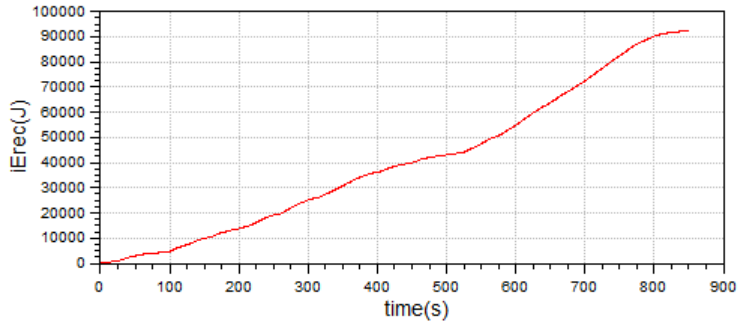

Fig. 21. Electricity produced in a simulated real driving cycle

The presented results show how energy recovery proceeds for a cycle reflecting a real driving cycle of a vehicle. It can be seen that recovered power varies over a wide range, from about 20 W to about 200 W, depending on the engine momentary demand for power. During the entire driving cycle of about 15 minutes, less than 100 kJ of electrical energy was recovered. This gives energy equivalent to that contained in about 10 grams of petrol, assuming that the efficiency of energy extraction from petrol is at the level of 30%. During the presented driving cycle, the vehicle consumed about 1.2 litres of fuel, which means average consumption of 9.3 l/100 km. Based on Fig. 20 and Fig. 21, i.e. real driving cycle simulation, it can be stated that the system works much more efficiently for higher loads associated with a faster travelling speed.

Conclusions

This paper presents an analysis of the external performance characteristic of the internal combustion engine system in the most significant range of speeds from the point of view of practical operation. The exhaust gas mean values of temperature and velocity in the exhaust manifold change approximately in proportion to the engine rotational speed. As the rpm value gets higher, the velocity of the medium increases, and so does the convective heat transfer in the exhaust system. The periodicity of combustion in the engine cylinders additionally involves formation of pressure waves, and the unsteadiness of the exhaust gas outflow leads to considerable unsteadiness in the flow through the exhaust system. Pulsations seem to have a much greater effect on convection than the mean velocity of the exhaust gas flow. This results in an intensive heat exchange in the applied energy recovery system based on the TEM.

The evaluated factors determining the efficiency of heat recovery from exhaust gases are the length of the pipe segment connecting the collector to the heat exchanger, the length of the heat exchanger and the exchanger heat capacity. It was noticed that the heat flux transferred by the recovery system is non-monotonic depending on the length of the connecting pipe. The length should be selected so as to avoid a hot portion of the exhaust gas being pushed rapidly through the recovery heat exchanger. Generally, the shorter the connecting pipe, the more heat is recovered.

It was also observed that the heat capacity of the heat exchanger has a significant effect on the performance and efficiency of the energy recovery system. Low heat capacity leads to high dynamics of the recovery system operation, which results in rapid changes in the exchanger temperatures. This can create high thermal stresses in the system, leading to overheating and, consequently, destruction of the TEM. Lower heat capacity causes faster heating and, as a result, a decrease in heat flux conducted from the gas. Higher heat capacity enables partial accumulation of heat in the heat exchanger during the engine operation under a high load and its slow release under smaller loads or even in the standstill phase. However, too high heat capacity leads to lower

temperature of the heat exchanger, and in consequence lower TEM efficiency. So, such a system should be optimized for a specific engine.

Analysing a real driving cycle of about 15 minutes, less than 100 kJ of electrical energy was recovered. This gives energy equivalent to that contained in about 0.01 litres of petrol, assuming that the efficiency of energy extraction from petrol is at the level of 30%. During the presented driving cycle, the vehicle consumed about 1.2 litres of fuel, which means average consumption at the level of 9.3 l/100 km. The energy recovered by the regenerative braking system greatly exceeds this value. The TEM-based recovery system is more effective for constant driving at high speed. No detailed calculations were performed of the economic costs of manufacture, assembly and operation of the thermoelectric module embedded in the engine exhaust system. However, based on the presented data it seems that, under the adopted assumptions corresponding roughly to the devices available on the market, the installation of such systems nowadays may be economically unjustified in most cases of the car use.

Acknowledgments

This work was supported by the Polish National Science Centre from Grant 2016/23/B/ST8/03133.

References

[1] Rychter T., Teodorczyk A., Teoria Silników Tłokowych. Wydawnictwa Komunikacji i Łączności; 2006.

[2] Gabriel-Buenaventura, A., Azzopardi, B,. Energy recovery systems for retrofitting in internal combustion engine vehicles: A review of techniques. Renewable and Sustainable Energy Reviews, Vol. 41, pp. 955-964, 2015.

[3] Karvonen, M., Kapoor, R., Uusitalo, A., Ojanen, V., Technology competition in the internal combustion engine waste heat recovery: a patent landscape analysis. Journal of Cleaner Production, Vol. 112, pp. 3735-3743, 2016.

[4] Saidur, R., Rezaei, M., Muzammil, W.K., Hassan, M.H., Paria, S., Hasanuzzaman, M., Technologies to recover exhaust heat from internal combustion engines. Renewable and Sustainable Energy Reviews, Vol. 16, pp. 5649-5659, 2012.

[5] Nolas, G. S., Sharp, J., Goldsmid, H. J., Thermoelectrics, Basic Principles and New Materials Developments. Springer-Verlag Berlin Heidelberg, New York, 2001.

[6] Chen L., Gong J., Sun F., Chih W., Effect of heat transfer on the performance of thermoelectric generators. International Journal of Thermal Sciences, 2002, Vol. 41, pp.95–99.

[7] Mohamed E. S., Development and performance analysis of a TEG system using exhaust recovery for a light diesel vehicle with assessment of fuel economy and emissions. Applied Thermal Engineering, 2019, Vol. 147, pp.661–674.

[8] Liu X., Deng Y.D., Zhang K., Xu M., Xu Y., Su C.Q., Experiments and simulations on heat exchangers in thermoelectric generator for automotive application. Applied Thermal Engineering, Vol. 71, pp. 364-370, 2014.

[9] Niu Z., Diao H., Yu S., Jiao K., Du Q., Shu G., Investigation and design optimization of exhaust-based thermoelectric generator system for internal combustion engine. Energy Conversion and Management, Vol. 85, pp. 85-101, 2014.

[10] Su C.Q., Wang W.S., Liu X., Deng Y.D., Simulation and experimental study on thermal optimization of the heat exchanger for automotive exhaust-based thermoelectric generators. Case Studies in Thermal Engineering Vol. 4, pp. 85-91, 2014.

[11] Buchalik R., Buczkowski D., Przybyla G., Nowak G., Investigation of Waste Heat Recovery for Automobile Application Based on a Thermoelectric Module. Journal of KONES Powertrain and Transport, 2016, Vol. 23, No. 4, DOI: 10.5604/12314005.1217185.

[12] Buchalik R., Rogozinski K., Nowak G., The potential of thermoelectric energy harvesting in vehicles equipped with ICE. Combustion Engines. 2019, 179(4), 70-74. DOI: 10.19206/CE-2019-411.

[13] Boost Theory. AVL AST documentation, AVL List GmbH , Graz, 2018